



Entergy Operations, Inc.
1340 Echelon Parkway
Jackson, MS 39213-8298
Tel 601 368 5758

Michael A. Krupa
Director
Nuclear Safety & Licensing

CNRO-2003-00035

September 3, 2003

U.S. Nuclear Regulatory Commission
ATTN: Document Control Desk
Washington, DC 20555-0001

SUBJECT: Entergy Operations, Inc.
Response to Request for Additional Information Pertaining to
Relaxation Request to NRC Order EA-03-009 for In-Core
Instrumentation Nozzles

Arkansas Nuclear One, Unit 2
Docket No. 50-368
License No. NPF-29

REFERENCE: 1. NRC Order EA-03-009, "Issuance of Order Establishing Interim
Inspection Requirements for Reactor Pressure Vessel Heads at
Pressurized Water Reactors," dated February 11, 2003

2. Entergy Operations, Inc. Letter CNRO-2003-00033 to the NRC,
"Relaxation Request to NRC Order EA 03-009," dated August 27,
2003

Pursuant to Section IV.F of NRC Order EA-03-009, (Reference #1), Entergy Operations, Inc. (Entergy) requests relaxation from Section IV.C(1)(b) of the Order for Arkansas Nuclear One, Unit 2 (ANO-2). Specifically, Section IV.C(1)(b) of the Order requires either an ultrasonic test (UT) or a wetted surface examination using eddy current testing (ECT) or dye penetrant testing (PT) be performed on the total population of reactor pressure vessel (RPV) head penetration nozzles. Compliance with Section IV.C(1)(b) does not allow the use of a combination of inspection techniques; therefore, Entergy is requesting that a combination of techniques and supplementary analysis be allowed for determining the condition of the In-Core Instrumentation (ICI) nozzles at ANO-2. Enclosure 1 of this letter contains the relaxation request for ANO-2. Enclosure 2 contains a copy of the fracture mechanics analysis report (Engineering Report M-EP-2003-003, Rev. 0) that supports this request.

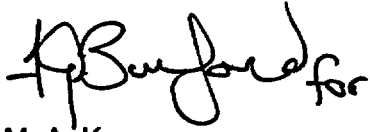
Engineering Report M-EP-2003-003, Rev. 0 utilizes information pertaining to material properties and analytical methods provided by Dominion Engineering, Inc. via Dominion letter L-4162-00-1, "Material Properties and Modeling Methods Used in ANO Unit 2 Welding Residual Stress Analysis." Entergy provided this letter to the NRC staff via Reference #2.

This letter contains new commitments as identified in Enclosure 3.

A101

Should you have any questions, please contact Guy Davant at (601) 368-5756.

Sincerely,

A handwritten signature in black ink, appearing to read "M. A. Krupa for".

M. A. Krupa
Director, Nuclear Safety & Licensing

MAK/GHD/bal

Enclosure: 1. Relaxation Request #3 for Arkansas Nuclear One, Unit 2
 2. Engineering Report M-EP-2003-003, Rev. 1
 3. Licensee-Identified Commitments

cc: Mr. C. G. Anderson (ANO)
 Mr. W. A. Eaton (ECH)
 Mr. G. A. Williams (ECH)

Mr. T. W. Alexion, NRR Project Manager (ANO-2)
Mr. R. L. Bywater, NRC Senior Resident Inspector (ANO)
Mr. T. P. Gwynn, NRC Region IV Regional Administrator

ENCLOSURE 1

CNRO-2003-00035

**ARKANSAS NUCLEAR ONE, UNIT 2
RELAXATION REQUEST #3**

**ENTERGY OPERATIONS, INC.
ARKANSAS NUCLEAR ONE, UNIT 2**

RELAXATION REQUEST #3 TO NRC ORDER EA-03-009

I. ASME COMPONENTS AFFECTED

Arkansas Nuclear One, Unit 2 (ANO-2) has ninety (90) ASME Class 1 reactor pressure vessel (RPV) head penetration nozzles comprised of eighty-one (81) Control Element Drive Mechanism (CEDM) nozzles, eight (8) In-Core Instrument (ICI) nozzles, and one (1) vent line nozzle. This request pertains to the ICI nozzles only. The locations of RPV head penetrations are provided in Figure 1.

II. REQUIREMENTS

The NRC issued Order EA-03-009 (the Order) that modified the current licenses at nuclear facilities utilizing pressurized water reactors (PWRs), which includes ANO-2. The NRC Order establishes inspection requirements for RPV head penetration nozzles. In accordance with Section IV.A of NRC Order EA-03-009, the ANO-2 susceptibility category is "high" based on a calculated value of 12.4 effective degradation years (EDY) at the beginning of the upcoming fall refueling outage.

Section IV.C of the Order states in part:

"All Licensees shall perform inspections of the RPV head using the following techniques and frequencies:

- (1) For those plants in the High category, RPV head and head penetration nozzle inspections shall be performed using the following techniques every refueling outage.
 - (a) Bare metal visual examination of 100% of the RPV head surface (including 360° around each RPV head penetration nozzle), AND
 - (b) Either:
 - (i) Ultrasonic testing of each RPV head penetration nozzle (i.e., nozzle base material) from two (2) inches above the J-groove weld to the bottom of the nozzle and an assessment to determine if leakage has occurred into the interference fit zone, OR
 - (ii) Eddy current testing or dye penetrant testing of the wetted surface of each J-groove weld and RPV head penetration nozzle base material to at least two (2) inches above the J-groove weld."

Entergy is performing a bare metal visual examination of the ICI nozzles in accordance with Section IV.C(1)(a) of the Order.

III. REASON FOR REQUEST

Section IV.F of the Order states:

"Licensees proposing to deviate from the requirements of this Order shall seek relaxation of this Order pursuant to the procedure specified below. The Director, Office of Nuclear Reactor Regulation, may, in writing, relax or rescind any of the above conditions upon demonstration by the Licensee of good cause. A request for relaxation regarding inspection of specific nozzles shall also address the following criteria:

- (1) The proposed alternative(s) for inspection of specific nozzles will provide an acceptable level of quality and safety, or
- (2) Compliance with this Order for specific nozzles would result in hardship or unusual difficulty without a compensating increase in the level of quality and safety.

"Requests for relaxation associated with specific penetration nozzles will be evaluated by the NRC staff using its procedure for evaluating proposed alternatives to the ASME Code in accordance with 10 CFR 50.55a(a)(3)."

Pursuant to Section IV.F(1) of the Order, Entergy Operations, Inc. (Entergy) requests relaxation from the requirements of Section IV.C(1)(b). Entergy plans to inspect RPV head ICI penetration nozzles at ANO-2 using the ultrasonic testing (UT) method in accordance with Section IV.C(1)(b)(i) of the Order to the maximum extent possible. However, limitations due to nozzle configuration cause reduced UT inspection coverage of each nozzle. These are discussed below.

A. Counterbore Blind Zone

ICI nozzles are manufactured with a counterbore as shown in Figure 2. Due to lift-off of the UT transducers at the counterbore, a UT blind zone exists at the upper hillside location (180° azimuth) of each ICI nozzle. Measuring approximately 0.88 inches in axial length, the bottom of the blind zone is located 1.080 inches above the top of the J-groove weld. Centered at the upper hillside location of each nozzle, the counterbore blind zone has a circumferential extent of 82°. See Figure 6 for additional details.

It should also be noted that the blind zone associated with the counter bore does not exist at any other azimuthal locations along the circumference of the ICI nozzle. Due to the RPV head angle at the ICI locations, the counterbore is significantly closer to the J-groove weld on the upper hillside of the nozzle than on the lower hillside. Specifically, the distance from the top of the J-groove weld to the bottom of the counterbore blind zone on the lower hillside of the ICI nozzle is 9.96 inches as shown in Figures 6 and 7. At the 90° and 270° azimuthal locations, the counter bore is approximately 4.64 inches above the top of the J-groove weld. See Figure 8 for additional details.

B. Blind Zone at Nozzle Bottom

A blind zone exists along the bottom of each ICI nozzle and varies from approximately 0.2 inch to 0.5 inch. This blind zone occurs due to loss of couplant as the transducers traverse across the bottom end of the nozzle. This problem is further compounded by the configuration of the ICI nozzle bottom which is cut to match the contour of the RPV head. See Figures 3, 4, and 5 for additional information.

IV. PROPOSED ALTERNATIVE AND BASIS FOR USE

Paragraph IV.C(1)(b)(i) of the Order requires that the UT inspection of each RPV head penetration nozzle encompass "from two (2) inches above the J-groove weld to the bottom of the nozzle." Due to the reasons stated above, Entergy requests relaxation from this requirement for ANO-2 ICI nozzles and proposes a three-step alternative, which involves the use of analysis, UT examination, and surface examination techniques, as described below.

A. Proposed Alternative

1. Analysis

An analysis has been performed to ensure that an unidentified surface crack in the counterbore blind zone will extend along the length, into an inspectable region, at least one operating cycle prior to growing through the thickness. The analysis, based on design information and actual UT data obtained during the previous refueling outage, is discussed in further detail in Section IV.B.1 below and is fully documented in Engineering Report M-EP-2003-003, Rev. 0 (Enclosure 2). Based on this analysis, no examination of the counterbore region is required.

2. UT Examination

The ID of each ICI nozzle (i.e., nozzle base material) shall be ultrasonically examined in accordance with Section IV.C(1)(b)(i) except as follows:

- a) For the area of the counterbore blind zone that falls within two (2) inches above the J-groove weld on the upper hillside; and
- b) For the area of the nozzle end blind zone.

In addition to the UT examination, an assessment to determine if leakage has occurred into the interference fit zone will be performed, as currently specified in Section IV.C(1)(b)(i) of the Order.

3. Augmented Inspection Plan

Because meaningful UT data cannot be collected at the bottom of the ICI nozzle, Entergy will augment the UT inspection with a surface examination of the nozzle ID, OD, and J-groove weld area that falls within the blind zone at the nozzle end. As previously mentioned, the nozzle end blind zone varies in length from 0.2 inch to 0.5 inch

depending on probe location (see Figures 3, 4 and 5). This augmented inspection plan will be performed on a sample of the ICI nozzle population. The examination methods and sampling plan are described below.

a) Examination Method

The augmented inspections will be performed using the manual PT examination method as the primary technique. Because the PT examination method cannot distinguish acceptable fabrication discontinuities from primary water stress corrosion cracking (PWSCC), PT indications are conservatively assumed to be PWSCC. Under these conditions, PT indications will be investigated by either:

- (i) Supplemental inspection using the ECT examination method; or
- (ii) Grinding followed by additional PT examinations.

b) Sampling Plan

Entergy will select two (2) of the eight ICI nozzles for augmented inspection. The size of the sampling population may increase based on the following criteria:

- (i) If PWSCC is identified in any ICI nozzle during the performance of the UT inspections, that nozzle will be included in the augmented inspection scope.
- (ii) If PWSCC is confirmed in an ICI nozzle during the performance of the augmented inspections, the remaining ICI nozzles will be added to the augmented inspection scope.

Entergy will provide in the 60-day report for ANO-2, as required by the Order, specific inspection information including the type, extent, and results of inspections and results of inspections performed on the ICI nozzles.

B. Basis for Use

1. Analysis

The extent of the proposed alternative is established by an engineering evaluation comprised of a finite element stress analysis and fracture mechanics model of the ICI nozzle counterbore blind zone. The purpose of this engineering evaluation is to ensure that an unidentified surface crack in the counterbore blind zone will extend along the length, into an inspectable region, at least one operating cycle prior to growing through the thickness.

Only an ID fracture mechanic analysis is required for this justification. This is due to the fact that the OD surface of the nozzle is not in a reactor coolant environment which promotes PWSCC. The UT exam discussed in Section IV.A.1 confirms there is no OD crack on the nozzle creating a leak path, and the triple point examination confirms there is no leak path through the weld.

Additionally the leak assessment examination above the weld confirms there is no leak through the weld butter. Hence, PWSCC can only be initiated on the ID surface of the counterbore blind zone. Both circumferential and axial cracks were evaluated; however, detailed fracture mechanics of the circumferential crack was not required because the ID and $\frac{1}{4}$ thickness axial stress is predominately compressive in the 82° arc being evaluated.

The finite element-based stress analysis and the fracture mechanics evaluation are described below. For additional details pertaining to the engineering evaluation and its conclusions, see Engineering Report M-EP-2003-003, Rev. 0 (Enclosure 2).

a) Stress Analysis

A finite element-based stress analysis representing the eight (8) ANO-2 ICI nozzle penetrations was performed by Dominion Engineering, Inc. (DEI) using best estimates of as-built geometries based on previous UT and available design information, and the material yield strength of the eight nozzles from the same heat number. General dimensions for reactor head and ICI nozzles were obtained from Westinghouse/Combustion Engineering (CE) design drawings and documents. To accommodate a potentially longer downhill side fillet weld as shown in the UT data, the fillet weld dimension in the model was increased from 3/16 inch to 7/16 inch. The counterbore was not explicitly modeled; rather, the elements were angled and tapered to transition from the 4.750-inch ID below the counterbore to the 4.625-inch ID above the counterbore. The actual counterbore is 0.25 inch high with a 1-to-4 (depth-to-length) taper; this transition precludes the need to evaluate stress concentrations such as required per ASME Section III, Subsection NB-3680 for transitions with less than a 1-to-3 transition.

Consideration of a Circumferential Crack in the Counterbore Blind Zone

Entergy considered a circumferential crack located on the ID surface, spanning the full 82° circumferential extent of the blind zone (see Figure 6). A circumferential crack, if propagated through-wall, could potentially lead to ejection of the associated nozzle. For this circumferential crack growth to occur, both the PWSCC environment and a conducive tensile axial stress field must exist. The DEI axial stress finite element analysis data were reviewed for locations at the upper hillside and those angles spanning 45° on either side of the 180° azimuth (135° and 157.5°) that would encompass the circumferential extent of the counterbore blind zone.

From previous fracture mechanics evaluations for the CEDM nozzles, it was shown that no crack growth will occur for an applied hoop stress of 10 ksi; that is, the resulting applied stress intensity factor is below the threshold value of 8.19 ksi $\sqrt{\text{in}}$ needed for crack growth.

The stresses at the ID and at the 25% through-wall location, covering a 90° circumferential span around the ICI nozzle, are predominantly compressive. Hence, the initiation of a circumferential crack in the

counterbore blind zone is precluded and presents no safety significance by not inspecting this region.

b) Fracture Mechanics Evaluation

Safety analyses performed by the EPRI Materials Reliability Program (MRP) have demonstrated that axial cracks in the nozzle tube material do not pose a challenge to the structural integrity of the nozzle. Axial cracks, if allowed to exist undetected for sufficient periods of time can produce a primary boundary leak that can cause damage to the reactor vessel head (carbon steel) and create a conducive environment for initiating and propagating OD circumferential cracks. These conditions challenge the pressure boundary; hence, critical importance is paid to proper periodic inspection and to the disposition of cracks that may be discovered. Therefore, proper analyses are essential to ascertain the nature of axial crack growth such that appropriate determination can be accomplished.

Several crack sizes were evaluated in the counterbore blind zone on the upper hillside. Crack aspect ratios typical of ASME Section XI (6-to-1 and 10-to-1 length-to-depth) and another aspect ratio emphasizing deep flaws (4-to-1) were evaluated to maximize through-wall growth while accommodating growth along the length of the ICI nozzle. These evaluations also considered a case in which the half-length of the crack was less than the remaining length needed to grow to the end of the blind zone. Summaries of crack depths and lengths used to evaluate the counterbore blind zone are presented in the table below.

Crack Case ID	Description	Crack Depth. (inch)	Crack Length (inch)
1	Aspect ratio of 6-to-1 with depth initially 25% through-wall	0.1	.06
2	Aspect ratio of 10-to-1 with an initial length of 0.4 inch	0.04	0.4
3	Aspect ratio of 4-to-1 with depth initially 25% through-wall	0.1	0.4
4	Aspect ratio of 6-to-1 with the crack spanning the length of the blind zone	0.147	0.88

In the PWSCC crack growth evaluation, the acceptability of the crack is determined by its extension outside the counterbore blind zone to a detectable length in greater than one operating cycle prior to growing through-wall. The minimum detectable crack was assumed to be 0.04 inch (2 mm) based on EPRI demonstrations. For conservatism, the detectability threshold was set at 0.16 inch. That is, a crack contained within the

counterbore blind zone must propagate along the length of the nozzle a distance measured from the tip of the crack to the edge of the blind zone plus an axial distance of 0.16 inch to ensure proper detection. The results of the crack growth evaluations are presented in the table below.

Crack Case ID	Propagation Length (inch)	Time to Reach Propagation Length (years)	Time to Grow Through-Wall (years)
1	0.3	10.94	13.74
2	0.4	> 40	> 40
3	0.4	20.98	23.34
4	0.16	3.83	6.99

A review of the stress output shows the through thickness and axial distribution of hoop stresses on the lower hillside (0° azimuth) of the nozzle to be higher than that of the upper hillside for the same relative distance above the J-groove weld. That is, for the length of the nozzle 1.08 inches above the top of the weld on the lower hillside, plus a region 0.88 inch beyond that (equivalent to the span of the counterbore blind zone on the upper hillside), the stress distribution was generally higher. However, the counterbore blind zone on the lower hillside is 9.96 inches above the top of the J-groove weld and is, therefore, not subject to the requirements of the Order. Because of the higher stress field, it is reasonable to presume that under equivalent conditions, a crack could initiate in this equivalent lower hillside area more readily than on the upper hillside. However, this region is inspectable via UT; thus, the most susceptible location based on stresses is addressed by the current inspection coverage.

c) Conclusions

The engineering evaluation supports the following conclusions:

- (i) The upper hillside (180° azimuth) of the ICI nozzle above the top of the J-groove weld possesses the highest hoop stresses in the vicinity of the counterbore for which a UT blind zone exists.
- (ii) The conservatisms used in the analysis (pressure applied to crack faces and high crack length-to-depth aspect ratio) provide assurance that an undetected crack in the counterbore blind zone on the upper hillside will not grow through-wall prior to extending out of the blind zone into an inspectable region in less than one operating cycle.

- (iii) The area above the J-groove weld on the lower hillside of the ICI nozzle is in a higher stress field than the area on the upper hillside. Because of this, the lower hillside area is more susceptible to crack initiation than the upper hillside. However, this area is inspected by UT.
- (iv) The ID surface crack on the upper hillside either did not show any potential for crack growth, or the growth in the axial direction reached a detectable area of the nozzle in at least one operating cycle prior to the crack growing through-wall. Hence, an ID surface crack in a region above the J-groove weld on the upper hillside is not significant in that it does not affect nozzle integrity.
- (v) No potential exists for an ID circumferential crack to be located in the counterbore blind zone due to the predominant compressive axial stress field spanning 45° on either side of the upper hillside of the ICI nozzle.

This analysis incorporates a crack-growth formula different from that described in Footnote 1 of the Order, as provided in EPRI Report MRP-55. Entergy is aware that the NRC staff has not yet completed a final assessment regarding the acceptability of the EPRI report. If the NRC staff finds that the crack-growth formula in MRP-55 is unacceptable, Entergy shall revise its analysis that justifies relaxation of the Order within 30 days after the NRC informs Entergy of an NRC-approved crack-growth formula. If Entergy's revised analysis shows that the crack growth acceptance criteria are exceeded prior to the end of Operating Cycle 17 (following the upcoming refueling outage), Entergy will, within 72 hours, submit to the NRC written justification for continued operation. If the revised analysis shows that the crack growth acceptance criteria are exceeded during the subsequent operating cycle, Entergy shall, within 30 days, submit the revised analysis for NRC review. If the revised analysis shows that the crack growth acceptance criteria are not exceeded during either Operating Cycle 17 or the subsequent operating cycle, Entergy shall, within 30 days, submit a letter to the NRC confirming that its analysis has been revised. Any future crack-growth analyses performed for Operating Cycle 17 and future cycles for RPV head penetrations will be based on an NRC-acceptable crack growth rate formula.

2. UT Examination

The UT inspection probe to be used to inspect the ANO-2 ICI nozzles consists of seven (7) individual transducers. The configuration of the probe has been optimized for maximum coverage. UT inspection of ICI nozzles will be performed using a combination of time-of-flight diffraction (TOFD) and standard 0° pulse-echo techniques. The TOFD approach utilizes two pairs of 0.250-inch diameter, 55° refracted-longitudinal wave transducers aimed at each other. One of the transducers transmits sound into the inspection volume while the other receives the reflected and diffracted signals as they interact with the material. There will be one TOFD pair scanning in the axial direction of the penetration nozzle tube and one TOFD pair scanning in the circumferential

direction of the tube. The TOFD technique is primarily used to detect and characterize planar-type defects within the full volume of the tube.

The standard 0° pulse-echo ultrasonic approach utilizes one 0.250-inch diameter straight beam transducer. The 0° technique is used to:

- Plot the penetration nozzle OD location and J-groove weld location,
- Locate and size any laminar-type defects that may be encountered, and
- Monitor the back-wall signal response to detect leakage that may occur in the interference regions of the RPV head penetration.

The UT inspection procedures and techniques to be utilized at ANO-2 have been satisfactorily demonstrated under the EPRI Materials Reliability Program (MRP) Inspection Demonstration Program.

3. Augmented Inspection Plan

Augmenting UT examination of the nozzle base material with surface examination ensures the ICI nozzle is adequately examined to determine its condition. The augmented inspection plan will only be used for those portions of the nozzles that could not be inspected by UT or excluded by analysis. The bases for the examination method and sampling plan are described below.

a) Examination Method

The augmented inspections will be performed using the PT examination method as the primary technique. Entergy believes the use of PT to augment UT is acceptable for ensuring that the required areas not excluded by analysis are inspected. The Order recognizes and allows the use of PT as acceptable for evaluating the condition of nozzle surfaces. Augmenting the UT examination of the nozzle base material with PT ensures the nozzle is adequately examined to determine its condition.

As discussed in Section IV.A.3.a), above, Entergy may use ECT to investigate indications identified by PT. ECT is also an acceptable technique for evaluating such indications. As with PT, the Order recognizes and allows the use of ECT as acceptable for evaluating the condition of nozzles and associated J-groove welds.

b) Sampling Plan

Entergy believes that to require examination of every ICI nozzle rather than inspecting in accordance with the sampling plan would impose hardships without a compensating increase in the level of quality and safety. The basis for this position is summarized below:

(i) Low Probability of PWSCC

The likelihood of finding a PWSCC crack in an ANO-2 ICI nozzle is low based on available industry data. Specifically:

- (1) Each ICI nozzle at ANO-2 was manufactured by Huntington Alloy using heat number NX2696 of SB-166, N06600. For this particular heat of material, there is no known industry history of PWSCC.
- (2) High yield strength materials are more susceptible to PWSCC. The lowest yield strength for nozzle material known to have cracked is 37 ksi. The yield strength of the ANO-2 ICI nozzles is 31.5 ksi, which is significantly lower.
- (3) While the industry has identified PWSCC in control element drive mechanism (CEDM) nozzles, there is no industry history of PWSCC in ICI nozzles.

(ii) High Personnel Dose

As stated above, augmented inspections will be performed using the PT examination method. Entergy estimates personnel performing PT on all eight ICI nozzles would receive a radiation dose ranging between 2.4 and 4.5 man-REM.

The preferred method of investigating rounded PT indications in weld metal is supplemental inspection using the ECT examination method. The ECT equipment that would be used to perform these supplemental inspections is being developed and has not been field proven. However, based on similar inspections, Entergy estimates performing supplemental ECT on all eight ICI nozzles will involve a radiation exposure of approximately 1 man-REM. The dose estimate for performing PT with supplemental ECT on all eight nozzles would be approximately 3.4 to 5.5 man-REM.

Entergy has not estimated the radiation dose associated with grinding activities to investigate rounded indications. However, we expect the dose to be higher than that estimated for performing PT with supplemental ECT because of extended personnel stay-time under the RPV head involved with grinding activities.

(iii) Adverse Impact to Nozzle Base Material

As discussed above, the PT examination method cannot distinguish acceptable rounded indications from the surface extension of a PWSCC crack on a weld. Therefore, PT indications may be explored by grinding if the ECT process is not available. Because grinding of the weld metal and/or nozzle base material causes localized work-hardening, ground areas of the nozzle and weld will experience an increased susceptibility to PWSCC.

In summary, there is no industry history of PWSCC in ICI nozzles. Furthermore, UT inspections of nozzle regions with the higher stresses, which are believed to be more susceptible to PWSCC, are being inspected volumetrically. UT inspection of the more susceptible regions combined with the surface examinations of the nozzle end blind zone, no industry

experience of PWSCC, and the low susceptible ICI material properties provides assurance that the proposed sample plan will provide an acceptable level of quality and safety.

V. CONCLUSION

Section IV.F of NRC Order EA-03-009 states:

"Licensees proposing to deviate from the requirements of this Order shall seek relaxation of this Order pursuant to the procedure specified below. The Director, Office of Nuclear Reactor Regulation, may, in writing, relax or rescind any of the above conditions upon demonstration by the Licensee of good cause. A request for relaxation regarding inspection of specific nozzles shall also address the following criteria:

- (1) The proposed alternative(s) for inspection of specific nozzles will provide an acceptable level of quality and safety, or
- (2) Compliance with this Order for specific nozzles would result in hardship or unusual difficulty without a compensating increase in the level of quality and safety."

Section IV.C(1)(b) of the Order establishes a minimum set of RPV head penetration nozzle inspection requirements to identify the presence of cracks in penetration nozzles that could lead to leakage of reactor coolant and wastage of RPV head material.

Entergy believes the proposed alternative, described in Section IV, provides an acceptable level of quality and safety by utilizing inspections and supplemental analysis to determine the condition of the ANO-2 ICI nozzles. The technical basis for the supplemental analysis of the proposed alternative is documented in Engineering Report M-EP-2003-003, Rev. 0, which is contained in Enclosure 2 of this letter. Therefore, Entergy requests that the proposed alternative be authorized pursuant to Section IV.F of the Order.



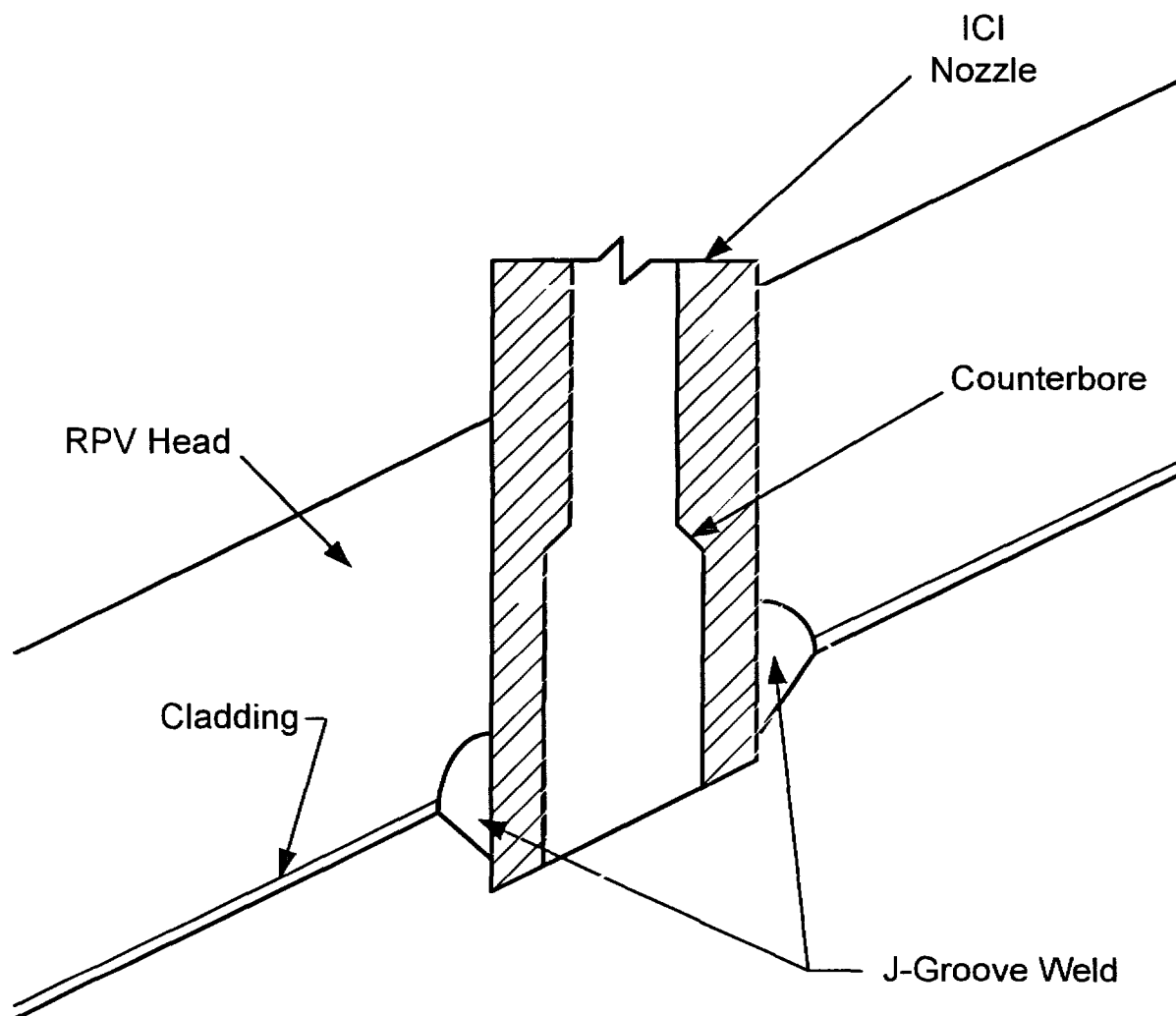


FIGURE 2
ICI NOZZLE CONFIGURATION

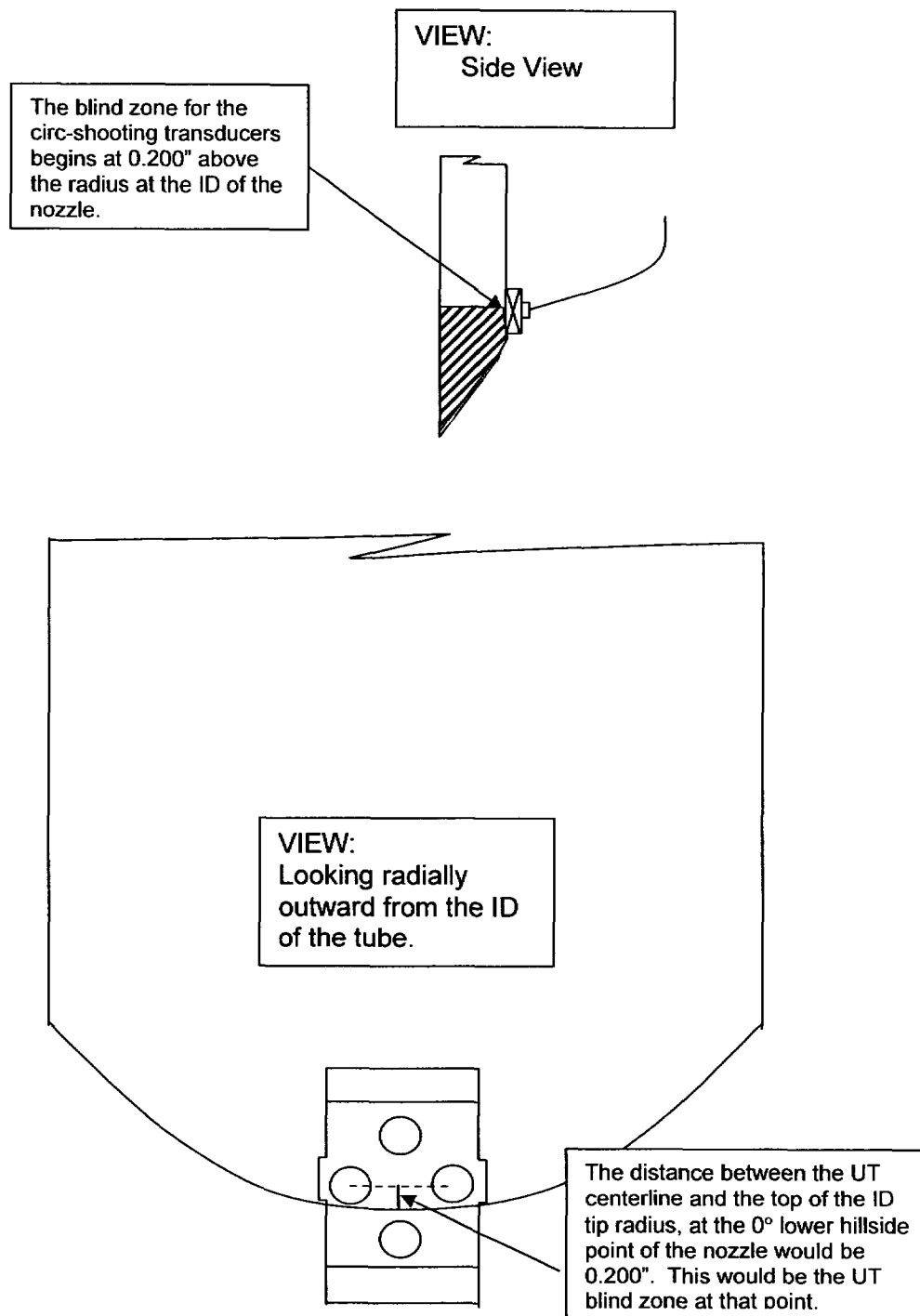


FIGURE 3
UT INSPECTION PROBE
END OF NOZZLE – LOWER HILLSIDE POSITION

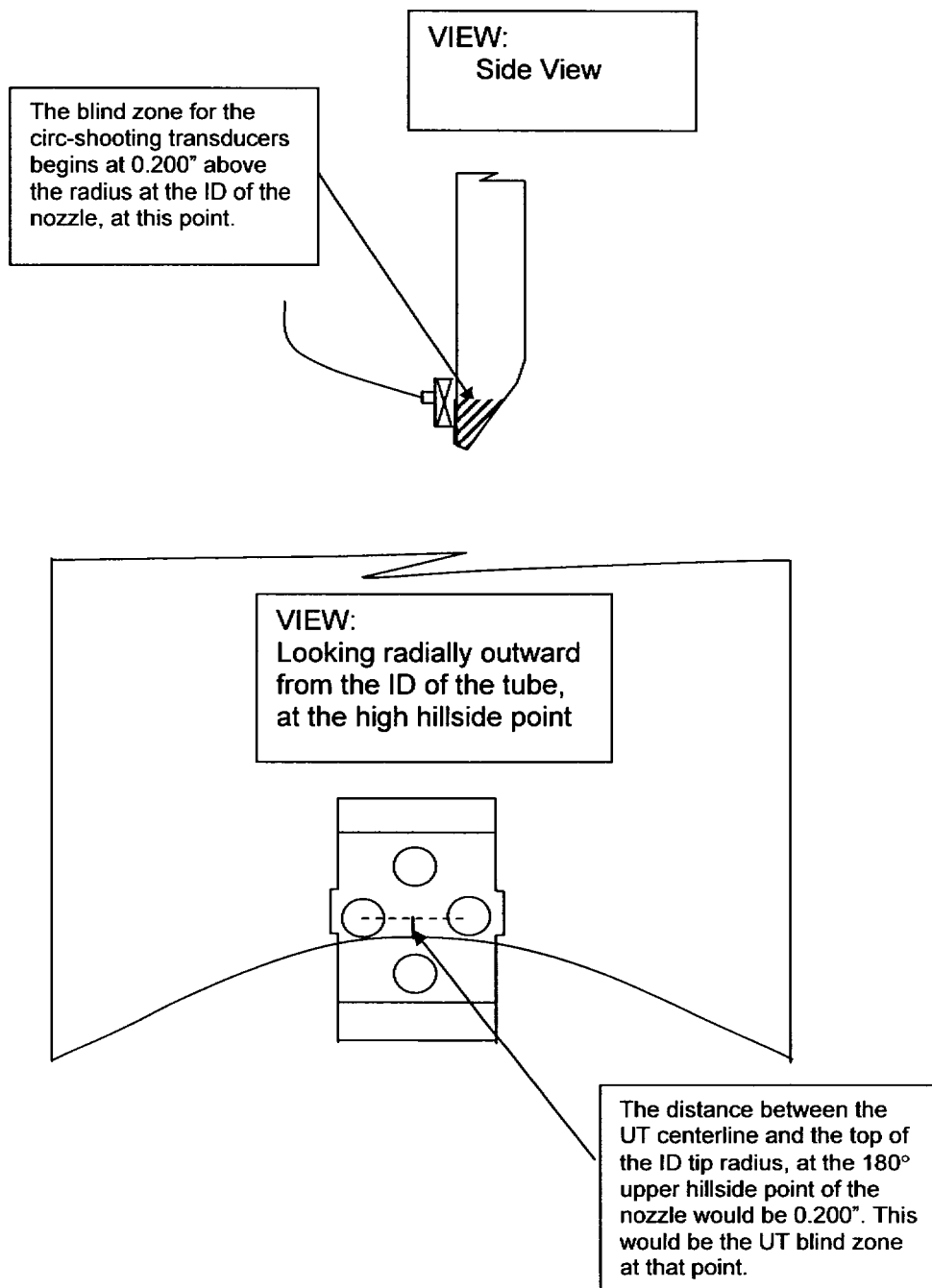


FIGURE 4
UT INSPECTION PROBE
END OF NOZZLE- UPPER HILLSIDE POSITION

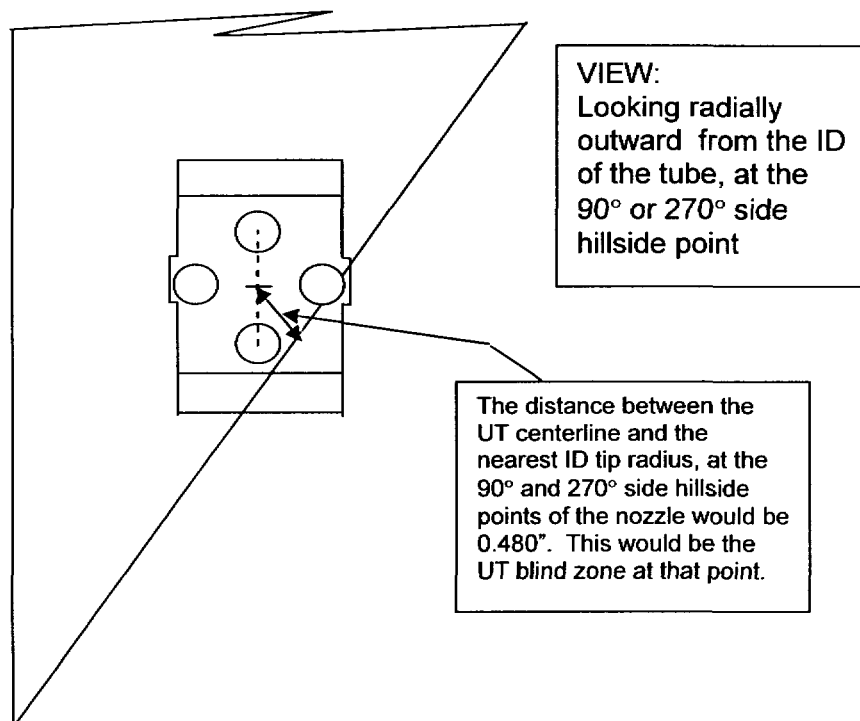


FIGURE 5
UT INSPECTION PROBE
END OF NOZZLE – SIDE VIEW @ 90° and 270°

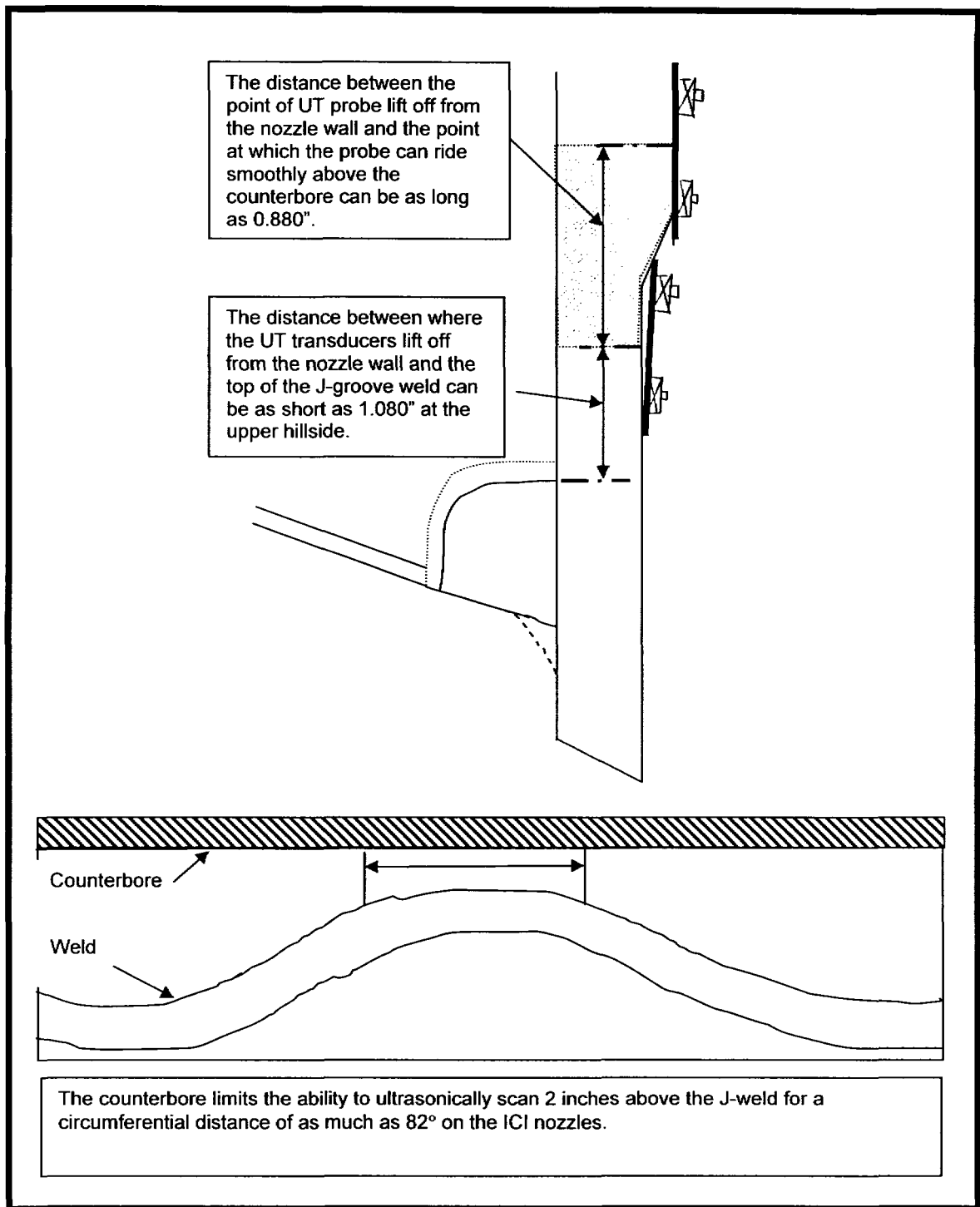


FIGURE 6
COUNTERBORE – UPPER HILLSIDE POSITION

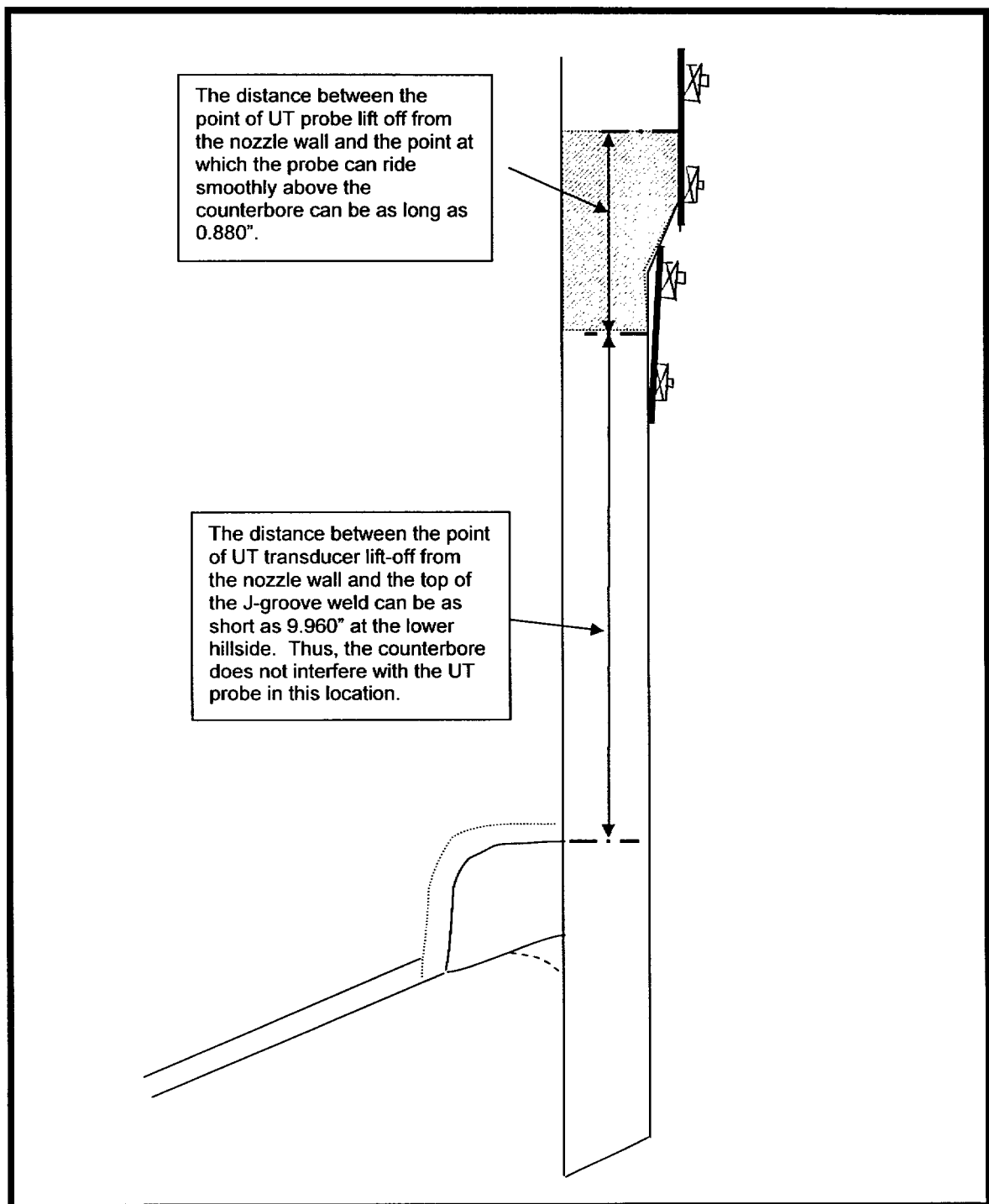


FIGURE 7
COUNTERBORE – LOWER HILLSIDE POSITION

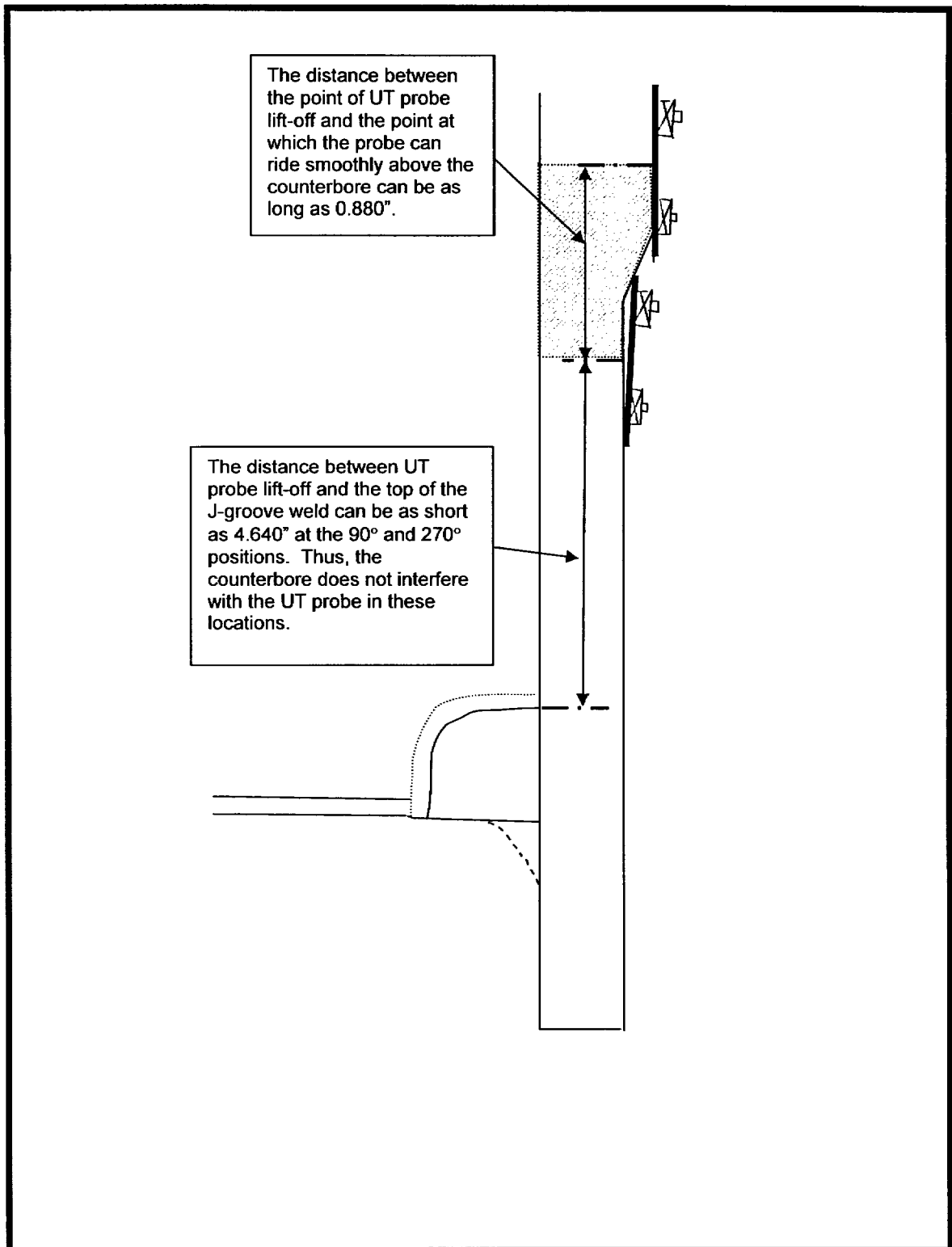


FIGURE 8
COUNTERBORE @ 90° AND 270° POSITIONS

ENCLOSURE 2

CNRO-2003-00035

ENGINEERING REPORT M-EP-2003-003, REV. 0

**FRACTURE MECHANICS ANALYSIS FOR THE ASSESSMENT OF THE
POTENTIAL FOR PRIMARY WATER STRESS CORROSION CRACK (PWSCC)
GROWTH IN THE UNINSPECTED REGIONS OF THE
IN-CORE INSTRUMENTATION (ICI) NOZZLES AT
ARKANSAS NUCLEAR ONE UNIT 2**



ENTERGY NUCLEAR SOUTH
Engineering Report Coversheet

Fracture Mechanics Analysis for the Assessment of the Potential for Primary Water Stress Corrosion Crack (PWSCC) Growth in the Un-Inspected Regions of the In-Core Instrumentation (ICI) Nozzles at Arkansas Nuclear One Unit 2

Engineering Report Type:

New ☒ Revision ☐ Deleted ☐ Superceded ☐

Applicable Site(s)

ANO ☒ Echelon ☒ GGNS ☐ RBS ☐ WF3

Report Origin: ☒ ENS ☐ Vendor **Safety-Related:** ☒ Yes ☐ No

Vendor Document No. _____

Prepared by:

Brian C. Khay
Responsible Engineer

Date: 9/3/03

Comments:

☐ Yes

☐ No

Attached:

☐ Yes

☐ No

Verified/
Reviewed by:

J. J. Britton
Design Verifier/Reviewer

Date: 9/3/03

☒ Yes

☐ No

☐ Yes

☒ No

Approved by:

R. L. L.
Responsible Supervisor or
Responsible Central Engineering Manager
(for multiple site reports only)

Date: 9/3/01

☐ Yes

☒ No

☐ Yes

☐ No

RECOMMENDATION FOR APPROVAL FORM

Prepared by: <u>Brian C. Gray</u>	Date: <u>9/3/03</u>	Comments: <input type="checkbox"/> Yes	Attached: <input type="checkbox"/> Yes
<u>William Lino</u> 9/3/03 Responsible Engineer		<input type="checkbox"/> No	<input type="checkbox"/> No
Concurrence: <u>[Signature]</u>	Date: <u>9/3/03</u>	<input checked="" type="checkbox"/> Yes	<input type="checkbox"/> Yes
Responsible Engineering Manager, ANO		<input type="checkbox"/> No	<input checked="" type="checkbox"/> No
Concurrence: <u>Not Applicable</u>	Date: _____	<input type="checkbox"/> Yes	<input type="checkbox"/> Yes
Responsible Engineering Manager, GGNS		<input type="checkbox"/> No	<input type="checkbox"/> No
Concurrence: <u>Not Applicable</u>	Date: _____	<input type="checkbox"/> Yes	<input type="checkbox"/> Yes
Responsible Engineering Manager, RBS		<input type="checkbox"/> No	<input type="checkbox"/> No
Concurrence: <u>Not Applicable</u>	Date: _____	<input type="checkbox"/> Yes	<input type="checkbox"/> Yes
Responsible Engineering Manager, WF3		<input type="checkbox"/> No	<input type="checkbox"/> No

Table of Contents

Section	Title	Page Number
	Table of Contents	3
	List of Attachments	4
	List of Tables	4
	List of Figures	5
1.0	PURPOSE	6
2.0	GIVEN CONDITIONS AND KNOWN VALUES	8
2.1	ICI Nozzle Material, Operating Conditions, and Geometry	8
2.2	Dimensions of the Welds and Counterbore Areas	9
2.3	Orientation and Dimensions of UT Blind Zone on the ICI Nozzles	10
3.0	METHOD OF ANALYSIS	11
3.1	Finite Element Stress Analysis of ANO-2 ICI Nozzles	11
3.2	ID Surface Flaw Fracture Mechanics Model	15
3.3	PWSCC Growth Model	17
3.4	Iterative Mathcad Model for Stress Curve-Fitting and Flaw Growth Evaluation	18
3.5	Consideration of a Circumferential Flaw in the Un-Inspectable Region	23
4.0	DISCUSSION AND RESULTS	25
4.1	Discussion	25
4.2	Results of the ID Surface Flaw Evaluation	26
5.0	CONCLUSIONS	33
6.0	REFERENCES	34

List of Attachments

Attachment Number	Content of Attachment	Number of Pages
1	Design Input Record from ANO-2 for the ICI Nozzles	4
2	NDE Limitations for ICI Nozzles	2
3	Dominion Engineering Inc. Nodal Stress and Coordinate Data (Including Transmittal E-mails)	18
4	Mathcad Worksheet for Flaw Case 1: 25% Through-wall Flaw with an Initial Aspect Ratio of 6-to-1 (Length-to-Depth) Centered in the Blind zone	42
5	Mathcad Worksheet for Flaw Case 2: 0.4 Inch Long with an Initial Aspect Ratio of 10-to-1 (Length-to-Depth) Centered in the Blind zone	42
6	Mathcad Worksheet for Flaw Case 3: 25% Through-wall Flaw with a Initial Aspect Ratio of 4-to-1 (Length-to-Depth) Centered in the Blind zone	42
7	Mathcad Worksheet for Flaw Case 4: A Flaw Spanning the Entire 0.88-Inch Length of the Blind zone with an Initial 6-to-1 Aspect Ratio (Length-to-Depth)	42

Total Pages of Attachments: 192**List of Tables**

Table Number	Title	Page Number
1	Dimensions from Tangent Line Datum Plane to specified locations on the ICI Nozzle	9
2	Summary of flaw depths and lengths used to evaluate the blind zone on the uphill side above the top of the weld (Blind zone begins a distance 1.08 inches above the top of the weld and extends 0.88 inch)	26
3	Results of PWSCC flaw growth evaluations in the length and depth directions	27

List of Figures

Figure Number	Title	Page Number
1	ANO-2 ICI Geometry from the Bottom of the Nozzle	8
2	Measured ICI Nozzle Locations from Tangent Line Datum	9
3	Counterbore at the Uphill Side (180°) Position	10
4	Hoop stress contours for the ICI nozzle. High tensile stresses occur in the weld and adjacent tube material	13
5	Hoop stress contours in the upper portion (closer to the intersection with the reactor head) of the ICI nozzle	13
6	Close-up of the uphill side (180° azimuth) hoop stress in the vicinity of the J-groove weld and counterbore region	14
7	SICF shown as a function of normalized crack depth for the “a-tip” (left figure) and the “c-tip” (right figure)	16
8	ID Axial Stress Distribution Spanning 45° on Either Side (90° Total) of Uphill	23
9	25% Through-Wall Position Axial Stress Distribution Spanning 45° on Either Side (90° Total) of Uphill	24
10	Flaw Case 1—Depth Growth (top) and Length Growth (bottom) versus number of operating years	28
11	Flaw Case 2—Depth Growth (top) and Length Growth (bottom) versus number of operating years	29
12	Flaw Case 3—Depth Growth (top) and Length Growth (bottom) versus number of operating years	30
13	Flaw Case 4—Depth Growth (top) and Length Growth (bottom) versus number of operating years	31

1.0 PURPOSE

The US Nuclear Regulatory Commission (NRC) issued Order EA-03-009 [Ref. 1], which modified licenses, requiring inspection of all Control Element Drive Mechanism (CEDM), In-Core Instrumentation (ICI), and vent penetration nozzles in the reactor vessel head. Paragraph IV.C.1.b of the Order requires the inspection to cover a region from the bottom of the nozzle to two (2.0) inches above the J-groove weld.

The Combustion Engineering (CE) design for the ICI nozzles consists of a 5.563-inch outside diameter (OD) nozzle, inserted into the reactor vessel head at a 56.2833° angle with the horizontal, with the portion of the nozzle extending below the inside surface of the vessel cut to the same angle. The inside diameter (ID) of the ICI nozzle is counter-bored from a diameter of 4.625 inches to 4.750 inches at a height of 1.377 inches above the top of the J-groove weld on the uphill side (180° azimuth), and approximately 10.092 inches from top of the J-groove weld on the downhill side (0° azimuth), based on design drawings. (These dimensions are taken from Attachment 1 and shown in Figures 1 and 2.) This counterbore region of the nozzle above the J-groove weld represents a challenge to interrogate the nozzle with Ultrasonic Testing (UT). Figures 1 and 2 show the typical layout and geometry of the ICI nozzle, while Figure 3 schematically depicts the un-inspectable regions with UT due to the configuration of the counterbore. This un-inspectable region, measuring 0.88 inch in axial length and extending circumferentially around the ID for 82°, above the top of the J-weld on the uphill side (as shown in Figure 3), is defined as the UT Blind zone (hereafter referred to as the blind zone). Due to the offset distance between the low hill side (0° azimuth) and high hillside (180°) of the nozzle at the attachment J-groove weld, the blind zone is closer to weld at the high hillside than it is on the low hillside. On the high (or uphill) side, the distance from the top of the J-groove weld to the bottom of the blind zone is 1.08 inches (Figure 3), whereas the same measurement on the downhill and mid-plane locations are 9.96 inches and 4.06 inches, respectively, a distance outside the requirements of the Order. Thus, only a small arc length of the nozzle (82°, from Attachment 2 and Figure 3) above the top of the weld on the uphill side cannot be examined with UT.

The unexamined region of the ICI nozzles in the counterbore region above the J-weld provides a location for surface flaws to exist with the potential to grow through the thickness of the nozzle prior to extending beyond the limits of the blind zone, into a detectable region. This is especially a concern on the uphill side of the nozzle, where the blind zone is only 1.08 inches from the top of the weld and in an area subject to the accompanying high stress field of the J-weld. An ID surface flaw could exist in this 0.88 inch-long blind zone.

In order to exclude the blind zone areas above the weld in the counterbore region from the inspection campaign, a relaxation of the Order is required pursuant to the requirements prescribed in Section IV.F and footnote 2 of the order [Ref. 1].

The purpose of this engineering report is to ensure that an unidentified surface flaw in the blind zone will extend along the length, into an inspectable region, at least one operating cycle prior to growing through the thickness. Only an ID fracture mechanic analysis is required for this justification. This is due to the fact that the OD surface of the nozzle is not in a reactor coolant environment which promotes PWSCC. The UT exam confirms there is no OD flaw on the nozzle creating a leak path, and the triple point examination confirms there is no leak path through the weld. Additionally the leak assessment examination above the weld confirms there is no leak through the butter. Hence, PWSCC can only be initiated on the ID surface of the blind zone. ID surface axial and circumferential flaws will be considered in the analysis.

2.0 GIVEN CONDITIONS AND KNOWN VALUES

2.1 ICI Nozzle Material, Operating Conditions, and Geometry:

Pipe Material: SB-167, Gr. 70 [Ref. 2a]

Pipe Outside Diameter:

$D_o = 5.563 \text{ in. } +0.000/-0.001 \text{ in.}$ [Ref. 2a]

Pipe Inside Diameter, above counterbore:

$D_{i1} = 4.625 \text{ in. } \pm 0.01 \text{ in.}$ [Ref. 2b]

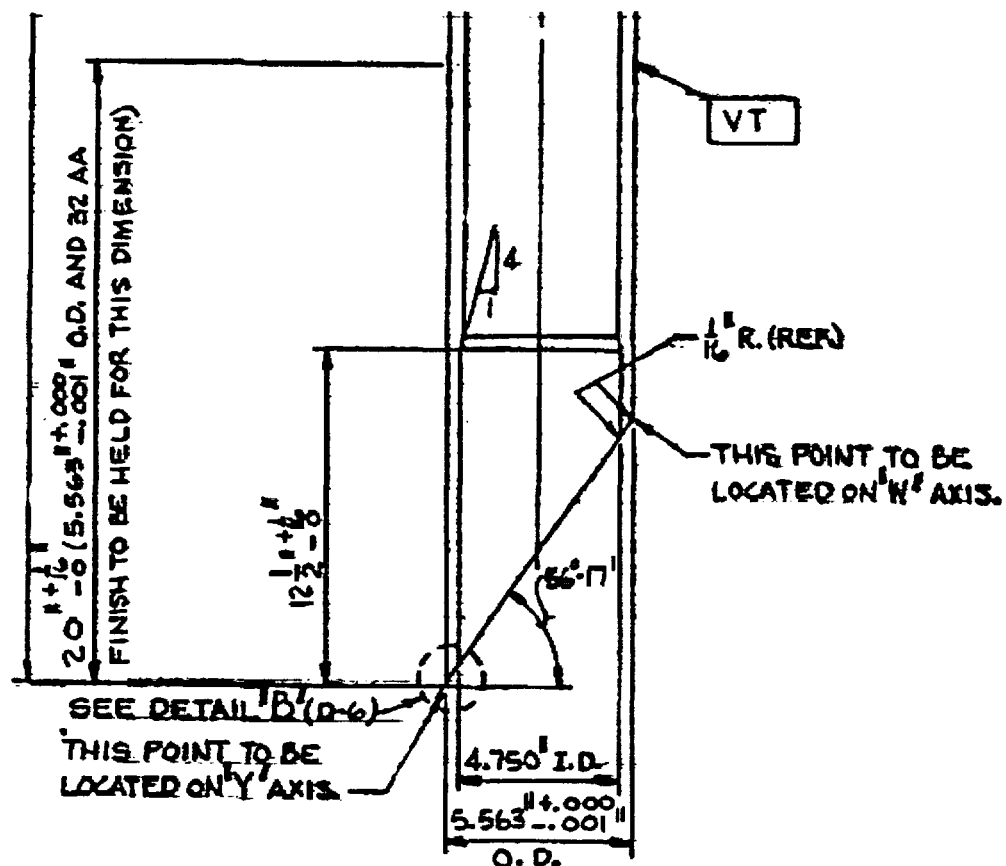
Pipe Inside Diameter, below counterbore:

$D_{i2} = 4.750 \text{ in. } \pm 0.01 \text{ in.}$ [Ref. 2b]

Operating Pressure = 2235 psi [Ref. 3]

Operating Temperature = 604°F. Reference 4 gives a value of 594.8°F, but 604°F will conservatively be used.

Figure 1: ANO-2 ICI Geometry from the Bottom of the Nozzle (from Ref. 2a)



2.2 Dimensions of the Welds and Counterbore Areas:

The elevations and heights of the ICI nozzles and weld positions were obtained from design drawings and transmitted in a Design Input Record from ANO (shown Attachment 1). The figure and table below provide a summary of these inputs:

Figure 2: Measured ICI Nozzle Locations from Tangent Line Datum

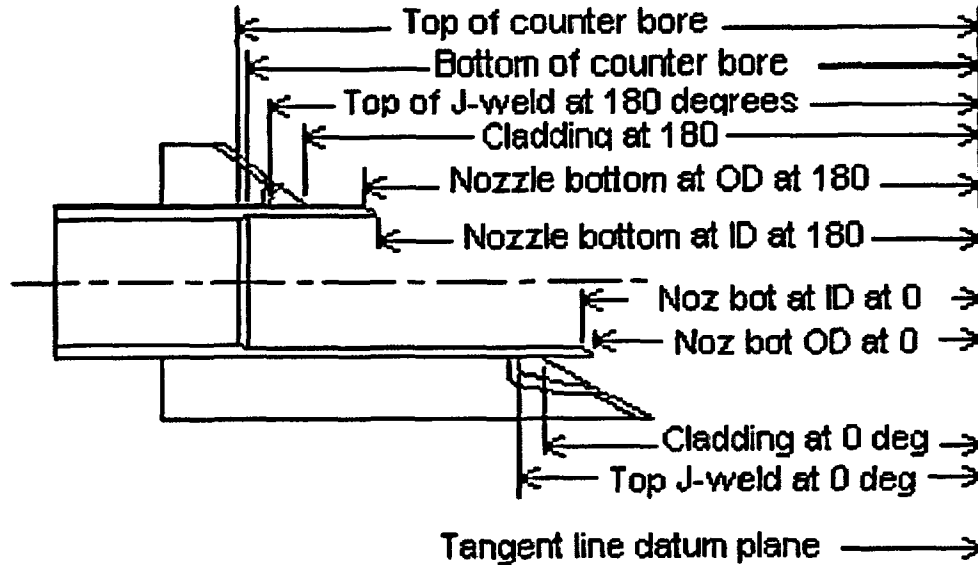
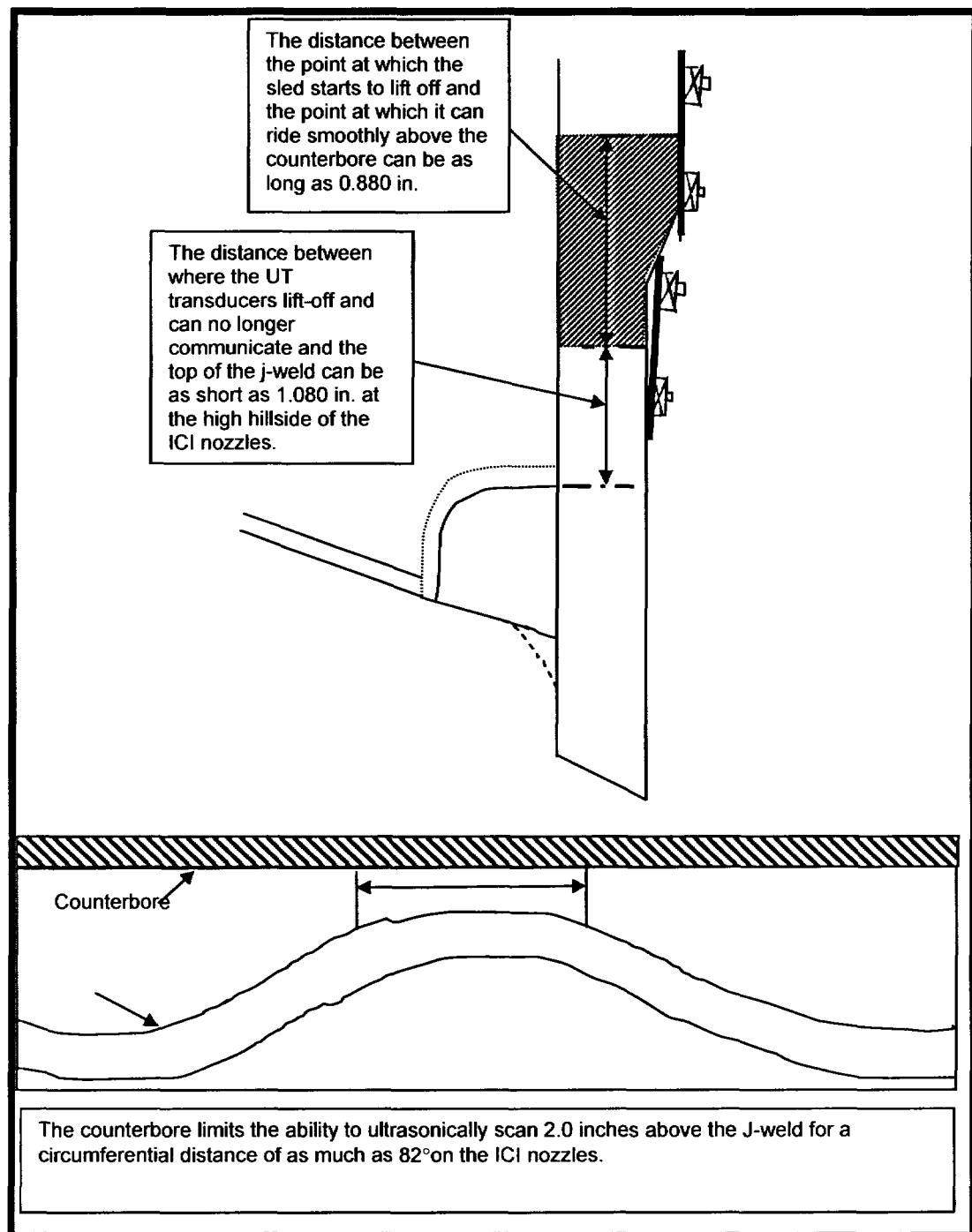


Table 1: Dimensions from Tangent Line Datum Plane to specified locations on the ICI Nozzle

Dimension from the tangent line datum plane to:	ANO-2 (inches)	W-3 (inches)
Top of counter bore transition	48.625	55.094
Bottom of counter bore transition	48.375	54.844
Top of J-weld at the 180 degree (high hill side) azimuth location	46.998	53.440
Intersection of the projected cladding surface and the nozzle OD at the 180 degree (high hill side) azimuth location	46.211	52.655
Bottom (sharp corner) of the nozzle at the OD surface at the 180 degree (high hill side) azimuth location	44.211	50.618
Bottom (sharp corner) of the nozzle at the ID surface at the 180 degree (high hill side) azimuth location	43.602	50.031
Top of J-weld at the 0 degree (low hill side) azimuth location	38.283	45.008
Intersection of the projected cladding surface and the nozzle OD at the 0 degree (low hill side) azimuth location	37.875	44.589
Bottom (sharp corner) of the nozzle at the ID surface at the 0 degree (low hill side) azimuth location	36.484	43.180
Bottom (sharp corner) of the nozzle at the OD surface at the 0 degree (low hill side) azimuth location	35.875	42.594

2.3 Orientation and Dimensions of UT Blind Zone on the ICI Nozzles

Figure 3: Counterbore at the Uphill Side (180°) Position—the UT Blind zone starting point is 1.080 inches above the top of weld. The Axial length of the UT Blind zone is 0.880 inch. The arc length of limitation for 2" scanning above the weld is 82° [shown in Attachment 2]



3.0 METHOD OF ANALYSIS

The analysis used to determine the impact of not examining the blind zone of the ICI nozzle above the top of the weld in the counterbore region on the uphill side consists of a detailed finite element stress analysis combined with an ID surface flaw fracture mechanics model. The fracture mechanics model evaluates an ID-initiated part through-wall axial crack in a cylinder, located in the 0.88-inch blind zone region above the top of the weld on the uphill side of the ICI nozzle. Additional consideration of an ID circumferential surface flaw is provided in Section 3.5

The following sections provide details of the finite element stress analysis and the accompanying fracture mechanics evaluation.

3.1 Finite Element Stress Analysis of ANO-2 ICI Nozzles

A finite element-based stress analysis representing the eight (8) ANO-2 ICI penetrations was performed by Dominion Engineering Inc. (DEI) using best estimates of as-built geometries based on previous UT and available design information, and the material yield strength of the eight nozzles from the same heat number. General dimensions for reactor head and ICI nozzles were obtained from Westinghouse/CE design drawings and documents. To accommodate a potentially longer downhill side fillet weld as shown in the UT data, the fillet weld dimension in the model was increased from 3/16 inch to 7/16 inch. The counterbore was not explicitly modeled due to computational resource restraints and modeling simplifications; rather, the elements were angled and tapered to transition from the 4.750-inch ID below the counterbore to the 4.625-inch ID above the counterbore. The actual counterbore is 0.25 inch high with a 1-to-4 (depth-to-length) taper; this transition precludes the need to evaluate stress concentrations such as required per ASME Section III, subsection NB-3680 [Ref. 5] for transitions with less than a 1-to-3 transition.

The finite element analysis (FEA) modeling steps using the above geometry data and assumptions to obtain the necessary stress (residual+operating) distribution in the ICI nozzle followed the process and methodology described in Reference 6a. The modeling steps were as follows:

- 1.) The finite element mesh consisted of 3-dimensional solid (brick) elements. Four elements were used to model the tube wall and similar refinement was carried to the attaching J-weld. As referenced above, one row of angled elements represented the transition from the 4.750-inch ID below the counterbore to the 4.625-inch ID above the counterbore.
- 2.) The ICI nozzle material, possessing the same yield strength for all nozzles, resulting from a single heat of material, was modeled with a monotonic stress-strain curve. The yield strength of the nozzles was referenced to the room temperature yield strength of the stress strain curve described in Reference 6a. Temperature-dependent stress-strain curves needed to model the nonlinear

welding process were obtained by indexing the temperature-dependent drop of the yield strength.

- 3.) The weld material was modeled as elastic-perfectly plastic for the weld simulation. This approximation is considered reasonable since most of the plastic strain in the weld metal occurs at high temperatures where metals do not work-harden significantly [Ref. 6b]. The temperature in the weld is always high during the welding process, and once the weld begins to cool, the temperatures in the weld at which strain hardening would persist are of limited duration [Ref. 6b]. This was borne out by the comparison between the analysis-based residual stress distribution and that obtained from experiments [Ref. 6c].
- 4.) The weld is simulated by two passes based on studies presented in Reference 6a.
- 5.) After completing the weld, a simulated hydro-test load step is applied to the model. The hydro-test step followed the fabrication practice.
- 6.) The model is then subjected to a normal operating schedule of normal heat up to steady state conditions at operating pressure. The residual plus operating stresses, once steady state has been achieved, are obtained for further analysis. The nodal stresses of interest are stored in an output file. These stresses are then transferred to an Excel spreadsheet for use in fracture mechanics analysis.

The stress contours for the ICI nozzle obtained from the finite element analysis are presented in Figures 4 through 6. The hoop stress contour color scheme is as follows:

Dark Navy blue → from Minimum (Compression) to -10 ksi

Royal blue → from -10 to 0 ksi

Light blue → from 0 to 10 ksi

Light green → from 10 to 20 ksi

Green → from 20 to 30 ksi

Yellow green → from 30 to 40 ksi

→ from 40 to 50 ksi

Red → from 50 to 100 ksi

Figure 4: Hoop stress contours for the ICI nozzle. High tensile stresses occur in the weld and adjacent tube material.

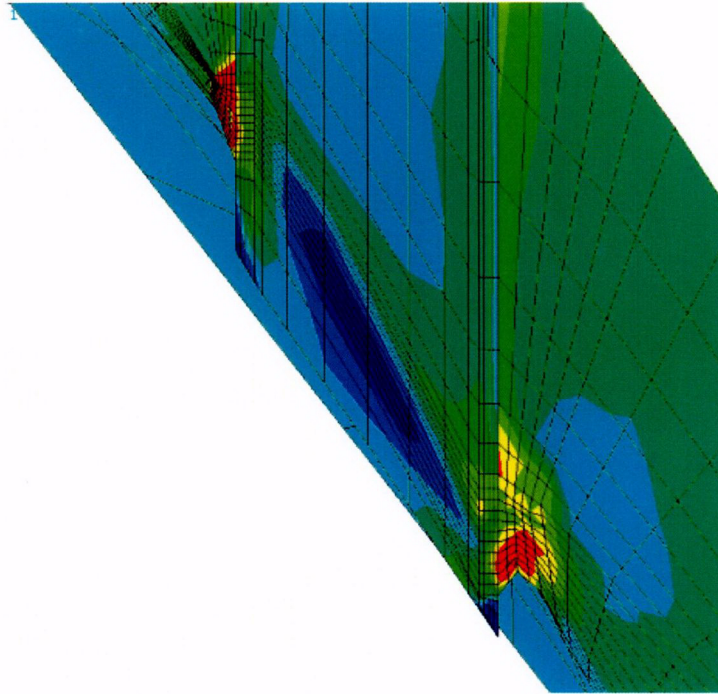


Figure 5: Hoop stress contours in the upper portion (closer to the intersection with the reactor head) of the ICI nozzle

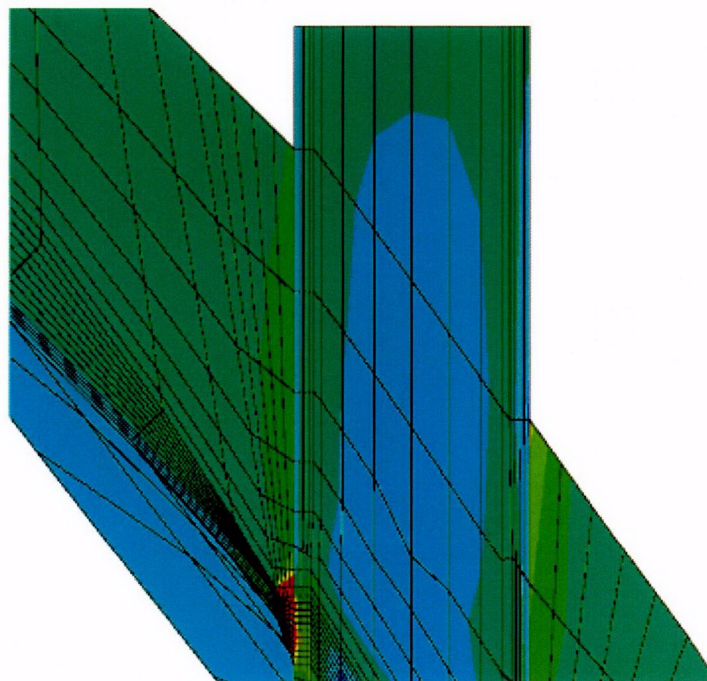
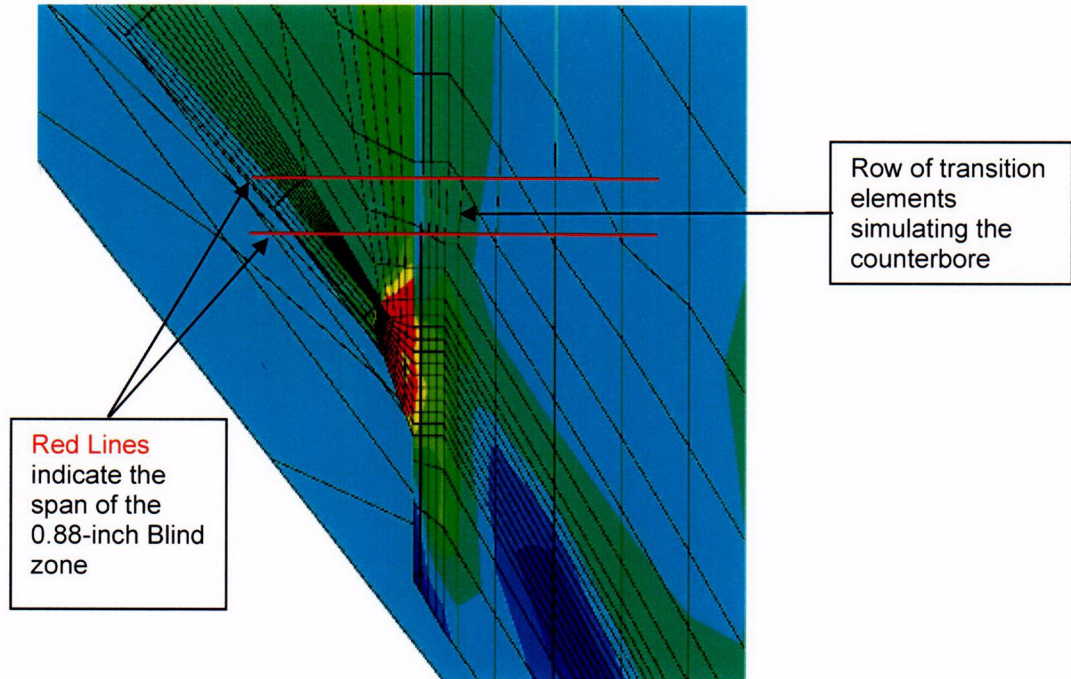


Figure 6: Close-up of the uphill side (180° azimuth) hoop stress in the vicinity of the J-groove weld and counterbore region



The nodal stresses for locations of interest were provided by DEI and were tabulated in Reference 6d. (This data is also shown in Attachment 3.) The location of the weld bottom at each azimuth was maintained at the node row ending with “601”, while the top of the weld at each azimuth was the node row ending with “1301”. The blind zone is shown on Figure 6 as an overlay to the stress contours.

From the stress data in Attachment 3, the uphill side (the 80000 series nodes from the stress data) hoop stresses are the second highest in the ICI nozzle above the weld; the downhill side above the weld has higher hoop stresses, and these will be addressed in Section 4.2. Additionally, axial stresses used to evaluate circumferentially flaws were tabulated in Reference 6e and contained in Attachment 3. These stresses and the potential of circumferential flaws in the blind zone will be discussed in more detail in Section 3.5.

The nodal stress data from the DEI analyses are imported into the respective Mathcad worksheet (discussed later) for further processing to obtain the pertinent stress distributions required for the fracture mechanics analysis described in Section 3.2. Additional processing of the nodal stress data is described in Section 3.4.2.

3.2 ID Surface Flaw Fracture Mechanics Model

The model used to evaluate an ID surface flaw contained in the 0.88-inch Blind zone above the top of the weld is described in detail in Reference 7, and was originally presented in a NASA Publication, Reference 8. This model evaluates an axial, part through-wall flaw on the ID surface of a cylinder, subject to an arbitrary stress distribution (up to a cubic polynomial fit). This model is valid for a ratio of mean radius (R_{mean})-to-thickness (t) between 1.0 and 300. Since the ICI nozzle has R_m/t equal to 6.4, this model is considered applicable.

The fracture mechanics model [Ref. 8] gives the equation for the stress intensity factor (SIF) for both deepest point of the crack and the tip of the flaw along the surface, as follows:

$$K_I = \left(\frac{\pi}{Q} a \right)^{0.5} * \left(\sum_{i=0}^3 \sigma_i G_a \right) \quad \text{for the SIF at the deepest point of the flaw}$$

$$K_I = \left(\frac{\pi}{Q} c \right)^{0.5} * \left(\sum_{i=0}^3 \sigma_i G_{ci} \right) \quad \text{for the SIF at the tip of the flaw on the surface}$$

where:

K_I is the applied Stress Intensity Factor, or SIF $\{ ksi\sqrt{in} \}$

Q = Crack shape factor; defined as

$$Q = 1 + 1.464 \cdot \left(\frac{a}{c} \right)^{1.65} \quad \text{when } a/c \leq 1.0 \text{ and,}$$

$$Q = 1 + 1.464 \cdot \left(\frac{c}{a} \right)^{1.65} \quad \text{when } a/c > 1.0$$

a = Crack depth {inch}

c = Crack half flaw length {inch}

σ_i = Coefficients of the stress polynomial describing the hoop stress variation through the crack depth. Describes the power loading on the crack face.

$G_{a,i}$ = Stress Intensity Correction Factors (SICF) for the deepest point, which are provided in tables in Reference 8.

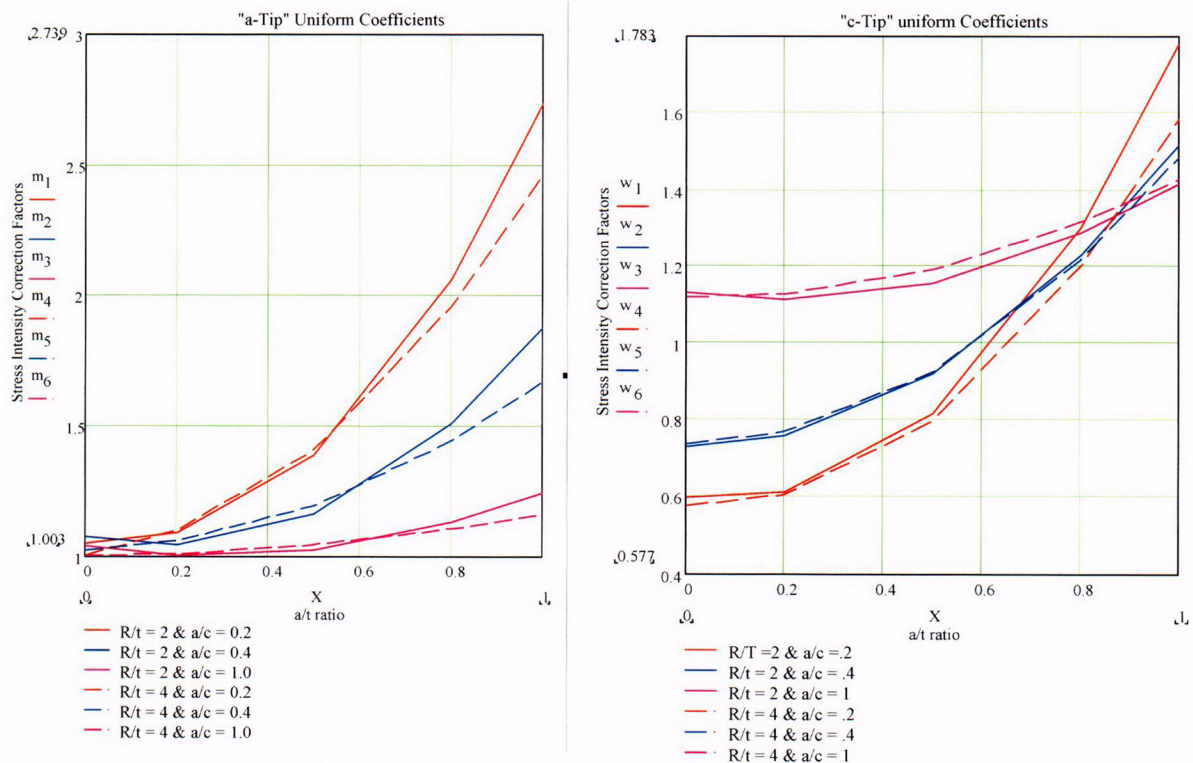
$G_{c,i}$ = Stress Intensity Correction Factors (SICF) for the surface tip, which are provided in tables in Reference 8.

In Reference 3, SICFs are presented for both the depth-point of the crack ("a-tip") and for the surface point of the crack ("c-tip"). Separate tables are provided for

internal (ID) and external (OD) surface cracks. In addition, the values are provided in association with the R_m/t ratio, a/c ratio (flaw aspect ratio), and a/t ratio (normalized crack depth). The SICF tables are large, and a suitable interpolation scheme is necessary to obtain proper coefficients dependent on crack size and shape for a given cylindrical geometry. Selected SICFs from the tables

for internal cracks for two different R_m/t ratios and a/c ratios are presented in Figure 7 below.

Figure 7: SICF shown as a function of normalized crack depth for the “a-tip” (left figure) and the “c-tip” (right figure). These figures show that simple linear interpolation would not provide accurate coefficients. These figures also show that a proper R_m/t is essential to provide a reasonably accurate estimate of the SIF



The figure above shows two features that are significant:

- 1.) The interpolation used to obtain the SICF must be carefully performed such that the value accurately represents the crack geometry. This is accommodated by selecting a suitable order for the curve-fitting polynomial prior to performing an interpolation to obtain the specific value. This aspect is discussed in further detail below;

- 2.) The correct R_m/t ratio is essential for obtaining a reasonably accurate estimate of the SIF. Using a higher ratio will tend to underestimate the SIF and hence under predict the crack growth.

Both these features have been considered in the development of the analysis model such that a reasonable, yet conservative, estimate of the SIF is obtained. This SIF is the critical input to determine the rate of PWSCC growth in the ICI nozzle. The growth model is discussed in Section 3.3.

3.3 PWSCC Growth Model

To evaluate the potential for crack growth due to PWSCC, the crack growth rate equation from EPRI Report MRP-55 [Ref. 9] was used. The crack growth rate as a function of the SIF with a correction for temperature effects is given as [Ref. 9]:

$$\frac{da}{dt} = \exp \left[-\frac{Q_g}{R} \left(\frac{1}{T} - \frac{1}{T_{ref}} \right) \right] \cdot \alpha \cdot (K - K_{th})^\beta$$

Where:

da/dt = crack growth rate at temperature T {meters/second}

Q_g = thermal activation energy for crack growth {31.0 kcal/mole}

R = universal gas constant { 1.103×10^{-3} kcal/mole-°R}

T = absolute operating temperature at crack tip {°R}

T_{ref} = absolute reference temperature for data normalization {1076.67 °R}

α = crack growth amplitude of 2.67×10^{-12}

K = crack tip SIF {MPa \sqrt{m} }

K_{th} = threshold SIF for crack growth {MPa \sqrt{m} }

β = exponent of 1.16

The above equation represents the seventy-fifth (75th) percentile curve. Since the PWSCC crack growth of interest is in the primary water, this model would provide a reasonably conservative crack growth.

3.4 Iterative Mathcad Model for Stress Curve-Fitting and Flaw Growth Evaluation

3.4.1 Mathcad Worksheet Format

The analytical scheme was developed using Mathcad [Ref. 10] which facilitates calculations (including recursive) in a logical manner. Reference 7, Appendix B, provides an annotated version of the ID surface crack worksheet used in the current analysis. In the paragraphs below the general approach used to develop the worksheet is presented. The three (3) parts of the Mathcad worksheet requiring user input is discussed in detail.

The first part of the Mathcad worksheet contains a section of imported FEA stress and elevation data for the ID, OD, and other locations through the thickness of the ICI nozzle. This section highlights the significant difference between the methodology used in Reference 7 for the CEDM nozzle evaluations and the current fracture mechanics evaluation for the counterbore region in the ICI nozzles: the “reversal” of the elevations obtained from the nodal stress and location data from DEI’s FEA models. For the CEDM nozzles, the reference point and “0”-elevation point is the bottom of the nozzle, since the bottom is level. For the ICI models, DEI indexed their data from the lowest part of the nozzle for each azimuth. For example, the ID corner on the uphill side represents the zero 0-elevation; due to the nozzle cut angle, the OD corner is at a higher elevation. DEI provided data for locations and stresses from the bottom to the top of the nozzle (as shown in Attachment 3). The CEDM evaluations and iterative loops considered a surface flaw in the nozzle below the weld growing axially upwards in the length direction. However, for a flaw in the counterbore region above the top of the weld in the ICI nozzles, due to the stress field being much higher axially down toward the weld, the flaw growth would be in the opposite direction. In order to avoid changes to the loop structure used for the CEDM analyses [Ref. 7] and definitions, the elevations referenced from the bottom of the ICI nozzle were modified to reference from the top of the nozzle as given in the FEA output data.

The second part of the worksheet requires the proper identification for the analysis being performed. In this region the component and the reference location in that component are identified. Immediately below the identification entry are the geometric landmark entries. For an ID surface crack, three entries are required and these are:

- 1.) The location of a reference line (for example, the Blind zone location) referenced to the top of the ICI nozzle from the FEA data (not the true top of the ICI nozzle from Reference 2a {**Ref_{Point}**}).

- 2.) The location of the crack with respect to the reference line (Upper crack tip at the reference line, center of crack at the reference line or lower crack tip at the reference line) {Val}
- 3.) The distance to the top of the weld, measured downward from the nozzle bottom {Elev_{Strs.Dist}}.

The third part of each Mathcad worksheet contains the inputs for crack dimensions, tube geometry, internal pressure, years of operation, iteration limit, operating temperature, constants for the PWSCC crack growth parameters, and the flaw geometry. It should be noted that the crack growth is performed using metric units; hence, those constants are required to be in metric units. The remainder of this sheet does not require user input. The

calculation shown is simple arithmetic to determine the values necessary for the analysis. The remaining parts of the Mathcad worksheet involving the regression of the stress data and the iterative analysis for flaw growth are discussed in Sections 3.4.2 and 3.4.3, respectively.

3.4.2 Regression Analysis of Axial and Through-Wall Stress Distributions

A regression analysis on the FEA stress data is required to obtain the appropriate stress distribution to be used in the determination of the SIF. Regression (that is, curve-fitting) of the stresses is needed because the SIF formulation is based on use of a uniform stress distribution along the length of the tube. However, the stress field in the nozzle above the weld, starting at the top of the nozzle where it intersects the reactor head, increases in magnitude as the top of the weld is approached. Consequently, if an assumed crack located in the vicinity of the reference line (in the blind zone) were to grow by PWSCC, it would be subjected to an increasing stress field. Thus, to use the stress distribution at the initial crack location would lead to an underestimate of the SIF, since the SIF is directly proportional to the applied stress. In order to obtain a reasonably representative SIF under the prevailing stress field variation, a moving average scheme was developed. This scheme is as follows:

- 1.) For the initial crack location, the stress distribution at the two crack tips (lower and upper) and the crack center are averaged to produce an average stress field that is applied to the crack. It is this stress distribution that is used to ascertain whether there exists a potential for PWSCC crack growth. This method is considered reasonable since it is similar to the superposition principle used in finite element-based SICF determination.
- 2.) The remaining portion of the nozzle extending from the lower crack tip to the top of the weld is divided into twenty (20) equal segments.

- 3.) The stress distribution in the first segment, below the lower crack tip, is an arithmetic average of the first three initial crack region distributions (the lower tip, center of crack and the upper tip) plus the distribution in the first segment. Thus, when the crack enters the first segment the magnitude of the stress distribution is appropriately increased to account for the increased applied stress. Similarly, as the crack progresses downward, out of the blind zone and toward the top of the weld through the various segments, the applied stress distribution is adjusted accordingly. The small extent of the length between the reference line and the top of the weld can be sufficiently accommodated by the twenty-segment characterization.

To accomplish this averaging scheme, the nodal stresses at the five (5) nodal locations through the nozzle thickness and the variation along the length of are individually regressed with a polynomial curve-fit. For the nodal stresses along the length of the nozzle, a fourth-order polynomial was used to fit the stresses in the region of interest (that is, the length of nozzle above the top of the flaw for some reasonable distance and the length below the bottom of the flaw, toward the top of the weld. The distance chosen for the axial curve-fit was evaluated for each set of stresses through the thickness to provide for precision in the area of interest and to avoid either under predicting or highly overshooting the stresses with the resulting polynomial. Reference 7 provides details on the importance of selecting a limited region for regression. Significant variation in stresses might produce errors in the determination of the SIF, which in turn could lead to an inaccurate estimate in crack growth. The regression is performed along the nozzle axis at each of the five (5) locations individually. The result of the regression provides the spatial coefficients required to describe the stress distribution. The nodal stress data representing the region of interest, from the top of the nozzle (elevation "0") to an elevation just below the top of the weld, is selected. In this manner, it is expected that proper representation of the stress distribution, pertinent to crack initiation and growth, can be accurately described. For the through-thickness stress distribution, a third-order polynomial was used to fit the stresses at each axial elevation. The results of the regression are contained in the Mathcad worksheets in Attachments 4 through 7. From these curves, it is evident that in the regions of interest, the fourth-order regression of the stresses along the length of the ICI nozzle provides an adequate representation of the stress distribution.

In the through-thickness regression, the nozzle thickness was assumed to be equal to the minimum section thickness to simplify application to the fracture mechanics iterative loop; that is, the nozzle below the counterbore with a minimum thickness (factoring in tolerances) of $[(5.563-0.001)-(4.750+0.010)]/2 = 0.401$ inch was used. To simplify the computations for the fracture mechanics loop, it was assumed that that thickness of the entire

nozzle above the weld was 0.401 inch. This is conservative, since the thickness above the counterbore (0.4635 inch), which is 13.5% thicker than the thinner section, has slightly lower stresses (owing to it being further removed from the highly stressed weld region) and a greater thickness through which a similarly sized flaw can propagate. Thus, the five (5) nodal stresses for the thicker section were assumed to be the equivalent nodal stresses for a thinner section in that region. As discussed previously,

the 1-to-4 taper on the counterbore is sufficient to not incur any stress concentrations in the model; furthermore, the residual stress effects in this region are muted, and the applied stresses from the operating pressure govern above the counterbore around the full circumference, as shown in Figure 5.

Following the determination of the five polynomial equations for the axial distribution of stresses, the through-wall stress distribution for the three locations defined by the crack and the twenty segments are established. The distributions at the twenty-three locations are subjected to a third order polynomial regression to obtain the coefficients describing the through-wall distributions. These coefficients are used within the recursive loop to assign the coefficients based on the current crack location. The five axial distributions are used for the ID surface crack.

3.4.3 Iterative Analysis to Determine Stress Intensity Correction Factors (SICFs)

For the ID surface crack, the SICF coefficients were incorporated in two data tables. The first table contains the geometry data (R_m/t , a/c and a/t) and the second table consists of the SICF data for the appropriate cylinder and crack geometry. The values for the data were obtained from Reference 8 and were subsequently used in Reference 7 for the CEDM nozzle flaw evaluation. The data contained in the two tables were regressed into function statements with an appropriate polynomial order. The data for cylindrical geometries with R_m/t ratios ranging from one (1) to four (4) were regressed with a third-order polynomial, and for those above four, a second-order polynomial was used. The selection of the polynomial order was based on matching the value in the table given, for a selected set of independent variables, with that obtained from the interpolation performed using the regressed coefficients. In this manner the accuracy of the regression-interpolation method was established. The interpolation equation was defined outside the recursive loop and function call was made inside the loop using the pertinent variables at the time of the call.

The recursive loop starts the calculation scheme to determine the crack growth for a specified time period under the prevailing conditions of applied stress. The first few statements are the initialization parameters. The calculation algorithm begins with the assignment of the through-wall stress

coefficients based on the current crack location. Once the four coefficients (uniform, linear, quadratic and cubic) are assigned, the through-wall stress distribution is used as the basis to establish the stress distribution along the crack face in the crack depth direction. That is, the stresses through the thickness are used to determine the stress along the crack face for application in the determination of the SIF in accordance with Reference 8. Once again, five locations along the crack depth were used to define the crack face distribution. The stresses representing the crack face values were regressed with a third-order polynomial to obtain the stress coefficients that would be used in the determination. At this point, the internal pressure is added to the SICF coefficient for the uniform term. Therefore, the crack face is subjected to an additional stress representing the internal pressure.

Following the determination of the stress coefficients, the function call to obtain the four SICF coefficients is made. In this case the two function calls were necessary to account for the "a-tip" and the "c-tip". The crack shape factor ("Q") was then computed using the appropriate crack dimensions. The SIF is calculated separately for the "a-tip" and the "c-tip" using the stress coefficients, appropriate SICFs and crack dimensions. The calculated SIFs were converted to metric units for the computation of crack growth. The crack growth rate, based on the prevailing SIF was computed in metric units. Once this was done, a conditional branch statement was used to calculate the crack growth within the prescribed time increment. The crack growth was computed in English units by converting the calculated crack growth rate in meters-per-second to inches-per-hour. Thus, the crack growth extent was obtained in inches for the specified time period. Since the operating time was selected to be forty (40) years and the number of iterations chosen at eight thousand (8000), the time increment for each crack growth block was approximately forty-four (44) hours. After the calculations were performed, all necessary information (crack growth, SIFs etc.) was assigned to an output variable such that it is stored in an array. The last step of the recursive loop consisted of updating the essential parameters (namely, the index, crack length, time increment etc.). This loop was annotated in Appendix B of Reference 7 to show the various steps.

Graphical displays of the results for flaw size in the depth direction, flaw growth in the length direction, the total flaw half length, and the SIFs for the number of operating years complete the work sheet. The Mathcad plots are used to determine whether or not the crack in the blind zone will grow through the thickness prior to extending beyond the blind zone and into an inspectable region. Tabular results of this analysis are shown in Table 3 of Section 4.0.

3.5 Consideration of a Circumferential Flaw in the Un-Inspectable Region

With the location of the blind zone above the top of the weld, the safety concerns of a circumferential flaw are significant. A circumferential flaw located on the ID surface, spanning the full 82° circumferential extent of the blind zone (from Figure 3), has the potential to grow through thickness and around the length of the ICI nozzle, thus creating an ejection mechanism leading to a loss of coolant accident. For this circumferential flaw growth to occur, both the PWSCC environment and a conducive tensile axial stress field must exist. The DEI axial stress FEA data in Attachment 3 were reviewed for locations at the uphill side and those angles spanning 45° on either side of the 180° azimuth (135° and 157.5°) that would encompass the circumferential extent of the blind zone.

From previous fracture mechanics evaluations for the CEDM nozzles (Reference 7), it was shown that no flaw growth will occur for an applied hoop stress of 10 ksi; that is, the resulting applied stress intensity factor is below the threshold value of $8.19 \text{ ksi} \sqrt{\text{in}}$ needed for flaw growth. With this premise applied to the axial stress distributions for growth of a circumferential flaw, Figures 8 and 9, below, show the axial stress distribution for the 135° to 225° azimuths.

Figure 8: ID Axial Stress Distribution Spanning 45° on Either Side (90° Total) of Uphill

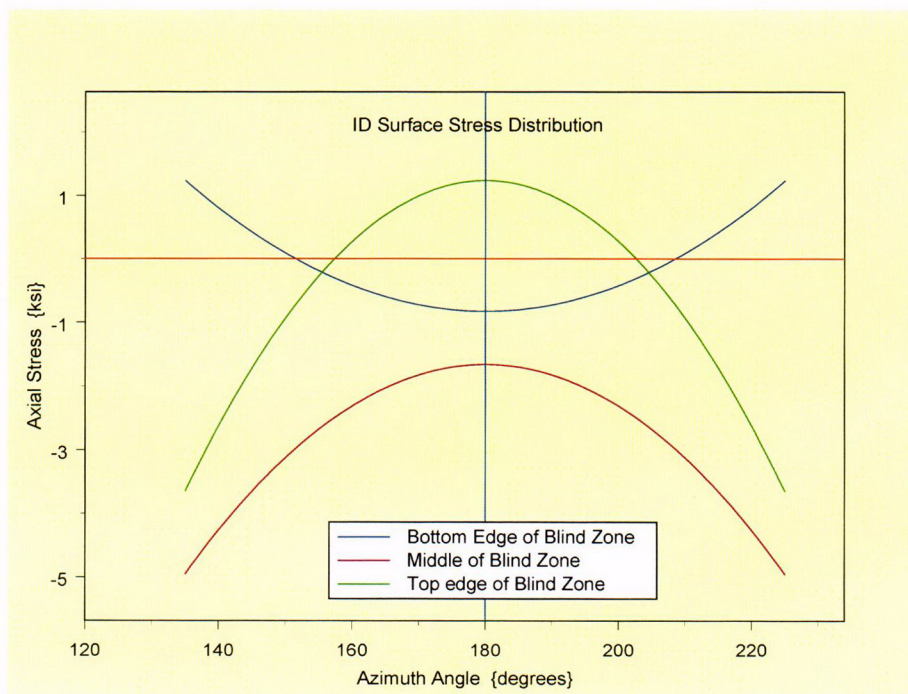
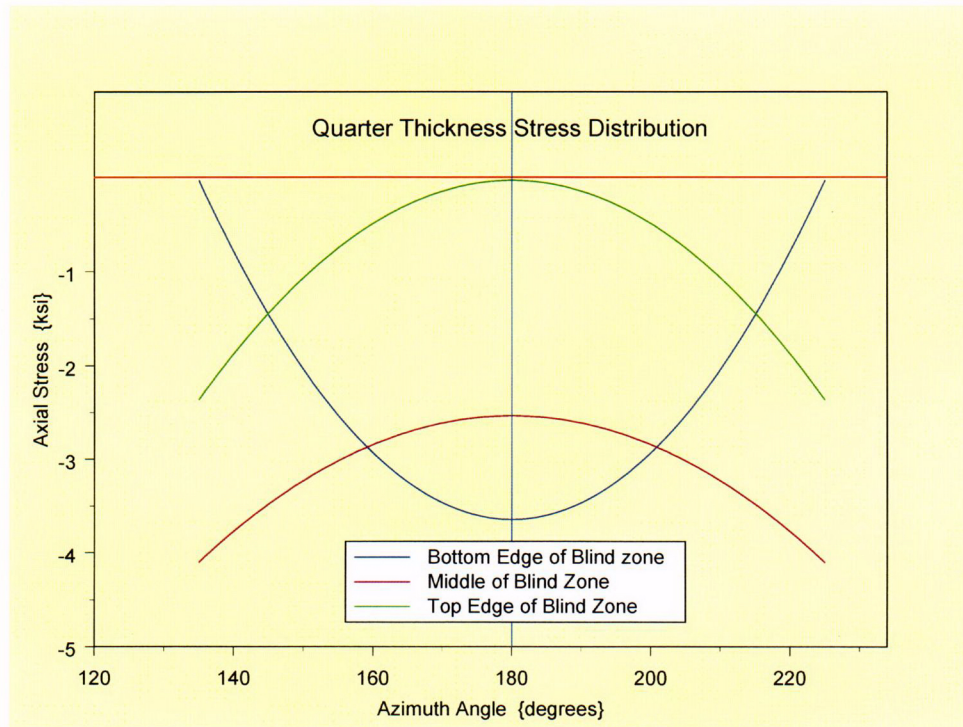


Figure 9: 25% Through-Wall Position Axial Stress Distribution Spanning 45° on Either Side (90° Total) of Uphill



From Figures 8 and 9, the stresses at the ID and at the 25% through-wall locations, covering a 90° circumferential span around the ICI nozzle, are predominantly compressive. Hence, the initiation of a circumferential flaw in the blind zone above the top of the weld on the uphill side (180° azimuth) is precluded, thus presenting no safety significance by not inspecting this region.

4.0 DISCUSSION AND RESULTS

4.1 Discussion

The goal of the inspection program designed for the reactor vessel head penetrations is to ensure that the postulated crack in the vicinity of the blind zone does not reach the weld or propagate through-wall during the upcoming operating cycle following the refueling outage when the inspections are performed. Safety analyses performed by the MRP have demonstrated that axial cracks in the nozzle tube material do not pose a challenge to the structural integrity of the nozzle. Axial cracks, if allowed to exist undetected for sufficient periods of time can produce a primary boundary leak that can cause damage to the reactor vessel head (carbon steel) and create a conducive environment for initiating and propagating OD circumferential cracks. These conditions challenge the pressure boundary; hence, critical importance is paid to proper periodic inspection and to the disposition of cracks that may be discovered. Therefore, proper analyses are essential to ascertain the nature of axial crack growth such that appropriate determination can be accomplished.

The analyses performed in this report were designed to capture the behavior of postulated ID part through-wall flaws that might exist in the blind zone region of the ICI nozzle, above the top of the weld, in the vicinity of the counterbore, on the uphill side. These would tend to grow along the tube ID, into the high stress field at the top of the weld, and through the thickness above the top of the weld.

The design review of the reactor vessel head construction, the detailed residual stress analyses, selection of representative fracture mechanics models, and the application of a suitable crack growth law has provided the bases for arriving at a comprehensive and prudent decision.

The axial crack geometry is selected for evaluation because this crack has the potential for propagation into the pressure boundary weld (the J-groove weld and the ICI nozzle). At all locations above the weld, the ID and the interior are in tension. The OD of the nozzle experiences slight compression in the counterbore transition region and low tension just below this region before ramping to a high tensile stress field at the top of the weld; this is due to the complex, three-dimensional ovalization of the ICI nozzle resulting from the welding process.

The fracture mechanics evaluation considered the crack face to be subjected to the operating reactor coolant system (RCS) pressure. This is accomplished by arithmetically adding the RCS pressure to the uniform stress coefficient in the ID surface crack. In this manner, the stress imposed on the crack is accurately and conservatively modeled. The moving average technique was previously verified in Appendix D of Reference 7 to be an accurate yet conservative depiction of stress application to the crack face. In this evaluation, the axial distribution of the stresses along the axis was kept constant. In this manner, the moving average method should provide results that have the same distribution at all locations along the tube axis.

This implies the through-wall distribution is invariant along the length of the tube. The results of the analysis showed that the stress distribution across the wall remained unchanged along the axis of the tube. Therefore, the moving stress averaging method is validated for the ID surface crack model.

4.2 Results of the ID Surface Flaw Evaluation

Several flaw sizes were evaluated in the blind zone region above the weld on the uphill side. Flaw aspect ratios typical of ASME Section XI (6-to-1 and 10-to-1 on length-to-depth) and another emphasizing deep flaws (4-to-1 aspect ratio) were evaluated that sought to maximize growth through-wall while accommodating growth along the length of the ICI nozzle. These evaluations also considered a case where the half length ("c") of the flaw was less than the remaining length needed to grow to the end of the blind zone. Additionally, for those low aspect ratios (4-to-1 and 6-to-1), a conservative depth of 25% of the wall thickness (0.100 inch) was assumed. With this depth, a flaw need only propagate 0.3 inch through the thickness to reach through-wall, whereas the flaw along the length must extend 0.4 inch (measured from the tip of the flaw on the ID surface to the edge of the blind zone, plus an additional 0.16 inch in order to become detectable). Table 2 below shows the assumed flaw sizes based on these aspect ratios.

Table 2: Summary of flaw depths and lengths used to evaluate the blind zone on the uphill side above the top of the weld (Blind zone begins a distance 1.08 inches above the top of the weld and extends 0.88 inch)

Flaw Case ID	Description	Flaw Depth (in.)	Flaw length (in.)
1	Aspect ratio of 6-to-1 with depth initially 25% through-wall	0.1	0.6
2	Aspect ratio of 10-to-1 with an initial length of 0.4 inch	0.04	0.4
3	Aspect ratio of 4-to-1 with depth initially 25% through-wall	0.1	0.4
4	Flaw spanning the length of the Blind zone with 6-to-1 aspect ratio	0.147	0.88

In the PWSCC flaw growth evaluation, the acceptability of the flaw is determined by its extension outside of the blind zone region, to a detectable length, prior to growing through the thickness, with at least one fuel cycle (1.5 years) between the length and depth growths reaching these values. From Reference 11, the minimum detectable length of a flaw was 2 mm (0.08 inch), with all flaws in the EPRI demonstration between 2 mm and 4 mm (0.16 inch) being detected. Thus, the detectability threshold in the Mathcad worksheets in Attachments 4 through 7 was set to 0.16 inch(or 4 mm). That is, a flaw contained within the 0.88-inch Blind zone must

propagate along the length of the nozzle a distance measured from the tip of the flaw to the edge of the blind zone (mathematically, this is $BZ_length/2 - c_0$, where BZ_length is the blind zone length and c_0 is the initial half flaw length), plus an additional axial distance of 0.16 to ensure proper detection. This length is defined as the Propagation Length, **Prop_Length**, in the Mathcad worksheets shown in Attachments 4 through 7. At the same time, the growth through the thickness is limited to reaching through-wall from the initial depth, a_0 . Table 3 below provides the results of the flaw growth evaluation for each of the four (4) flaw cases given in Table 2. The detailed Mathcad worksheets are contained in Attachments 4 through 7.

Table 3: Results of PWSCC flaw growth evaluations in the length and depth directions.

Flaw Case ID	Prop_Length {in.} ($BZ_length/2 - c_0 + 0.16$ in.)	Time to reach Prop_Length (years)	Time to go Through-wall (in.)
1	0.3	10.94	13.74
2	0.4	> 40	> 40
3	0.4	20.98	23.34
4	0.16	3.83	6.99

These results suggest that a sufficiently deep flaw in the 0.88-inch blind zone above the top of the weld on the uphill side (180° azimuth) would grow to a detectable length at least one fuel cycle (1.5 years) prior to growing through-wall. Graphical details of the depth and length flaw growth are shown in Figures 10 through 13.

Figure 10: Flaw Case 1—Depth Growth (top) and Length Growth (bottom) versus number of operating years. For Flaw Case 1, the growth through-wall occurs in 13.74 years. The length growth into an inspectable region occurs in 10.94 years.

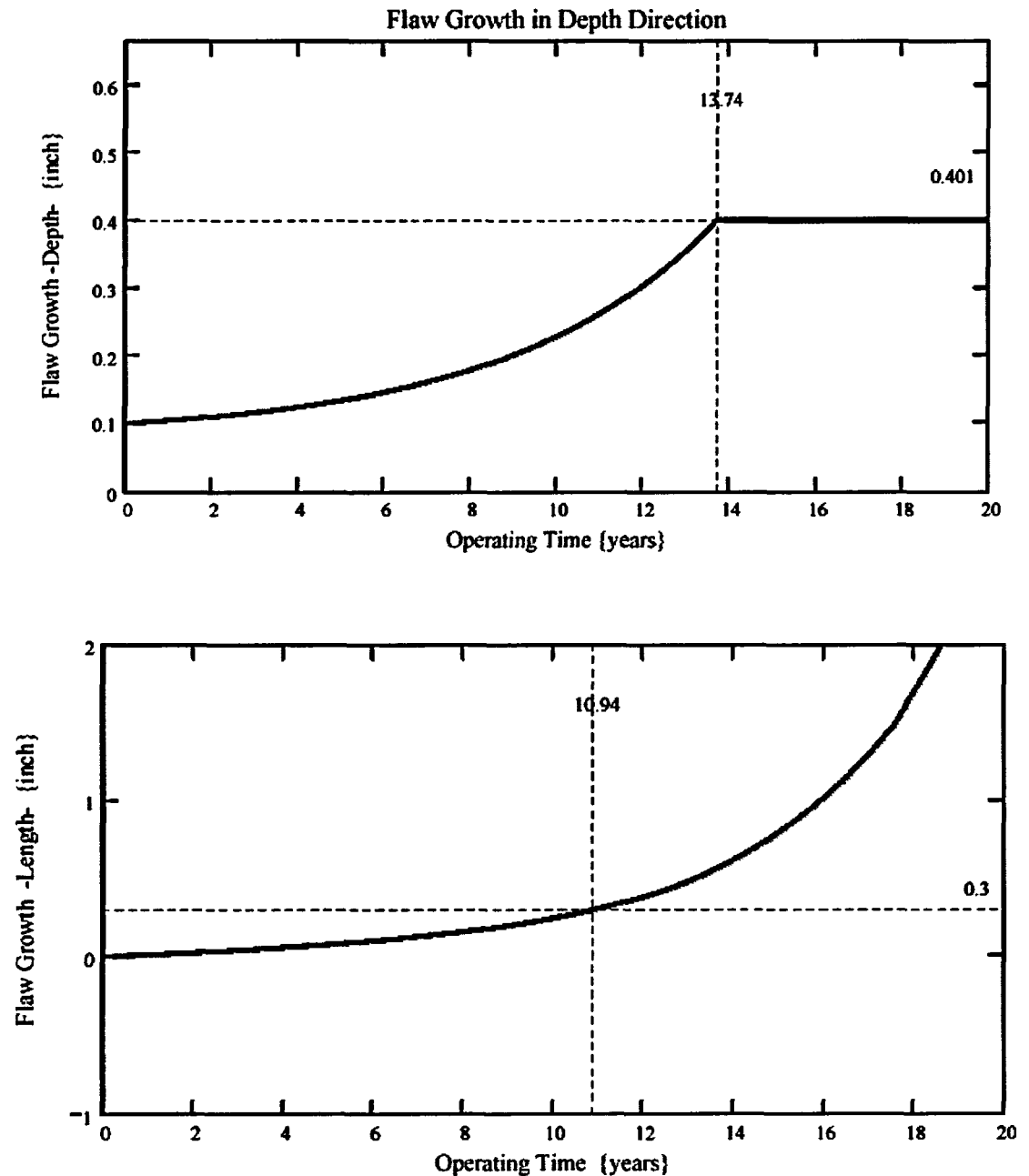


Figure 11: Flaw Case 2—Depth Growth (top) and Length Growth (bottom) versus number of operating years. For Flaw Case 2, no growth in either the depth or length direction occurs within 40 years.

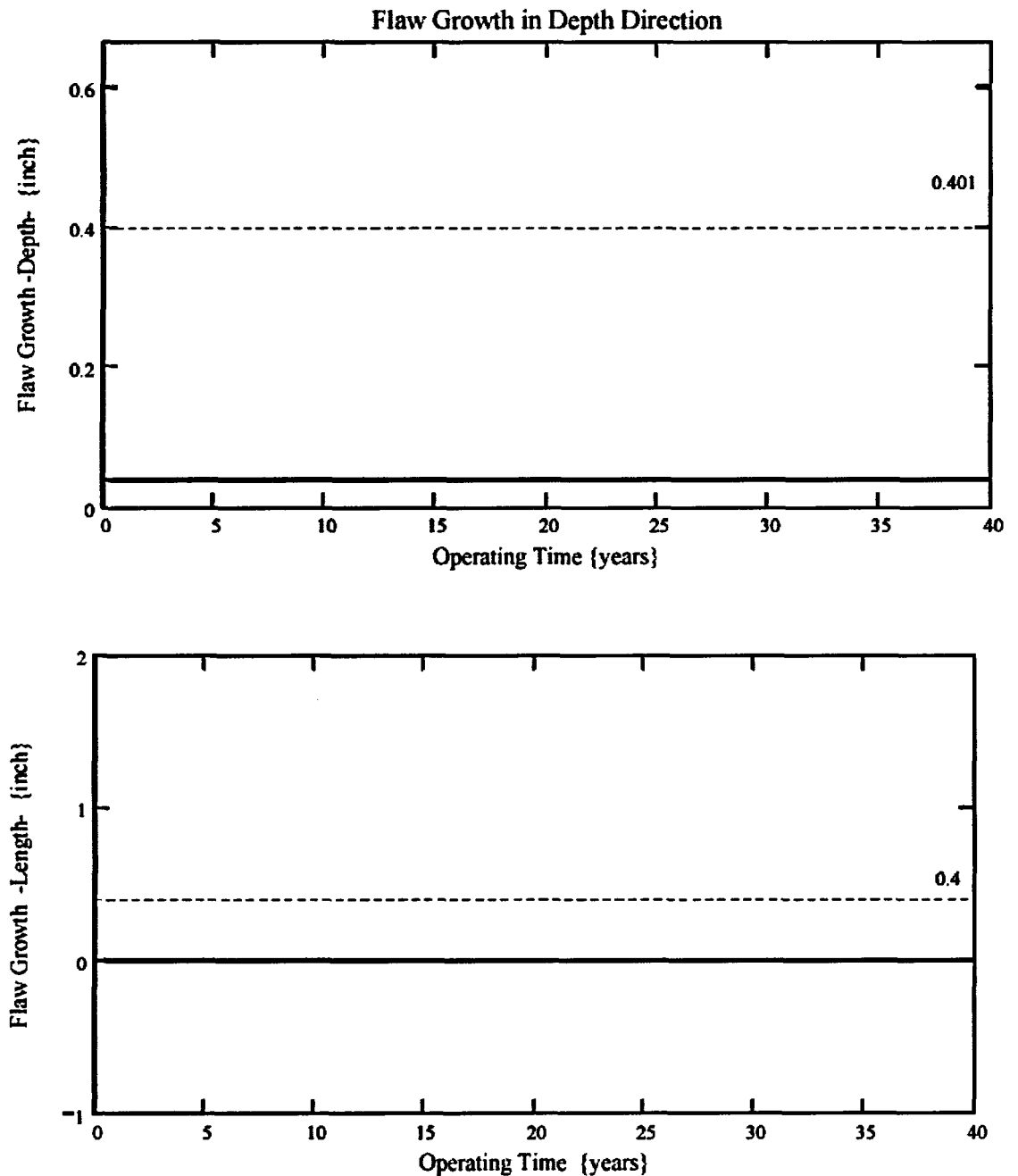


Figure 12: Flaw Case 3—Depth Growth (top) and Length Growth (bottom) versus number of operating years. For Flaw Case 3, the growth through-wall occurs in 23.34 years. The length growth into an inspectable region occurs in 20.98 years.

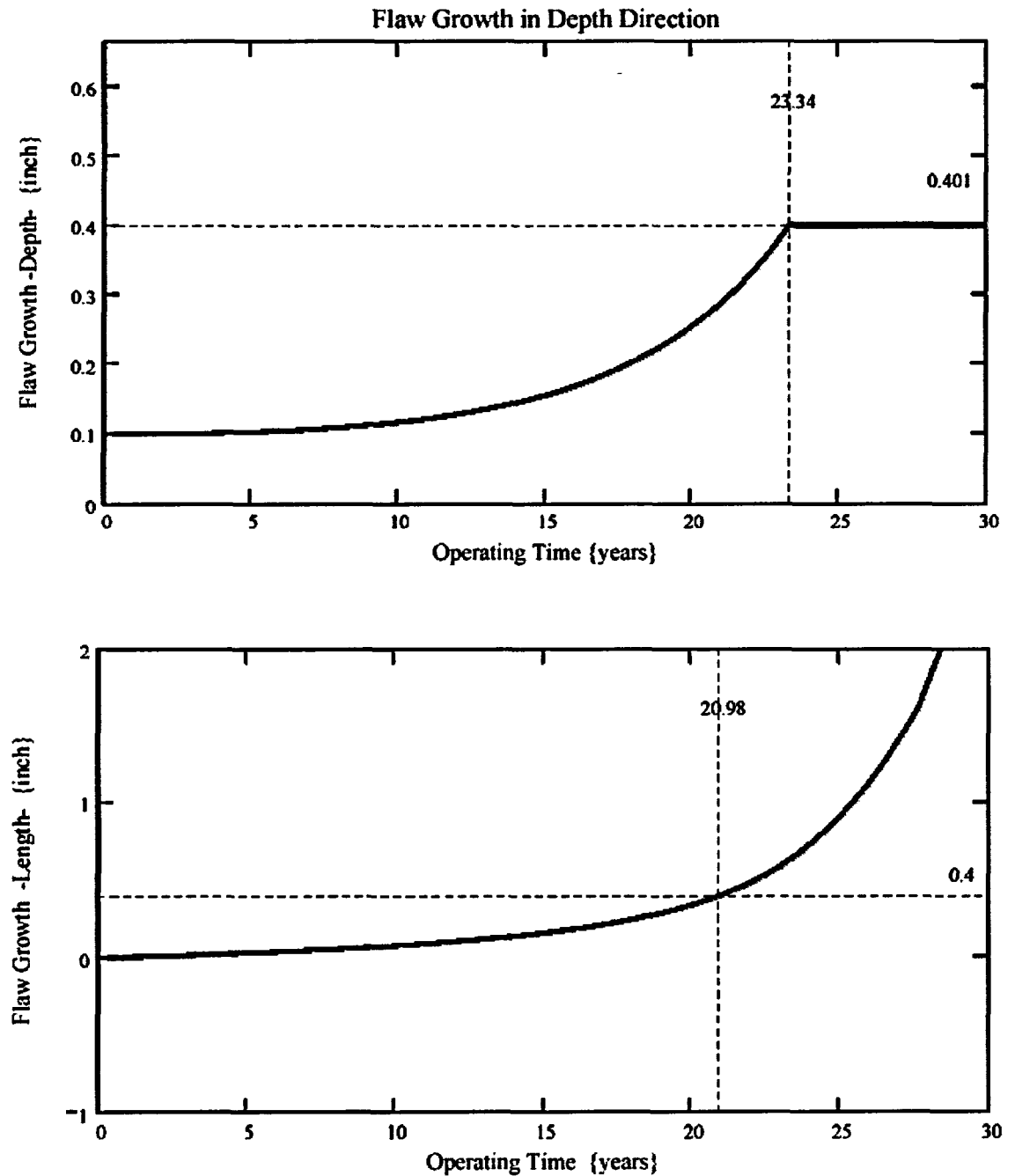
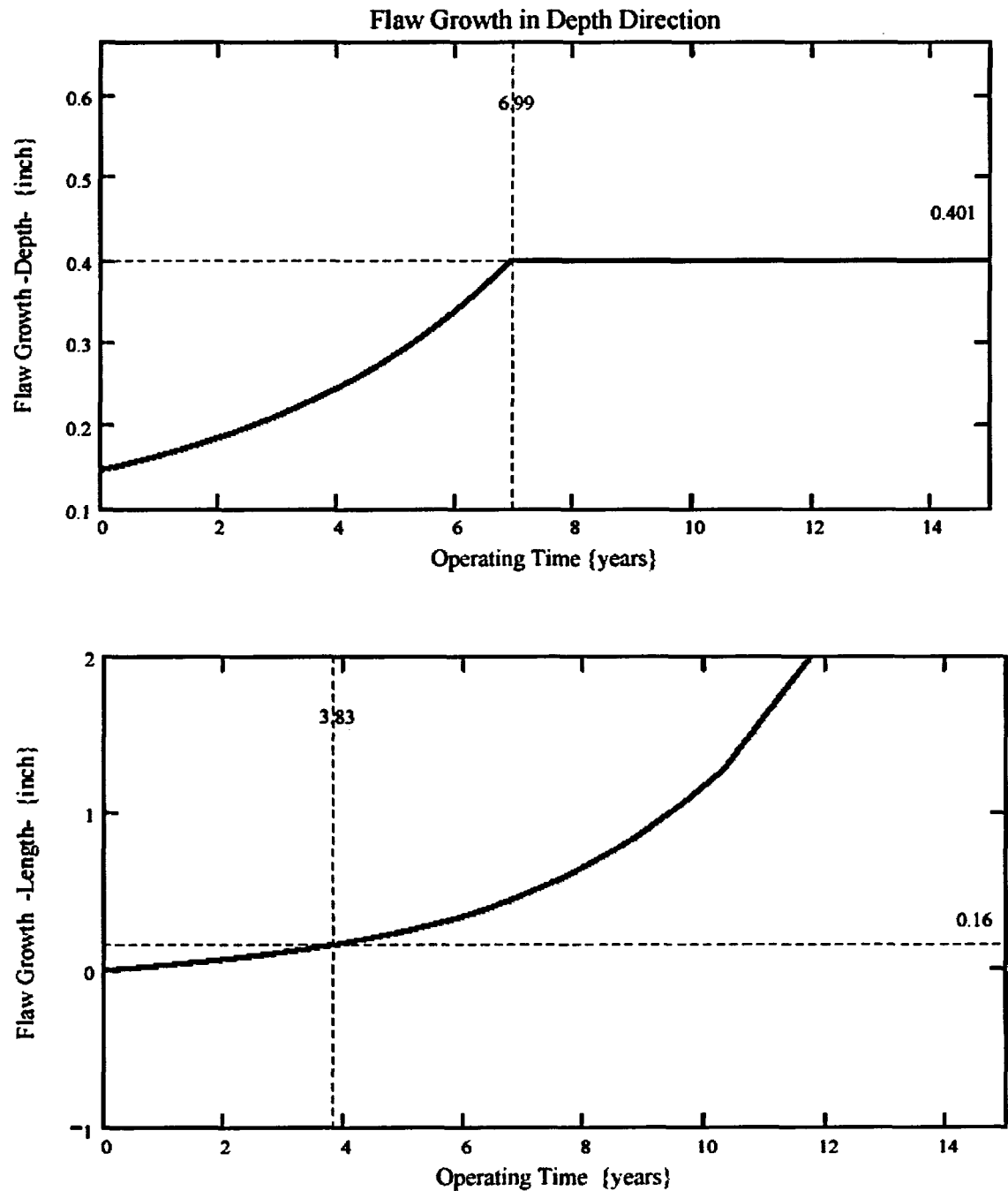


Figure 13: Flaw Case 4—Depth Growth (top) and Length Growth (bottom) versus number of operating years. For Flaw Case 4, the growth through-wall occurs in 6.99 years. The length growth into an inspectable region occurs in 3.83 years.



A review of DEI's FEA stress output shows the through thickness and axial distribution of hoop stresses on the downhill side (0° azimuth) of the nozzle to be higher than that for the uphill side for the same relative distance above the weld. That is, for the length of the nozzle 1.08 inches above the top of the weld on the downhill side, plus a region 0.88 inch beyond that (equivalent to the span of the blind zone on the uphill side), the stress distribution was similar in through-wall behavior but generally higher in magnitude. The counterbore region on the downhill side, however, is 9.96 inches above the top of the weld and not subject to the requirements of the Order. Because of the higher stress field, it is reasonable to presume that under equivalent conditions, a flaw could initiate in this equivalent downhill side area more readily than on the uphill side. However, this region is inspected via UT; thus, the most susceptible location based on stresses is addressed by the current inspection coverage.

5.0 CONCLUSIONS

The evaluation performed and presented in the preceding sections support the following conclusions:

- 1) The uphill side (180° azimuth) of the ICI nozzle above the top of the weld possesses the highest (hoop) stresses in the vicinity of the counterbore for which a UT blind zone exists.
- 2) The developed fracture mechanics model, incorporating a method to account for applied stress distribution variation along the ICI nozzle length, has been shown to be a reasonably realistic yet conservative representation of the expected crack growth and morphology.
- 3) The conservatisms used in the analysis (pressure applied to crack faces and high flaw length-to-depth aspect ratio) provide assurance that an undetected crack in the 0.88-inch Blind zone region above the top of the weld on the uphill side (180° azimuth) will extend out of the blind zone and into an inspectable region at least one operating cycle prior to growth through the thickness.
- 4) Though the downhill side (0° azimuth) of the ICI nozzle at an equivalent distance above the top of the weld is in a higher stress field and more susceptible to crack initiation, it is inspected by UT.
- 5) The ID surface crack on the uphill side either did not show any potential for crack growth, or the crack growth in the axial direction reached a detectable area at least one operating cycle prior to the crack growing through-wall. Hence, an ID surface crack in a region above the weld on the uphill side is not significant.
- 6) No potential exists for an ID circumferential crack to be located in the 82° circumferential extent of the blind zone due to the predominant compressive axial stress field spanning 45° on either side of the uphill side (180° azimuth) of the ICI nozzle.

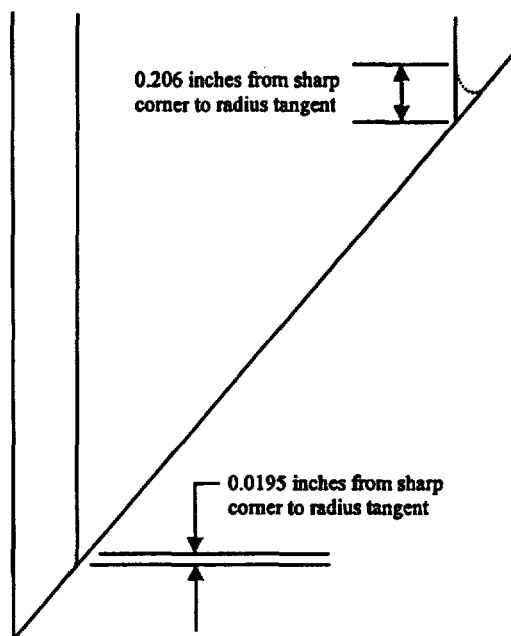
6.0 REFERENCES

- 1) NRC Order; Issued by letter EA-03-009 addressed to "Holders of Licenses for Operating Pressurized Water Reactors"; dated February 11, 2003.
- 2) a.) ANO Drawing No. M-2001-C2-24 (DRN 03-1315), "Closure Head Instrument Nozzle Details"
b.) ANO Drawing No. M-2001-C2-107-3, "Closure Head Nozzle Requirements"
- 3) ANO Calculation No. 86-E-0036-39 "Analytical Report for Arkansas Nuclear One – Unit 2 Reactor Vessel"; prepared by Combustion Engineering, Inc.; dated August 1974.
- 4) ANO Calculation No. 02-E-0003-01, Rev. 0, "Time at Temperature Assessment for ANO-2 RV Head Nozzles Revised for Power Uprate"; dated 2/28/02.
- 5) ASME Boiler and Pressure Vessel Code, Section III NB, 1992 Edition.
- 6) a) "PWSCC of Alloy 600 Materials in PWR Primary System Penetrations"; EPRI TR-103696; Electric Power Research Institute, Palo Alto, CA; July 1994.
b) "BWR Vessel and Internals Project – Evaluation of crack growth in BWR Stainless Steel RPV Internals (BWRVIP-14)"; EPRI TR-105873; Electric Power Research Institute, Palo Alto, CA; March 1996.
c) "BWR Vessel and Internals Project – Evaluation of crack growth in BWR Nickel Base Austenitic Alloys in RPV Internals (BWRVIP-59)"; EPRI TR-108710; Electric Power Research Institute, Palo Alto, CA; December 1998.
d) Dominion Engineering Inc. e-mails E-4162-00-4, E-4162-00-5, and E-4162-00-6 containing the nodal stress and coordinate data for ANO-2 ICI Analysis; J. Broussard and S. Ahnert (DEI) to B. Gray (Entergy); dated August 25 & 26, 2003.
e) Dominion Engineering Inc. e-mail E-4162-00-9 containing axial stress and elevation data for all node locations above the top of the weld; J. Broussard (DEI) to B. Gray (Entergy); dated September 3, 2003.
- 7) Entergy Nuclear South/Central Engineering Programs Engineering Report No. M-EP-2003-002, Rev. 01, "Fracture Mechanics Analysis for the Assessment of the Potential for Primary Water Stress Corrosion Crack (PWSCC) Growth in the Un-Insepected Regions of the Control Element Drive Mechanism (CEDM) Nozzles at Arkansas Nuclear One Unit 2"; dated August 26, 2003. [Previously sent to the NRC Under Relaxation Request transmittal CNRO-2003-00033, dated August 25, 2003.]
- 8) "Stress Intensity Factors for Part-Through Surface Cracks in Hollow Cylinders": S. R. Mettu et al; NASA TM-111707; Prepared by Lockheed Engineering & Science Services; Houston, Texas; July 1992.
- 9) "Materials reliability Program (MRP) Crack Growth Rates for Evaluating Primary Water Stress Corrosion cracking (PWSCC) of Thick Wall Alloy 600 Material": MRP-55, Revision 1; Electric Power Research Institute (EPRI); dated November 13, 2002.

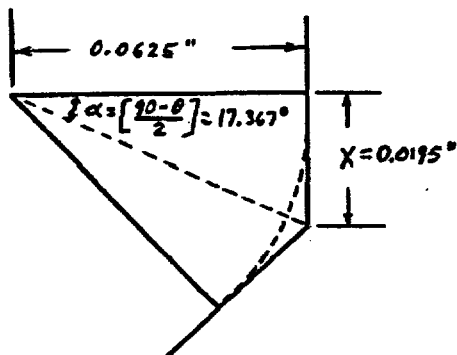
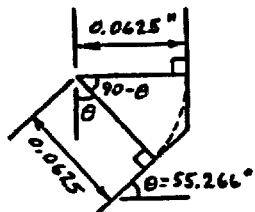
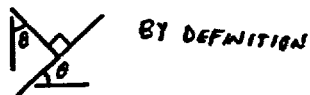
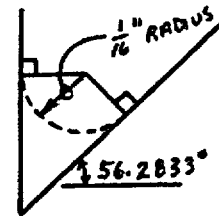
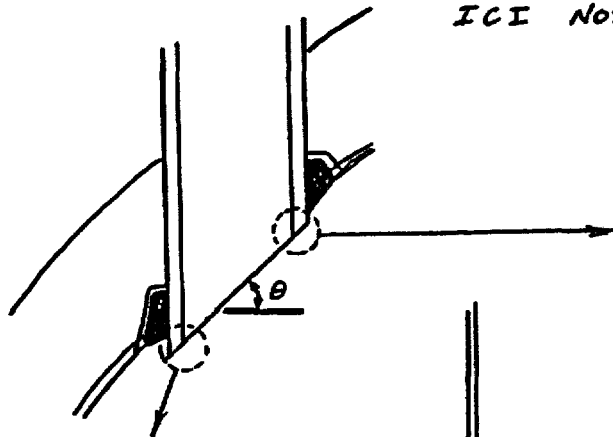
- 10) Mathcad – 11; Data Analysis Products Division; Mathsoft Inc.; Seattle WA; November 2002.
- 11) EPRI NDE Demonstration Report; “MRP Inspection Demonstration Program – Wesdyne Qualification”: Transmitted by e-mail from B. Rassler (EPRI) to K. C. Panther (Entergy); Dated 3/27/2003.

Page <u>1</u> of <u>1</u>	
Design Input Revision <u>0</u>	
<u>DESIGN INPUT RECORD</u>	
Document Type: _____	
Document Number: _____	Document Revision: _____
Design Objective: (Attach additional sheets as required)	
<p>The purpose of this Design Input Record is to establish the applicable design inputs associated with the In-Core Instrument (ICI) nozzle configurations at ANO-2 and Waterford-3. This information will be used as input to fracture mechanics evaluations being prepared in accordance with ASME Section XI, part IWB-3600 to evaluate flaw propagation associated with potential future nozzle repairs due to PWSCC cracking in Alloy 600 material.</p>	
Design Inputs: (Identify requirement and how it is applied. Ref. DC-141, Sec. 5.1.2)	
See attached sheets	
Contributing Disciplines:	
NOTE 1	
Mechanical	_____
I & C	_____
Electrical	_____
Civil	_____
Piping	_____
Structures	_____
Engineering programs	_____
Other	_____
NOTE 1: The contributing discipline engineer shall provide his/her name beside the appropriate block.	
-Lead Discipline Mechanical	
-Prepared by (DA) Jamie GoBell	Date 07/21/03
Lead Design/Responsible Engineer <u>JAI BRINHADESAM</u>	Date _____
Lead Discipline Reviewer Nara Ray	Date 7-24-03
-Lead Discipline Supervisor William Sims	Date 7-30-03

The NDE limitations for the ICI nozzles are provided relative to the point at which the blend radius begins on the inside surface of the bottom of the nozzle. The dimensions provided for the head cladding surface to the bottom of the ICI nozzle are provided relative to the "sharp corner" points before the points are blended to a 1/16 inch radius. To define the NDE limitations, the vertical distance from the "sharp corner" points up to the tangent point of the blend radius with the vertical face of the nozzle have to be considered. The sketch below shows those dimensions for the zero and 180 degree azimuth positions on the nozzle. At the 90 and 270 degree azimuth positions, the dimension is 1/16 inch. The calculations of the values in the figure below are shown on the following page. It should be noted that on the low hill side, the smaller cutoff angle from the Waterford 3 ICI nozzle configuration was more conservative and was used, and on the upper hill side, the larger cutoff angle from the ANO-2 ICI nozzle configuration was more conservative and was used.

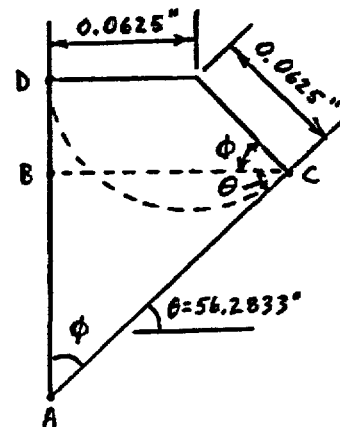


ICI NOZZLE



$$X = 0.0625" \tan 17.367^\circ$$

$$X = 0.0195"$$



$$\phi = 90 - \theta = 33.7167^\circ$$

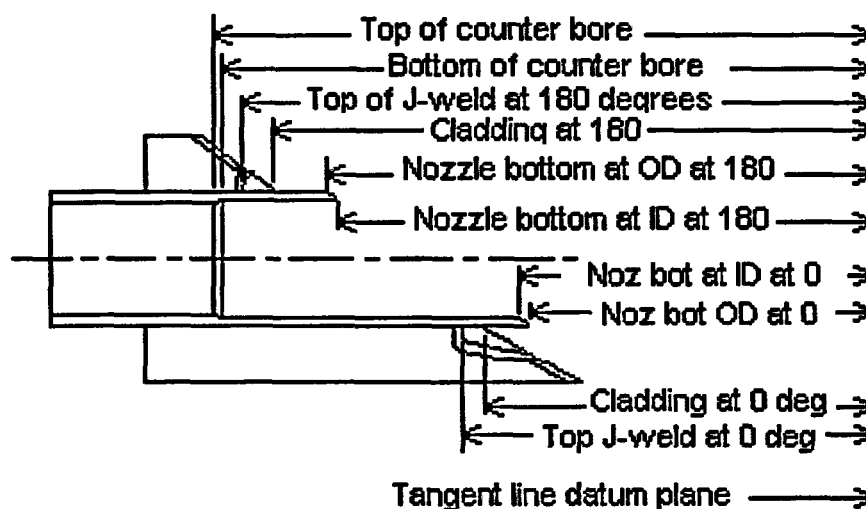
$$\overline{BC} = 0.0625" + 0.0625 \cos \phi = 0.1145"$$

$$\overline{BD} = 0.0625 \sin \phi = 0.0347"$$

$$\overline{AB} = \overline{BC} / \tan \phi = 0.1715"$$

$$\overline{AD} = \overline{AB} + \overline{BD} = 0.2062"$$

The dimensions of the ICI nozzles relative to the J-groove welds and cladding surface inside the head were calculated relative to the "tangent line" that defines the radius of curvature of the head. These dimensional references are depicted in the sketch below.



Because there is a slight variation in the location of the ICI nozzles at Waterford 3 relative to the centerline of the head, there is a very slight variation in the values calculated from nozzle to nozzle. Because the variation is very small, only one set of values is reported in the tabulated data. If desired, the specific values for a specific nozzle can be extracted from the Excel spreadsheet that calculated the values. The values for ANO-2 and Waterford 3 were calculated using Excel spreadsheets, and the results are summarized in the table below.

Dimension from the tangent line datum plane to:	ANO-2 (inches)	W-3 (inches)
Top of counter bore transition	48.625	55.094
Bottom of counter bore transition	48.375	54.844
Top of J-weld at the 180 degree (high hill side) azimuth location	46.998	53.440
Intersection of the projected cladding surface and the nozzle OD at the 180 degree (high hill side) azimuth location	46.211	52.655
Bottom (sharp corner) of the nozzle at the OD surface at the 180 degree (high hill side) azimuth location	44.211	50.618
Bottom (sharp corner) of the nozzle at the ID surface at the 180 degree (high hill side) azimuth location	43.602	50.031
Top of J-weld at the 0 degree (low hill side) azimuth location	38.283	45.008
Intersection of the projected cladding surface and the nozzle OD at the 0 degree (low hill side) azimuth location	37.875	44.589
Bottom (sharp corner) of the nozzle at the ID surface at the 0 degree (low hill side) azimuth location	36.484	43.180
Bottom (sharp corner) of the nozzle at the OD surface at the 0 degree (low hill side) azimuth location	35.875	42.594

Page 1 of 2
Design Input Revision 0

DESIGN INPUT RECORD

Document Type: N/A
Document Number: N/A Document Revision: N/A

Design Objective: (Attach additional sheets as required)

The following dimensions of the ultrasonic (UT) examination blind zone associated with the counterbore region at the 180° high hillside location of the incore instrumentation (ICI) nozzles at ANO-2 were obtained based on a review of UT data obtained during 2R15 for 7 of 8 ICI nozzles. These dimensions represent worst case measurements.

Dimension from Top of J-weld to Bottom of Counterbore Blind Zone: 1.080"

Axial Length of UT Blind Zone: 0.880"

Arc Length or Circumferential Extent of Counterbore Blind Zone: 82°

Attached to this coversheet is a sketch which identifies the UT "blind zone" of the counterbore region at the 180° high hillside location of the ICI nozzles at ANO-2. The sketch provided is only meant to aid in visualizing the location of the blind zone, and is not meant to be taken as an accurate depiction of the nozzle configuration. The sketch is not to scale.

Design Inputs: (Identify requirement and how it is applied. Ref. DC-141, Sec. 5.1.2)
(See attached sheets, drawings, and photographs)

Contributing Disciplines:
NOTE 1

Mechanical	N/A	N/A
I & C	N/A	N/A
Electrical	N/A	N/A
Civil	N/A	N/A
Piping	N/A	N/A
Structures	N/A	N/A
Engineering programs	N/A	N/A
Other	N/A	N/A

NOTE 1: The contributing discipline engineer shall provide his/her name beside the appropriate block.

-Lead Discipline Mechanical

-Prepared by (DA) Ronnie Swain (Entergy Level III)

Lead Design/Responsible Engineer

Lead Discipline Reviewer

-Lead Discipline Supervisor

*For telecon on 9-3-03, 1200 hrs,
Jack Weeks for Ronnie Swain*

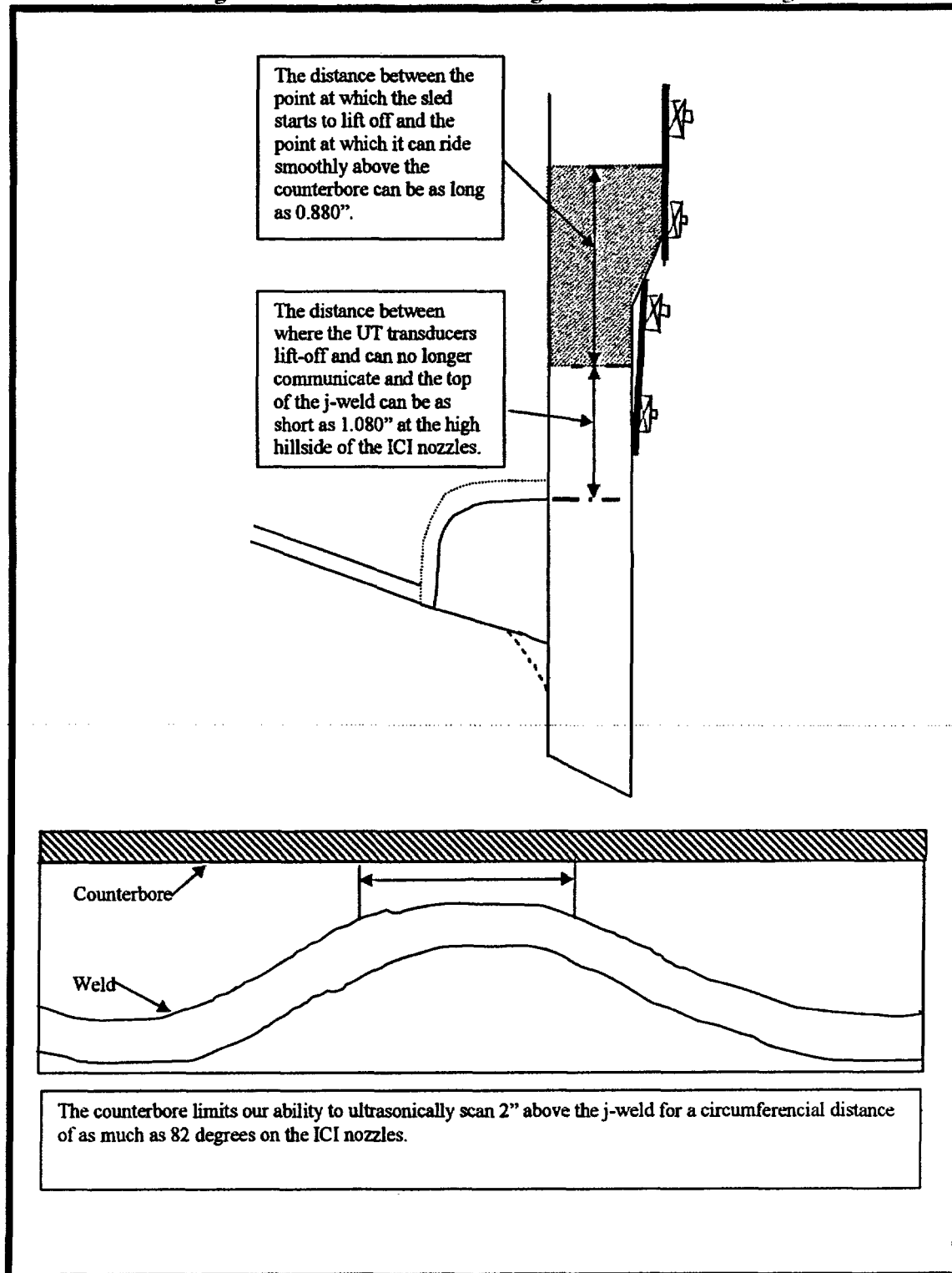
Date	<u>9-3-03</u>
Date	<u>N/A</u>
Date	<u>N/A</u>
Date	<u>N/A</u>

COUNTERBORE AT HIGH HILLSIDE POSITION

UT blind zone starting point = 1.080" above top of weld

Axial length of UT blind zone = 0.880"

Arc length of limitation for 2" scanning above the weld = 82 degrees



GRAY, BRIAN C

From: Stephen Ahnert [sahnert@domeng.com]
Sent: Monday, August 25, 2003 1:18 PM
To: GRAY, BRIAN C
Subject: E-4162-00-4 ANO2 ICI Results Above Weld



ANO2ICIC.ICIdata
post.results.t...



ICI Uphill Hoop
Stress Plot.pd...

Brian-

Attached are the ANO2 ICI hoop stress results, reported in the nozzle coordinate system, for the uphill half of the nozzle (40,000's - 80,000's planes) above the top of the weld. The axial heights shown in the attachment are measured from the lowest point on the tube at the node's circumferential plane (e.g. node 71403's axial height is measured from node 70001).

Since the ICI nozzle model includes an ID counterbore, the wall thickness is not constant along the nozzle axis. Furthermore, because of the angle of the element mesh, the ID transition does not occur between the same two nodes at every circumferential plane. For the 5 planes included in this transmittal, the ID transition occurs between the following nodes.

40,000's plane	41901 - 42001
50,000's plane	51801 - 51901
60,000's plane	61701 - 61801
70,000's plane	71601 - 71701
80,000's plane	81601 - 81701

Below the transition, the inner radius is 2.375", while above the transition, the radius shrinks to 2.3125". Between the nodes, the radius shrinks linearly. I've also attached a plot focusing on the uphill portion of the nozzle above the weld.

If you have any questions or comments, please do not hesitate to contact me or John at 703-437-1155.

Sincerely,
Stephen Ahnert

ANO2ICIC
40000's Plane (90 degrees from downhill)

Hoop Stresses		% Through Wall			
NODE	ID	25	50	75	OD
41401.	16446.	15541.	13421.	12339.	12594.
41501.	14314.	13452.	11688.	10418.	10601.
41601.	8445.	9350.	9998.	11033.	13072.
41701.	1075.	5098.	8684.	12018.	14641.
41801.	1335.	5111.	9178.	12550.	14555.
41901.	3151.	6164.	9256.	12135.	13611.
42001.	1484.	5279.	8515.	11674.	14273.
42101.	3802.	6228.	8417.	10542.	12607.
42201.	13096.	12072.	11966.	11842.	11007.

ANO2ICIC
50000's Plane (112.5 degrees from downhill)

Hoop Stresses		% Through Wall			
NODE	ID	25	50	75	OD
51401.	13439.	11150.	11288.	12991.	19269.
51501.	12560.	10399.	9501.	9540.	9172.
51601.	6466.	7661.	9531.	11608.	13143.
51701.	866.	4582.	8870.	12570.	14646.
51801.	906.	5050.	9540.	13377.	15336.
51901.	2748.	6200.	9745.	13166.	15292.
52001.	3543.	6551.	9276.	12078.	14330.
52101.	7325.	8780.	10127.	11427.	12628.
52201.	13142.	11794.	11231.	10665.	9629.

ANO2ICIC
60000's Plane (135 degrees from downhill)

Hoop Stresses		% Through Wall			
NODE	ID	25	50	75	OD
61401.	15760.	12973.	11684.	10977.	12678.
61501.	12143.	11320.	11164.	11425.	12767.
61601.	5816.	7062.	8246.	9521.	10482.
61701.	6278.	8097.	10246.	11831.	12131.
61801.	8396.	9921.	11212.	12104.	12473.
61901.	8947.	9990.	10471.	11176.	11617.
62001.	10693.	10537.	10595.	10597.	10475.
62101.	11570.	11146.	10777.	10457.	10165.
62201.	12332.	11207.	10505.	9847.	9088.

ANO2ICIC
70000's Plane (157.5 degrees from downhill)

Hoop Stresses		% Through Wall			
NODE	ID	25	50	75	OD
71401.	21920.	18904.	16819.	15479.	10386.
71501.	17603.	15506.	13062.	9850.	8222.
71601.	12704.	12514.	11586.	8619.	5497.
71701.	13761.	13841.	13644.	10194.	6625.
71801.	15399.	15288.	13268.	9179.	5658.
71901.	15955.	15242.	11918.	8363.	5274.

72001.	15901.	13994.	11179.	8633.	6165.
72101.	14346.	12527.	10824.	9449.	8173.
72201.	11030.	10495.	10124.	9793.	9527.

ANO2ICIC
80000's Plane (180 degrees from downhill)

Hoop Stresses		% Through Wall			
NODE	ID	25	50	75	OD
81401.	23147.	21559.	19292.	16085.	9729.
81501.	19425.	18188.	15780.	11381.	8207.
81601.	15065.	14581.	13132.	6189.	-109.
81701.	16707.	16175.	15560.	8890.	2754.
81801.	17399.	17177.	15044.	8136.	2316.
81901.	17412.	17487.	12883.	7180.	2298.
82001.	17115.	15794.	11377.	7821.	4387.
82101.	15304.	13024.	10766.	9067.	7453.
82201.	10308.	10119.	10032.	9951.	9936.

ANO2ICIC
Node Locations

		% Through Wall			
NODE	ID	25	50	75	OD
41401.	3.8310	3.8310	3.8310	3.8310	3.8310
41501.	4.3383	4.3383	4.3383	4.3383	4.3383
41601.	5.0383	5.0383	5.0383	5.0383	5.0383
41701.	6.0041	6.0041	6.0041	6.0041	6.0041
41801.	7.3368	7.3368	7.3368	7.3368	7.3368
41901.	8.6238	8.7618	8.8998	9.0378	9.1757
42001.	11.7131	11.7131	11.7131	11.7131	11.7131
42101.	15.2141	15.2141	15.2141	15.2141	15.2141
42201.	21.2702	21.2702	21.2702	21.2702	21.2702
51401.	4.0867	4.0867	4.0867	4.0867	4.0867
51501.	4.5620	4.5620	4.5620	4.5620	4.5620
51601.	5.2230	5.2230	5.2230	5.2230	5.2230
51701.	6.1423	6.2728	6.4034	6.5339	6.6645
51801.	7.3069	7.3354	7.3638	7.3923	7.4208
51901.	9.1989	9.1989	9.1989	9.1989	9.1989
52001.	11.6719	11.6719	11.6719	11.6719	11.6719
52101.	15.1113	15.1113	15.1113	15.1113	15.1113
52201.	19.9532	19.9532	19.9532	19.9532	19.9532
61401.	4.2688	4.2688	4.2688	4.2688	4.2688
61501.	4.7171	4.7171	4.7171	4.7171	4.7171
61601.	5.3452	5.3959	5.4466	5.4973	5.5480
61701.	6.1904	6.1992	6.2079	6.2167	6.2255
61801.	7.4589	7.4589	7.4589	7.4589	7.4589
61901.	9.1874	9.1874	9.1874	9.1874	9.1874
62001.	11.6096	11.6096	11.6096	11.6096	11.6096
62101.	15.0039	15.0039	15.0039	15.0039	15.0039
62201.	18.8368	18.8368	18.8368	18.8368	18.8368
71401.	4.3860	4.3860	4.3860	4.3860	4.3860
71501.	4.8127	4.8100	4.8074	4.8047	4.8020
71601.	5.4444	5.4370	5.4297	5.4223	5.4149
71701.	6.2649	6.2649	6.2649	6.2649	6.2649

71801.	7.4647	7.4647	7.4647	7.4647	7.4647
71901.	9.1581	9.1581	9.1581	9.1581	9.1581
72001.	11.5484	11.5484	11.5484	11.5484	11.5484
72101.	14.9222	14.9222	14.9222	14.9222	14.9222
72201.	18.0908	18.0908	18.0908	18.0908	18.0908
81401.	4.4536	4.4536	4.4536	4.4536	4.4536
81501.	4.8639	4.8639	4.8639	4.8639	4.8639
81601.	5.1825	5.2486	5.3148	5.3810	5.4472
81701.	6.2761	6.2761	6.2761	6.2761	6.2761
81801.	7.4543	7.4543	7.4543	7.4543	7.4543
81901.	9.1289	9.1289	9.1289	9.1289	9.1289
82001.	11.5090	11.5090	11.5090	11.5090	11.5090
82101.	14.8917	14.8917	14.8917	14.8917	14.8917
82201.	17.8288	17.8288	17.8288	17.8288	17.8288

GRAY, BRIAN C

From: Stephen Ahnert [sahnert@domeng.com]
Sent: Monday, August 25, 2003 1:58 PM
To: GRAY, BRIAN C
Subject: E-4162-00-5 ANO2 ICI Results up to Weld Top



ANO2ICIC.nodeloc. ANO2ICIC.datapos
results.txt (... t.results.txt ...

Brian-

Here is the data for the ICI nozzle up to the weld top. This info was previously sent to Jai, which is why I thought you might have it already. I've also included the detailed node locations for the nozzle below the bottom of the weld, where the element mesh is not straight across the wall of the nozzle.

Stephen

ANO2ICIC

Node Locations Below Weld Bottom

NODE	ID	% Through Wall			OD
		25	50	75	
1.	0.6979	0.5235	0.3490	0.1745	0.0000
101.	0.8029	0.7201	0.6372	0.5543	0.4715
201.	0.8633	0.8330	0.8028	0.7726	0.7423
301.	0.8979	0.8979	0.8979	0.8979	0.8979
10001.	0.6448	0.4836	0.3224	0.1612	0.0000
10101.	0.8557	0.7791	0.7026	0.6260	0.5494
10201.	0.9768	0.9489	0.9209	0.8930	0.8651
10301.	1.0464	1.0464	1.0464	1.0464	1.0464
20001.	0.4935	0.3701	0.2468	0.1234	0.0000
20101.	0.8988	0.8402	0.7816	0.7231	0.6645
20201.	1.1317	1.1103	1.0889	1.0675	1.0462
20301.	1.2654	1.2654	1.2654	1.2654	1.2654
30001.	0.2671	0.2003	0.1335	0.0668	0.0000
30101.	0.9090	0.8773	0.8456	0.8139	0.7821
30201.	1.2777	1.2662	1.2546	1.2430	1.2315
30301.	1.4896	1.4896	1.4896	1.4896	1.4896
40001.	0.0000	0.0000	0.0000	0.0000	0.0000
40101.	0.8726	0.8726	0.8726	0.8726	0.8726
40201.	1.3739	1.3739	1.3739	1.3739	1.3739
40301.	1.6618	1.6618	1.6618	1.6618	1.6618
50001.	0.0000	0.0668	0.1335	0.2003	0.2671
50101.	1.0655	1.0972	1.1289	1.1606	1.1923
50201.	1.6776	1.6891	1.7007	1.7123	1.7239
50301.	2.0292	2.0292	2.0292	2.0292	2.0292
60001.	0.0000	0.1234	0.2468	0.3701	0.4935
60101.	1.2091	1.2677	1.3263	1.3848	1.4434
60201.	1.9036	1.9250	1.9464	1.9678	1.9891
60301.	2.3026	2.3026	2.3026	2.3026	2.3026
70001.	0.0000	0.1612	0.3224	0.4836	0.6448
70101.	1.3062	1.3828	1.4593	1.5359	1.6124
70201.	2.0566	2.0845	2.1124	2.1404	2.1683
70301.	2.4876	2.4876	2.4876	2.4876	2.4876
80001.	0.0000	0.1745	0.3490	0.5235	0.6979
80101.	1.3646	1.4475	1.5303	1.6132	1.6961
80201.	2.1485	2.1787	2.2090	2.2392	2.2695
80301.	2.5988	2.5988	2.5988	2.5988	2.5988

ANO2ICIC

0's Plane (0 degrees from downhill)

NODE	HEIGHT	ID	% Through Wall			OD
			25	50	75	
1.	0.3490	330.	-16634.	-22706.	-21399.	-19763.
101.	0.6372	15313.	-4281.	-17786.	-14429.	-10809.
201.	0.8028	26820.	18769.	-3643.	-5548.	397.
301.	0.8979	27575.	27463.	11589.	12114.	23130.
401.	1.1242	26017.	27633.	24092.	27004.	45053.
501.	1.3505	28242.	28868.	30962.	40738.	54823.
601.	1.5768	20921.	27864.	35821.	45523.	53450.
701.	1.8031	11964.	23787.	33856.	42567.	51113.
801.	2.0295	9687.	17779.	27821.	30215.	40313.
901.	2.2558	19668.	19737.	25207.	27694.	34390.
1001.	2.4821	37434.	31888.	27565.	24410.	27638.
1101.	2.7084	43325.	40161.	32465.	26020.	30372.
1201.	2.9347	40046.	40036.	37953.	30641.	32887.
1301.	3.1610	35368.	35925.	38751.	36110.	38087.

ANO2ICIC

10000's Plane (22.5 degrees from downhill)

NODE	HEIGHT	ID	% Through Wall			OD
			25	50	75	
10001.	0.3224	11817.	-3000.	-15292.	-17046.	-14741.
10101.	0.7026	23129.	8947.	-4634.	-7335.	-4914.
10201.	0.9209	26611.	19814.	8851.	6956.	15400.
10301.	1.0464	25592.	22193.	16673.	20834.	32108.
10401.	1.2671	23008.	21479.	22537.	28149.	43356.
10501.	1.4878	14243.	18187.	24429.	31101.	45101.
10601.	1.7085	5755.	14592.	23974.	31574.	40756.
10701.	1.9292	984.	12514.	24300.	33893.	38241.
10801.	2.1499	5267.	13512.	21660.	26329.	31416.
10901.	2.3706	16884.	18312.	19651.	22167.	28262.
11001.	2.5913	26961.	22846.	19899.	18757.	23492.
11101.	2.8120	32152.	29086.	25470.	21444.	27068.
11201.	3.0327	32793.	33052.	30915.	26565.	30561.
11301.	3.2534	31892.	32130.	31968.	28400.	35085.

ANO2ICIC

20000's Plane (45 degrees from downhill)

NODE	HEIGHT	ID	% Through Wall			OD
			25	50	75	
20001.	0.2468	20018.	12176.	2142.	-4565.	-4829.
20101.	0.7816	17823.	13195.	8703.	7199.	11360.
20201.	1.0889	13018.	9830.	11177.	16535.	29313.
20301.	1.2654	8173.	7762.	11434.	21752.	29049.
20401.	1.4771	2810.	6438.	11829.	18313.	24836.
20501.	1.6888	-2122.	3625.	11444.	19199.	25718.
20601.	1.9005	-6511.	-381.	9736.	18601.	26353.
20701.	2.1122	-7277.	-1422.	7250.	16568.	19341.
20801.	2.3239	-1618.	3555.	9846.	16479.	19018.
20901.	2.5356	5060.	8571.	11061.	13316.	13608.
21001.	2.7474	10775.	11353.	11467.	13710.	15707.
21101.	2.9591	17210.	16185.	13444.	12720.	18141.

21201.	3.1708	22055.	21876.	19604.	17419.	19194.
21301.	3.3825	22420.	22298.	20957.	19614.	22892.

ANO2ICIC

30000's Plane (67.5 degrees from downhill)

NODE	HEIGHT	ID	% Through Wall			OD
			25	50	75	
30001.	0.1335	8133.	7529.	8405.	8807.	9444.
30101.	0.8456	2509.	4841.	8075.	13153.	14854.
30201.	1.2546	-3159.	185.	6565.	15336.	19781.
30301.	1.4896	-8698.	-3807.	4486.	15633.	21762.
30401.	1.6905	-10607.	-5127.	4368.	16593.	23105.
30501.	1.8915	-11697.	-6146.	3629.	14221.	21065.
30601.	2.0924	-12130.	-5767.	3348.	11915.	24052.
30701.	2.2934	-10623.	-4097.	2790.	9076.	14421.
30801.	2.4943	-6605.	-1271.	4055.	10985.	18666.
30901.	2.6953	-846.	1412.	5279.	8673.	12195.
31001.	2.8963	5966.	4457.	6294.	8822.	10450.
31101.	3.0972	12453.	8583.	8083.	7942.	9098.
31201.	3.2982	17413.	13069.	11816.	9951.	7765.
31301.	3.4991	19608.	16481.	14640.	15484.	12007.

ANO2ICIC

40000's Plane (90 degrees from downhill)

NODE	HEIGHT	ID	% Through Wall			OD
			25	50	75	
40001.	0.0000	5256.	6249.	9996.	13433.	14867.
40101.	0.8726	-3168.	1103.	7186.	13071.	17896.
40201.	1.3739	-10727.	-3806.	6415.	17046.	27965.
40301.	1.6618	-15878.	-7317.	4861.	18322.	29000.
40401.	1.8519	-16192.	-7314.	4927.	19781.	31004.
40501.	2.0421	-15973.	-6986.	3677.	16010.	23384.
40601.	2.2322	-15040.	-6183.	2945.	11781.	22918.
40701.	2.4223	-12838.	-5543.	3656.	10925.	15784.
40801.	2.6124	-9517.	-5798.	1581.	9281.	16033.
40901.	2.8026	-4550.	-4030.	1975.	7726.	11560.
41001.	2.9927	1807.	-217.	3770.	8108.	7520.
41101.	3.1828	6378.	3651.	5439.	8875.	4032.
41201.	3.3729	10031.	6751.	6671.	6664.	1885.
41301.	3.5631	13966.	12498.	11967.	14062.	6061.

ANO2ICIC

50000's Plane (112.5 degrees from downhill)

NODE	HEIGHT	ID	% Through Wall			OD
			25	50	75	
50001.	0.1335	1855.	4938.	9186.	12671.	15099.
50101.	1.1289	-3205.	1648.	8628.	15241.	19737.
50201.	1.7007	-10751.	-4274.	5271.	16542.	24718.
50301.	2.0292	-15595.	-6154.	6009.	20523.	29654.
50401.	2.2096	-17582.	-8682.	3168.	15984.	27678.
50501.	2.3900	-16129.	-8492.	3069.	14915.	22125.
50601.	2.5704	-14648.	-7789.	3245.	13265.	20801.
50701.	2.7508	-13026.	-7342.	3631.	13180.	19786.
50801.	2.9312	-11837.	-6347.	2955.	12010.	19650.
50901.	3.1116	-10397.	-4769.	2256.	10236.	16691.

51001.	3.2920	-7427.	-2667.	3304.	7906.	12458.
51101.	3.4724	-2850.	583.	4589.	10291.	8319.
51201.	3.6528	2957.	3567.	5248.	8049.	4998.
51301.	3.8332	9365.	8955.	10723.	13578.	7031.

ANO2ICIC

60000's Plane (135 degrees from downhill)

NODE	HEIGHT	ID	% Through Wall			OD
			25	50	75	
60001.	0.2468	7021.	5842.	5526.	6093.	7368.
60101.	1.3263	3640.	3465.	5318.	7600.	11311.
60201.	1.9464	-905.	1001.	5440.	12219.	21693.
60301.	2.3026	-3267.	2518.	8632.	17598.	31596.
60401.	2.4751	-6647.	884.	9919.	20233.	34996.
60501.	2.6476	-5744.	986.	10615.	22120.	33405.
60601.	2.8200	-5329.	2056.	10825.	22691.	31650.
60701.	2.9925	-4932.	2805.	11187.	22210.	31425.
60801.	3.1650	-4264.	3369.	11827.	19607.	30392.
60901.	3.3374	-2796.	4582.	11807.	20853.	29935.
61001.	3.5099	30.	5642.	12469.	18196.	26233.
61101.	3.6824	4197.	7650.	12858.	18879.	21916.
61201.	3.8549	9685.	10612.	13445.	16308.	19536.
61301.	4.0273	14607.	13634.	15404.	17649.	19056.

ANO2ICIC

70000's Plane (157.5 degrees from downhill)

NODE	HEIGHT	ID	% Through Wall			OD
			25	50	75	
70001.	0.3224	1473.	-3036.	-6641.	-12104.	-17020.
70101.	1.4593	20460.	16006.	11035.	2785.	-6169.
70201.	2.1124	21212.	17465.	16798.	18497.	17342.
70301.	2.4876	22297.	22154.	23184.	29005.	38650.
70401.	2.6542	21709.	23715.	25857.	31252.	45358.
70501.	2.8208	20455.	24110.	27879.	33527.	45849.
70601.	2.9874	19387.	24320.	28835.	34759.	46036.
70701.	3.1541	18829.	24621.	28661.	36197.	47360.
70801.	3.3207	18551.	24450.	28707.	32753.	47292.
70901.	3.4873	18254.	23886.	28207.	33211.	44358.
71001.	3.6539	18196.	23178.	27689.	31919.	41466.
71101.	3.8205	19769.	23334.	27730.	34376.	41884.
71201.	3.9871	22441.	23108.	26486.	30105.	41124.
71301.	4.1537	23836.	22198.	21340.	20204.	32077.

ANO2ICIC

80000's Plane (180 degrees from downhill)

NODE	HEIGHT	ID	% Through Wall			OD
			25	50	75	
80001.	0.3490	-11742.	-11463.	-12940.	-22469.	-28317.
80101.	1.5303	32201.	29001.	20291.	4279.	-13369.
80201.	2.2090	30297.	28052.	24882.	23328.	16928.
80301.	2.5988	32705.	32454.	32437.	35963.	40476.
80401.	2.7617	35478.	35651.	35700.	37186.	47454.
80501.	2.9246	35664.	35774.	37391.	40265.	51097.
80601.	3.0875	35636.	36135.	38433.	41721.	53338.
80701.	3.2503	35307.	36675.	38189.	44045.	56253.

80801.	3.4132	34605.	35864.	37199.	40276.	55808.
80901.	3.5761	33503.	34531.	36673.	40156.	51744.
81001.	3.7390	32045.	32671.	34572.	38781.	48869.
81101.	3.9018	30301.	31492.	34115.	41212.	53934.
81201.	4.0647	28270.	28386.	32739.	36470.	51629.
81301.	4.2276	26390.	25687.	24607.	22680.	44523.

GRAY, BRIAN C

From: Stephen Ahnert [sahnert@domeng.com]
Sent: Tuesday, August 26, 2003 1:34 PM
To: GRAY, BRIAN C
Subject: E-4162-00-6 ANO2 ICI Results Above Weld (Downhill Plane)



ANO2ICIC.ICIdata
post2.results....

Brian-

Attached are the hoop stress results and node locations for the ICI nozzle at the downhill (0's) plane above the top of the weld . The axial heights shown in the attachment are measured from the lowest point on the tube at the node's circumferential plane (node 5 for the downhill plane). The ID counterbore transition occurs between nodes 2001 and 2101.

Stephen

ANO2ICIC

0's Plane (0 degrees from downhill)

Hoop Stresses		% Through Wall			
NODE	ID	25	50	75	OD
1401.	31359.	29908.	29337.	29599.	28489.
1501.	26330.	23785.	21351.	19924.	17183.
1601.	22264.	20269.	17426.	11969.	-417.
1701.	17018.	15329.	12768.	6665.	-2122.
1801.	15282.	14896.	13020.	9080.	4869.
1901.	16043.	15499.	13486.	9127.	5185.
2001.	16153.	14788.	10629.	6368.	2547.
2101.	14853.	10204.	5245.	1131.	-2825.
2201.	13403.	12899.	12285.	11712.	11405.

ANO2ICIC

Node Locations

		% Through Wall			
NODE	ID	25	50	75	OD
1401.	3.4831	3.4831	3.4831	3.4831	3.4831
1501.	4.1328	4.1328	4.1328	4.1328	4.1328
1601.	4.9976	4.9976	4.9976	4.9976	4.9976
1701.	6.1486	6.1486	6.1486	6.1486	6.1486
1801.	7.6805	7.6805	7.6805	7.6805	7.6805
1901.	9.7195	9.7195	9.7195	9.7195	9.7195
2001.	12.7631	12.6025	12.4419	12.2813	12.1207
2101.	16.0453	16.0453	16.0453	16.0453	16.0453
2201.	25.4095	25.4095	25.4095	25.4095	25.4095

GRAY, BRIAN C

From: John Broussard [jbroussard@domeng.com]
Sent: Wednesday, September 03, 2003 11:00 AM
To: GRAY, BRIAN C
Subject: E-4162-00-9, Axial Stresses in the ICI nozzle at and above the weld



ANO2ICIC.axial.res
ults.txt (13...

Brian,

Per our conversation, attached is a text file containing through-wall axial stresses (cylindrical coordinate system centered on the nozzle) and node elevations (relative to the lowest point on the nozzle) for every circumferential plane around the nozzle. If you have any questions or require further information, do not hesitate to call or e-mail.

John Broussard, P.E.
Dominion Engineering, Inc.
E-mail: jbroussard@domeng.com
Phone : 703-437-7826 x236
Fax : 703-437-0780

ANO2ICIC - Stresses Above the Weld
0's Plane (0 degrees from downhill)

Axial Stresses		% Through Wall			
NODE	ID	25	50	75	OD
1301.	19134.	19841.	23185.	23594.	23602.
1401.	21283.	22477.	23786.	24530.	26400.
1501.	24244.	23406.	22564.	19655.	15696.
1601.	21617.	21652.	21873.	20331.	10326.
1701.	15755.	17788.	20296.	20152.	14481.
1801.	14607.	16765.	19586.	19917.	19366.
1901.	13693.	15556.	17456.	17722.	17673.
2001.	11799.	12422.	12271.	12235.	12122.
2101.	9528.	8143.	6757.	5463.	4009.
2201.	7582.	6930.	5926.	4908.	4268.

ANO2ICIC - Stresses Above the Weld
10000's Plane (22.5 degrees from downhill)

Axial Stresses		% Through Wall			
NODE	ID	25	50	75	OD
11301.	22586.	22533.	23312.	23359.	25490.
11401.	23861.	23539.	24158.	26607.	33571.
11501.	23450.	22379.	21257.	19017.	16595.
11601.	21170.	20405.	20232.	18786.	12381.
11701.	16771.	17940.	19555.	19168.	15399.
11801.	15537.	17110.	19041.	19315.	18815.
11901.	14317.	15543.	16831.	17585.	17957.
12001.	11514.	11890.	11821.	11647.	11801.
12101.	8776.	7616.	6655.	5694.	4550.
12201.	6698.	6114.	5295.	4480.	3935.

ANO2ICIC - Stresses Above the Weld
20000's Plane (45 degrees from downhill)

Axial Stresses		% Through Wall			
NODE	ID	25	50	75	OD
21301.	32078.	30339.	27899.	25016.	23002.
21401.	32246.	29745.	27938.	28428.	31653.
21501.	28287.	26285.	24046.	22044.	21592.
21601.	21901.	20929.	19971.	18562.	16355.
21701.	17934.	18215.	18706.	17913.	16267.
21801.	15767.	16723.	17588.	17926.	17999.
21901.	13734.	14661.	15815.	16924.	18084.
22001.	10646.	10362.	10036.	9985.	10015.
22101.	5882.	5455.	5297.	5132.	4810.
22201.	5389.	5108.	4877.	4619.	4334.

ANO2ICIC - Stresses Above the Weld
30000's Plane (67.5 degrees from downhill)

Axial Stresses		% Through Wall			
NODE	ID	25	50	75	OD
31301.	33568.	30437.	28273.	26492.	21121.
31401.	32613.	29501.	25741.	23410.	20830.
31501.	27804.	26658.	25076.	23609.	24053.

31601.	20992.	20323.	19276.	18062.	16687.
31701.	14110.	14247.	14670.	14920.	14942.
31801.	10324.	11615.	13167.	14307.	15302.
31901.	9890.	10413.	11095.	11524.	11672.
32001.	7802.	8304.	8650.	8901.	9102.
32101.	3146.	3772.	4392.	4997.	5563.
32201.	4854.	4611.	4694.	4781.	4601.

ANO2ICIC - Stresses Above the Weld
40000's Plane (90 degrees from downhill)

Axial Stresses		% Through Wall			
NODE	ID	25	50	75	OD
41301.	27693.	26366.	24818.	23340.	16693.
41401.	27076.	25745.	22225.	20007.	19364.
41501.	21642.	20426.	18131.	16185.	16290.
41601.	15264.	15112.	14377.	13926.	14193.
41701.	5004.	6885.	8509.	10424.	12026.
41801.	4640.	6420.	8493.	10387.	11537.
41901.	6519.	7330.	8271.	9065.	9330.
42001.	4302.	5572.	6738.	7940.	8892.
42101.	2449.	3416.	4343.	5245.	6088.
42201.	5189.	4721.	4770.	4821.	4469.

ANO2ICIC - Stresses Above the Weld
50000's Plane (112.5 degrees from downhill)

Axial Stresses		% Through Wall			
NODE	ID	25	50	75	OD
51301.	16932.	15839.	16310.	16729.	13390.
51401.	17627.	14595.	12835.	12324.	17720.
51501.	13191.	10239.	7842.	6261.	5158.
51601.	5842.	6039.	6398.	6923.	7504.
51701.	-27.	1914.	4198.	6352.	7716.
51801.	1264.	2980.	4949.	6577.	7463.
51901.	3160.	4250.	5485.	6675.	7363.
52001.	2524.	3586.	4636.	5927.	6956.
52101.	3505.	4084.	4668.	5242.	5741.
52201.	5464.	4957.	4932.	4859.	4472.

ANO2ICIC - Stresses Above the Weld
60000's Plane (135 degrees from downhill)

Axial Stresses		% Through Wall			
NODE	ID	25	50	75	OD
61301.	3896.	2573.	4347.	6737.	10416.
61401.	4814.	1456.	-147.	-1041.	-1614.
61501.	1261.	65.	-337.	-772.	-206.
61601.	-4868.	-4016.	-3343.	-2306.	-1074.
61701.	-3529.	-2279.	-543.	975.	1729.
61801.	245.	1119.	2071.	2887.	3455.
61901.	2525.	3025.	3391.	3945.	4307.
62001.	4204.	4306.	4570.	4750.	4811.
62101.	4855.	4863.	4957.	5065.	5104.
62201.	5488.	5162.	5144.	5053.	4823.

ANO2ICIC - Stresses Above the Weld
70000's Plane (157.5 degrees from downhill)

Axial Stresses		% Through Wall			
NODE	ID	25	50	75	OD
71301.	454.	-2163.	-4850.	-6703.	7792.
71401.	1834.	-2115.	-5846.	-9511.	-16830.
71501.	-421.	-3135.	-6430.	-9855.	-11198.
71601.	-2819.	-3261.	-4224.	-5131.	-5407.
71701.	-456.	-938.	-1350.	-1472.	-1504.
71801.	2658.	1946.	1324.	405.	-449.
71901.	4736.	4256.	3468.	2646.	1820.
72001.	5760.	5395.	4874.	4328.	3705.
72101.	5827.	5450.	5223.	5032.	4769.
72201.	5466.	5304.	5258.	5137.	5049.

ANO2ICIC - Stresses Above the Weld
80000's Plane (180 degrees from downhill)

Axial Stresses		% Through Wall			
NODE	ID	25	50	75	OD
81301.	238.	-3173.	-8173.	-11550.	15902.
81401.	2159.	-1729.	-7605.	-15001.	-24613.
81501.	-662.	-3054.	-7027.	-11418.	-13552.
81601.	-1163.	-2032.	-4603.	-6545.	-7444.
81701.	1946.	456.	-1865.	-3592.	-4364.
81801.	4652.	3396.	1590.	-159.	-1737.
81901.	6022.	5282.	3800.	2360.	1009.
82001.	6542.	6050.	5056.	4230.	3328.
82101.	6161.	5674.	5320.	5006.	4621.
82201.	5431.	5323.	5257.	5112.	5062.

ANO2ICIC
Node Elevations Above the Weld

		% Through Wall			
NODE	ID	25	50	75	OD
1301.	3.1610	3.1610	3.1610	3.1610	3.1610
1401.	3.4831	3.4831	3.4831	3.4831	3.4831
1501.	4.1328	4.1328	4.1328	4.1328	4.1328
1601.	4.9976	4.9976	4.9976	4.9976	4.9976
1701.	6.1486	6.1486	6.1486	6.1486	6.1486
1801.	7.6805	7.6805	7.6805	7.6805	7.6805
1901.	9.7195	9.7195	9.7195	9.7195	9.7195
2001.	12.7631	12.6025	12.4419	12.2813	12.1207
2101.	16.0453	16.0453	16.0453	16.0453	16.0453
2201.	25.4095	25.4095	25.4095	25.4095	25.4095
11301.	3.2534	3.2534	3.2534	3.2534	3.2534
11401.	3.5665	3.5665	3.5665	3.5665	3.5665
11501.	4.1839	4.1839	4.1839	4.1839	4.1839
11601.	5.0137	5.0137	5.0137	5.0137	5.0137
11701.	6.1290	6.1290	6.1290	6.1290	6.1290
11801.	7.6279	7.6279	7.6279	7.6279	7.6279
11901.	9.6425	9.6425	9.6425	9.6425	9.6425
12001.	12.3503	12.2141	12.0780	11.9418	11.8056
12101.	15.9895	15.9895	15.9895	15.9895	15.9895
12201.	25.0944	25.0944	25.0944	25.0944	25.0944

21301.	3.3825	3.3825	3.3825	3.3825	3.3825
21401.	3.6821	3.6821	3.6821	3.6821	3.6821
21501.	4.2630	4.2630	4.2630	4.2630	4.2630
21601.	5.0509	5.0509	5.0509	5.0509	5.0509
21701.	6.1198	6.1198	6.1198	6.1198	6.1198
21801.	7.5697	7.5697	7.5697	7.5697	7.5697
21901.	9.5365	9.5365	9.5365	9.5365	9.5365
22001.	12.2045	11.8805	11.5564	11.2324	10.9084
22101.	15.8235	15.8235	15.8235	15.8235	15.8235
22201.	24.1971	24.1971	24.1971	24.1971	24.1971
31301.	3.4991	3.4991	3.4991	3.4991	3.4991
31401.	3.7829	3.7829	3.7829	3.7829	3.7829
31501.	4.3262	4.3262	4.3262	4.3262	4.3262
31601.	5.0695	5.0695	5.0695	5.0695	5.0695
31701.	6.0867	6.0867	6.0867	6.0867	6.0867
31801.	7.4786	7.4786	7.4786	7.4786	7.4786
31901.	9.3834	9.4289	9.4744	9.5199	9.5655
32001.	11.9898	11.9898	11.9898	11.9898	11.9898
32101.	15.5564	15.5564	15.5564	15.5564	15.5564
32201.	22.8542	22.8542	22.8542	22.8542	22.8542
41301.	3.5631	3.5631	3.5631	3.5631	3.5631
41401.	3.8310	3.8310	3.8310	3.8310	3.8310
41501.	4.3383	4.3383	4.3383	4.3383	4.3383
41601.	5.0383	5.0383	5.0383	5.0383	5.0383
41701.	6.0041	6.0041	6.0041	6.0041	6.0041
41801.	7.3368	7.3368	7.3368	7.3368	7.3368
41901.	8.6238	8.7618	8.8998	9.0378	9.1757
42001.	11.7131	11.7131	11.7131	11.7131	11.7131
42101.	15.2141	15.2141	15.2141	15.2141	15.2141
42201.	21.2702	21.2702	21.2702	21.2702	21.2702
51301.	3.8332	3.8332	3.8332	3.8332	3.8332
51401.	4.0867	4.0867	4.0867	4.0867	4.0867
51501.	4.5620	4.5620	4.5620	4.5620	4.5620
51601.	5.2230	5.2230	5.2230	5.2230	5.2230
51701.	6.1423	6.2728	6.4034	6.5339	6.6645
51801.	7.3069	7.3354	7.3638	7.3923	7.4208
51901.	9.1989	9.1989	9.1989	9.1989	9.1989
52001.	11.6719	11.6719	11.6719	11.6719	11.6719
52101.	15.1113	15.1113	15.1113	15.1113	15.1113
52201.	19.9532	19.9532	19.9532	19.9532	19.9532
61301.	4.0273	4.0273	4.0273	4.0273	4.0273
61401.	4.2688	4.2688	4.2688	4.2688	4.2688
61501.	4.7171	4.7171	4.7171	4.7171	4.7171
61601.	5.3452	5.3959	5.4466	5.4973	5.5480
61701.	6.1904	6.1992	6.2079	6.2167	6.2255
61801.	7.4589	7.4589	7.4589	7.4589	7.4589
61901.	9.1874	9.1874	9.1874	9.1874	9.1874
62001.	11.6096	11.6096	11.6096	11.6096	11.6096
62101.	15.0039	15.0039	15.0039	15.0039	15.0039
62201.	18.8368	18.8368	18.8368	18.8368	18.8368
71301.	4.1537	4.1537	4.1537	4.1537	4.1537
71401.	4.3860	4.3860	4.3860	4.3860	4.3860
71501.	4.8127	4.8100	4.8074	4.8047	4.8020
71601.	5.4444	5.4370	5.4297	5.4223	5.4149
71701.	6.2649	6.2649	6.2649	6.2649	6.2649
71801.	7.4647	7.4647	7.4647	7.4647	7.4647

71901.	9.1581	9.1581	9.1581	9.1581	9.1581
72001.	11.5484	11.5484	11.5484	11.5484	11.5484
72101.	14.9222	14.9222	14.9222	14.9222	14.9222
72201.	18.0908	18.0908	18.0908	18.0908	18.0908
81301.	4.2276	4.2276	4.2276	4.2276	4.2276
81401.	4.4536	4.4536	4.4536	4.4536	4.4536
81501.	4.8639	4.8639	4.8639	4.8639	4.8639
81601.	5.1825	5.2486	5.3148	5.3810	5.4472
81701.	6.2761	6.2761	6.2761	6.2761	6.2761
81801.	7.4543	7.4543	7.4543	7.4543	7.4543
81901.	9.1289	9.1289	9.1289	9.1289	9.1289
82001.	11.5090	11.5090	11.5090	11.5090	11.5090
82101.	14.8917	14.8917	14.8917	14.8917	14.8917
82201.	17.8288	17.8288	17.8288	17.8288	17.8288

Arkansas Nuclear One Unit 2

**Primary Water Stress Corrosion Crack Growth Analysis for an ICI ID Surface Flaw
Uphill (180°), in the Blind Zone above the Top of the J-Groove Weld
Developed by Central Engineering Programs, Entergy Operations Inc.**

Flaw Case 1: 25% Through-Wall Flaw with a 6-to-1 Flaw Length-to-Depth Aspect Ratio, Located at the Center of the Blind Zone

Calculation Basis: MRP 75 th Percentile and Flaw Face Pressurized

Mean Radius -to- Thickness Ratio:- " R_m/t " – between 1.0 and 300.0

Note : *The Metric form of the equation from EPRI MRP was used 55-Rev. 1 . A correction factor is applied in the determination of the crack extension to convert the units of meters per second to the value in inches per hour .*

ID Surface Flaw

User Input:

The Dominion Engineering Inc. (DEI) finite element model nodal elevations and hoop stresses for the uphill side (180° azimuth) of the ICI nozzle are brought into the Mathcad worksheet from data supplied in Reference 6d. The data are composed of the nodal elevations (in inches), along with the ID, 25% through-wall (tw), 50% tw, 75% tw, and OD hoop stresses, beginning at the top of the weld (nodal line 81301) and extending to the top of the nozzle in the FEA model, which is at the point where the nozzle intersects the reactor vessel head.

The DEI FEA data has elevation referenced from the bottom of the ICI nozzle. The elevations of the node points in the DEI FEA model, beginning at the top of the weld (nodal line 81301), are as follows:

$i := 0..9$

Node_line_i := ID_elev_fea_i := QT_elev_fea_i := MD_elev_fea_i := TQ_elev_fea_i := OD_elev_fea_i :=

81301	4.2276	4.2276	4.2276	4.2276	4.2276
81401	4.4536	4.4536	4.4536	4.4536	4.4536
81501	4.8639	4.8639	4.8639	4.8639	4.8639
81601	5.1825	5.2486	5.3148	5.3810	5.4472
81701	6.2761	6.2761	6.2761	6.2761	6.2761
81801	7.4543	7.4543	7.4543	7.4543	7.4543
81901	9.1289	9.1289	9.1289	9.1289	9.1289
82001	11.5090	11.5090	11.5090	11.5090	11.5090
82101	14.8917	14.8917	14.8917	14.8917	14.8917
82201	17.8288	17.8288	17.8288	17.8288	17.8288

The corresponding stresses at these nodes are

ID_stress_fea_i := QT_stress_fea_i := MD_stress_fea_i := TQ_stress_fea_i := OD_stress_fea_i :=

26.390
23.147
19.425
15.065
16.707
17.399
17.412
17.115
15.304
10.308

25.687
21.559
18.188
14.581
16.175
17.177
17.487
15.794
13.024
10.119

24.607
19.292
15.780
13.132
15.560
15.044
12.883
11.377
10.766
10.032

22.680
16.085
11.381
6.189
8.890
8.136
7.180
7.821
9.067
9.951

44.523
9.729
8.207
-0.109
2.74
2.316
2.298
4.387
7.453
9.936

Blind Zone and Counterbore Reference dimensions:

From design drawings (Ref. 2a and 2b) and the design input of Attachment 1, the following dimensions are used to locate the counterbore bottom and blind zone locations (bottom, top, and middle) as referenced from the nodal coordinates of the DEI FEA model.

$$\text{Actual_cbore_bottom_elev} := \text{ID_elev_fea}_0 + 1.377$$

$$\text{Actual_cbore_bottom_elev} = 5.6046$$

$$\text{topweld_to_bottom_BZ} := 1.08$$

$$\text{BZ_length} := 0.88$$

$$\text{elev_to_mid_BZ} := \text{ID_elev_fea}_0 + \text{topweld_to_bottom_BZ} + \frac{\text{BZ_length}}{2}$$

$$\text{elev_to_mid_BZ} = 5.7476$$

$$\text{bottom_of_BZ} := \text{ID_elev_fea}_0 + \text{topweld_to_bottom_BZ}$$

$$\text{bottom_of_BZ} = 5.3076$$

$$\text{top_of_BZ} := \text{ID_elev_fea}_0 + \text{topweld_to_bottom_BZ} + \text{BZ_length}$$

$$\text{top_of_BZ} = 6.1876$$

For stress averaging and fracture mechanics purposes, the reference coordinate system--with a "0" elevation at the bottom of the nozzle, at the ID corner--must be converted into a new coordinate system with the top of the nozzle (nodal line 82201) as the new "0" elevation.. The positive direction along this new coordinate system will be towards nodal line 81301, which is the top of the weld. This modification facilitates a fracture mechanics model more ammenable to the surface flaw loop structure previously developed in Reference 7.

The following iterative loops convert the five (5) through-wall stress components--ID, 25% tw (QT), 50% tw (MD), 75% tw (TQ), and OD--and the associated elevations, initially given in the DEI FEA model, into the "new" coordinate system, referenced from the top of the nozzle where it meets the reactor vessel head.

```

ID_conv := | Top ← ID_elev_fea9
            | j ← 9
            | i ← 0
            | while j ≥ 0
            |   | ID_elev_convi ← Top - ID_elev_feaj
            |   | ID_stressi ← ID_stress_feaj
            |   | output(i, 0) ← ID_elev_convi
            |   | output(i, 1) ← ID_stressi
            |   | j ← j - 1
            |   | i ← i + 1
            | output
  
```

$$\text{ID_elev} := \text{ID_conv}^{\langle 0 \rangle}$$

$$\text{ID_stress} := \text{ID_conv}^{\langle 1 \rangle}$$

```

QT_conv := | Top ← QT_elev_fea9
            | j ← 9
            | i ← 0
            | while j ≥ 0
            |   | QT_elev_convi ← Top – QT_elev_feaj
            |   | QT_stressi ← QT_stress_feaj
            |   | output(i, 0) ← QT_elev_convi
            |   | output(i, 1) ← QT_stressi
            |   | j ← j – 1
            |   | i ← i + 1
            | output
  
```

QT_elev := QT_conv⁽⁰⁾

QT_stress := QT_conv⁽¹⁾

```

MD_conv := | Top ← MD_elev_fea9
            | j ← 9
            | i ← 0
            | while j ≥ 0
            |   | MD_elev_convi ← Top – MD_elev_feaj
            |   | MD_stressi ← MD_stress_feaj
            |   | output(i, 0) ← MD_elev_convi
            |   | output(i, 1) ← MD_stressi
            |   | j ← j – 1
            |   | i ← i + 1
            | output
  
```

MD_elev := MD_conv⁽⁰⁾

MD_stress := MD_conv⁽¹⁾

```

TQ_conv := | Top ← TQ_elev_fea9
            | j ← 9
            | i ← 0
            | while j ≥ 0
            |   | TQ_elev_convi ← Top - TQ_elev_feaj
            |   | TQ_stressi ← TQ_stress_feaj
            |   | output(i, 0) ← TQ_elev_convi
            |   | output(i, 1) ← TQ_stressi
            |   | j ← j - 1
            |   | i ← i + 1
            | output
  
```

TQ_elev := TQ_conv⁽⁰⁾

TQ_stress := TQ_conv⁽¹⁾

```

OD_conv := | Top ← OD_elev_fea9
            | j ← 9
            | i ← 0
            | while j ≥ 0
            |   | OD_elev_convi ← Top - OD_elev_feaj
            |   | OD_stressi ← OD_stress_feaj
            |   | output(i, 0) ← OD_elev_convi
            |   | output(i, 1) ← OD_stressi
            |   | j ← j - 1
            |   | i ← i + 1
            | output
  
```

OD_elev := OD_conv⁽⁰⁾

OD_stress := OD_conv⁽¹⁾

ID_elev_i =

0
2.9371
6.3198
8.6999
10.3745
11.5527
12.6463
12.9649
13.3752
13.6012

QT_elev_i =

0
2.9371
6.3198
8.6999
10.3745
11.5527
12.5802
12.9649
13.3752
13.6012

MD_elev_i =

0
2.9371
6.3198
8.6999
10.3745
11.5527
12.514
12.9649
13.3752
13.6012

TQ_elev_i =

0
2.9371
6.3198
8.6999
10.3745
11.5527
12.4478
12.9649
13.3752
13.6012

OD_elev_i =

0
2.9371
6.3198
8.6999
10.3745
11.5527
12.3816
12.9649
13.3752
13.6012

ID_stress_i =

10.308
15.304
17.115
17.412
17.399
16.707
15.065
19.425
23.147
26.39

QT_stress_i =

10.119
13.024
15.794
17.487
17.177
16.175
14.581
18.188
21.559
25.687

MD_stress_i =

10.032
10.766
11.377
12.883
15.044
15.56
13.132
15.78
19.292
24.607

TQ_stress_i =

9.951
9.067
7.821
7.18
8.136
8.89
6.189
11.381
16.085
22.68

OD_stress_i =

9.936
7.453
4.387
2.298
2.316
2.74
-0.109
8.207
9.729
44.523

The two sets of five arrays given above are the elevations measured from the top of the ICI nozzle from the FEA model down to the top of the J-weld and the corresponding hoop stresses in the modified coordinate system (MCS).

Additional Geometry in Modified Coordinate System

The top of the J-groove weld in the MCS is equal to the last entry in the ID_elev array:

$$\text{Top_Jweld} := \text{ID_elev}_9$$

$$\text{Top_Jweld} = 13.6012$$

The location of the top of the UT blind zone (BZ) in the MCS (as measured from the ID surface) is

$$\text{BZ_top} := \text{Top_Jweld} - (\text{topweld_to_bottom_BZ} + \text{BZ_length})$$

$$\text{BZ_top} = 11.6412$$

The midpoint of the BZ in the MCS is

$$\text{BZ_mid} := \text{BZ_top} + \frac{\text{BZ_length}}{2}$$

$$\text{BZ_mid} = 12.0812$$

The bottom of the BZ in the MCS is

$$\text{BZ_bottom} := \text{BZ_top} + \text{BZ_length}$$

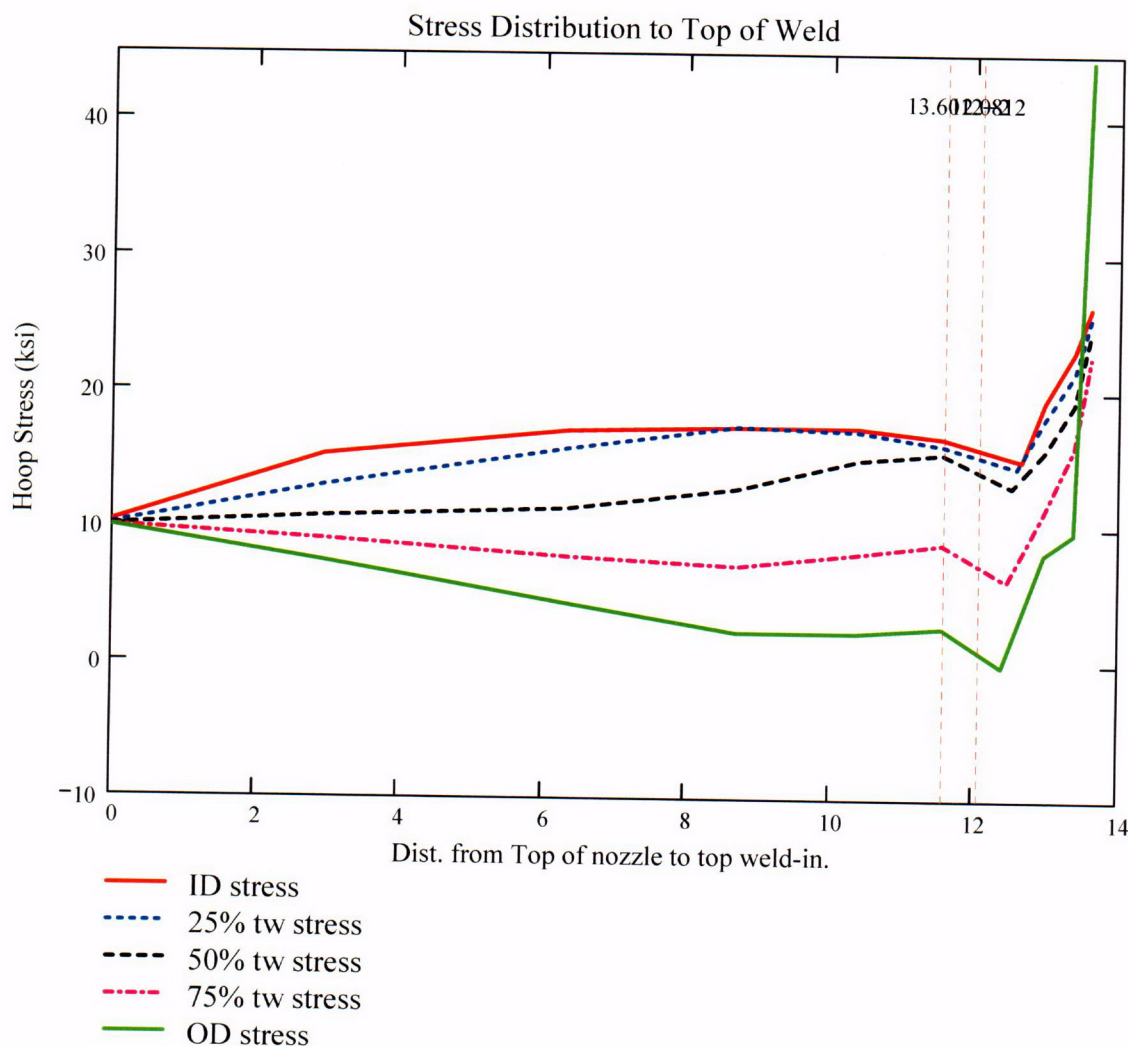
$$\text{BZ_bottom} = 12.5212$$

The location of the actual counterbore (from design drawings) in the MCS:

$$\text{cbore_elev} := \text{Top_Jweld} - 1.377$$

$$\text{cbore_elev} = 12.2242$$

From the MCS, the stress distribution from elevation 0 (the top of the ICI nozzle where it intersects the RV head) to the top of the weld is graphically shown below.



For the ID surface flaw model, the reference point is the location along the axis of the nozzle used to locate the flaw. For this analysis, the reference point is considered at the mid-height of the blind zone.

Ref_{Point} := BZ_{mid}

To place the flaw with respect to the reference point, the flaw tips and center can be located as follows:

- 1) The Upper "c- tip" located at the reference point (Enter 1)
- 2) The Center of the flaw at the reference point (Enter 2)
- 3) The lower "c- tip" located at the reference point (Enter 3).

Val := 2

The Input Below is the point below the blind zone region where stresses will be considered for curve-fitting. This point is taken as the top of the weld, since the stress distribution changes drastically within the weld region. Enter this dimension or variable below.

Elev_{Strs.Dist} := Top_Jweld The elevation to the point of maximum stress to consider
(Axial distance from elevation 0 in the MCS).

ICI Nozzle Geometry Input Data:

od := 5.563 - 0.001 Tube OD, in inches (The value from Ref. 2a, is 5.563" +0.00/-0.001)

id1 := 4.625 + 0.01 Maximum Tube ID above counterbore, in inches
(The value from Ref. 2b is 4.625" +/- 0.010")

id2 := 4.750 + 0.01 Maximum Tube ID below counterbore, in inches
(The value from Ref. 2b is 4.750" +/- 0.010")

$$t1 := \frac{(od - id1)}{2}$$

Minimum wall thickness above the counterbore, in inches

$$t1 = 0.4635$$

$$t2 := \frac{(od - id2)}{2}$$

Minimum wall thickness below the counterbore, in inches

$$t2 = 0.401$$

$$R_o := \frac{od}{2}$$

$$R_o = 2.781$$

$$R_{id1} := \frac{id1}{2}$$

$$R_{id1} = 2.3175$$

$$R_{id2} := \frac{id2}{2} \quad R_{id2} = 2.38$$

$$R_{m1} := R_{id1} + \frac{t1}{2} \quad R_{m1} = 2.54925$$

$$R_{m2} := R_{id2} + \frac{t2}{2} \quad R_{m2} = 2.5805$$

$$R_t := \frac{R_{m2}}{t2} \quad R_t = 6.43516$$

$$\frac{R_o}{t2} = 6.93516$$

Flaw Geometry Input Data:

A postulated flaw could exist in the 0.88" UT Blindzone that occurs 1.08" above the top of the J-weld at the uphill (180°) location. The flaw length (c) and depth (a) constitute the input parameters. This flaw represents an internal surface crack in a cylinder, as described in Reference 8.

$AR_0 := 6$ The flaw length-to-depth aspect ratio. This is a ratio common to ASME Section XI, and one sufficient to promote flaw growth through the thickness.

$$t2 \cdot .25 = 0.10025$$

$a_0 := 0.1$ Initial Flaw Depth of the ID surface flaw in the blind zone above the top of the weld on the uphill side. The minimum detectable depth of a surface flaw from UT demonstrations [Ref. 11] was 8% throughwall. Conservatively, a 25% throughwall flaw is assumed. This flaw is sufficiently deep to see the stress field developed through the thickness.

$L_m := a_0 \cdot AR_0$ Initial Flaw Length of an ID surface flaw in the counterbore region, in inches. The length was determined by assuming a 6-to-1 flaw length-to-depth aspect ratio. Half the flaw length (0.3 inch) was placed below the mid-height of the blind zone, while the other half was placed above the mid-height.

$$L = 0.6$$

$c_0 := \frac{L}{2}$ The half flaw length used in the fracture mechanics model

Additional Input Data:

$P_{Int} := 2.235$ Design Operating Pressure (internal) [Ref. 3]

Years := 40 Number of Operating Years

$I_{lim} := 8000$ Iteration limit for Crack Growth loop

$T_{mm} := 604$ Conservative Operating Temperature for the head, in degrees F. Ref. 4 gives a value of 594.8 deg. F following power uprate.

$\alpha_{0c} := 2.67 \cdot 10^{-12}$ Constant in MRP-55 PWSCC Model for I-600 Wrought @ 617 deg. F [Ref. 9]

$Q_g := 31.0$ Thermal activation Energy for Crack Growth {MRP} [Ref. 9]

$T_{ref} := 617$ Reference Temperature for normalizing Data deg. F [Ref. 9]

$Tim_{opr} := 365.2422 \cdot 24 \cdot \text{Years}$ Numer of operating hours in a year

$CF_{inhr} := 1.417 \cdot 10^5$ Correction factor to convert meters per second to inches per hour

$C_{blk} := \frac{Tim_{opr}}{I_{lim}}$ Calculation block size for the crack growth iteration loop

$C_{blk} = 43.82906$

$Prnt_{blk} := \left\lceil \frac{I_{lim}}{50} \right\rceil$

$C_{01} := e^{\left[\frac{-Q_g}{1.103 \cdot 10^{-3}} \cdot \left(\frac{1}{T+459.67} - \frac{1}{T_{ref}+459.67} \right) \right]} \cdot \alpha_{0c}$ Temperature Correction for Coefficient Alpha from EPRI MRP-55, Revision 1 [Ref. 9]

$C_0 := 1.0C_{01}$ 75th percentile from MRP-55 Revision 1 [Ref. 9]

The flaw model used for a postulated flaw within the counterbore region on the uphill side of the ICI nozzle is an internal surface flaw in a cylinder, subject to an arbitrary stress distribution.

To allow for a "moving average" of through-thickness stress values as the flaw extends along the length of the ICI ID surface, the length from the bottom tip of the of the initial flaw in the blind zone to the stress distribution upper limit--Elev_{Strs.Dist}--is broken into 20 equal segments. Note that due to the MCS used, with a 0 elevation occurring at the TOP of the nozzle, the term "U_{Tip}" (implying the upper tip of the flaw) is actually the physical bottom tip of the flaw, closer to the top of the weld. U_{Tip} is the term used in Reference 7 for the CEDM nozzles, and thus it will continue to be used in the ICI nozzle evaluation.

$$FL_{Cntr} := \begin{cases} Ref_{Point} - c_0 & \text{if Val} = 1 \\ Ref_{Point} & \text{if Val} = 2 \\ Ref_{Point} + c_0 & \text{otherwise} \end{cases} \quad \begin{array}{l} \text{Flaw center Location at the mid-point of} \\ \text{the blind zone region} \end{array}$$

$$U_{Tip} := FL_{Cntr} + c_0$$

$$U_{Tip} = 12.3812$$

$$Inc_{Strs.avg} := \frac{Elev_{Strs.Dist} - U_{Tip}}{20}$$

$$Inc_{Strs.avg} = 0.061$$

No User Input is required beyond this Point

Regression of Through-Thickness Stresses as a Function of Axial Elevation

Because of the minor variation in stresses occurring at the top of the nozzle where it intersects the reactor head and the need to accurately curve fit stresses in the region of interest in the BZ, the entire range of stresses is not appropriate to curve fit. To accommodate an area below and above the BZ region, the first two data points in each of the elevation and stress arrays were removed from consideration in the curve fitting equations. This is a reasonable assumption, given that in the completely through-wall tensile stress field that exists in the nozzle above the top of the J-weld, a flaw centered in the BZ region is likely to grow through the thickness entirely (in addition to growth along the surface of the nozzle) rather than grow very long into an area close to the top of the head or below the top of the J-weld (i.e., elevation ranges not included in the stress polynomial curve fit). Initially, a **fourth (4th)** order polynomial was chosen for axial stress regression. After regression, the stress at the mid-height of the blind zone (12.0812 inches in the MCS) is checked.

Regression for ID stresses:

$k := 0..6$

$$ID_elev_cf := \begin{pmatrix} 8.6999 \\ 10.3745 \\ 11.5527 \\ 12.6463 \\ 12.9649 \\ 13.3752 \\ 13.6012 \end{pmatrix} \quad ID_stress_cf := \begin{pmatrix} 17.412 \\ 17.399 \\ 16.707 \\ 15.065 \\ 19.425 \\ 23.147 \\ 26.39 \end{pmatrix}$$

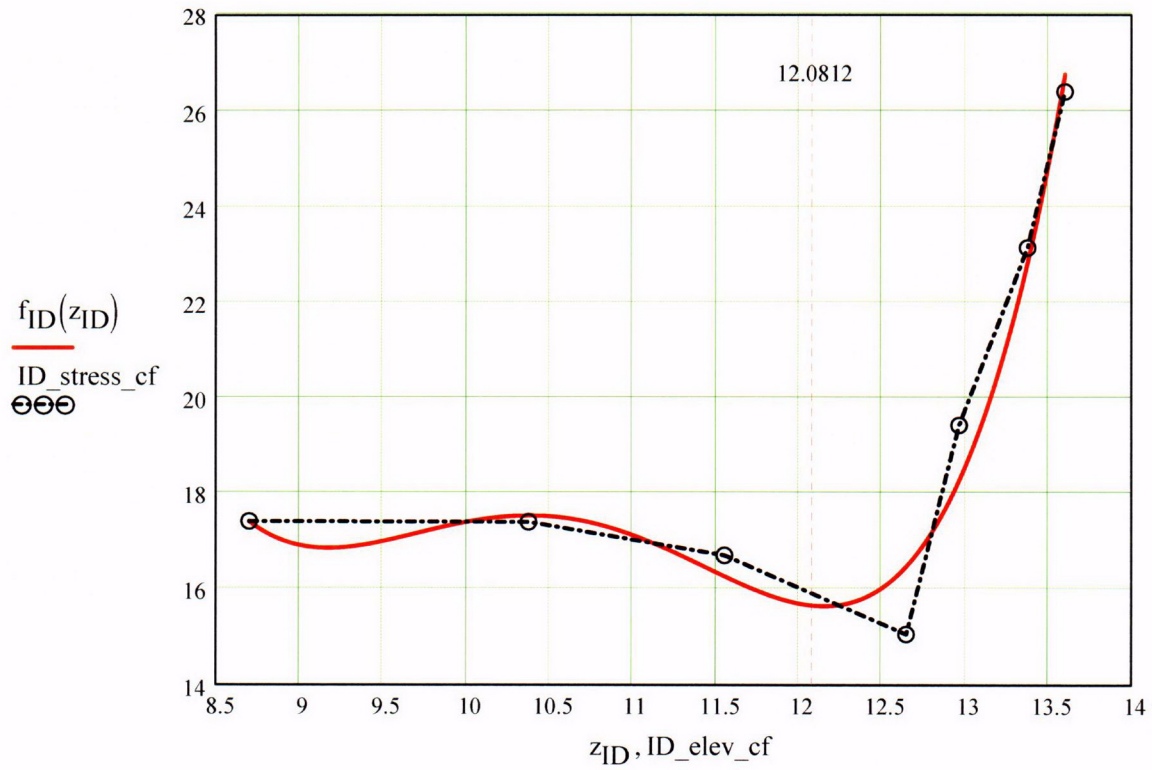
$$R_{ID} := \text{regress}(ID_elev_cf, ID_stress_cf, 4)$$

$$z_{ID} := 8.6999, 8.701.. \text{Top_Jweld}$$

$$R_{ID} = \begin{pmatrix} 3 \\ 3 \\ 4 \\ 2920.01158 \\ -1120.32621 \\ 161.1276 \\ -10.23275 \\ 0.24206 \end{pmatrix}$$

ID_elev _i =	ID_stress _i =
0	10.308
2.9371	15.304
6.3198	17.115
8.6999	17.412
10.3745	17.399
11.5527	16.707
12.6463	15.065
12.9649	19.425
13.3752	23.147
13.6012	26.39

$$f_{ID}(z_{ID}) := \text{interp}(R_{ID}, ID_elev_cf, ID_stress_cf, z_{ID})$$



$$f_{ID}(12.0812) = 15.66367$$

Regression for 25% throughwall stresses:

$$QT_elev_cf := \begin{pmatrix} 8.6999 \\ 10.3745 \\ 11.5527 \\ 12.5802 \\ 12.9649 \\ 13.3752 \\ 13.6012 \end{pmatrix} \quad QT_stress_cf := \begin{pmatrix} 17.487 \\ 17.177 \\ 16.175 \\ 14.581 \\ 18.188 \\ 21.559 \\ 25.687 \end{pmatrix}$$

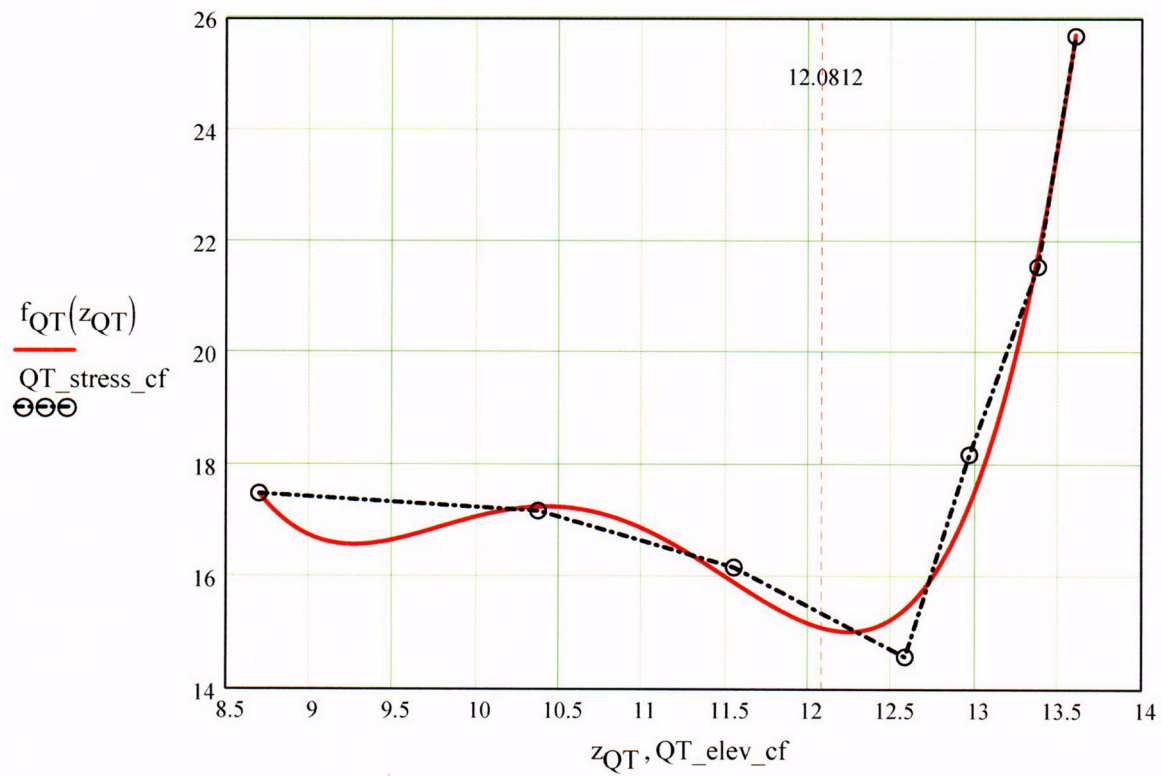
$$R_{QT} := \text{regress}(QT_elev_cf, QT_stress_cf, 4)$$

$$z_{QT} := 8.6999, 8.701 \dots \text{Top_Jweld}$$

$$R_{QT} = \begin{pmatrix} 3 \\ 3 \\ 4 \\ 3362.70255 \\ -1281.45936 \\ 182.93207 \\ -11.53275 \\ 0.27085 \end{pmatrix}$$

QT_elev _i =	QT_stress _i =
0	10.119
2.9371	13.024
6.3198	15.794
8.6999	17.487
10.3745	17.177
11.5527	16.175
12.5802	14.581
12.9649	18.188
13.3752	21.559
13.6012	25.687

$$f_{QT}(z_{QT}) := \text{interp}(R_{QT}, QT_elev_cf, QT_stress_cf, z_{QT})$$



$$f_{QT}(12.0812) = 15.09487$$

C08

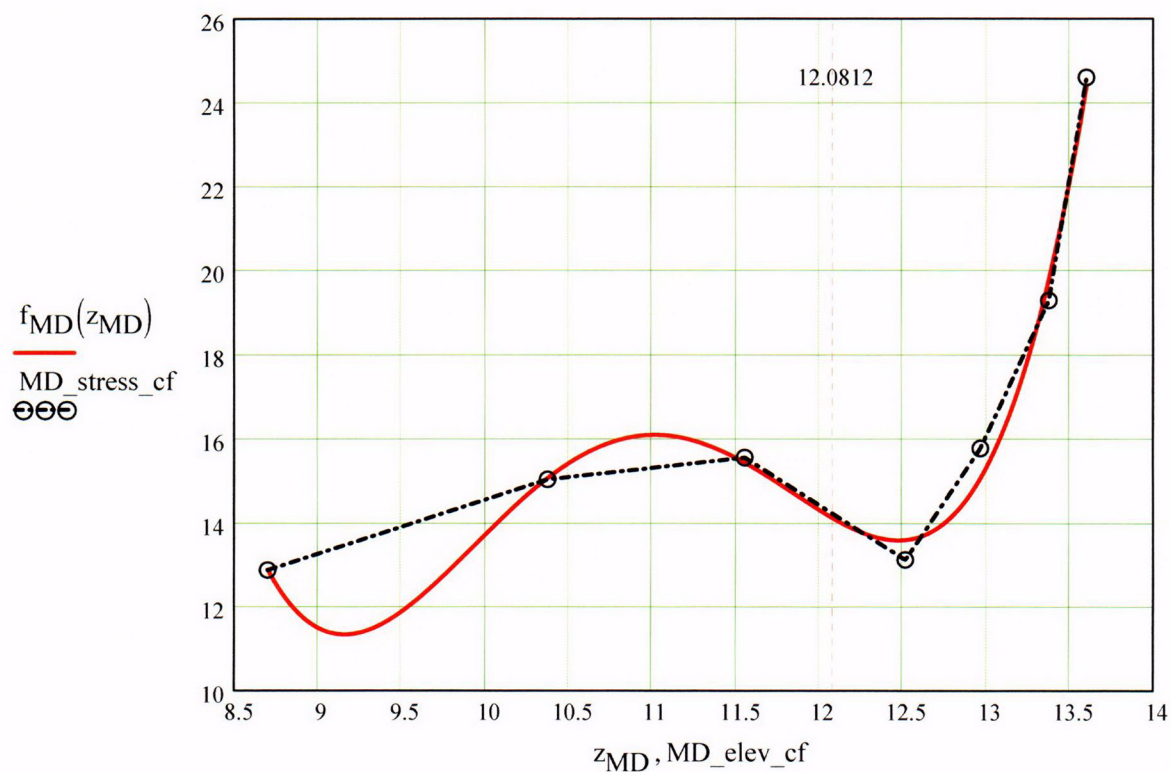
Regression for 50% throughwall stresses:

$$\text{MD_elev_cf} := \begin{pmatrix} 8.6999 \\ 10.3745 \\ 11.5527 \\ 12.514 \\ 12.9649 \\ 13.3752 \\ 13.6012 \end{pmatrix} \quad \text{MD_stress_cf} := \begin{pmatrix} 12.883 \\ 15.044 \\ 15.56 \\ 13.132 \\ 15.78 \\ 19.292 \\ 24.607 \end{pmatrix}$$

$$\begin{aligned} R_{\text{MD}} &:= \text{regress}(\text{MD_elev_cf}, \text{MD_stress_cf}, 4) \\ z_{\text{MD}} &:= 8.6999, 8.701 \dots \text{Top_Jweld} \end{aligned} \quad R_{\text{MD}} = \begin{pmatrix} 3 \\ 3 \\ 4 \\ 6270.57353 \\ -2357.44561 \\ 330.23769 \\ -20.39106 \\ 0.46849 \end{pmatrix}$$

MD_elev _i	MD_stress _i
0	10.032
2.9371	10.766
6.3198	11.377
8.6999	12.883
10.3745	15.044
11.5527	15.56
12.514	13.132
12.9649	15.78
13.3752	19.292
13.6012	24.607

$$f_{\text{MD}}(z_{\text{MD}}) := \text{interp}(R_{\text{MD}}, \text{MD_elev_cf}, \text{MD_stress_cf}, z_{\text{MD}})$$



$$f_{MD}(12.0812) = 14.11569$$

Regression for 75% throughwall stresses:

$$TQ_elev_cf := \begin{pmatrix} 8.6999 \\ 10.3745 \\ 11.5527 \\ 12.4478 \\ 12.9649 \\ 13.3752 \\ 13.6012 \end{pmatrix}$$

$$TQ_stress_cf := \begin{pmatrix} 7.18 \\ 8.136 \\ 8.89 \\ 6.189 \\ 11.381 \\ 16.085 \\ 22.68 \end{pmatrix}$$

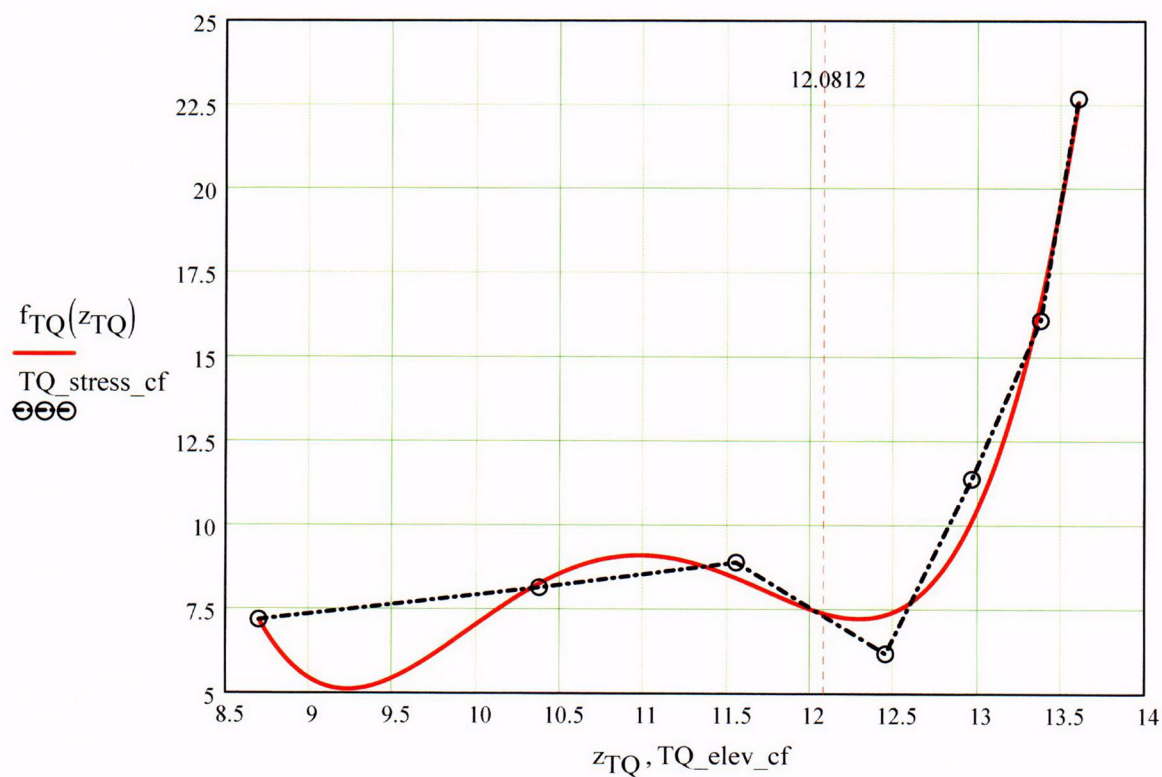
$$R_{TQ} := \text{regress}(TQ_elev_cf, TQ_stress_cf, 4)$$

$$z_{TQ} := 8.6999, 8.701 \dots \text{Top_Jweld}$$

$$R_{TQ} = \begin{pmatrix} 3 \\ 3 \\ 4 \\ 6772.44513 \\ -2552.34739 \\ 358.42617 \\ -22.21167 \\ 0.51271 \end{pmatrix}$$

$TQ_elev_i =$	$TQ_stress_i =$
0	9.951
2.9371	9.067
6.3198	7.821
8.6999	7.18
10.3745	8.136
11.5527	8.89
12.4478	6.189
12.9649	11.381
13.3752	16.085
13.6012	22.68

$$f_{TQ}(z_{TQ}) := \text{interp}(R_{TQ}, TQ_elev_cf, TQ_stress_cf, z_{TQ})$$



$$f_{TQ}(12.0812) = 7.37343$$

Regression for OD stresses:

kk := 0..5

$$\text{OD_elev_cf} := \begin{pmatrix} 10.3745 \\ 11.5527 \\ 12.3816 \\ 12.9649 \\ 13.3752 \\ 13.6012 \end{pmatrix} \quad \text{OD_stress_cf} := \begin{pmatrix} 2.316 \\ 2.74 \\ -0.109 \\ 8.207 \\ 9.729 \\ 44.523 \end{pmatrix}$$

$R_{OD} := \text{regress}(\text{OD_elev_cf}, \text{OD_stress_cf}, 4$

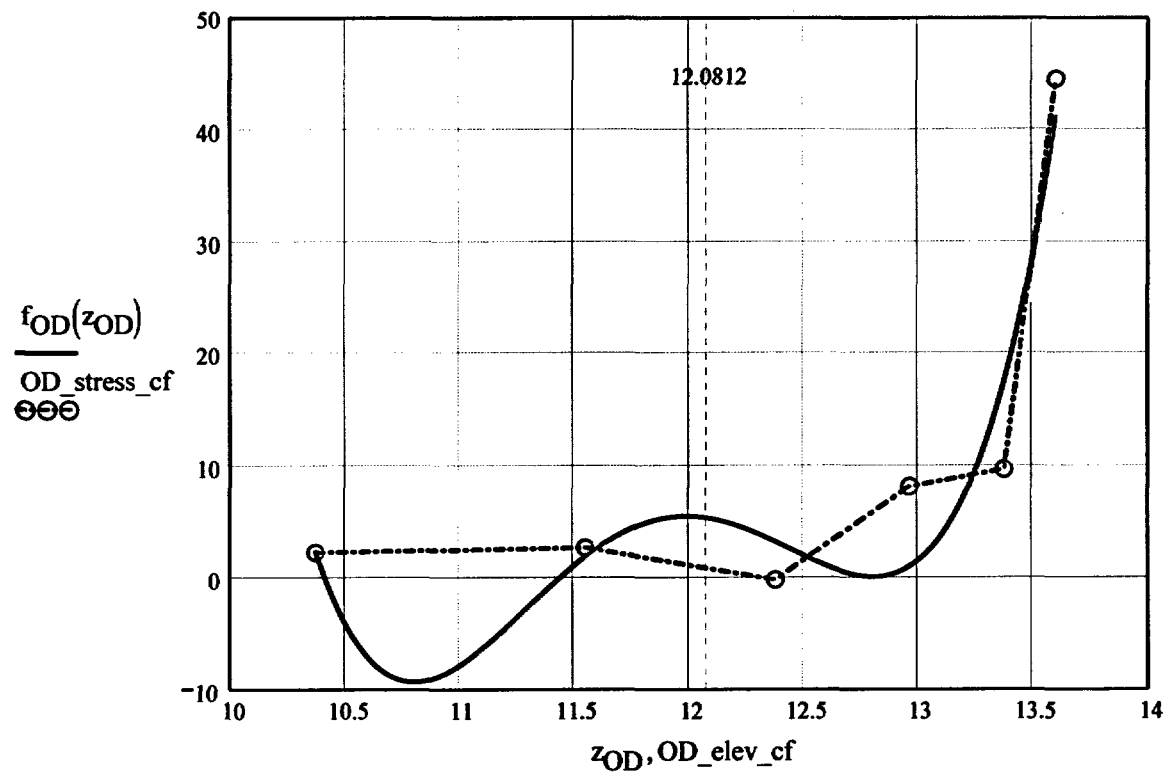
$z_{OD} := 10.3745, 10.376 \dots \text{Top_Jweld}$

$$R_{OD} = \begin{pmatrix} 3 \\ 3 \\ 4 \\ 1.83727 \times 10^5 \\ -62394.03658 \\ 7925.4618 \\ -446.31291 \\ 9.40247 \end{pmatrix}$$

OD_elev_i = OD_stress_i =

OD_elev _i	OD_stress _i
0	9.936
2.9371	7.453
6.3198	4.387
8.6999	2.298
10.3745	2.316
11.5527	2.74
12.3816	-0.109
12.9649	8.207
13.3752	9.729
13.6012	44.523

$f_{OD}(z_{OD}) := \text{interp}(R_{OD}, \text{OD_elev_cf}, \text{OD_stress_cf}, z_{OD})$



$$f_{OD}(12.0812) = 5.39079$$

Calculation to develop Stress Profiles for Analysis

This analysis for the axial stress regression and the through-wall stress regression is the same as that used for the CEDM Nozzles (in Ref. 7) with the exception that the axial stresses are fit with a fourth-order polynomial, rather than a third-order polynomial, to accommodate greater precision.

$$N_{\text{ww}} := 20 \quad \text{Number of locations for stress profiles}$$

$$\text{Loc}_0 := \text{FL}_{\text{Cntr}} - L$$

$$\text{FL}_{\text{Cntr}} = 12.0812$$

$$L = 0.6$$

$$i := 1..N + 3$$

$$\text{Incr}_i := \begin{cases} c_0 & \text{if } i < 4 \\ \text{IncStrs.avg} & \text{otherwise} \end{cases}$$

$$\text{Loc}_i := \text{Loc}_{i-1} + \text{Incr}_i$$

$$\text{SID}_i := R_{\text{ID}_3} + R_{\text{ID}_4} \cdot \text{Loc}_i + R_{\text{ID}_5} \cdot (\text{Loc}_i)^2 + R_{\text{ID}_6} \cdot (\text{Loc}_i)^3 + R_{\text{ID}_7} \cdot (\text{Loc}_i)^4$$

$$\text{SQT}_i := R_{\text{QT}_3} + R_{\text{QT}_4} \cdot \text{Loc}_i + R_{\text{QT}_5} \cdot (\text{Loc}_i)^2 + R_{\text{QT}_6} \cdot (\text{Loc}_i)^3 + R_{\text{QT}_7} \cdot (\text{Loc}_i)^4$$

$$\text{SMD}_i := R_{\text{MD}_3} + R_{\text{MD}_4} \cdot \text{Loc}_i + R_{\text{MD}_5} \cdot (\text{Loc}_i)^2 + R_{\text{MD}_6} \cdot (\text{Loc}_i)^3 + R_{\text{MD}_7} \cdot (\text{Loc}_i)^4$$

$$\text{STQ}_i := R_{\text{TQ}_3} + R_{\text{TQ}_4} \cdot \text{Loc}_i + R_{\text{TQ}_5} \cdot (\text{Loc}_i)^2 + R_{\text{TQ}_6} \cdot (\text{Loc}_i)^3 + R_{\text{TQ}_7} \cdot (\text{Loc}_i)^4$$

$$\text{SOD}_i := R_{\text{OD}_3} + R_{\text{OD}_4} \cdot \text{Loc}_i + R_{\text{OD}_5} \cdot (\text{Loc}_i)^2 + R_{\text{OD}_6} \cdot (\text{Loc}_i)^3 + R_{\text{OD}_7} \cdot (\text{Loc}_i)^4$$

$$j := 1..N$$

$$S_{\text{id}_j} := \begin{cases} \frac{\text{SID}_j + \text{SID}_{j+1} + \text{SID}_{j+2}}{3} & \text{if } j = 1 \\ \frac{S_{\text{id}_{j-1}} \cdot (j+1) + \text{SID}_{j+2}}{j+2} & \text{otherwise} \end{cases}$$

$$S_{\text{qt}_j} := \begin{cases} \frac{\text{SQT}_j + \text{SQT}_{j+1} + \text{SQT}_{j+2}}{3} & \text{if } j = 1 \\ \frac{S_{\text{qt}_{j-1}} \cdot (j+1) + \text{SQT}_{j+2}}{j+2} & \text{otherwise} \end{cases}$$

$$S_{md_j} := \begin{cases} \frac{SMD_j + SMD_{j+1} + SMD_{j+2}}{3} & \text{if } j = 1 \\ \frac{S_{md_{j-1}} \cdot (j+1) + SMD_{j+2}}{j+2} & \text{otherwise} \end{cases}$$

$$S_{tq_j} := \begin{cases} \frac{STQ_j + STQ_{j+1} + STQ_{j+2}}{3} & \text{if } j = 1 \\ \frac{S_{tq_{j-1}} \cdot (j+1) + STQ_{j+2}}{j+2} & \text{otherwise} \end{cases}$$

$$S_{od_j} := \begin{cases} \frac{SOD_j + SOD_{j+1} + SOD_{j+2}}{3} & \text{if } j = 1 \\ \frac{S_{od_{j-1}} \cdot (j+1) + SOD_{j+2}}{j+2} & \text{otherwise} \end{cases}$$

Through-Wall Stress Distribution for ID Flaws (i.e. ID to OD Stress distribution)

$$u_0 := 0.000$$

$$u_1 := 0.25$$

$$u_2 := 0.50$$

$$u_3 := 0.75$$

$$u_4 := 1.00$$

$$Y := \text{stack}(u_0, u_1, u_2, u_3, u_4)$$

$$\text{SIG}_1 := \text{stack}(S_{id_1}, S_{qt_1}, S_{md_1}, S_{tq_1}, S_{od_1})$$

$$\text{SIG}_2 := \text{stack}(S_{id_2}, S_{qt_2}, S_{md_2}, S_{tq_2}, S_{od_2})$$

$$\text{SIG}_3 := \text{stack}(S_{id_3}, S_{qt_3}, S_{md_3}, S_{tq_3}, S_{od_3})$$

$$\text{SIG}_4 := \text{stack}(S_{id_4}, S_{qt_4}, S_{md_4}, S_{tq_4}, S_{od_4})$$

$$\text{SIG}_5 := \text{stack}(S_{id_5}, S_{qt_5}, S_{md_5}, S_{tq_5}, S_{od_5})$$

$$\text{SIG}_6 := \text{stack}(S_{id_6}, S_{qt_6}, S_{md_6}, S_{tq_6}, S_{od_6})$$

$$\text{SIG}_7 := \text{stack}(S_{id_7}, S_{qt_7}, S_{md_7}, S_{tq_7}, S_{od_7})$$

$$\text{SIG}_8 := \text{stack}(S_{id_8}, S_{qt_8}, S_{md_8}, S_{tq_8}, S_{od_8})$$

$$\text{SIG}_9 := \text{stack}(S_{id_9}, S_{qt_9}, S_{md_9}, S_{tq_9}, S_{od_9})$$

$$\text{SIG}_{10} := \text{stack}(S_{id_{10}}, S_{qt_{10}}, S_{md_{10}}, S_{tq_{10}}, S_{od_{10}})$$

$$\text{SIG}_{11} := \text{stack}(S_{id_{11}}, S_{qt_{11}}, S_{md_{11}}, S_{tq_{11}}, S_{od_{11}})$$

$$\text{SIG}_{12} := \text{stack}(S_{id_{12}}, S_{qt_{12}}, S_{md_{12}}, S_{tq_{12}}, S_{od_{12}})$$

$$\text{SIG}_{13} := \text{stack}(S_{id_{13}}, S_{qt_{13}}, S_{md_{13}}, S_{tq_{13}}, S_{od_{13}})$$

$$\text{SIG}_{14} := \text{stack}(S_{id_{14}}, S_{qt_{14}}, S_{md_{14}}, S_{tq_{14}}, S_{od_{14}})$$

$$\text{SIG}_{15} := \text{stack}(S_{id_{15}}, S_{qt_{15}}, S_{md_{15}}, S_{tq_{15}}, S_{od_{15}})$$

$$\text{SIG}_{16} := \text{stack}(S_{id_{16}}, S_{qt_{16}}, S_{md_{16}}, S_{tq_{16}}, S_{od_{16}})$$

$$\text{SIG}_{17} := \text{stack}(S_{id_{17}}, S_{qt_{17}}, S_{md_{17}}, S_{tq_{17}}, S_{od_{17}})$$

$$\text{SIG}_{18} := \text{stack}(S_{id_{18}}, S_{qt_{18}}, S_{md_{18}}, S_{tq_{18}}, S_{od_{18}})$$

$$\text{SIG}_{19} := \text{stack}(S_{id_{19}}, S_{qt_{19}}, S_{md_{19}}, S_{tq_{19}}, S_{od_{19}})$$

$$\text{SIG}_{20} := \text{stack}(S_{id_{20}}, S_{qt_{20}}, S_{md_{20}}, S_{tq_{20}}, S_{od_{20}})$$

Regression of Through-Wall Stress distribution to Obtain Stress Coefficients Using a Third Order Polynomial

$$\text{IDRG}_1 := \text{regress}(Y, \text{SIG}_1, 3)$$

$$\text{IDRG}_2 := \text{regress}(Y, \text{SIG}_2, 3)$$

$$\text{IDRG}_3 := \text{regress}(Y, \text{SIG}_3, 3)$$

$$\text{IDRG}_4 := \text{regress}(Y, \text{SIG}_4, 3)$$

$$\text{IDRG}_5 := \text{regress}(Y, \text{SIG}_5, 3)$$

$$\text{IDRG}_6 := \text{regress}(Y, \text{SIG}_6, 3)$$

$$\text{IDRG}_7 := \text{regress}(Y, \text{SIG}_7, 3)$$

$$\text{IDRG}_8 := \text{regress}(Y, \text{SIG}_8, 3)$$

$$\text{IDRG}_9 := \text{regress}(Y, \text{SIG}_9, 3)$$

$$\text{IDRG}_{10} := \text{regress}(Y, \text{SIG}_{10}, 3)$$

$$\text{IDRG}_{11} := \text{regress}(Y, \text{SIG}_{11}, 3)$$

$$\text{IDRG}_{12} := \text{regress}(Y, \text{SIG}_{12}, 3)$$

$$\text{IDRG}_{13} := \text{regress}(Y, \text{SIG}_{13}, 3)$$

$$\text{IDRG}_{14} := \text{regress}(Y, \text{SIG}_{14}, 3)$$

$$\text{IDRG}_{15} := \text{regress}(Y, \text{SIG}_{15}, 3)$$

$$\text{IDRG}_{16} := \text{regress}(Y, \text{SIG}_{16}, 3)$$

$$\text{IDRG}_{17} := \text{regress}(Y, \text{SIG}_{17}, 3)$$

$$\text{IDRG}_{18} := \text{regress}(Y, \text{SIG}_{18}, 3)$$

$$\text{IDRG}_{19} := \text{regress}(Y, \text{SIG}_{19}, 3)$$

$$\text{IDRG}_{20} := \text{regress}(Y, \text{SIG}_{20}, 3)$$

**Stress Distribution in the tube. Stress influence coefficients obtained from
thrid-order polynomial curve fit to the throughwall stress distribution**

Data Files for Flaw Shape Factors from NASA SC04 Model [Ref. 8]

{NO INPUT Required}

**Mettu Raju Newman Sivakumar Forman Solution of ID Part throughwall
Flaw in Cyinder**

Jsb :=

	0	1	2
0	1.000	0.200	0.000
1	1.000	0.200	0.200
2	1.000	0.200	0.500
3	1.000	0.200	0.800
4	1.000	0.200	1.000
5	1.000	0.400	0.000
6	1.000	0.400	0.200
7	1.000	0.400	0.500
8	1.000	0.400	0.800
9	1.000	0.400	1.000
10	1.000	1.000	0.000
11	1.000	1.000	0.200
12	1.000	1.000	0.500
13	1.000	1.000	0.800
14	1.000	1.000	1.000
15	2.000	0.200	0.000
16	2.000	0.200	0.200
17	2.000	0.200	0.500
18	2.000	0.200	0.800
19	2.000	0.200	1.000
20	2.000	0.400	0.000
21	2.000	0.400	0.200
22	2.000	0.400	0.500
23	2.000	0.400	0.800
24	2.000	0.400	1.000
25	2.000	1.000	0.000
26	2.000	1.000	0.200
27	2.000	1.000	0.500
28	2.000	1.000	0.800
29	2.000	1.000	1.000
30	4.000	0.200	0.000
31	4.000	0.200	0.200
32	4.000	0.200	0.500
33	4.000	0.200	0.800

34	4.000	0.200	1.000
35	4.000	0.400	0.000
36	4.000	0.400	0.200
37	4.000	0.400	0.500
38	4.000	0.400	0.800
39	4.000	0.400	1.000
40	4.000	1.000	0.000
41	4.000	1.000	0.200
42	4.000	1.000	0.500
43	4.000	1.000	0.800
44	4.000	1.000	1.000
45	10.000	0.200	0.000
46	10.000	0.200	0.200
47	10.000	0.200	0.500
48	10.000	0.200	0.800
49	10.000	0.200	1.000
50	10.000	0.400	0.000
51	10.000	0.400	0.200
52	10.000	0.400	0.500
53	10.000	0.400	0.800
54	10.000	0.400	1.000
55	10.000	1.000	0.000
56	10.000	1.000	0.200
57	10.000	1.000	0.500
58	10.000	1.000	0.800
59	10.000	1.000	1.000
60	300.000	0.200	0.000
61	300.000	0.200	0.200
62	300.000	0.200	0.500
63	300.000	0.200	0.800
64	300.000	0.200	1.000
65	300.000	0.400	0.000
66	300.000	0.400	0.200
67	300.000	0.400	0.500
68	300.000	0.400	0.800
69	300.000	0.400	1.000
70	300.000	1.000	0.000
71	300.000	1.000	0.200
72	300.000	1.000	0.500
73	300.000	1.000	0.800
74	300.000	1.000	1.000

Sambi :=

	0	1	2	3	4	5	6	7
0	1.076	0.693	0.531	0.434	0.608	0.083	0.023	0.009
1	1.056	0.647	0.495	0.408	0.615	0.085	0.027	0.013
2	1.395	0.767	0.557	0.446	0.871	0.171	0.069	0.038
3	2.53	1.174	0.772	0.58	1.554	0.363	0.155	0.085
4	3.846	1.615	0.995	0.716	2.277	0.544	0.233	0.127
5	1.051	0.689	0.536	0.444	0.74	0.112	0.035	0.015
6	1.011	0.646	0.504	0.421	0.745	0.119	0.041	0.02
7	1.149	0.694	0.529	0.435	0.916	0.181	0.073	0.04
8	1.6	0.889	0.642	0.51	1.334	0.307	0.132	0.073
9	2.087	1.093	0.761	0.589	1.752	0.421	0.183	0.101
10	0.992	0.704	0.534	0.506	1.044	0.169	0.064	0.032
11	0.987	0.701	0.554	0.491	1.08	0.182	0.067	0.034
12	1.01	0.709	0.577	0.493	1.116	0.2	0.078	0.041
13	1.07	0.73	0.623	0.523	1.132	0.218	0.095	0.051
14	1.128	0.75	0.675	0.556	1.131	0.229	0.11	0.06
15	1.049	0.673	0.519	0.427	0.6	0.078	0.021	0.008
16	1.091	0.661	0.502	0.413	0.614	0.083	0.025	0.012
17	1.384	0.764	0.556	0.446	0.817	0.15	0.058	0.031
18	2.059	1.033	0.708	0.545	1.3	0.291	0.123	0.067
19	2.739	1.301	0.858	0.643	1.783	0.421	0.18	0.099
20	1.075	0.674	0.527	0.436	0.73	0.072	0.044	0.021
21	1.045	0.659	0.511	0.425	0.76	0.122	0.043	0.021
22	1.16	0.71	0.536	0.441	0.919	0.197	0.064	0.034
23	1.51	0.854	0.623	0.498	1.231	0.271	0.114	0.062
24	1.876	0.995	0.71	0.555	1.519	0.317	0.161	0.089
25	1.037	0.732	0.594	0.505	1.132	0.192	0.07	0.035
26	1.003	0.707	0.577	0.493	1.113	0.19	0.071	0.036
27	1.023	0.714	0.58	0.495	1.155	0.207	0.08	0.042
28	1.129	0.774	0.619	0.521	1.286	0.247	0.098	0.052
29	1.242	0.84	0.661	0.549	1.416	0.285	0.115	0.061
30	1.003	0.649	0.511	0.43	0.577	0.07	0.015	0.005
31	1.097	0.666	0.511	0.426	0.606	0.079	0.023	0.01
32	1.405	0.776	0.567	0.46	0.797	0.141	0.054	0.028
33	1.959	0.996	0.692	0.542	1.201	0.262	0.108	0.059
34	2.461	1.197	0.808	0.619	1.586	0.37	0.154	0.085
35	1.024	0.668	0.528	0.451	0.737	0.11	0.033	0.015
36	1.057	0.666	0.52	0.439	0.77	0.123	0.042	0.021
37	1.193	0.715	0.545	0.454	0.924	0.174	0.068	0.036
38	1.443	0.828	0.614	0.509	1.219	0.263	0.109	0.059
39	1.665	0.934	0.681	0.565	1.487	0.339	0.143	0.078
40	1.005	0.72	0.597	0.518	1.119	0.188	0.068	0.034

	1.000	0.712	0.588	0.511	1.128	0.194	0.072	0.037
41	1.009	0.713	0.588	0.511	1.128	0.194	0.072	0.037
42	1.041	0.726	0.594	0.515	1.191	0.214	0.082	0.043
43	1.105	0.768	0.623	0.536	1.316	0.248	0.097	0.05
44	1.162	0.81	0.653	0.558	1.428	0.277	0.109	0.055
45	0.973	0.635	0.499	0.446	0.579	0.07	0.016	0.005
46	1.115	0.673	0.514	0.438	0.607	0.079	0.023	0.01
47	1.427	0.783	0.571	0.462	0.791	0.138	0.052	0.027
48	1.872	0.96	0.671	0.529	1.179	0.253	0.104	0.056
49	2.23	1.108	0.757	0.594	1.548	0.356	0.149	0.081
50	0.992	0.656	0.52	0.443	0.733	0.109	0.032	0.014
51	1.072	0.672	0.523	0.441	0.777	0.125	0.043	0.021
52	1.217	0.723	0.549	0.456	0.936	0.176	0.069	0.036
53	1.393	0.806	0.601	0.493	1.219	0.259	0.106	0.056
54	1.521	0.875	0.647	0.528	1.469	0.328	0.135	0.071
55	0.994	0.715	0.59	0.518	1.114	0.187	0.068	0.035
56	1.015	0.715	0.588	0.512	1.14	0.197	0.074	0.038
57	1.05	0.729	0.596	0.515	1.219	0.221	0.085	0.044
58	1.09	0.76	0.618	0.532	1.348	0.255	0.099	0.051
59	1.118	0.788	0.639	0.55	1.456	0.282	0.109	0.056
60	0.936	0.62	0.486	0.405	0.582	0.068	0.015	0.005
61	1.145	0.681	0.514	0.42	0.613	0.081	0.024	0.011
62	1.459	0.79	0.569	0.454	0.79	0.138	0.051	0.026
63	1.774	0.917	0.641	0.501	1.148	0.239	0.096	0.051
64	1.974	1.008	0.696	0.537	1.482	0.328	0.134	0.07
65	0.982	0.651	0.512	0.427	0.721	0.103	0.031	0.013
66	1.095	0.677	0.52	0.431	0.782	0.127	0.045	0.022
67	1.244	0.727	0.546	0.446	0.946	0.18	0.071	0.037
68	1.37	0.791	0.585	0.473	1.201	0.253	0.102	0.054
69	1.438	0.838	0.618	0.496	1.413	0.31	0.126	0.066

$$W := \text{Jsb}^{(0)}$$

$$X := \text{Jsb}^{(1)}$$

$$Y := \text{Jsb}^{(2)}$$

$$a_U := \text{Sambi}^{(0)}$$

$$a_L := \text{Sambi}^{(1)}$$

$$a_Q := \text{Sambi}^{(2)}$$

$$a_C := \text{Sambi}^{(3)}$$

$$c_U := \text{Sambi}^{(4)}$$

$$c_L := \text{Sambi}^{(5)}$$

$$c_Q := \text{Sambi}^{(6)}$$

$$c_C := \text{Sambi}^{(7)}$$

$$n := \begin{cases} 3 & \text{if } R_t \leq 4.0 \\ 2 & \text{otherwise} \end{cases}$$

"a-Tip" Uniform Term

$$M_{aU} := \text{augment}(W, X, Y) \quad V_{aU} := a_U \quad R_{aU} := \text{regress}(M_{aU}, V_{aU}, n)$$

$$f_{aU}(W, X, Y) := \text{interp} \left[R_{aU}, M_{aU}, V_{aU}, \begin{pmatrix} W \\ X \\ Y \end{pmatrix} \right]$$

$$f_{aU}(4, .4, .8) = 1.7089$$

Check Calculation

Linear Term

$$M_{aL} := \text{augment}(W, X, Y) \quad V_{aL} := a_L \quad R_{aL} := \text{regress}(M_{aL}, V_{aL}, n)$$

$$f_{aL}(W, X, Y) := \text{interp} \left[R_{aL}, M_{aL}, V_{aL}, \begin{pmatrix} W \\ X \\ Y \end{pmatrix} \right]$$

$$f_{aL}(4, .4, .8) = 0.93393$$

Check Calculation

Quadratic Term

$$M_{aQ} := \text{augment}(W, X, Y) \quad V_{aQ} := a_Q \quad R_{aQ} := \text{regress}(M_{aQ}, V_{aQ}, n)$$

$$f_{aQ}(W, X, Y) := \text{interp} \left[R_{aQ}, M_{aQ}, V_{aQ}, \begin{pmatrix} W \\ X \\ Y \end{pmatrix} \right]$$

$$f_{aQ}(4, .4, .8) = 0.67668 \quad \text{Check Calculation}$$

Cubic Term

$$M_{aC} := \text{augment}(W, X, Y) \quad V_{aC} := a_C$$

$$R_{aC} := \text{regress}(M_{aC}, V_{aC}, n)$$

$$f_{aC}(W, X, Y) := \text{interp} \left[R_{aC}, M_{aC}, V_{aC}, \begin{pmatrix} W \\ X \\ Y \end{pmatrix} \right]$$

$$f_{aC}(4, .4, .8) = 0.54151 \quad \text{Check Calculation}$$

"C" Tip Coefficients

Uniform Term

$$M_{cU} := \text{augment}(W, X, Y) \quad V_{cU} := c_U$$

$$R_{cU} := \text{regress}(M_{cU}, V_{cU}, n)$$

$$f_{cU}(W, X, Y) := \text{interp} \left[R_{cU}, M_{cU}, V_{cU}, \begin{pmatrix} W \\ X \\ Y \end{pmatrix} \right]$$

$$f_{cU}(4, .4, .8) = 1.31015 \quad \text{Check Calculation}$$

Linear Term

$$M_{cL} := \text{augment}(W, X, Y) \quad V_{cL} := c_L$$

$$R_{cL} := \text{regress}(M_{cL}, V_{cL}, n)$$

$$f_{cL}(W, X, Y) := \text{interp} \left[R_{cL}, M_{cL}, V_{cL}, \begin{pmatrix} W \\ X \\ Y \end{pmatrix} \right]$$

$$f_{cL}(2, .4, .8) = 0.28509 \quad \text{Check Calculation}$$

Quadratic Term

$$M_{cQ} := \text{augment}(W, X, Y) \quad V_{cQ} := c_Q \quad R_{cQ} := \text{regress}(M_{cQ}, V_{cQ}, n)$$

$$f_{cQ}(W, X, Y) := \text{interp} \left[R_{cQ}, M_{cQ}, V_{cQ}, \begin{pmatrix} W \\ X \\ Y \end{pmatrix} \right]$$

$$f_{cQ}(4, .4, .8) = 0.11797 \quad \text{Check Calculation}$$

Cubic Term

$$M_{cC} := \text{augment}(W, X, Y) \quad V_{cC} := c_C \quad R_{cC} := \text{regress}(M_{cC}, V_{cC}, n)$$

$$f_{cC}(W, X, Y) := \text{interp} \left[R_{cC}, M_{cC}, V_{cC}, \begin{pmatrix} W \\ X \\ Y \end{pmatrix} \right]$$

$$f_{cC}(4, .4, .8) = 0.06384 \quad \text{Check Calculation}$$

Calculations : Recursive calculations to estimate flaw growth

Recursive Loop for Calculation of PWSCC Crack Growth

```

CGRsambi := | j ← 0
              | a0 ← a0
              | c0 ← c0
              | t ← t2
              | NCB0 ← Cblk
              | while j ≤ Ilim
                |   | σ0 ← | IDRG13 if cj ≤ c0
                |   |      | IDRG23 if c0 < cj ≤ c0 + IncStrs.avg
                |   |      | IDRG33 if c0 + IncStrs.avg < cj ≤ c0 + 2·IncStrs.avg
                |   |      | IDRG43 if c0 + 2·IncStrs.avg < cj ≤ c0 + 3·IncStrs.avg
                |   |      | IDRG53 if c0 + 3·IncStrs.avg < cj ≤ c0 + 4·IncStrs.avg
                |   |      | IDRG63 if c0 + 4·IncStrs.avg < cj ≤ c0 + 5·IncStrs.avg
                |   |      | IDRG73 if c0 + 5·IncStrs.avg < cj ≤ c0 + 6·IncStrs.avg
                |   |      | IDRG83 if c0 + 6·IncStrs.avg < cj ≤ c0 + 7·IncStrs.avg
                |   |      | IDRG93 if c0 + 7·IncStrs.avg < cj ≤ c0 + 8·IncStrs.avg
                |   |      | IDRG103 if c0 + 8·IncStrs.avg < cj ≤ c0 + 9·IncStrs.avg
                |   |      | IDRG113 if c0 + 9·IncStrs.avg < cj ≤ c0 + 10·IncStrs.avg
                |   |      | IDRG123 if c0 + 10·IncStrs.avg < cj ≤ c0 + 11·IncStrs.avg
                |   |      | IDRG133 if c0 + 11·IncStrs.avg < cj ≤ c0 + 12·IncStrs.avg
                |   |      | IDRG143 if c0 + 12·IncStrs.avg < cj ≤ c0 + 13·IncStrs.avg
                |   |      | IDRG153 if c0 + 13·IncStrs.avg < cj ≤ c0 + 14·IncStrs.avg

```


	IDRG _{16₃} if $c_0 + 14 \cdot \text{IncStrs.avg} < c_j \leq c_0 + 15 \cdot \text{IncStrs.avg}$
	IDRG _{17₃} if $c_0 + 15 \cdot \text{IncStrs.avg} < c_j \leq c_0 + 16 \cdot \text{IncStrs.avg}$
	IDRG _{18₃} if $c_0 + 16 \cdot \text{IncStrs.avg} < c_j \leq c_0 + 17 \cdot \text{IncStrs.avg}$
	IDRG _{19₃} if $c_0 + 17 \cdot \text{IncStrs.avg} < c_j \leq c_0 + 18 \cdot \text{IncStrs.avg}$
	IDRG _{20₃} otherwise
$\sigma_1 \leftarrow$	IDRG _{1₄} if $c_j \leq c_0$
	IDRG _{2₄} if $c_0 < c_j \leq c_0 + \text{IncStrs.avg}$
	IDRG _{3₄} if $c_0 + \text{IncStrs.avg} < c_j \leq c_0 + 2 \cdot \text{IncStrs.avg}$
	IDRG _{4₄} if $c_0 + 2 \cdot \text{IncStrs.avg} < c_j \leq c_0 + 3 \cdot \text{IncStrs.avg}$
	IDRG _{5₄} if $c_0 + 3 \cdot \text{IncStrs.avg} < c_j \leq c_0 + 4 \cdot \text{IncStrs.avg}$
	IDRG _{6₄} if $c_0 + 4 \cdot \text{IncStrs.avg} < c_j \leq c_0 + 5 \cdot \text{IncStrs.avg}$
	IDRG _{7₄} if $c_0 + 5 \cdot \text{IncStrs.avg} < c_j \leq c_0 + 6 \cdot \text{IncStrs.avg}$
	IDRG _{8₄} if $c_0 + 6 \cdot \text{IncStrs.avg} < c_j \leq c_0 + 7 \cdot \text{IncStrs.avg}$
	IDRG _{9₄} if $c_0 + 7 \cdot \text{IncStrs.avg} < c_j \leq c_0 + 8 \cdot \text{IncStrs.avg}$
	IDRG _{10₄} if $c_0 + 8 \cdot \text{IncStrs.avg} < c_j \leq c_0 + 9 \cdot \text{IncStrs.avg}$
	IDRG _{11₄} if $c_0 + 9 \cdot \text{IncStrs.avg} < c_j \leq c_0 + 10 \cdot \text{IncStrs.avg}$
	IDRG _{12₄} if $c_0 + 10 \cdot \text{IncStrs.avg} < c_j \leq c_0 + 11 \cdot \text{IncStrs.avg}$
	IDRG _{13₄} if $c_0 + 11 \cdot \text{IncStrs.avg} < c_j \leq c_0 + 12 \cdot \text{IncStrs.avg}$
	IDRG _{14₄} if $c_0 + 12 \cdot \text{IncStrs.avg} < c_j \leq c_0 + 13 \cdot \text{IncStrs.avg}$
	IDRG _{15₄} if $c_0 + 13 \cdot \text{IncStrs.avg} < c_j \leq c_0 + 14 \cdot \text{IncStrs.avg}$
	IDRG _{16₄} if $c_0 + 14 \cdot \text{IncStrs.avg} < c_j \leq c_0 + 15 \cdot \text{IncStrs.avg}$

	IDRG ₁₇ ₄	if $c_0 + 15 \cdot \text{IncStrs.avg} < c_j \leq c_0 + 16 \cdot \text{IncStrs.avg}$
	IDRG ₁₈ ₄	if $c_0 + 16 \cdot \text{IncStrs.avg} < c_j \leq c_0 + 17 \cdot \text{IncStrs.avg}$
	IDRG ₁₉ ₄	if $c_0 + 17 \cdot \text{IncStrs.avg} < c_j \leq c_0 + 18 \cdot \text{IncStrs.avg}$
	IDRG ₂₀ ₄	otherwise
$\sigma_2 \leftarrow$	IDRG ₁ ₅	if $c_j \leq c_0$
	IDRG ₂ ₅	if $c_0 < c_j \leq c_0 + \text{IncStrs.avg}$
	IDRG ₃ ₅	if $c_0 + \text{IncStrs.avg} < c_j \leq c_0 + 2 \cdot \text{IncStrs.avg}$
	IDRG ₄ ₅	if $c_0 + 2 \cdot \text{IncStrs.avg} < c_j \leq c_0 + 3 \cdot \text{IncStrs.avg}$
	IDRG ₅ ₅	if $c_0 + 3 \cdot \text{IncStrs.avg} < c_j \leq c_0 + 4 \cdot \text{IncStrs.avg}$
	IDRG ₆ ₅	if $c_0 + 4 \cdot \text{IncStrs.avg} < c_j \leq c_0 + 5 \cdot \text{IncStrs.avg}$
	IDRG ₇ ₅	if $c_0 + 5 \cdot \text{IncStrs.avg} < c_j \leq c_0 + 6 \cdot \text{IncStrs.avg}$
	IDRG ₈ ₅	if $c_0 + 6 \cdot \text{IncStrs.avg} < c_j \leq c_0 + 7 \cdot \text{IncStrs.avg}$
	IDRG ₉ ₅	if $c_0 + 7 \cdot \text{IncStrs.avg} < c_j \leq c_0 + 8 \cdot \text{IncStrs.avg}$
	IDRG ₁₀ ₅	if $c_0 + 8 \cdot \text{IncStrs.avg} < c_j \leq c_0 + 9 \cdot \text{IncStrs.avg}$
	IDRG ₁₁ ₅	if $c_0 + 9 \cdot \text{IncStrs.avg} < c_j \leq c_0 + 10 \cdot \text{IncStrs.avg}$
	IDRG ₁₂ ₅	if $c_0 + 10 \cdot \text{IncStrs.avg} < c_j \leq c_0 + 11 \cdot \text{IncStrs.avg}$
	IDRG ₁₃ ₅	if $c_0 + 11 \cdot \text{IncStrs.avg} < c_j \leq c_0 + 12 \cdot \text{IncStrs.avg}$
	IDRG ₁₄ ₅	if $c_0 + 12 \cdot \text{IncStrs.avg} < c_j \leq c_0 + 13 \cdot \text{IncStrs.avg}$
	IDRG ₁₅ ₅	if $c_0 + 13 \cdot \text{IncStrs.avg} < c_j \leq c_0 + 14 \cdot \text{IncStrs.avg}$
	IDRG ₁₆ ₅	if $c_0 + 14 \cdot \text{IncStrs.avg} < c_j \leq c_0 + 15 \cdot \text{IncStrs.avg}$
	IDRG ₁₇ ₅	if $c_0 + 15 \cdot \text{IncStrs.avg} < c_j \leq c_0 + 16 \cdot \text{IncStrs.avg}$
	IDRG ₁₈	if $c_0 + 16 \cdot \text{IncStrs.avg} < c_j \leq c_0 + 17 \cdot \text{IncStrs.avg}$

		IDRG_{19_5} if $c_0 + 17 \cdot \text{IncStrs.avg} < c_j \leq c_0 + 18 \cdot \text{IncStrs.avg}$ IDRG_{20_5} otherwise
$\sigma_3 \leftarrow$		IDRG_{1_6} if $c_j \leq c_0$ IDRG_{2_6} if $c_0 < c_j \leq c_0 + \text{IncStrs.avg}$ IDRG_{3_6} if $c_0 + \text{IncStrs.avg} < c_j \leq c_0 + 2 \cdot \text{IncStrs.avg}$ IDRG_{4_6} if $c_0 + 2 \cdot \text{IncStrs.avg} < c_j \leq c_0 + 3 \cdot \text{IncStrs.avg}$ IDRG_{5_6} if $c_0 + 3 \cdot \text{IncStrs.avg} < c_j \leq c_0 + 4 \cdot \text{IncStrs.avg}$ IDRG_{6_6} if $c_0 + 4 \cdot \text{IncStrs.avg} < c_j \leq c_0 + 5 \cdot \text{IncStrs.avg}$ IDRG_{7_6} if $c_0 + 5 \cdot \text{IncStrs.avg} < c_j \leq c_0 + 6 \cdot \text{IncStrs.avg}$ IDRG_{8_6} if $c_0 + 6 \cdot \text{IncStrs.avg} < c_j \leq c_0 + 7 \cdot \text{IncStrs.avg}$ IDRG_{9_6} if $c_0 + 7 \cdot \text{IncStrs.avg} < c_j \leq c_0 + 8 \cdot \text{IncStrs.avg}$ IDRG_{10_6} if $c_0 + 8 \cdot \text{IncStrs.avg} < c_j \leq c_0 + 9 \cdot \text{IncStrs.avg}$ IDRG_{11_6} if $c_0 + 9 \cdot \text{IncStrs.avg} < c_j \leq c_0 + 10 \cdot \text{IncStrs.avg}$ IDRG_{12_6} if $c_0 + 10 \cdot \text{IncStrs.avg} < c_j \leq c_0 + 11 \cdot \text{IncStrs.avg}$ IDRG_{13_6} if $c_0 + 11 \cdot \text{IncStrs.avg} < c_j \leq c_0 + 12 \cdot \text{IncStrs.avg}$ IDRG_{14_6} if $c_0 + 12 \cdot \text{IncStrs.avg} < c_j \leq c_0 + 13 \cdot \text{IncStrs.avg}$ IDRG_{15_6} if $c_0 + 13 \cdot \text{IncStrs.avg} < c_j \leq c_0 + 14 \cdot \text{IncStrs.avg}$ IDRG_{16_6} if $c_0 + 14 \cdot \text{IncStrs.avg} < c_j \leq c_0 + 15 \cdot \text{IncStrs.avg}$ IDRG_{17_6} if $c_0 + 15 \cdot \text{IncStrs.avg} < c_j \leq c_0 + 16 \cdot \text{IncStrs.avg}$ IDRG_{18_6} if $c_0 + 16 \cdot \text{IncStrs.avg} < c_j \leq c_0 + 17 \cdot \text{IncStrs.avg}$ IDRG_{19_6} if $c_0 + 17 \cdot \text{IncStrs.avg} < c_j \leq c_0 + 18 \cdot \text{IncStrs.avg}$

$\left| \text{IDRG}_{20_6} \text{ otherwise} \right.$

$$\xi_0 \leftarrow \sigma_0$$

$$\xi_1 \leftarrow \sigma_0 + \sigma_1 \cdot \left(\frac{0.25 \cdot a_j}{t} \right) + \sigma_2 \cdot \left(\frac{0.25 \cdot a_j}{t} \right)^2 + \sigma_3 \cdot \left(\frac{0.25 \cdot a_j}{t} \right)^3$$

$$\xi_2 \leftarrow \sigma_0 + \sigma_1 \cdot \left(\frac{0.5 \cdot a_j}{t} \right) + \sigma_2 \cdot \left(\frac{0.5 \cdot a_j}{t} \right)^2 + \sigma_3 \cdot \left(\frac{0.5 \cdot a_j}{t} \right)^3$$

$$\xi_3 \leftarrow \sigma_0 + \sigma_1 \cdot \left(\frac{0.75 \cdot a_j}{t} \right) + \sigma_2 \cdot \left(\frac{0.75 \cdot a_j}{t} \right)^2 + \sigma_3 \cdot \left(\frac{0.75 \cdot a_j}{t} \right)^3$$

$$\xi_4 \leftarrow \sigma_0 + \sigma_1 \cdot \left(\frac{1.0 \cdot a_j}{t} \right) + \sigma_2 \cdot \left(\frac{1.0 \cdot a_j}{t} \right)^2 + \sigma_3 \cdot \left(\frac{1.0 \cdot a_j}{t} \right)^3$$

$$x_0 \leftarrow 0.0$$

$$x_1 \leftarrow 0.25$$

$$x_2 \leftarrow 0.5$$

$$x_3 \leftarrow 0.75$$

$$x_4 \leftarrow 1.0$$

$$X \leftarrow \text{stack}(x_0, x_1, x_2, x_3, x_4)$$

$$ST \leftarrow \text{stack}(\xi_0, \xi_1, \xi_2, \xi_3, \xi_4)$$

$$RG \leftarrow \text{regress}(X, ST, 3)$$

$$\sigma_{00} \leftarrow RG_3 + P_{\text{Int}}$$

$$\sigma_{10} \leftarrow RG_4$$

$$\sigma_{20} \leftarrow RG_5$$

$$\sigma_{30} \leftarrow RG_6$$

$$AR_j \leftarrow \frac{a_j}{c_j}$$

$$AT_j \leftarrow \frac{a_j}{t}$$

$$G_{\dots} \leftarrow f_{\dots}(R_{\dots}, AR_{\dots}, AT_{\dots})$$

$$-a u_j \cdot -a U(-T, -\infty, -\infty)$$

$$G_{al,j} \leftarrow f_{aL}(R_t, AR_j, AT_j)$$

$$G_{aq_j} \leftarrow f_{aQ}(R_t, AR_j, AT_j)$$

$$G_{ac_j} \leftarrow f_{aC}(R_t, AR_j, AT_j)$$

$$G_{cu_i} \leftarrow f_{cU}(R_t, AR_j, AT_j)$$

$$G_{cl,j} \leftarrow f_{cL}(R_t, AR_j, AT_j)$$

$$G_{cq_j} \leftarrow f_{cQ}(R_t, AR_j, AT_j)$$

$$G_{cc_i} \leftarrow f_{cC}(R_t, AR_j, AT_j)$$

$$Q_j \leftarrow \begin{cases} 1 + 1.464 \cdot \left(\frac{a_j}{c_j} \right)^{1.65} & \text{if } c_j \geq a_j \\ 1 + 1.464 \cdot \left(\frac{c_j}{a_j} \right)^{1.65} & \text{otherwise} \end{cases}$$

$$K_{a_j} \leftarrow \left(\frac{\pi \cdot a_j}{Q_j} \right)^{0.5} \cdot (\sigma_{00} \cdot G_{au_j} + \sigma_{10} \cdot G_{al_j} + \sigma_{20} \cdot G_{aq_j} + \sigma_{30} \cdot G_{ac_j})$$

$$K_{c_j} \leftarrow \left(\frac{\pi \cdot c_j}{Q_j} \right)^{0.5} \cdot (\sigma_{00} \cdot G_{cu_j} + \sigma_{10} \cdot G_{cl_j} + \sigma_{20} \cdot G_{cq_j} + \sigma_{30} \cdot G_{cc_j})$$

$$K_{\alpha_i} \leftarrow K_{a_i} \cdot 1.099$$

$$K_{\gamma_j} \leftarrow K_{c_j} \cdot 1.099$$

$$K_{\alpha_j} \leftarrow \begin{cases} 9.0 & \text{if } K_{\alpha_j} \leq 9.0 \\ K_{\alpha_j} & \text{otherwise} \end{cases}$$

$$K_{\gamma_j} \leftarrow \begin{cases} 9.0 & \text{if } K_{\gamma_j} \leq 9.0 \\ K_{\gamma_j} & \text{otherwise} \end{cases}$$

$$D_{a_i} \leftarrow C_0 \cdot (K_{\alpha_i} - 9.0)^{1.16}$$

$$|D| \leq |D|_{\text{CF}} + |C|, \text{ if } K \leq \aleph_n$$

$$D_{agj} \leftarrow \begin{cases} a_j \cdot CF_{inhr} \cdot C_{blk} & \text{if } K_{\gamma_j} > 80.0 \\ 4 \cdot 10^{-10} \cdot CF_{inhr} \cdot C_{blk} & \text{otherwise} \end{cases}$$

$$D_{cj} \leftarrow C_0 \cdot (K_{\gamma_j} - 9.0)^{1.16}$$

$$D_{cgj} \leftarrow \begin{cases} D_{cj} \cdot CF_{inhr} \cdot C_{blk} & \text{if } K_{\gamma_j} < 80.0 \\ 4 \cdot 10^{-10} \cdot CF_{inhr} \cdot C_{blk} & \text{otherwise} \end{cases}$$

$$\text{output}(j, 0) \leftarrow j$$

$$\text{output}(j, 1) \leftarrow a_j$$

$$\text{output}(j, 2) \leftarrow c_j - c_0$$

$$\text{output}(j, 3) \leftarrow D_{agj}$$

$$\text{output}(j, 4) \leftarrow D_{cgj}$$

$$\text{output}(j, 5) \leftarrow K_{a_j}$$

$$\text{output}(j, 6) \leftarrow K_{c_j}$$

$$\text{output}(j, 7) \leftarrow \frac{NCB_j}{365 \cdot 24}$$

$$\text{output}(j, 8) \leftarrow G_{au_j}$$

$$\text{output}(j, 9) \leftarrow G_{al_j}$$

$$\text{output}(j, 10) \leftarrow G_{aq_j}$$

$$\text{output}(j, 11) \leftarrow G_{ac_j}$$

$$\text{output}(j, 12) \leftarrow G_{cu_j}$$

$$\text{output}(j, 13) \leftarrow G_{cl_j}$$

$$\text{output}(j, 14) \leftarrow G_{cq_j}$$

$$\text{output}(j, 15) \leftarrow G_{cc_j}$$

$$j \leftarrow j + 1$$

$$a_i \leftarrow a_{i-1} + D_{a_i}$$

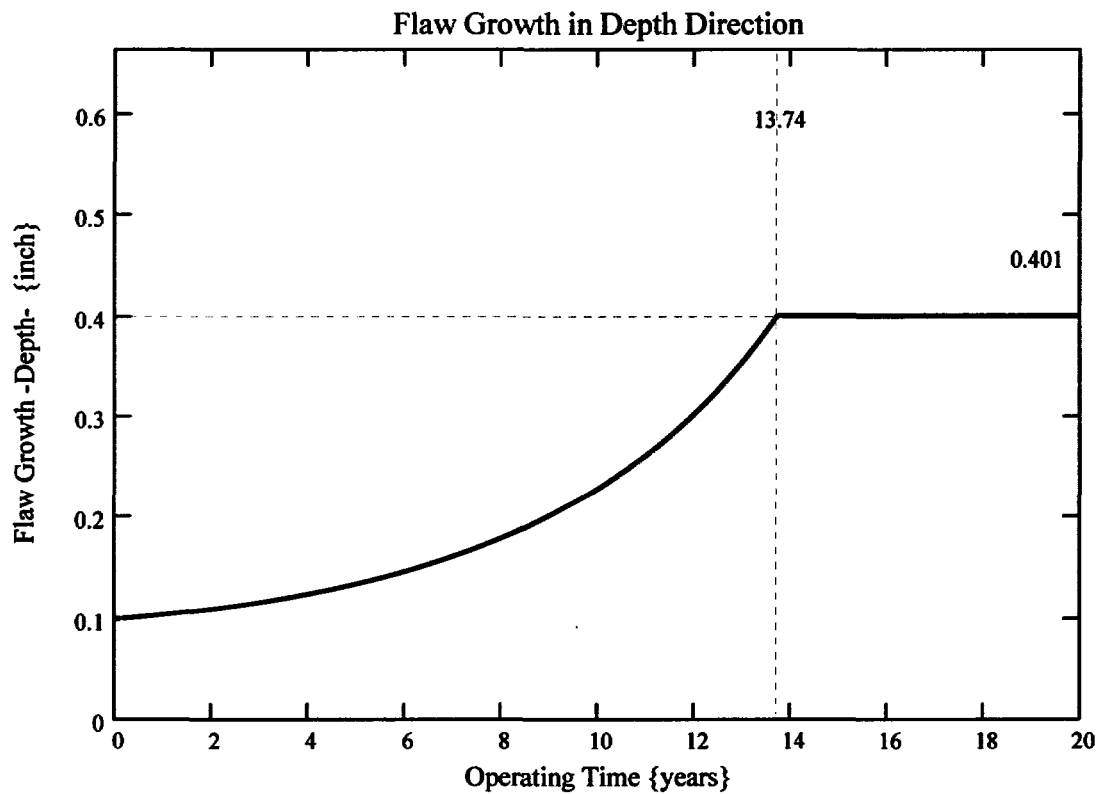
```

    εj-1
    cj ← cj-1 + Dcgj-1
    aj ←  $\begin{cases} t & \text{if } a_j \geq t \\ a_j & \text{otherwise} \end{cases}$ 
    NCBj ← NCBj-1 + Cblk
  output

```

$k_w := 0..I_{lim}$

The curve below shows the flaw growth through-wall and the operating time (in years) it takes to go through-wall.



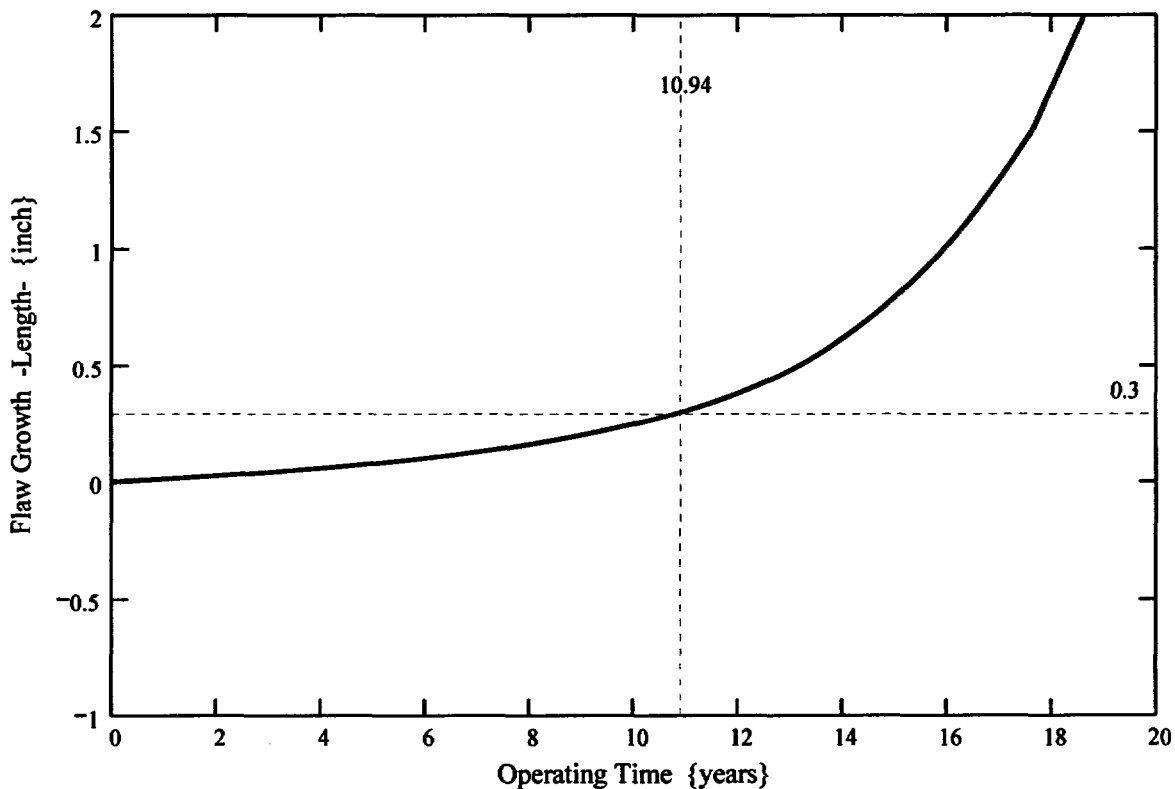
The propagation length for the ICI nozzles is defined as the length for which the initial flaw in the blind zone would extend out of the blind zone and grow to a detectable flaw. Reference 11 gives the minimum detectable flaw size of 4 mm (0.16) in length; thus, 0.16 inch was considered as this minimum detectable flaw length. This dimension is added to the end of the blind zone.

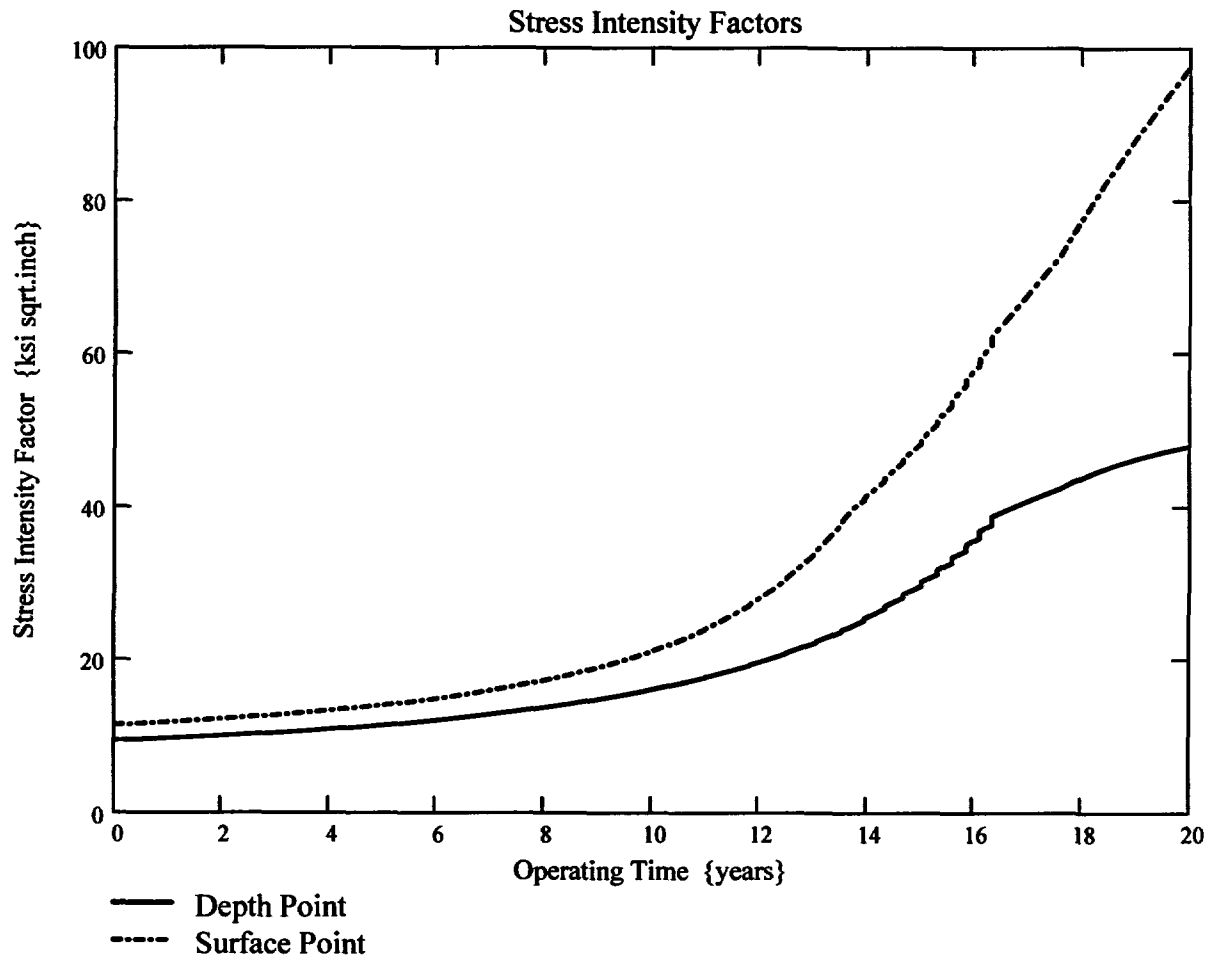
$$\text{Prop_Length} := \frac{\text{BZ_length}}{2} - c_0 + 0.16$$

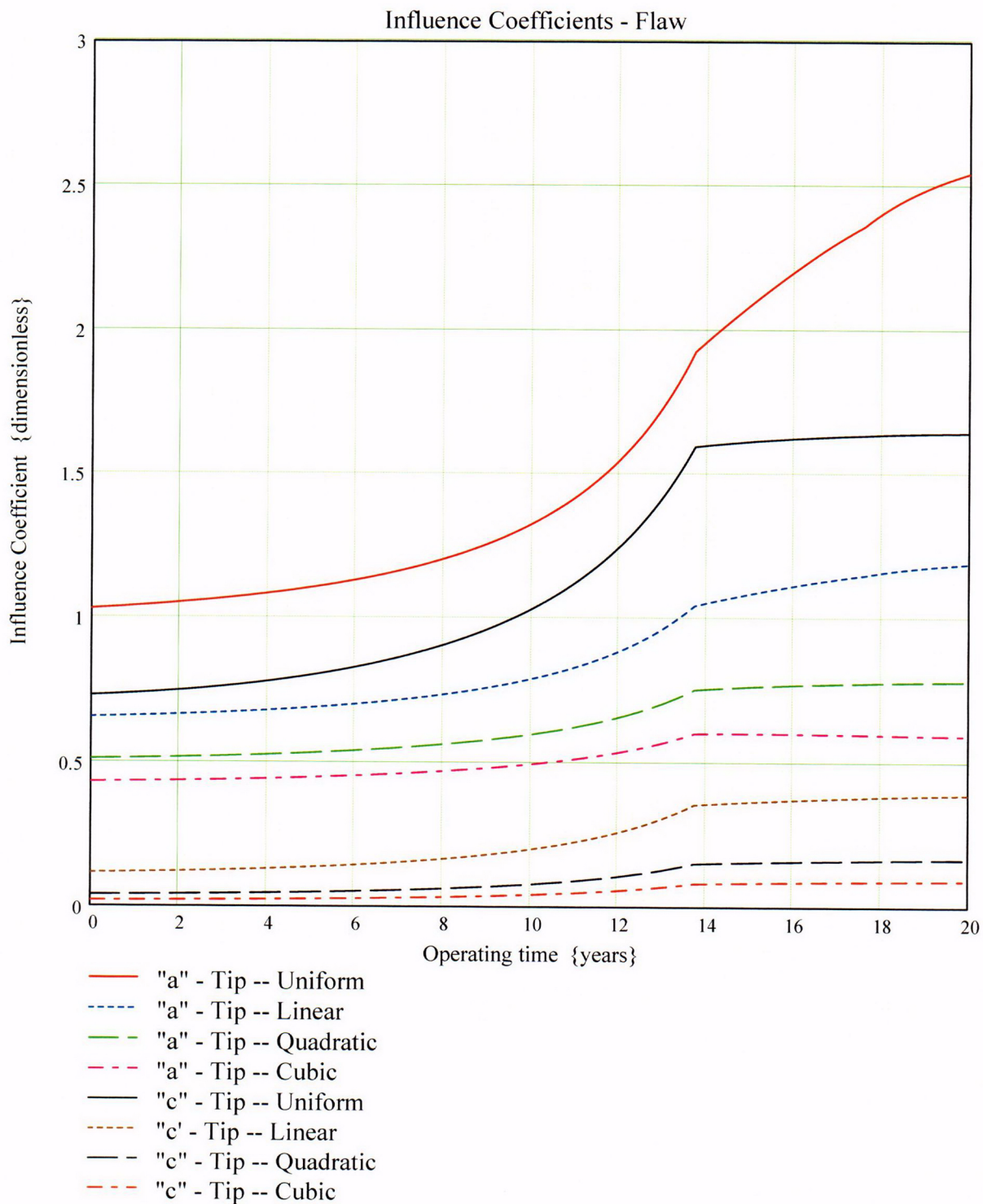
$$\text{Prop_Length} = 0.3$$

This implies that a flaw initially within the blindzone must grow 0.3 inch to become detectable via UT.

The curve below shows the flaw growth along the length of the ICI nozzle and the operating time (in years) it takes to reach the Prop_Length value defined above.







Arkansas Nuclear One Unit 2

Primary Water Stress Corrosion Crack Growth Analysis for an ICI ID Surface Flaw
Uphill (180°), in the Blind Zone above the Top of the J-Groove Weld
Developed by Central Engineering Programs, Entergy Operations Inc.

Flaw Case 2: 0.4-Inch Long Flaw with a 10-to-1 Flaw Length-to-Depth Aspect Ratio, Located at the Center of the Blind Zone

Calculation Basis: MRP 75 th Percentile and Flaw Face Pressurized

Mean Radius -to- Thickness Ratio:- " R_m/t " – between 1.0 and 300.0

Note : *The Metric form of the equation from EPRI MRP was used 55-Rev. 1 . A correction factor is applied in the determination of the crack extension to convert the units of meters per second to the value in inches per hour .*

ID Surface Flaw

User Input:

The Dominion Engineering Inc. (DEI) finite element model nodal elevations and hoop stresses for the uphill side (180° azimuth) of the ICI nozzle are brought into the Mathcad worksheet from data supplied in Reference 6d. The data are composed of the nodal elevations (in inches), along with the ID, 25% through-wall (tw), 50% tw, 75% tw, and OD hoop stresses, beginning at the top of the weld (nodal line 81301) and extending to the top of the nozzle in the FEA model, which is at the point where the nozzle intersects the reactor vessel head.

The DEI FEA data has elevation referenced from the bottom of the ICI nozzle. The elevations of the node points in the DEI FEA model, beginning at the top of the weld (nodal line 81301), are as follows:

$i := 0..9$

$\text{Node_line}_i := \text{ID_elev_fea}_i := \text{QT_elev_fea}_i := \text{MD_elev_fea}_i := \text{TQ_elev_fea}_i := \text{OD_elev_fea}_i :=$

81301	4.2276	4.2276	4.2276	4.2276	4.2276
81401	4.4536	4.4536	4.4536	4.4536	4.4536
81501	4.8639	4.8639	4.8639	4.8639	4.8639
81601	5.1825	5.2486	5.3148	5.3810	5.4472
81701	6.2761	6.2761	6.2761	6.2761	6.2761
81801	7.4543	7.4543	7.4543	7.4543	7.4543
81901	9.1289	9.1289	9.1289	9.1289	9.1289
82001	11.5090	11.5090	11.5090	11.5090	11.5090
82101	14.8917	14.8917	14.8917	14.8917	14.8917
82201	17.8288	17.8288	17.8288	17.8288	17.8288

The corresponding stresses at these nodes are

ID_stress_fea_i := QT_stress_fea_i := MD_stress_fea_i := TQ_stress_fea_i := OD_stress_fea_i :=

26.390
23.147
19.425
15.065
16.707
17.399
17.412
17.115
15.304
10.308

25.687
21.559
18.188
14.581
16.175
17.177
17.487
15.794
13.024
10.119

24.607
19.292
15.780
13.132
15.560
15.044
12.883
11.377
10.766
10.032

22.680
16.085
11.381
6.189
8.890
8.136
7.180
7.821
9.067
9.951

44.523
9.729
8.207
-0.109
2.74
2.316
2.298
4.387
7.453
9.936

Blind Zone and Counterbore Reference dimensions:

From design drawings (Ref. 2a and 2b) and the design input of Attachment 1, the following dimensions are used to locate the counterbore bottom and blind zone locations (bottom, top, and middle) as referenced from the nodal coordinates of the DEI FEA model.

$$\text{Actual_cbore_bottom_elev} := \text{ID_elev_fea}_0 + 1.377$$

$$\text{Actual_cbore_bottom_elev} = 5.6046$$

$$\text{topweld_to_bottom_BZ} := 1.08$$

$$\text{BZ_length} := 0.88$$

$$\text{elev_to_mid_BZ} := \text{ID_elev_fea}_0 + \text{topweld_to_bottom_BZ} + \frac{\text{BZ_length}}{2}$$

$$\text{elev_to_mid_BZ} = 5.7476$$

$$\text{bottom_of_BZ} := \text{ID_elev_fea}_0 + \text{topweld_to_bottom_BZ}$$

$$\text{bottom_of_BZ} = 5.3076$$

$$\text{top_of_BZ} := \text{ID_elev_fea}_0 + \text{topweld_to_bottom_BZ} + \text{BZ_length}$$

$$\text{top_of_BZ} = 6.1876$$

For stress averaging and fracture mechanics purposes, the reference coordinate system--with a "0" elevation at the bottom of the nozzle, at the ID corner--must be converted into a new coordinate system with the top of the nozzle (nodal line 82201) as the new "0" elevation.. The positive direction along this new coordinate system will be towards nodal line 81301, which is the top of the weld. This modification facilitates a fracture mechanics model more ammenable to the surface flaw loop structure previously developed in Reference 7.

The following iterative loops convert the five (5) through-wall stress components--ID, 25% tw (QT), 50% tw (MD), 75% tw (TQ), and OD--and the associated elevations, initially given in the DEI FEA model, into the "new" coordinate system, referenced from the top of the nozzle where it meets the reactor vessel head.

```

ID_conv := | Top ← ID_elev_fea9
            | j ← 9
            | i ← 0
            | while j ≥ 0
            |   | ID_elev_convi ← Top - ID_elev_feaj
            |   | ID_stressi ← ID_stress_feaj
            |   | output(i, 0) ← ID_elev_convi
            |   | output(i, 1) ← ID_stressi
            |   | j ← j - 1
            |   | i ← i + 1
            | output
  
```

$$\text{ID_elev} := \text{ID_conv}^{\langle 0 \rangle}$$

$$\text{ID_stress} := \text{ID_conv}^{\langle 1 \rangle}$$

```

QT_conv := | Top ← QT_elev_fea9
            | j ← 9
            | i ← 0
            | while j ≥ 0
            |   | QT_elev_convi ← Top - QT_elev_feaj
            |   | QT_stressi ← QT_stress_feaj
            |   | output(i,0) ← QT_elev_convi
            |   | output(i,1) ← QT_stressi
            |   | j ← j - 1
            |   | i ← i + 1
            | output
  
```

QT_elev := QT_conv⁽⁰⁾

QT_stress := QT_conv⁽¹⁾

```

MD_conv := | Top ← MD_elev_fea9
            | j ← 9
            | i ← 0
            | while j ≥ 0
            |   | MD_elev_convi ← Top - MD_elev_feaj
            |   | MD_stressi ← MD_stress_feaj
            |   | output(i,0) ← MD_elev_convi
            |   | output(i,1) ← MD_stressi
            |   | j ← j - 1
            |   | i ← i + 1
            | output
  
```

MD_elev := MD_conv⁽⁰⁾

MD_stress := MD_conv⁽¹⁾

```

TQ_conv := | Top ← TQ_elev_fea9
            | j ← 9
            | i ← 0
            | while j ≥ 0
            |   | TQ_elev_convi ← Top - TQ_elev_feaj
            |   | TQ_stressi ← TQ_stress_feaj
            |   | output(i, 0) ← TQ_elev_convi
            |   | output(i, 1) ← TQ_stressi
            |   | j ← j - 1
            |   | i ← i + 1
            | output
  
```

TQ_elev := TQ_conv⁽⁰⁾

TQ_stress := TQ_conv⁽¹⁾

```

OD_conv := | Top ← OD_elev_fea9
            | j ← 9
            | i ← 0
            | while j ≥ 0
            |   | OD_elev_convi ← Top - OD_elev_feaj
            |   | OD_stressi ← OD_stress_feaj
            |   | output(i, 0) ← OD_elev_convi
            |   | output(i, 1) ← OD_stressi
            |   | j ← j - 1
            |   | i ← i + 1
            | output
  
```

OD_elev := OD_conv⁽⁰⁾

OD_stress := OD_conv⁽¹⁾

ID_elev_i =

0
2.9371
6.3198
8.6999
10.3745
11.5527
12.6463
12.9649
13.3752
13.6012

QT_elev_i =

0
2.9371
6.3198
8.6999
10.3745
11.5527
12.5802
12.9649
13.3752
13.6012

MD_elev_i =

0
2.9371
6.3198
8.6999
10.3745
11.5527
12.514
12.9649
13.3752
13.6012

TQ_elev_i =

0
2.9371
6.3198
8.6999
10.3745
11.5527
12.4478
12.9649
13.3752
13.6012

OD_elev_i =

0
2.9371
6.3198
8.6999
10.3745
11.5527
12.3816
12.9649
13.3752
13.6012

ID_stress_i =

10.308
15.304
17.115
17.412
17.399
16.707
15.065
19.425
23.147
26.39

QT_stress_i =

10.119
13.024
15.794
17.487
17.177
16.175
14.581
18.188
21.559
25.687

MD_stress_i =

10.032
10.766
11.377
12.883
15.044
15.56
13.132
15.78
19.292
24.607

TQ_stress_i =

9.951
9.067
7.821
7.18
8.136
8.89
6.189
11.381
16.085
22.68

OD_stress_i =

9.936
7.453
4.387
2.298
2.316
2.74
-0.109
8.207
9.729
44.523

The two sets of five arrays given above are the elevations measured from the top of the ICI nozzle from the FEA model down to the top of the J-weld and the corresponding hoop stresses in the modified coordinate system (MCS).

Additional Geometry in Modified Coordinate System

The top of the J-groove weld in the MCS is equal to the last entry in the ID_elev array:

$$\text{Top_Jweld} := \text{ID_elev}_9$$

$$\text{Top_Jweld} = 13.6012$$

The location of the top of the UT blind zone (BZ) in the MCS (as measured from the ID surface) is

$$\text{BZ_top} := \text{Top_Jweld} - (\text{topweld_to_bottom_BZ} + \text{BZ_length})$$

$$\text{BZ_top} = 11.6412$$

The midpoint of the BZ in the MCS is

$$\text{BZ_mid} := \text{BZ_top} + \frac{\text{BZ_length}}{2}$$

$$\text{BZ_mid} = 12.0812$$

The bottom of the BZ in the MCS is

$$\text{BZ_bottom} := \text{BZ_top} + \text{BZ_length}$$

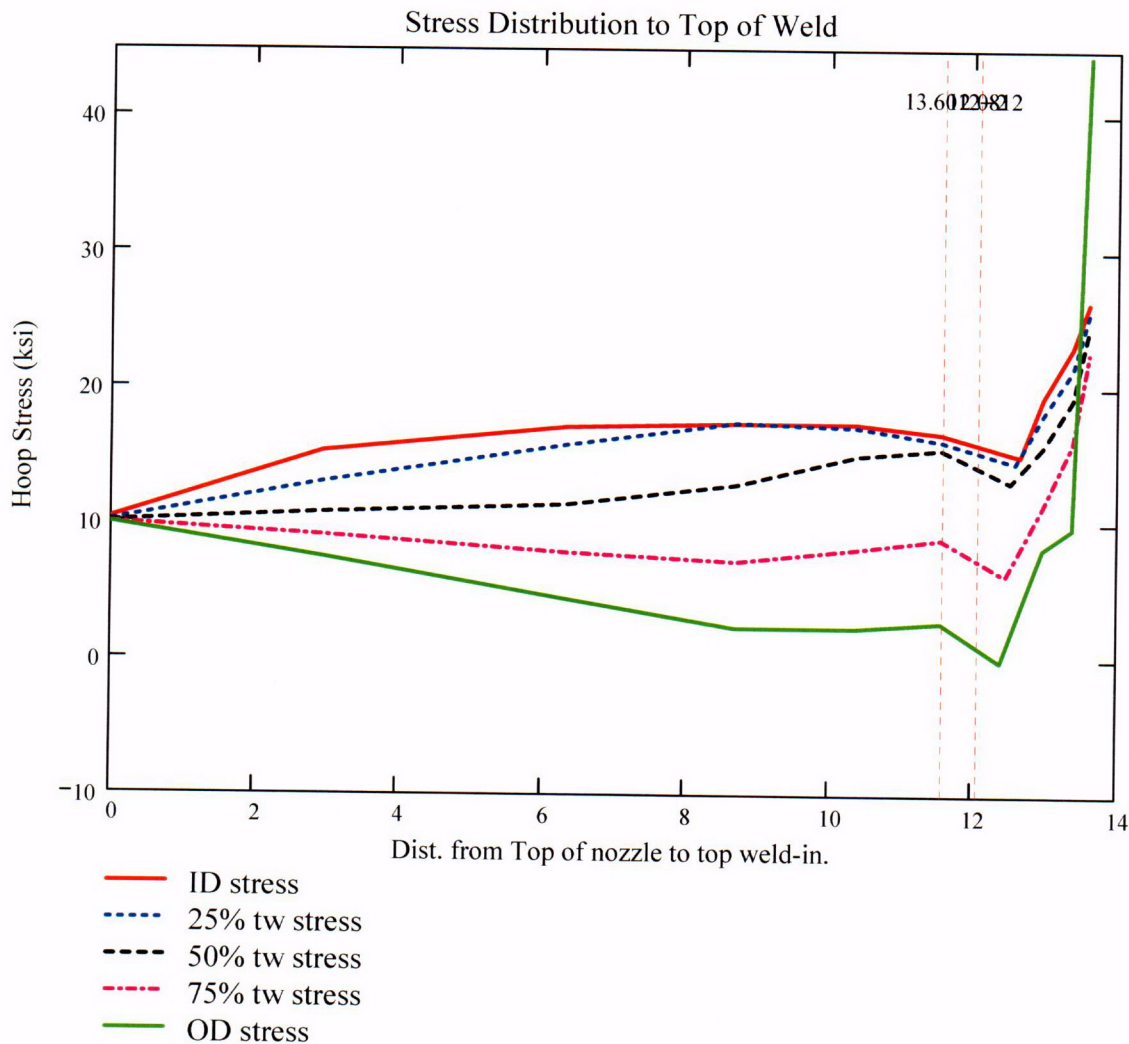
$$\text{BZ_bottom} = 12.5212$$

The location of the actual counterbore (from design drawings) in the MCS:

$$\text{cbore_elev} := \text{Top_Jweld} - 1.377$$

$$\text{cbore_elev} = 12.2242$$

From the MCS, the stress distribution from elevation 0 (the top of the ICI nozzle where it intersects the RV head) to the top of the weld is graphically shown below.



For the ID surface flaw model, the reference point is the location along the axis of the nozzle used to locate the flaw. For this analysis, the reference point is considered at the mid-height of the blind zone.

Ref_{Point} := BZ_{mid}

To place the flaw with respect to the reference point, the flaw tips and center can be located as follows:

- 1) The Upper "c- tip" located at the reference point (Enter 1)
- 2) The Center of the flaw at the reference point (Enter 2)
- 3) The lower "c- tip" located at the reference point (Enter 3).

Val := 2

The Input Below is the point below the blind zone region where stresses will be considered for curve-fitting. This point is taken as the top of the weld, since the stress distribution changes drastically within the weld region. Enter this dimension or variable below.

Elev_{Strs.Dist} := Top_Jweld The elevation to the point of maximum stress to consider
(Axial distance from elevation 0 in the MCS).

ICI Nozzle Geometry Input Data:

od := 5.563 – 0.001 Tube OD, in inches (The value from Ref. 2a, is 5.563" +0.00/-0.001)

id1 := 4.625 + 0.01 Maximum Tube ID above counterbore, in inches
(The value from Ref. 2b is 4.625" +/- 0.010")

id2 := 4.750 + 0.01 Maximum Tube ID below counterbore, in inches
(The value from Ref. 2b is 4.750" +/- 0.010")

$$t1 := \frac{(od - id1)}{2}$$

Minimum wall thickness above the counterbore, in inches

$$t1 = 0.4635$$

$$t2 := \frac{(od - id2)}{2}$$

Minimum wall thickness below the counterbore, in inches

$$t2 = 0.401$$

$$R_o := \frac{od}{2}$$

$$R_o = 2.781$$

$$R_{id1} := \frac{id1}{2}$$

$$R_{id1} = 2.3175$$

$$R_{id2} := \frac{id2}{2} \quad R_{id2} = 2.38$$

$$R_{m1} := R_{id1} + \frac{t1}{2} \quad R_{m1} = 2.54925$$

$$R_{m2} := R_{id2} + \frac{t2}{2} \quad R_{m2} = 2.5805$$

$$R_t := \frac{R_{m2}}{t2} \quad R_t = 6.43516$$

$$\frac{R_o}{t2} = 6.93516$$

Flaw Geometry Input Data:

A postulated flaw could exist in the 0.88" UT Blindzone that occurs 1.08" above the top of the J-weld at the uphill (180°) location. The flaw length (c) and depth (a) constitute the input parameters. This flaw represents an internal surface crack in a cylinder, as described in Reference 8.

$AR_0 := 10$ The flaw length-to-depth aspect ratio. This is a ratio common to ASME Section XI, and one sufficient to promote flaw growth through the thickness.

$$t2 \cdot 10 = 0.0401$$

$L_{in} := 0.4$ Initial Flaw Length of an ID surface flaw in the counterbore region, in inches. The length was based on a sufficiently long flaw (10-to-1 aspect ratio) with enough depth into the thickness (10%) to precipitate growth in both the depth and length directions. Half the flaw length (0.2 inch) was placed below the mid-height of the blind zone, while the other half was placed above the mid-height.

$a_0 := \frac{0.4}{AR_0}$ Initial Flaw Depth of the ID surface flaw in the blind zone above the top of the weld on the uphill side. The minimum detectable depth of a surface flaw from UT demonstrations [Ref. 11] was 8% throughwall. This flaw is 10% throughwall.

$$a_0 = 0.04$$

$c_0 := \frac{L}{2}$ The half flaw length used in the fracture mechanics model

Additional Input Data:

$P_{Int} := 2.235$ Design Operating Pressure (internal) [Ref. 3]

Years := 40 Number of Operating Years

$I_{lim} := 8000$ Iteration limit for Crack Growth loop

$T_{op} := 604$ Conservative Operating Temperature for the head, in degrees F. Ref. 4 gives a value of 594.8 deg. F following power uprate.

$\alpha_{0c} := 2.67 \cdot 10^{-12}$ Constant in MRP-55 PWSCC Model for I-600 Wrought @ 617 deg. F [Ref. 9]

$Q_g := 31.0$ Thermal activation Energy for Crack Growth {MRP} [Ref. 9]

$T_{ref} := 617$ Reference Temperature for normalizing Data deg. F [Ref. 9]

$Tim_{opr} := 365.2422 \cdot 24 \cdot \text{Years}$ Numer of operating hours in a year

$CF_{inhr} := 1.417 \cdot 10^5$ Correction factor to convert meters per second to inches per hour

$C_{blk} := \frac{Tim_{opr}}{I_{lim}}$ Calculation block size for the crack growth iteration loop

$C_{blk} = 43.82906$

$Prnt_{blk} := \left| \frac{I_{lim}}{50} \right|$

$C_{01} := e^{\left[\frac{-Q_g}{1.103 \cdot 10^{-3}} \cdot \left(\frac{1}{T+459.67} - \frac{1}{T_{ref}+459.67} \right) \right]} \cdot \alpha_{0c}$

Temperature Correction for Coefficient Alpha
from EPRI MRP-55, Revision 1 [Ref. 9]

$$C_0 := 1.0C_{01} \quad 75^{\text{th}} \text{ percentile from MRP-55 Revision 1 [Ref. 9]}$$

The flaw model used for a postulated flaw within the counterbore region on the uphill side of the ICI nozzle is an internal surface flaw in a cylinder, subject to an arbitrary stress distribution.

To allow for a "moving average" of through-thickness stress values as the flaw extends along the length of the ICI ID surface, the length from the bottom tip of the of the initial flaw in the blind zone to the stress distribution upper limit--ElevStrs.Dist--is broken into 20 equal segments. Note that due to the MCS used, with a 0 elevation occurring at the TOP of the nozzle, the term "U_{Tip}" (implying the upper tip of the flaw) is actually the physical bottom tip of the flaw, closer to the top of the weld. U_{Tip} is the term used in Reference 7 for the CEDM nozzles, and thus it will continue to be used in the ICI nozzle evaluation.

$$FL_{Cntr} := \begin{cases} Ref_{Point} - c_0 & \text{if Val} = 1 \\ Ref_{Point} & \text{if Val} = 2 \\ Ref_{Point} + c_0 & \text{otherwise} \end{cases} \quad \begin{array}{l} \text{Flaw center Location at the mid-point of} \\ \text{the blind zone region} \end{array}$$

$$U_{Tip} := FL_{Cntr} + c_0$$

$$U_{Tip} = 12.2812$$

$$Inc_{Strs.avg} := \frac{Elev_{Strs.Dist} - U_{Tip}}{20}$$

$$Inc_{Strs.avg} = 0.066$$

No User Input is required beyond this Point

Regression of Through-Thickness Stresses as a Function of Axial Elevation

Because of the minor variation in stresses occurring at the top of the nozzle where it intersects the reactor head and the need to accurately curve fit stresses in the region of interest in the BZ, the entire range of stresses is not appropriate to curve fit. To accommodate an area below and above the BZ region, the first two data points in each of the elevation and stress arrays were removed from consideration in the curve fitting equations. This is a reasonable assumption, given that in the completely through-wall tensile stress field that exists in the nozzle above the top of the J-weld, a flaw centered in the BZ region is likely to grow through the thickness entirely (in addition to growth along the surface of the nozzle) rather than grow very long into an area close to the top of the head or below the top of the J-weld (i.e., elevation ranges not included in the stress polynomial curve fit). Initially, a **fourth (4th)** order polynomial was chosen for axial stress regression. After regression, the stress at the mid-height of the blind zone (12.0812 inches in the MCS) is checked.

Regression for ID stresses:

$k := 0..6$

$$ID_elev_cf := \begin{pmatrix} 8.6999 \\ 10.3745 \\ 11.5527 \\ 12.6463 \\ 12.9649 \\ 13.3752 \\ 13.6012 \end{pmatrix} \quad ID_stress_cf := \begin{pmatrix} 17.412 \\ 17.399 \\ 16.707 \\ 15.065 \\ 19.425 \\ 23.147 \\ 26.39 \end{pmatrix}$$

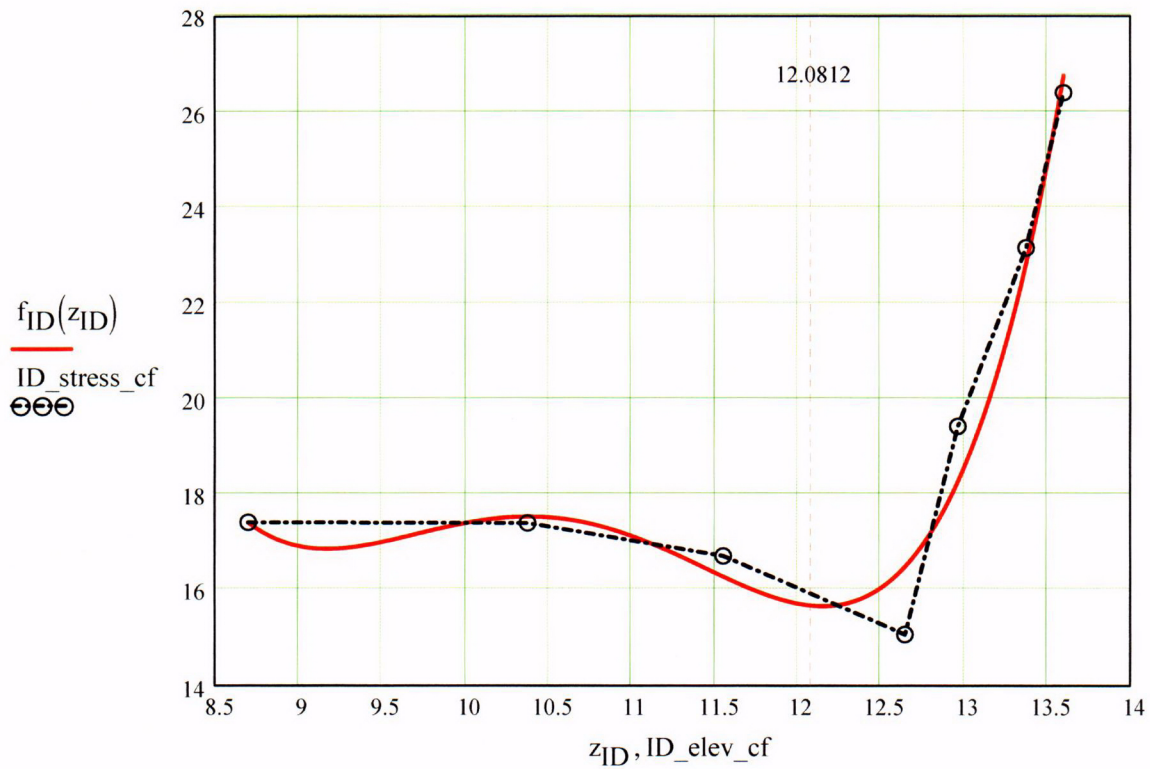
$R_{ID} := \text{regress}(ID_elev_cf, ID_stress_cf, 4)$

$z_{ID} := 8.6999, 8.701.. \text{Top_Jweld}$

$$R_{ID} = \begin{pmatrix} 3 \\ 3 \\ 4 \\ 2920.01158 \\ -1120.32621 \\ 161.1276 \\ -10.23275 \\ 0.24206 \end{pmatrix}$$

$ID_elev_i =$	$ID_stress_i =$
0	10.308
2.9371	15.304
6.3198	17.115
8.6999	17.412
10.3745	17.399
11.5527	16.707
12.6463	15.065
12.9649	19.425
13.3752	23.147
13.6012	26.39

$f_{ID}(z_{ID}) := \text{interp}(R_{ID}, ID_elev_cf, ID_stress_cf, z_{ID})$



$$f_{ID}(12.0812) = 15.66367$$

Regression for 25% throughwall stresses:

$$QT_elev_cf := \begin{pmatrix} 8.6999 \\ 10.3745 \\ 11.5527 \\ 12.5802 \\ 12.9649 \\ 13.3752 \\ 13.6012 \end{pmatrix} \quad QT_stress_cf := \begin{pmatrix} 17.487 \\ 17.177 \\ 16.175 \\ 14.581 \\ 18.188 \\ 21.559 \\ 25.687 \end{pmatrix}$$

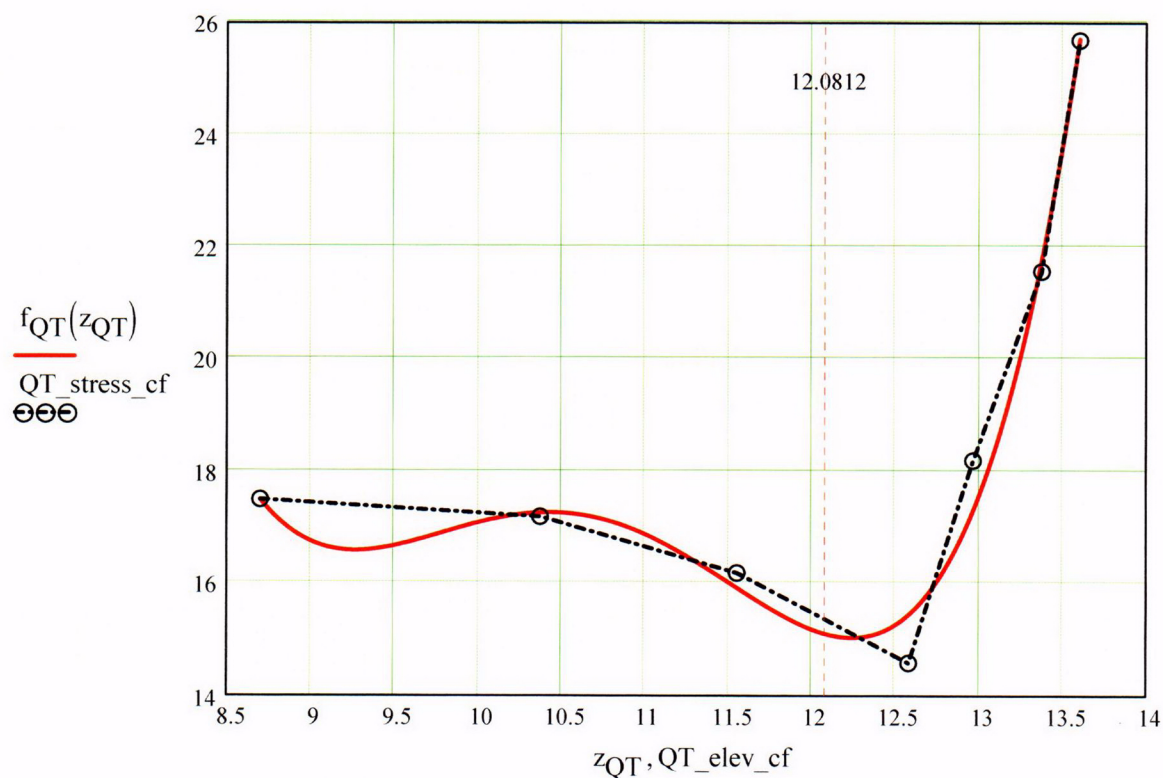
$$R_{QT} := \text{regress}(QT_elev_cf, QT_stress_cf, 4)$$

$$z_{QT} := 8.6999, 8.701 \dots \text{Top_Jweld}$$

$$R_{QT} = \begin{pmatrix} 3 \\ 3 \\ 4 \\ 3362.70255 \\ -1281.45936 \\ 182.93207 \\ -11.53275 \\ 0.27085 \end{pmatrix}$$

QT_elev _i =	QT_stress _i =
0	10.119
2.9371	13.024
6.3198	15.794
8.6999	17.487
10.3745	17.177
11.5527	16.175
12.5802	14.581
12.9649	18.188
13.3752	21.559
13.6012	25.687

$$f_{QT}(z_{QT}) := \text{interp}(R_{QT}, QT_elev_cf, QT_stress_cf, z_{QT})$$



$$f_{QT}(12.0812) = 15.09487$$

Regression for 50% throughwall stresses:

$$\text{MD_elev_cf} := \begin{pmatrix} 8.6999 \\ 10.3745 \\ 11.5527 \\ 12.514 \\ 12.9649 \\ 13.3752 \\ 13.6012 \end{pmatrix} \quad \text{MD_stress_cf} := \begin{pmatrix} 12.883 \\ 15.044 \\ 15.56 \\ 13.132 \\ 15.78 \\ 19.292 \\ 24.607 \end{pmatrix}$$

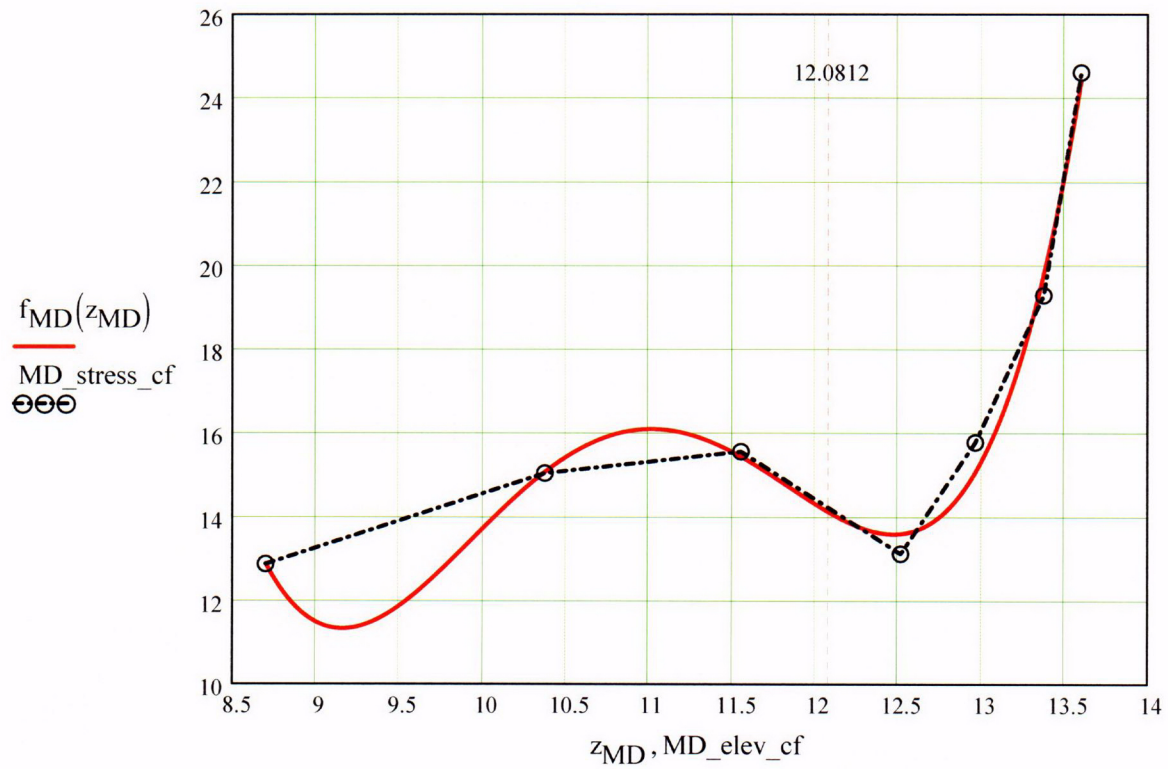
$$R_{\text{MD}} := \text{regress}(\text{MD_elev_cf}, \text{MD_stress_cf}, 4)$$

$$z_{\text{MD}} := 8.6999, 8.701 \dots \text{Top_Jweld}$$

$$R_{\text{MD}} = \begin{pmatrix} 3 \\ 3 \\ 4 \\ 6270.57353 \\ -2357.44561 \\ 330.23769 \\ -20.39106 \\ 0.46849 \end{pmatrix}$$

MD_elev _i	MD_stress _i
0	10.032
2.9371	10.766
6.3198	11.377
8.6999	12.883
10.3745	15.044
11.5527	15.56
12.514	13.132
12.9649	15.78
13.3752	19.292
13.6012	24.607

$$f_{\text{MD}}(z_{\text{MD}}) := \text{interp}(R_{\text{MD}}, \text{MD_elev_cf}, \text{MD_stress_cf}, z_{\text{MD}})$$



$$f_{MD}(12.0812) = 14.11569$$

Regression for 75% throughwall stresses:

$$TQ_elev_cf := \begin{pmatrix} 8.6999 \\ 10.3745 \\ 11.5527 \\ 12.4478 \\ 12.9649 \\ 13.3752 \\ 13.6012 \end{pmatrix}$$

$$TQ_stress_cf := \begin{pmatrix} 7.18 \\ 8.136 \\ 8.89 \\ 6.189 \\ 11.381 \\ 16.085 \\ 22.68 \end{pmatrix}$$

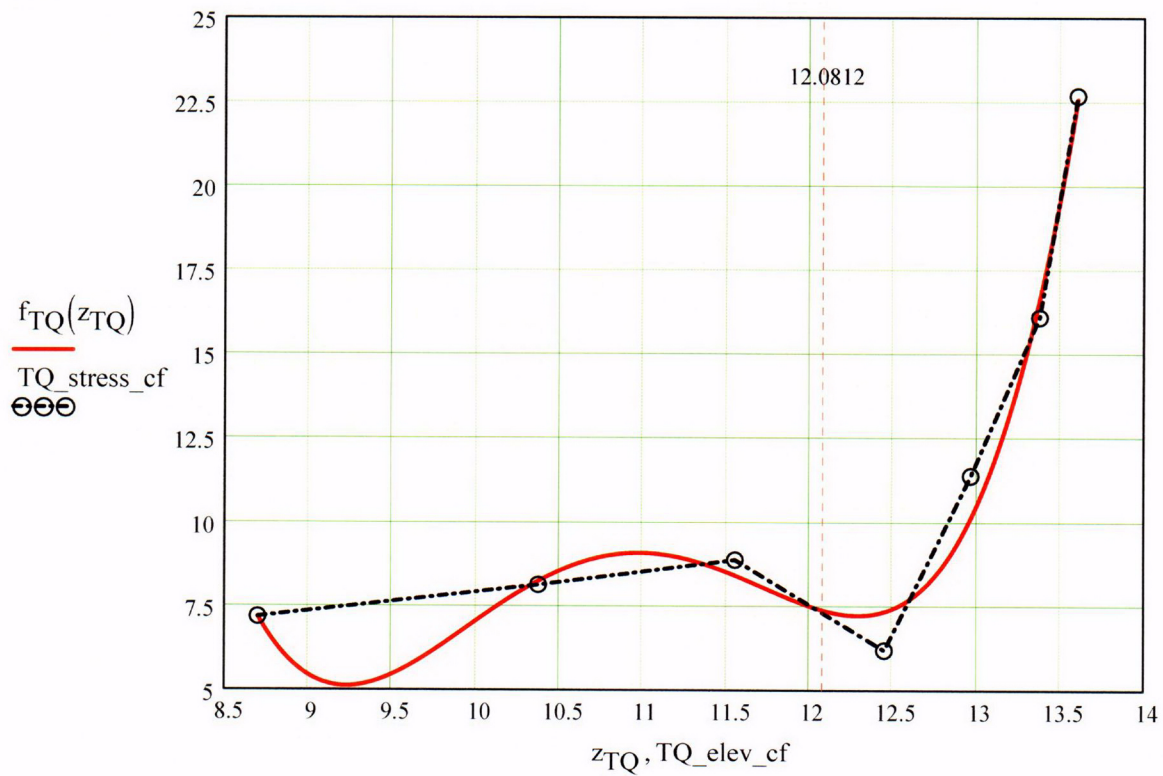
$$R_{TQ} := \text{regress}(TQ_elev_cf, TQ_stress_cf, 4)$$

$$z_{TQ} := 8.6999, 8.701 \dots \text{Top_Jweld}$$

$$R_{TQ} = \begin{pmatrix} 3 \\ 3 \\ 4 \\ 6772.44513 \\ -2552.34739 \\ 358.42617 \\ -22.21167 \\ 0.51271 \end{pmatrix}$$

$TQ_elev_i =$	$TQ_stress_i =$
0	9.951
2.9371	9.067
6.3198	7.821
8.6999	7.18
10.3745	8.136
11.5527	8.89
12.4478	6.189
12.9649	11.381
13.3752	16.085
13.6012	22.68

$$f_{TQ}(z_{TQ}) := \text{interp}(R_{TQ}, TQ_elev_cf, TQ_stress_cf, z_{TQ})$$



$$f_{TQ}(12.0812) = 7.37343$$

Regression for OD stresses:

kk := 0..5

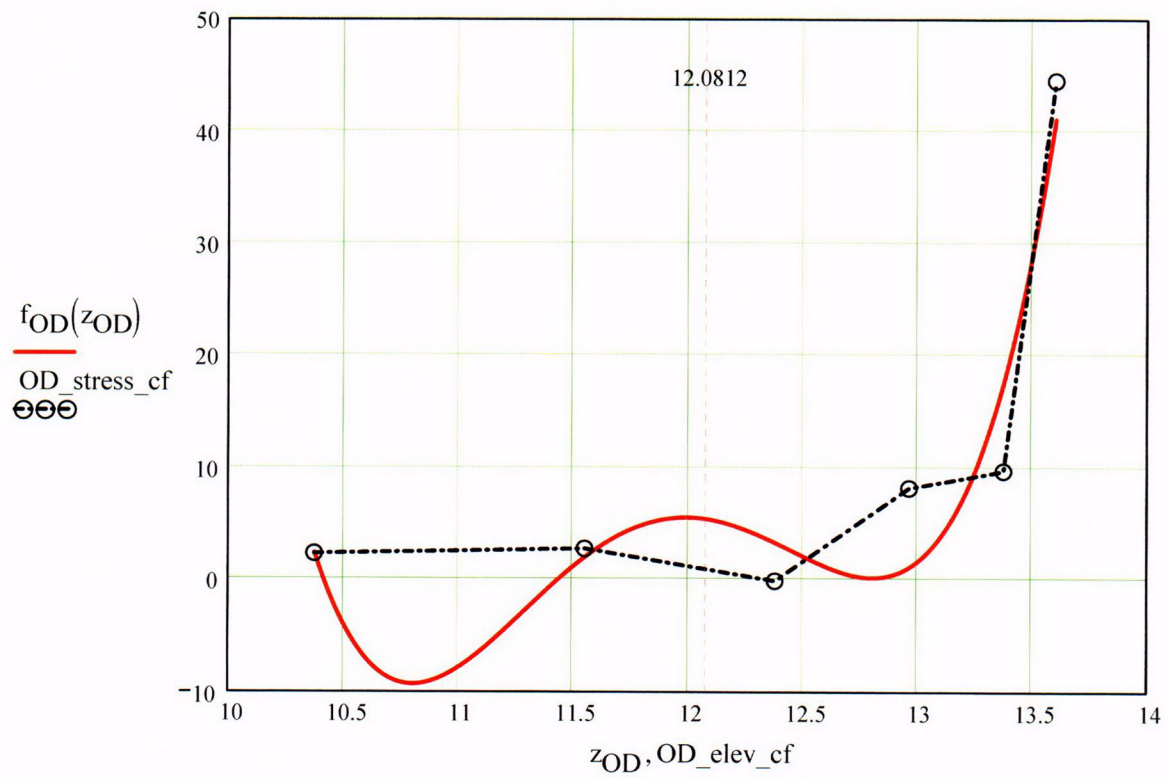
$$\text{OD_elev_cf} := \begin{pmatrix} 10.3745 \\ 11.5527 \\ 12.3816 \\ 12.9649 \\ 13.3752 \\ 13.6012 \end{pmatrix} \quad \text{OD_stress_cf} := \begin{pmatrix} 2.316 \\ 2.74 \\ -0.109 \\ 8.207 \\ 9.729 \\ 44.523 \end{pmatrix}$$

$$\begin{aligned} R_{OD} &:= \text{regress}(\text{OD_elev_cf}, \text{OD_stress_cf}, 4) \\ z_{OD} &:= 10.3745, 10.376 \dots \text{Top_Jweld} \end{aligned}$$

$$R_{OD} = \begin{pmatrix} 3 \\ 3 \\ 4 \\ 1.83727 \times 10^5 \\ -62394.03658 \\ 7925.4618 \\ -446.31291 \\ 9.40247 \end{pmatrix}$$

OD_elev _i	OD_stress _i
0	9.936
2.9371	7.453
6.3198	4.387
8.6999	2.298
10.3745	2.316
11.5527	2.74
12.3816	-0.109
12.9649	8.207
13.3752	9.729
13.6012	44.523

$$f_{OD}(z_{OD}) := \text{interp}(R_{OD}, \text{OD_elev_cf}, \text{OD_stress_cf}, z_{OD})$$



$$f_{OD}(12.0812) = 5.39079$$

Calculation to develop Stress Profiles for Analysis

This analysis for the axial stress regression and the through-wall stress regression is the same as that used for the CEDM Nozzles (in Ref. 7) with the exception that the axial stresses are fit with a fourth-order polynomial, rather than a third-order polynomial, to accommodate greater precision.

$$N_{\text{ww}} := 20 \quad \text{Number of locations for stress profiles}$$

$$\text{Loc}_0 := \text{FL}_{\text{Cntr}} - L$$

$$\text{FL}_{\text{Cntr}} = 12.0812$$

$$L = 0.4$$

$$i := 1..N + 3$$

$$\text{Incr}_i := \begin{cases} c_0 & \text{if } i < 4 \\ \text{IncStrs.avg} & \text{otherwise} \end{cases}$$

$$\text{Loc}_i := \text{Loc}_{i-1} + \text{Incr}_i$$

$$\text{SID}_i := R_{\text{ID}_3} + R_{\text{ID}_4} \cdot \text{Loc}_i + R_{\text{ID}_5} \cdot (\text{Loc}_i)^2 + R_{\text{ID}_6} \cdot (\text{Loc}_i)^3 + R_{\text{ID}_7} \cdot (\text{Loc}_i)^4$$

$$\text{SQT}_i := R_{\text{QT}_3} + R_{\text{QT}_4} \cdot \text{Loc}_i + R_{\text{QT}_5} \cdot (\text{Loc}_i)^2 + R_{\text{QT}_6} \cdot (\text{Loc}_i)^3 + R_{\text{QT}_7} \cdot (\text{Loc}_i)^4$$

$$\text{SMD}_i := R_{\text{MD}_3} + R_{\text{MD}_4} \cdot \text{Loc}_i + R_{\text{MD}_5} \cdot (\text{Loc}_i)^2 + R_{\text{MD}_6} \cdot (\text{Loc}_i)^3 + R_{\text{MD}_7} \cdot (\text{Loc}_i)^4$$

$$\text{STQ}_i := R_{\text{TQ}_3} + R_{\text{TQ}_4} \cdot \text{Loc}_i + R_{\text{TQ}_5} \cdot (\text{Loc}_i)^2 + R_{\text{TQ}_6} \cdot (\text{Loc}_i)^3 + R_{\text{TQ}_7} \cdot (\text{Loc}_i)^4$$

$$\text{SOD}_i := R_{\text{OD}_3} + R_{\text{OD}_4} \cdot \text{Loc}_i + R_{\text{OD}_5} \cdot (\text{Loc}_i)^2 + R_{\text{OD}_6} \cdot (\text{Loc}_i)^3 + R_{\text{OD}_7} \cdot (\text{Loc}_i)^4$$

$$j := 1..N$$

$$S_{\text{id}_j} := \begin{cases} \frac{\text{SID}_j + \text{SID}_{j+1} + \text{SID}_{j+2}}{3} & \text{if } j = 1 \\ \frac{S_{\text{id}_{j-1}} \cdot (j+1) + \text{SID}_{j+2}}{j+2} & \text{otherwise} \end{cases}$$

$$S_{\text{qt}_j} := \begin{cases} \frac{\text{SQT}_j + \text{SQT}_{j+1} + \text{SQT}_{j+2}}{3} & \text{if } j = 1 \\ \frac{S_{\text{qt}_{j-1}} \cdot (j+1) + \text{SQT}_{j+2}}{j+2} & \text{otherwise} \end{cases}$$

$$S_{md_j} := \begin{cases} \frac{SMD_j + SMD_{j+1} + SMD_{j+2}}{3} & \text{if } j = 1 \\ \frac{S_{md_{j-1}} \cdot (j+1) + SMD_{j+2}}{j+2} & \text{otherwise} \end{cases}$$

$$S_{tq_j} := \begin{cases} \frac{STQ_j + STQ_{j+1} + STQ_{j+2}}{3} & \text{if } j = 1 \\ \frac{S_{tq_{j-1}} \cdot (j+1) + STQ_{j+2}}{j+2} & \text{otherwise} \end{cases}$$

$$S_{od_j} := \begin{cases} \frac{SOD_j + SOD_{j+1} + SOD_{j+2}}{3} & \text{if } j = 1 \\ \frac{S_{od_{j-1}} \cdot (j+1) + SOD_{j+2}}{j+2} & \text{otherwise} \end{cases}$$

Through-Wall Stress Distribution for ID Flaws (i.e. ID to OD Stress distribution)

$$u_0 := 0.000$$

$$u_1 := 0.25$$

$$u_2 := 0.50$$

$$u_3 := 0.75$$

$$u_4 := 1.00$$

$$Y := \text{stack}(u_0, u_1, u_2, u_3, u_4)$$

$$\text{SIG}_1 := \text{stack}(S_{id_1}, S_{qt_1}, S_{md_1}, S_{tq_1}, S_{od_1})$$

$$\text{SIG}_2 := \text{stack}(S_{id_2}, S_{qt_2}, S_{md_2}, S_{tq_2}, S_{od_2})$$

$$\text{SIG}_3 := \text{stack}(S_{id_3}, S_{qt_3}, S_{md_3}, S_{tq_3}, S_{od_3})$$

$$\text{SIG}_4 := \text{stack}(S_{id_4}, S_{qt_4}, S_{md_4}, S_{tq_4}, S_{od_4})$$

$$\text{SIG}_5 := \text{stack}(S_{id_5}, S_{qt_5}, S_{md_5}, S_{tq_5}, S_{od_5})$$

$$\text{SIG}_6 := \text{stack}(S_{id_6}, S_{qt_6}, S_{md_6}, S_{tq_6}, S_{od_6})$$

$$\text{SIG}_7 := \text{stack}(S_{id_7}, S_{qt_7}, S_{md_7}, S_{tq_7}, S_{od_7})$$

$$\text{SIG}_8 := \text{stack}(S_{id_8}, S_{qt_8}, S_{md_8}, S_{tq_8}, S_{od_8})$$

$$\text{SIG}_9 := \text{stack}(S_{id_9}, S_{qt_9}, S_{md_9}, S_{tq_9}, S_{od_9})$$

$$\text{SIG}_{10} := \text{stack}(S_{id_{10}}, S_{qt_{10}}, S_{md_{10}}, S_{tq_{10}}, S_{od_{10}})$$

$$\text{SIG}_{11} := \text{stack}(S_{id_{11}}, S_{qt_{11}}, S_{md_{11}}, S_{tq_{11}}, S_{od_{11}})$$

$$\text{SIG}_{12} := \text{stack}(S_{id_{12}}, S_{qt_{12}}, S_{md_{12}}, S_{tq_{12}}, S_{od_{12}})$$

$$\text{SIG}_{13} := \text{stack}(S_{id_{13}}, S_{qt_{13}}, S_{md_{13}}, S_{tq_{13}}, S_{od_{13}})$$

$$\text{SIG}_{14} := \text{stack}(S_{id_{14}}, S_{qt_{14}}, S_{md_{14}}, S_{tq_{14}}, S_{od_{14}})$$

$$\text{SIG}_{15} := \text{stack}(S_{id_{15}}, S_{qt_{15}}, S_{md_{15}}, S_{tq_{15}}, S_{od_{15}})$$

$$\text{SIG}_{16} := \text{stack}(S_{id_{16}}, S_{qt_{16}}, S_{md_{16}}, S_{tq_{16}}, S_{od_{16}})$$

$$\text{SIG}_{17} := \text{stack}(S_{id_{17}}, S_{qt_{17}}, S_{md_{17}}, S_{tq_{17}}, S_{od_{17}})$$

$$\text{SIG}_{18} := \text{stack}(S_{id_{18}}, S_{qt_{18}}, S_{md_{18}}, S_{tq_{18}}, S_{od_{18}})$$

$$\text{SIG}_{19} := \text{stack}(S_{id_{19}}, S_{qt_{19}}, S_{md_{19}}, S_{tq_{19}}, S_{od_{19}})$$

$$\text{SIG}_{20} := \text{stack}(S_{id_{20}}, S_{qt_{20}}, S_{md_{20}}, S_{tq_{20}}, S_{od_{20}})$$

Regression of Through-Wall Stress distribution to Obtain Stress Coefficients Using a Third Order Polynomial

$$\text{IDRG}_1 := \text{regress}(Y, \text{SIG}_1, 3)$$

$$\text{IDRG}_2 := \text{regress}(Y, \text{SIG}_2, 3)$$

$$\text{IDRG}_3 := \text{regress}(Y, \text{SIG}_3, 3)$$

$$\text{IDRG}_4 := \text{regress}(Y, \text{SIG}_4, 3)$$

$$\text{IDRG}_5 := \text{regress}(Y, \text{SIG}_5, 3)$$

$$\text{IDRG}_6 := \text{regress}(Y, \text{SIG}_6, 3)$$

$$\text{IDRG}_7 := \text{regress}(Y, \text{SIG}_7, 3)$$

$$\text{IDRG}_8 := \text{regress}(Y, \text{SIG}_8, 3)$$

$$\text{IDRG}_9 := \text{regress}(Y, \text{SIG}_9, 3)$$

$$\text{IDRG}_{10} := \text{regress}(Y, \text{SIG}_{10}, 3)$$

$$\text{IDRG}_{11} := \text{regress}(Y, \text{SIG}_{11}, 3)$$

$$\text{IDRG}_{12} := \text{regress}(Y, \text{SIG}_{12}, 3)$$

$$\text{IDRG}_{13} := \text{regress}(Y, \text{SIG}_{13}, 3)$$

$$\text{IDRG}_{14} := \text{regress}(Y, \text{SIG}_{14}, 3)$$

$$\text{IDRG}_{15} := \text{regress}(Y, \text{SIG}_{15}, 3)$$

$$\text{IDRG}_{16} := \text{regress}(Y, \text{SIG}_{16}, 3)$$

$$\text{IDRG}_{17} := \text{regress}(Y, \text{SIG}_{17}, 3)$$

$$\text{IDRG}_{18} := \text{regress}(Y, \text{SIG}_{18}, 3)$$

$$\text{IDRG}_{19} := \text{regress}(Y, \text{SIG}_{19}, 3)$$

$$\text{IDRG}_{20} := \text{regress}(Y, \text{SIG}_{20}, 3)$$

Stress Distribution in the tube. *Stress influence coefficients obtained from third-order polynomial curve fit to the throughwall stress distribution*

Data Files for Flaw Shape Factors from NASA SC04 Model [Ref. 8]

{NO INPUT Required}

Mettu Raju Newman Sivakumar Forman Solution of ID Part throughwall Flaw in Cyinder

Jsb :=

	0	1	2
0	1.000	0.200	0.000
1	1.000	0.200	0.200
2	1.000	0.200	0.500
3	1.000	0.200	0.800
4	1.000	0.200	1.000
5	1.000	0.400	0.000
6	1.000	0.400	0.200
7	1.000	0.400	0.500
8	1.000	0.400	0.800
9	1.000	0.400	1.000
10	1.000	1.000	0.000
11	1.000	1.000	0.200
12	1.000	1.000	0.500
13	1.000	1.000	0.800
14	1.000	1.000	1.000
15	2.000	0.200	0.000
16	2.000	0.200	0.200
17	2.000	0.200	0.500
18	2.000	0.200	0.800
19	2.000	0.200	1.000
20	2.000	0.400	0.000
21	2.000	0.400	0.200
22	2.000	0.400	0.500
23	2.000	0.400	0.800
24	2.000	0.400	1.000
25	2.000	1.000	0.000
26	2.000	1.000	0.200
27	2.000	1.000	0.500
28	2.000	1.000	0.800
29	2.000	1.000	1.000
30	4.000	0.200	0.000
31	4.000	0.200	0.200
32	4.000	0.200	0.500
33	4.000	0.200	0.800

34	4.000	0.200	1.000
35	4.000	0.400	0.000
36	4.000	0.400	0.200
37	4.000	0.400	0.500
38	4.000	0.400	0.800
39	4.000	0.400	1.000
40	4.000	1.000	0.000
41	4.000	1.000	0.200
42	4.000	1.000	0.500
43	4.000	1.000	0.800
44	4.000	1.000	1.000
45	10.000	0.200	0.000
46	10.000	0.200	0.200
47	10.000	0.200	0.500
48	10.000	0.200	0.800
49	10.000	0.200	1.000
50	10.000	0.400	0.000
51	10.000	0.400	0.200
52	10.000	0.400	0.500
53	10.000	0.400	0.800
54	10.000	0.400	1.000
55	10.000	1.000	0.000
56	10.000	1.000	0.200
57	10.000	1.000	0.500
58	10.000	1.000	0.800
59	10.000	1.000	1.000
60	300.000	0.200	0.000
61	300.000	0.200	0.200
62	300.000	0.200	0.500
63	300.000	0.200	0.800
64	300.000	0.200	1.000
65	300.000	0.400	0.000
66	300.000	0.400	0.200
67	300.000	0.400	0.500
68	300.000	0.400	0.800
69	300.000	0.400	1.000
70	300.000	1.000	0.000
71	300.000	1.000	0.200
72	300.000	1.000	0.500
73	300.000	1.000	0.800
74	300.000	1.000	1.000

Sambi :=

	0	1	2	3	4	5	6	7
0	1.076	0.693	0.531	0.434	0.608	0.083	0.023	0.009
1	1.056	0.647	0.495	0.408	0.615	0.085	0.027	0.013
2	1.395	0.767	0.557	0.446	0.871	0.171	0.069	0.038
3	2.53	1.174	0.772	0.58	1.554	0.363	0.155	0.085
4	3.846	1.615	0.995	0.716	2.277	0.544	0.233	0.127
5	1.051	0.689	0.536	0.444	0.74	0.112	0.035	0.015
6	1.011	0.646	0.504	0.421	0.745	0.119	0.041	0.02
7	1.149	0.694	0.529	0.435	0.916	0.181	0.073	0.04
8	1.6	0.889	0.642	0.51	1.334	0.307	0.132	0.073
9	2.087	1.093	0.761	0.589	1.752	0.421	0.183	0.101
10	0.992	0.704	0.534	0.506	1.044	0.169	0.064	0.032
11	0.987	0.701	0.554	0.491	1.08	0.182	0.067	0.034
12	1.01	0.709	0.577	0.493	1.116	0.2	0.078	0.041
13	1.07	0.73	0.623	0.523	1.132	0.218	0.095	0.051
14	1.128	0.75	0.675	0.556	1.131	0.229	0.11	0.06
15	1.049	0.673	0.519	0.427	0.6	0.078	0.021	0.008
16	1.091	0.661	0.502	0.413	0.614	0.083	0.025	0.012
17	1.384	0.764	0.556	0.446	0.817	0.15	0.058	0.031
18	2.059	1.033	0.708	0.545	1.3	0.291	0.123	0.067
19	2.739	1.301	0.858	0.643	1.783	0.421	0.18	0.099
20	1.075	0.674	0.527	0.436	0.73	0.072	0.044	0.021
21	1.045	0.659	0.511	0.425	0.76	0.122	0.043	0.021
22	1.16	0.71	0.536	0.441	0.919	0.197	0.064	0.034
23	1.51	0.854	0.623	0.498	1.231	0.271	0.114	0.062
24	1.876	0.995	0.71	0.555	1.519	0.317	0.161	0.089
25	1.037	0.732	0.594	0.505	1.132	0.192	0.07	0.035
26	1.003	0.707	0.577	0.493	1.113	0.19	0.071	0.036
27	1.023	0.714	0.58	0.495	1.155	0.207	0.08	0.042
28	1.129	0.774	0.619	0.521	1.286	0.247	0.098	0.052
29	1.242	0.84	0.661	0.549	1.416	0.285	0.115	0.061
30	1.003	0.649	0.511	0.43	0.577	0.07	0.015	0.005
31	1.097	0.666	0.511	0.426	0.606	0.079	0.023	0.01
32	1.405	0.776	0.567	0.46	0.797	0.141	0.054	0.028
33	1.959	0.996	0.692	0.542	1.201	0.262	0.108	0.059
34	2.461	1.197	0.808	0.619	1.586	0.37	0.154	0.085
35	1.024	0.668	0.528	0.451	0.737	0.11	0.033	0.015
36	1.057	0.666	0.52	0.439	0.77	0.123	0.042	0.021
37	1.193	0.715	0.545	0.454	0.924	0.174	0.068	0.036
38	1.443	0.828	0.614	0.509	1.219	0.263	0.109	0.059
39	1.665	0.934	0.681	0.565	1.487	0.339	0.143	0.078
40	1.005	0.72	0.597	0.518	1.110	0.188	0.068	0.034

41	1.009	0.713	0.588	0.511	1.128	0.194	0.072	0.037
42	1.041	0.726	0.594	0.515	1.191	0.214	0.082	0.043
43	1.105	0.768	0.623	0.536	1.316	0.248	0.097	0.05
44	1.162	0.81	0.653	0.558	1.428	0.277	0.109	0.055
45	0.973	0.635	0.499	0.446	0.579	0.07	0.016	0.005
46	1.115	0.673	0.514	0.438	0.607	0.079	0.023	0.01
47	1.427	0.783	0.571	0.462	0.791	0.138	0.052	0.027
48	1.872	0.96	0.671	0.529	1.179	0.253	0.104	0.056
49	2.23	1.108	0.757	0.594	1.548	0.356	0.149	0.081
50	0.992	0.656	0.52	0.443	0.733	0.109	0.032	0.014
51	1.072	0.672	0.523	0.441	0.777	0.125	0.043	0.021
52	1.217	0.723	0.549	0.456	0.936	0.176	0.069	0.036
53	1.393	0.806	0.601	0.493	1.219	0.259	0.106	0.056
54	1.521	0.875	0.647	0.528	1.469	0.328	0.135	0.071
55	0.994	0.715	0.59	0.518	1.114	0.187	0.068	0.035
56	1.015	0.715	0.588	0.512	1.14	0.197	0.074	0.038
57	1.05	0.729	0.596	0.515	1.219	0.221	0.085	0.044
58	1.09	0.76	0.618	0.532	1.348	0.255	0.099	0.051
59	1.118	0.788	0.639	0.55	1.456	0.282	0.109	0.056
60	0.936	0.62	0.486	0.405	0.582	0.068	0.015	0.005
61	1.145	0.681	0.514	0.42	0.613	0.081	0.024	0.011
62	1.459	0.79	0.569	0.454	0.79	0.138	0.051	0.026
63	1.774	0.917	0.641	0.501	1.148	0.239	0.096	0.051
64	1.974	1.008	0.696	0.537	1.482	0.328	0.134	0.07
65	0.982	0.651	0.512	0.427	0.721	0.103	0.031	0.013
66	1.095	0.677	0.52	0.431	0.782	0.127	0.045	0.022
67	1.244	0.727	0.546	0.446	0.946	0.18	0.071	0.037
68	1.37	0.791	0.585	0.473	1.201	0.253	0.102	0.054
69	1.438	0.838	0.618	0.496	1.413	0.31	0.126	0.066

$$W_{\text{Jsb}} := \text{Jsb}^{(0)}$$

$$X := \text{Jsb}^{(1)}$$

$$Y := \text{Jsb}^{(2)}$$

$$a_U := \text{Sambi}^{(0)}$$

$$a_L := \text{Sambi}^{(1)}$$

$$a_Q := \text{Sambi}^{(2)}$$

$$a_C := \text{Sambi}^{(3)}$$

$$c_U := \text{Sambi}^{(4)}$$

$$c_L := \text{Sambi}^{(5)}$$

$$c_Q := \text{Sambi}^{(6)}$$

$$c_C := \text{Sambi}^{(7)}$$

$$n := \begin{cases} 3 & \text{if } R_t \leq 4.0 \\ 2 & \text{otherwise} \end{cases}$$

"a-Tip" Uniform Term

$$M_{aU} := \text{augment}(W, X, Y) \quad V_{aU} := a_U \quad R_{aU} := \text{regress}(M_{aU}, V_{aU}, n)$$

$$f_{aU}(W, X, Y) := \text{interp} \left[R_{aU}, M_{aU}, V_{aU}, \begin{pmatrix} W \\ X \\ Y \end{pmatrix} \right]$$

$$f_{aU}(4, .4, .8) = 1.7089$$

Check Calculation

Linear Term

$$M_{aL} := \text{augment}(W, X, Y) \quad V_{aL} := a_L \quad R_{aL} := \text{regress}(M_{aL}, V_{aL}, n)$$

$$f_{aL}(W, X, Y) := \text{interp} \left[R_{aL}, M_{aL}, V_{aL}, \begin{pmatrix} W \\ X \\ Y \end{pmatrix} \right]$$

$$f_{aL}(4, .4, .8) = 0.93393$$

Check Calculation

Quadratic Term

$$M_{aQ} := \text{augment}(W, X, Y) \quad V_{aQ} := a_Q \quad R_{aQ} := \text{regress}(M_{aQ}, V_{aQ}, n)$$

$$f_{aQ}(W, X, Y) := \text{interp} \left[R_{aQ}, M_{aQ}, V_{aQ}, \begin{pmatrix} W \\ X \\ Y \end{pmatrix} \right]$$

$$f_{aQ}(4, .4, .8) = 0.67668 \quad \text{Check Calculation}$$

Cubic Term

$$M_{aC} := \text{augment}(W, X, Y) \quad V_{aC} := a_C$$

$$R_{aC} := \text{regress}(M_{aC}, V_{aC}, n)$$

$$f_{aC}(W, X, Y) := \text{interp} \left[R_{aC}, M_{aC}, V_{aC}, \begin{pmatrix} W \\ X \\ Y \end{pmatrix} \right]$$

$$f_{aC}(4, .4, .8) = 0.54151 \quad \text{Check Calculation}$$

"C" Tip Coefficients

Uniform Term

$$M_{cU} := \text{augment}(W, X, Y) \quad V_{cU} := c_U$$

$$R_{cU} := \text{regress}(M_{cU}, V_{cU}, n)$$

$$f_{cU}(W, X, Y) := \text{interp} \left[R_{cU}, M_{cU}, V_{cU}, \begin{pmatrix} W \\ X \\ Y \end{pmatrix} \right]$$

$$f_{cU}(4, .4, .8) = 1.31015 \quad \text{Check Calculation}$$

Linear Term

$$M_{cL} := \text{augment}(W, X, Y) \quad V_{cL} := c_L$$

$$R_{cL} := \text{regress}(M_{cL}, V_{cL}, n)$$

$$f_{cL}(W, X, Y) := \text{interp} \left[R_{cL}, M_{cL}, V_{cL}, \begin{pmatrix} W \\ X \\ Y \end{pmatrix} \right]$$

$$f_{cL}(2, .4, .8) = 0.28509 \quad \text{Check Calculation}$$

Quadratic Term

$$M_{cQ} := \text{augment}(W, X, Y) \quad V_{cQ} := c_Q \quad R_{cQ} := \text{regress}(M_{cQ}, V_{cQ}, n)$$

$$f_{cQ}(W, X, Y) := \text{interp} \left[R_{cQ}, M_{cQ}, V_{cQ}, \begin{pmatrix} W \\ X \\ Y \end{pmatrix} \right]$$

$$f_{cQ}(4, .4, .8) = 0.11797 \quad \text{Check Calculation}$$

Cubic Term

$$M_{cC} := \text{augment}(W, X, Y) \quad V_{cC} := c_C \quad R_{cC} := \text{regress}(M_{cC}, V_{cC}, n)$$

$$f_{cC}(W, X, Y) := \text{interp} \left[R_{cC}, M_{cC}, V_{cC}, \begin{pmatrix} W \\ X \\ Y \end{pmatrix} \right]$$

$$f_{cC}(4, .4, .8) = 0.06384 \quad \text{Check Calculation}$$

Calculations : Recursive calculations to estimate flaw growth

Recursive Loop for Calculation of PWSCC Crack Growth

```

CGRsambi := | j ← 0
              | a0 ← a0
              | c0 ← c0
              | t ← t2
              | NCB0 ← Cblk
              | while j ≤ Ilim
                |   σ0 ← | IDRG1,3 if cj ≤ c0
                |         | IDRG2,3 if c0 < cj ≤ c0 + IncStrs.avg
                |         | IDRG3,3 if c0 + IncStrs.avg < cj ≤ c0 + 2·IncStrs.avg
                |         | IDRG4,3 if c0 + 2·IncStrs.avg < cj ≤ c0 + 3·IncStrs.avg
                |         | IDRG5,3 if c0 + 3·IncStrs.avg < cj ≤ c0 + 4·IncStrs.avg
                |         | IDRG6,3 if c0 + 4·IncStrs.avg < cj ≤ c0 + 5·IncStrs.avg
                |         | IDRG7,3 if c0 + 5·IncStrs.avg < cj ≤ c0 + 6·IncStrs.avg
                |         | IDRG8,3 if c0 + 6·IncStrs.avg < cj ≤ c0 + 7·IncStrs.avg
                |         | IDRG9,3 if c0 + 7·IncStrs.avg < cj ≤ c0 + 8·IncStrs.avg
                |         | IDRG10,3 if c0 + 8·IncStrs.avg < cj ≤ c0 + 9·IncStrs.avg
                |         | IDRG11,3 if c0 + 9·IncStrs.avg < cj ≤ c0 + 10·IncStrs.avg
                |         | IDRG12,3 if c0 + 10·IncStrs.avg < cj ≤ c0 + 11·IncStrs.avg
                |         | IDRG13,3 if c0 + 11·IncStrs.avg < cj ≤ c0 + 12·IncStrs.avg
                |         | IDRG14,3 if c0 + 12·IncStrs.avg < cj ≤ c0 + 13·IncStrs.avg
                |         | IDRG15,3 if c0 + 13·IncStrs.avg < cj ≤ c0 + 14·IncStrs.avg

```

	IDRG ₁₆ ₃	if $c_0 + 14 \cdot \text{IncStrs.avg} < c_j \leq c_0 + 15 \cdot \text{IncStrs.avg}$
	IDRG ₁₇ ₃	if $c_0 + 15 \cdot \text{IncStrs.avg} < c_j \leq c_0 + 16 \cdot \text{IncStrs.avg}$
	IDRG ₁₈ ₃	if $c_0 + 16 \cdot \text{IncStrs.avg} < c_j \leq c_0 + 17 \cdot \text{IncStrs.avg}$
	IDRG ₁₉ ₃	if $c_0 + 17 \cdot \text{IncStrs.avg} < c_j \leq c_0 + 18 \cdot \text{IncStrs.avg}$
	IDRG ₂₀ ₃	otherwise
$\sigma_1 \leftarrow$	IDRG ₁ ₄	if $c_j \leq c_0$
	IDRG ₂ ₄	if $c_0 < c_j \leq c_0 + \text{IncStrs.avg}$
	IDRG ₃ ₄	if $c_0 + \text{IncStrs.avg} < c_j \leq c_0 + 2 \cdot \text{IncStrs.avg}$
	IDRG ₄ ₄	if $c_0 + 2 \cdot \text{IncStrs.avg} < c_j \leq c_0 + 3 \cdot \text{IncStrs.avg}$
	IDRG ₅ ₄	if $c_0 + 3 \cdot \text{IncStrs.avg} < c_j \leq c_0 + 4 \cdot \text{IncStrs.avg}$
	IDRG ₆ ₄	if $c_0 + 4 \cdot \text{IncStrs.avg} < c_j \leq c_0 + 5 \cdot \text{IncStrs.avg}$
	IDRG ₇ ₄	if $c_0 + 5 \cdot \text{IncStrs.avg} < c_j \leq c_0 + 6 \cdot \text{IncStrs.avg}$
	IDRG ₈ ₄	if $c_0 + 6 \cdot \text{IncStrs.avg} < c_j \leq c_0 + 7 \cdot \text{IncStrs.avg}$
	IDRG ₉ ₄	if $c_0 + 7 \cdot \text{IncStrs.avg} < c_j \leq c_0 + 8 \cdot \text{IncStrs.avg}$
	IDRG ₁₀ ₄	if $c_0 + 8 \cdot \text{IncStrs.avg} < c_j \leq c_0 + 9 \cdot \text{IncStrs.avg}$
	IDRG ₁₁ ₄	if $c_0 + 9 \cdot \text{IncStrs.avg} < c_j \leq c_0 + 10 \cdot \text{IncStrs.avg}$
	IDRG ₁₂ ₄	if $c_0 + 10 \cdot \text{IncStrs.avg} < c_j \leq c_0 + 11 \cdot \text{IncStrs.avg}$
	IDRG ₁₃ ₄	if $c_0 + 11 \cdot \text{IncStrs.avg} < c_j \leq c_0 + 12 \cdot \text{IncStrs.avg}$
	IDRG ₁₄ ₄	if $c_0 + 12 \cdot \text{IncStrs.avg} < c_j \leq c_0 + 13 \cdot \text{IncStrs.avg}$
	IDRG ₁₅ ₄	if $c_0 + 13 \cdot \text{IncStrs.avg} < c_j \leq c_0 + 14 \cdot \text{IncStrs.avg}$
	IDRG ₁₆ ₄	if $c_0 + 14 \cdot \text{IncStrs.avg} < c_j \leq c_0 + 15 \cdot \text{IncStrs.avg}$

	IDRG ₁₇ ₄	if $c_0 + 15 \cdot \text{IncStrs.avg} < c_j \leq c_0 + 16 \cdot \text{IncStrs.avg}$
	IDRG ₁₈ ₄	if $c_0 + 16 \cdot \text{IncStrs.avg} < c_j \leq c_0 + 17 \cdot \text{IncStrs.avg}$
	IDRG ₁₉ ₄	if $c_0 + 17 \cdot \text{IncStrs.avg} < c_j \leq c_0 + 18 \cdot \text{IncStrs.avg}$
	IDRG ₂₀ ₄	otherwise
$\sigma_2 \leftarrow$	IDRG ₁ ₅	if $c_j \leq c_0$
	IDRG ₂ ₅	if $c_0 < c_j \leq c_0 + \text{IncStrs.avg}$
	IDRG ₃ ₅	if $c_0 + \text{IncStrs.avg} < c_j \leq c_0 + 2 \cdot \text{IncStrs.avg}$
	IDRG ₄ ₅	if $c_0 + 2 \cdot \text{IncStrs.avg} < c_j \leq c_0 + 3 \cdot \text{IncStrs.avg}$
	IDRG ₅ ₅	if $c_0 + 3 \cdot \text{IncStrs.avg} < c_j \leq c_0 + 4 \cdot \text{IncStrs.avg}$
	IDRG ₆ ₅	if $c_0 + 4 \cdot \text{IncStrs.avg} < c_j \leq c_0 + 5 \cdot \text{IncStrs.avg}$
	IDRG ₇ ₅	if $c_0 + 5 \cdot \text{IncStrs.avg} < c_j \leq c_0 + 6 \cdot \text{IncStrs.avg}$
	IDRG ₈ ₅	if $c_0 + 6 \cdot \text{IncStrs.avg} < c_j \leq c_0 + 7 \cdot \text{IncStrs.avg}$
	IDRG ₉ ₅	if $c_0 + 7 \cdot \text{IncStrs.avg} < c_j \leq c_0 + 8 \cdot \text{IncStrs.avg}$
	IDRG ₁₀ ₅	if $c_0 + 8 \cdot \text{IncStrs.avg} < c_j \leq c_0 + 9 \cdot \text{IncStrs.avg}$
	IDRG ₁₁ ₅	if $c_0 + 9 \cdot \text{IncStrs.avg} < c_j \leq c_0 + 10 \cdot \text{IncStrs.avg}$
	IDRG ₁₂ ₅	if $c_0 + 10 \cdot \text{IncStrs.avg} < c_j \leq c_0 + 11 \cdot \text{IncStrs.avg}$
	IDRG ₁₃ ₅	if $c_0 + 11 \cdot \text{IncStrs.avg} < c_j \leq c_0 + 12 \cdot \text{IncStrs.avg}$
	IDRG ₁₄ ₅	if $c_0 + 12 \cdot \text{IncStrs.avg} < c_j \leq c_0 + 13 \cdot \text{IncStrs.avg}$
	IDRG ₁₅ ₅	if $c_0 + 13 \cdot \text{IncStrs.avg} < c_j \leq c_0 + 14 \cdot \text{IncStrs.avg}$
	IDRG ₁₆ ₅	if $c_0 + 14 \cdot \text{IncStrs.avg} < c_j \leq c_0 + 15 \cdot \text{IncStrs.avg}$
	IDRG ₁₇ ₅	if $c_0 + 15 \cdot \text{IncStrs.avg} < c_j \leq c_0 + 16 \cdot \text{IncStrs.avg}$
	IDRG ₁₈	if $c_0 + 16 \cdot \text{IncStrs.avg} < c_j \leq c_0 + 17 \cdot \text{IncStrs.avg}$

		$\text{IDRG}_{19_5} \text{ if } c_0 + 17 \cdot \text{IncStrs.avg} < c_j \leq c_0 + 18 \cdot \text{IncStrs.avg}$ $\text{IDRG}_{20_5} \text{ otherwise}$
$\sigma_3 \leftarrow$		$\text{IDRG}_{1_6} \text{ if } c_j \leq c_0$ $\text{IDRG}_{2_6} \text{ if } c_0 < c_j \leq c_0 + \text{IncStrs.avg}$ $\text{IDRG}_{3_6} \text{ if } c_0 + \text{IncStrs.avg} < c_j \leq c_0 + 2 \cdot \text{IncStrs.avg}$ $\text{IDRG}_{4_6} \text{ if } c_0 + 2 \cdot \text{IncStrs.avg} < c_j \leq c_0 + 3 \cdot \text{IncStrs.avg}$ $\text{IDRG}_{5_6} \text{ if } c_0 + 3 \cdot \text{IncStrs.avg} < c_j \leq c_0 + 4 \cdot \text{IncStrs.avg}$ $\text{IDRG}_{6_6} \text{ if } c_0 + 4 \cdot \text{IncStrs.avg} < c_j \leq c_0 + 5 \cdot \text{IncStrs.avg}$ $\text{IDRG}_{7_6} \text{ if } c_0 + 5 \cdot \text{IncStrs.avg} < c_j \leq c_0 + 6 \cdot \text{IncStrs.avg}$ $\text{IDRG}_{8_6} \text{ if } c_0 + 6 \cdot \text{IncStrs.avg} < c_j \leq c_0 + 7 \cdot \text{IncStrs.avg}$ $\text{IDRG}_{9_6} \text{ if } c_0 + 7 \cdot \text{IncStrs.avg} < c_j \leq c_0 + 8 \cdot \text{IncStrs.avg}$ $\text{IDRG}_{10_6} \text{ if } c_0 + 8 \cdot \text{IncStrs.avg} < c_j \leq c_0 + 9 \cdot \text{IncStrs.avg}$ $\text{IDRG}_{11_6} \text{ if } c_0 + 9 \cdot \text{IncStrs.avg} < c_j \leq c_0 + 10 \cdot \text{IncStrs.avg}$ $\text{IDRG}_{12_6} \text{ if } c_0 + 10 \cdot \text{IncStrs.avg} < c_j \leq c_0 + 11 \cdot \text{IncStrs.avg}$ $\text{IDRG}_{13_6} \text{ if } c_0 + 11 \cdot \text{IncStrs.avg} < c_j \leq c_0 + 12 \cdot \text{IncStrs.avg}$ $\text{IDRG}_{14_6} \text{ if } c_0 + 12 \cdot \text{IncStrs.avg} < c_j \leq c_0 + 13 \cdot \text{IncStrs.avg}$ $\text{IDRG}_{15_6} \text{ if } c_0 + 13 \cdot \text{IncStrs.avg} < c_j \leq c_0 + 14 \cdot \text{IncStrs.avg}$ $\text{IDRG}_{16_6} \text{ if } c_0 + 14 \cdot \text{IncStrs.avg} < c_j \leq c_0 + 15 \cdot \text{IncStrs.avg}$ $\text{IDRG}_{17_6} \text{ if } c_0 + 15 \cdot \text{IncStrs.avg} < c_j \leq c_0 + 16 \cdot \text{IncStrs.avg}$ $\text{IDRG}_{18_6} \text{ if } c_0 + 16 \cdot \text{IncStrs.avg} < c_j \leq c_0 + 17 \cdot \text{IncStrs.avg}$ $\text{IDRG}_{19_6} \text{ if } c_0 + 17 \cdot \text{IncStrs.avg} < c_j \leq c_0 + 18 \cdot \text{IncStrs.avg}$

```

IDRG206 otherwise
ξ0 ← σ0
ξ1 ← σ0 + σ1 ·  $\left(\frac{0.25 \cdot a_j}{t}\right) + \sigma_2 \cdot \left(\frac{0.25 \cdot a_j}{t}\right)^2 + \sigma_3 \cdot \left(\frac{0.25 \cdot a_j}{t}\right)^3$ 
ξ2 ← σ0 + σ1 ·  $\left(\frac{0.5 \cdot a_j}{t}\right) + \sigma_2 \cdot \left(\frac{0.5 \cdot a_j}{t}\right)^2 + \sigma_3 \cdot \left(\frac{0.5 \cdot a_j}{t}\right)^3$ 
ξ3 ← σ0 + σ1 ·  $\left(\frac{0.75 \cdot a_j}{t}\right) + \sigma_2 \cdot \left(\frac{0.75 \cdot a_j}{t}\right)^2 + \sigma_3 \cdot \left(\frac{0.75 \cdot a_j}{t}\right)^3$ 
ξ4 ← σ0 + σ1 ·  $\left(\frac{1.0 \cdot a_j}{t}\right) + \sigma_2 \cdot \left(\frac{1.0 \cdot a_j}{t}\right)^2 + \sigma_3 \cdot \left(\frac{1.0 \cdot a_j}{t}\right)^3$ 
x0 ← 0.0
x1 ← 0.25
x2 ← 0.5
x3 ← 0.75
x4 ← 1.0
X ← stack(x0, x1, x2, x3, x4)
ST ← stack(ξ0, ξ1, ξ2, ξ3, ξ4)
RG ← regress(X, ST, 3)
σ00 ← RG3 + PInt
σ10 ← RG4
σ20 ← RG5
σ30 ← RG6
ARj ←  $\frac{a_j}{c_j}$ 
ATj ←  $\frac{a_j}{t}$ 
G... ← f... (R..., AR..., AT...)

```

$$G_{aq_j} \leftarrow f_{aQ}(R_t, AR_j, AT_j)$$

$$G_{cu_j} \leftarrow f_{cU}(R_t, AR_j, AT_j)$$

$$G_{cq_i} \leftarrow f_{cQ}(R_t, AR_j, AT_j)$$

$$Q_j \leftarrow \begin{cases} 1 + 1.464 \cdot \left(\frac{a_j}{c_j} \right)^{1.65} & \text{if } c_j \geq a_j \\ 1 + 1.464 \cdot \left(\frac{c_j}{a_j} \right)^{1.65} & \text{otherwise} \end{cases}$$

$$K_{a,j} \leftarrow \left(\frac{\pi \cdot a_j}{Q_j} \right)^{0.5} \cdot (\sigma_{00} \cdot G_{au,j} + \sigma_{10} \cdot G_{al,j} + \sigma_{20} \cdot G_{aq,j} + \sigma_{30} \cdot G_{ac,j})$$

$$K_{c_j} \leftarrow \left(\frac{\pi \cdot c_j}{Q_j} \right)^{0.5} \cdot (\sigma_{00} \cdot G_{cu_j} + \sigma_{10} \cdot G_{cl_j} + \sigma_{20} \cdot G_{cq_j} + \sigma_{30} \cdot G_{cc_j})$$

$$K_{\alpha_i} \leftarrow K_{a_i} \cdot 1.099$$

$$K_{\gamma_j} \leftarrow K_{c_j} \cdot 1.099$$

$$K_{\alpha_j} \leftarrow \begin{cases} 9.0 & \text{if } K_{\alpha_j} \leq 9.0 \\ K_{\alpha_j} & \text{otherwise} \end{cases}$$

$$K_{\gamma_j} \leftarrow \begin{cases} 9.0 & \text{if } K_{\gamma_j} \leq 9.0 \\ K_{\gamma_j} & \text{otherwise} \end{cases}$$

$$D_{a_i} \leftarrow C_0 \cdot (K_{\alpha_i} - 9.0)^{1.16}$$

$$|n| \leq |n|_{\text{CF}} + |n|_{\text{C}} \text{ if } K \leq \infty$$

$$D_{ag_j} \leftarrow \begin{cases} D_{a_j} \cdot CF_{inhr} \cdot C_{blk} & \text{if } K_{\gamma_j} \geq 80.0 \\ 4 \cdot 10^{-10} \cdot CF_{inhr} \cdot C_{blk} & \text{otherwise} \end{cases}$$

$$D_{c_j} \leftarrow C_0 \cdot (K_{\gamma_j} - 9.0)^{1.16}$$

$$D_{cg_j} \leftarrow \begin{cases} D_{c_j} \cdot CF_{inhr} \cdot C_{blk} & \text{if } K_{\gamma_j} < 80.0 \\ 4 \cdot 10^{-10} \cdot CF_{inhr} \cdot C_{blk} & \text{otherwise} \end{cases}$$

$$\text{output}(j, 0) \leftarrow j$$

$$\text{output}(j, 1) \leftarrow a_j$$

$$\text{output}(j, 2) \leftarrow c_j - c_0$$

$$\text{output}(j, 3) \leftarrow D_{ag_j}$$

$$\text{output}(j, 4) \leftarrow D_{cg_j}$$

$$\text{output}(j, 5) \leftarrow K_{a_j}$$

$$\text{output}(j, 6) \leftarrow K_{c_j}$$

$$\text{output}(j, 7) \leftarrow \frac{NCB_j}{365 \cdot 24}$$

$$\text{output}(j, 8) \leftarrow G_{au_j}$$

$$\text{output}(j, 9) \leftarrow G_{al_j}$$

$$\text{output}(j, 10) \leftarrow G_{aq_j}$$

$$\text{output}(j, 11) \leftarrow G_{ac_j}$$

$$\text{output}(j, 12) \leftarrow G_{cu_j}$$

$$\text{output}(j, 13) \leftarrow G_{cl_j}$$

$$\text{output}(j, 14) \leftarrow G_{cq_j}$$

$$\text{output}(j, 15) \leftarrow G_{cc_j}$$

$$j \leftarrow j + 1$$

$$a_i \leftarrow a_{i-1} + D_{a_i}$$

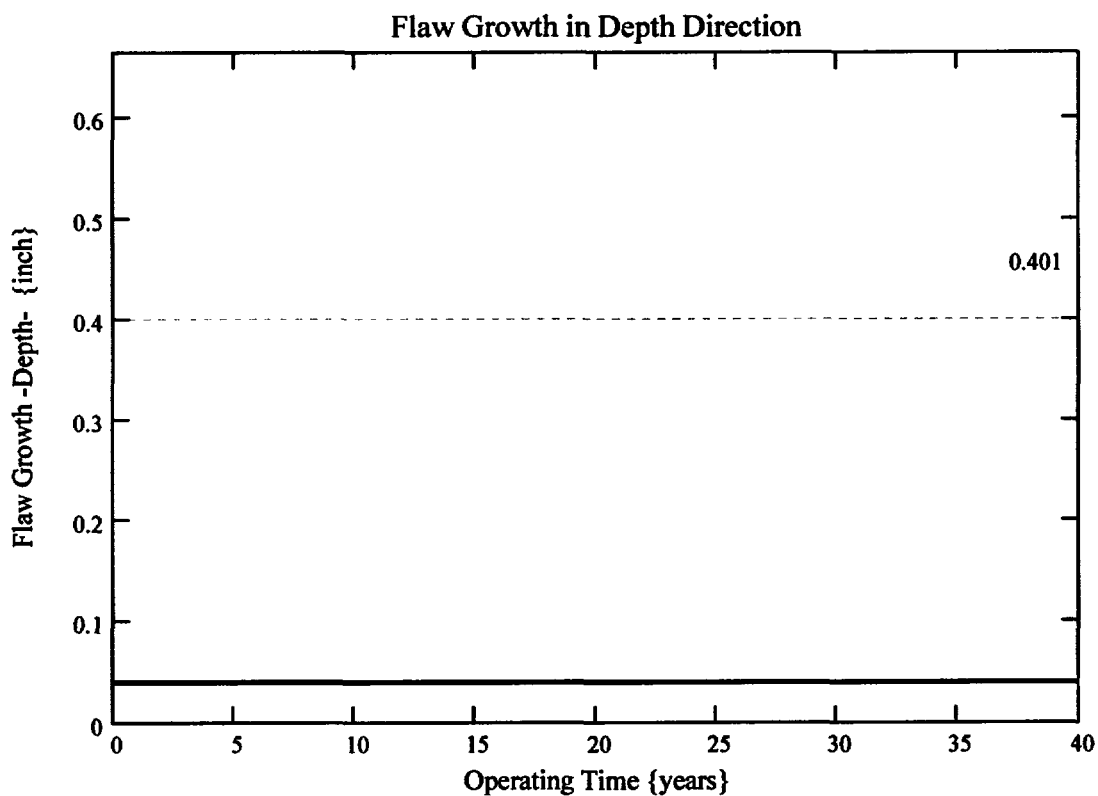

```

    "cj-1"
    cj ← cj-1 + Dcgj-1
    aj ← | t if aj ≥ t
          | aj otherwise
    NCBj ← NCBj-1 + Cblk
  output

```

$k_w := 0..I_{lim}$

The curve below shows the flaw growth through-wall and the operating time (in years) it takes to go through-wall.



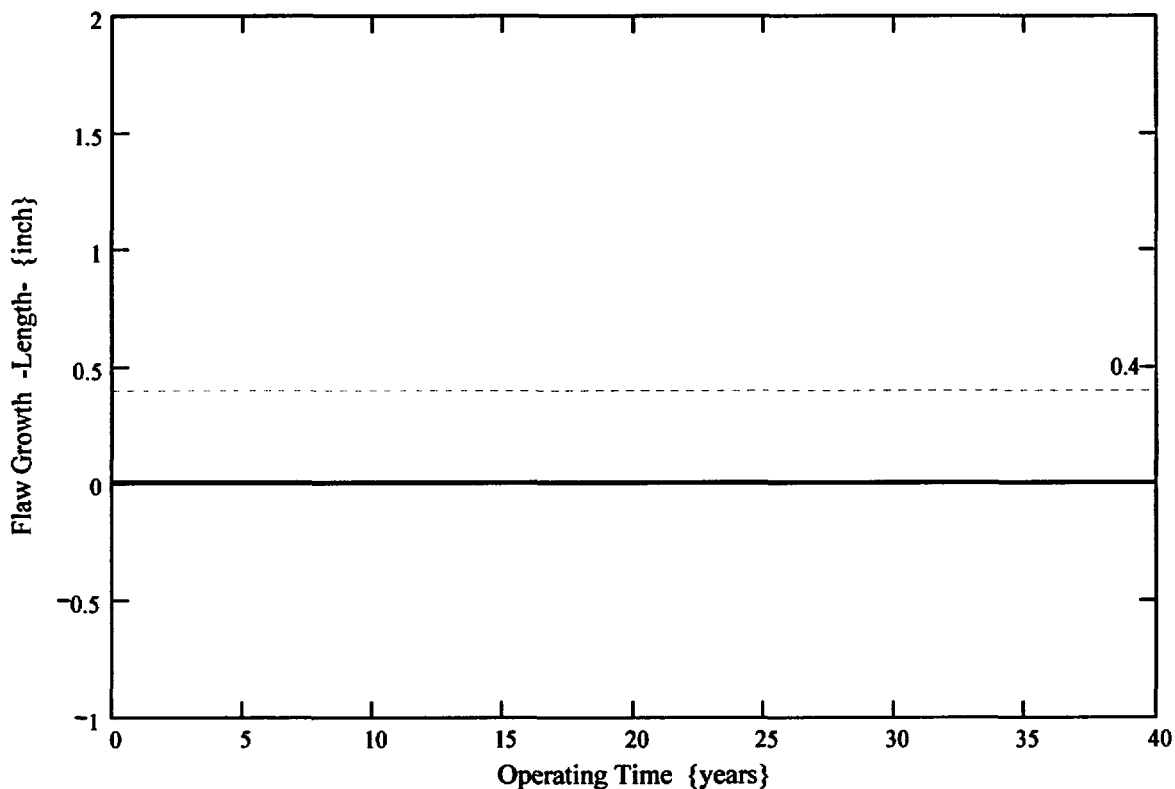
The propagation length for the ICI nozzles is defined as the length for which the initial flaw in the blind zone would extend out of the blind zone and grow to a detectable flaw. Reference 11 gives the minimum detectable flaw size of 4 mm (0.16) in length; thus, 0.16 inch was considered as this minimum detectable flaw length. This dimension is added to the end of the blind zone.

$$\text{Prop_Length} := \frac{\text{BZ_length}}{2} - c_0 + 0.16$$

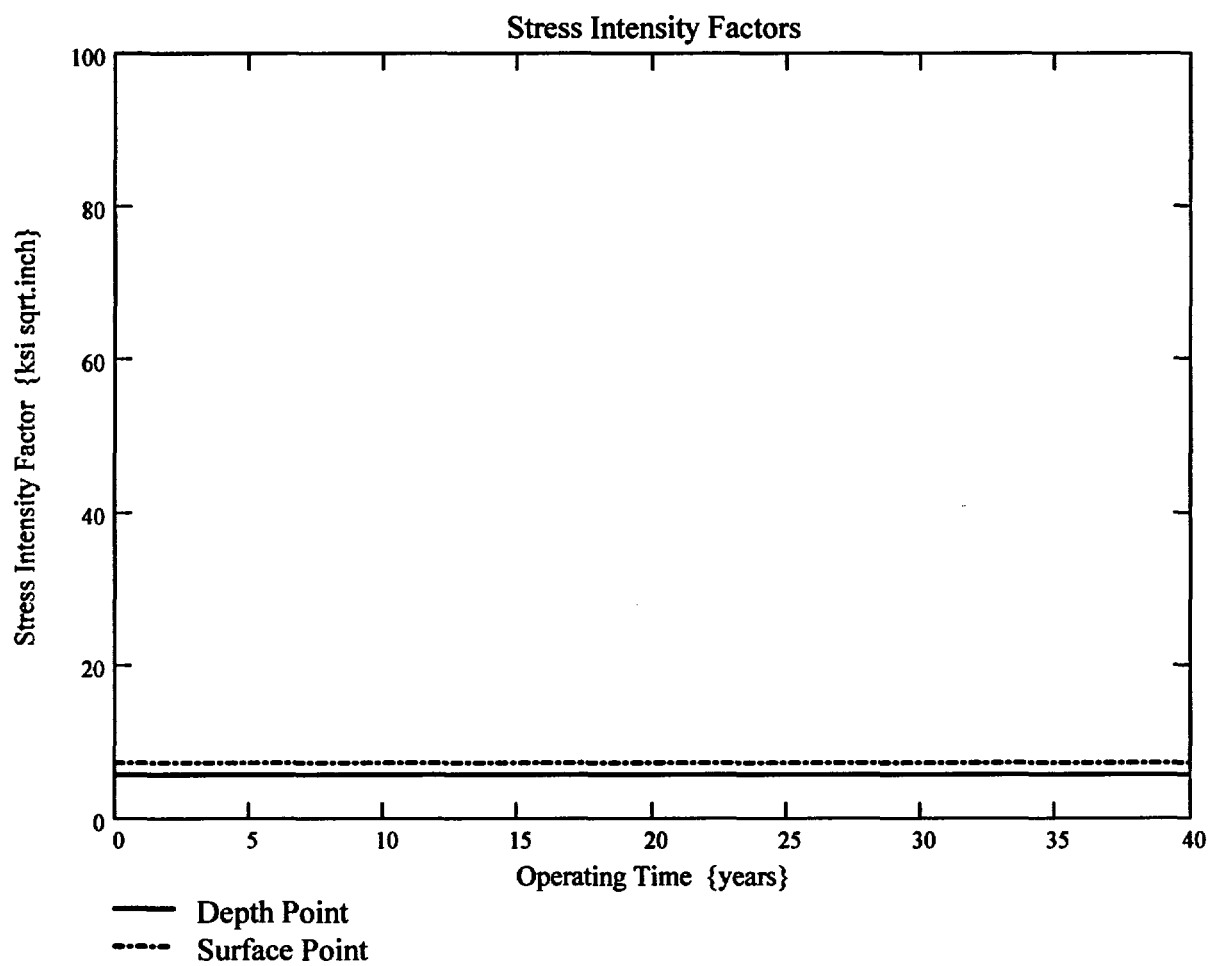
$$\text{Prop_Length} = 0.4$$

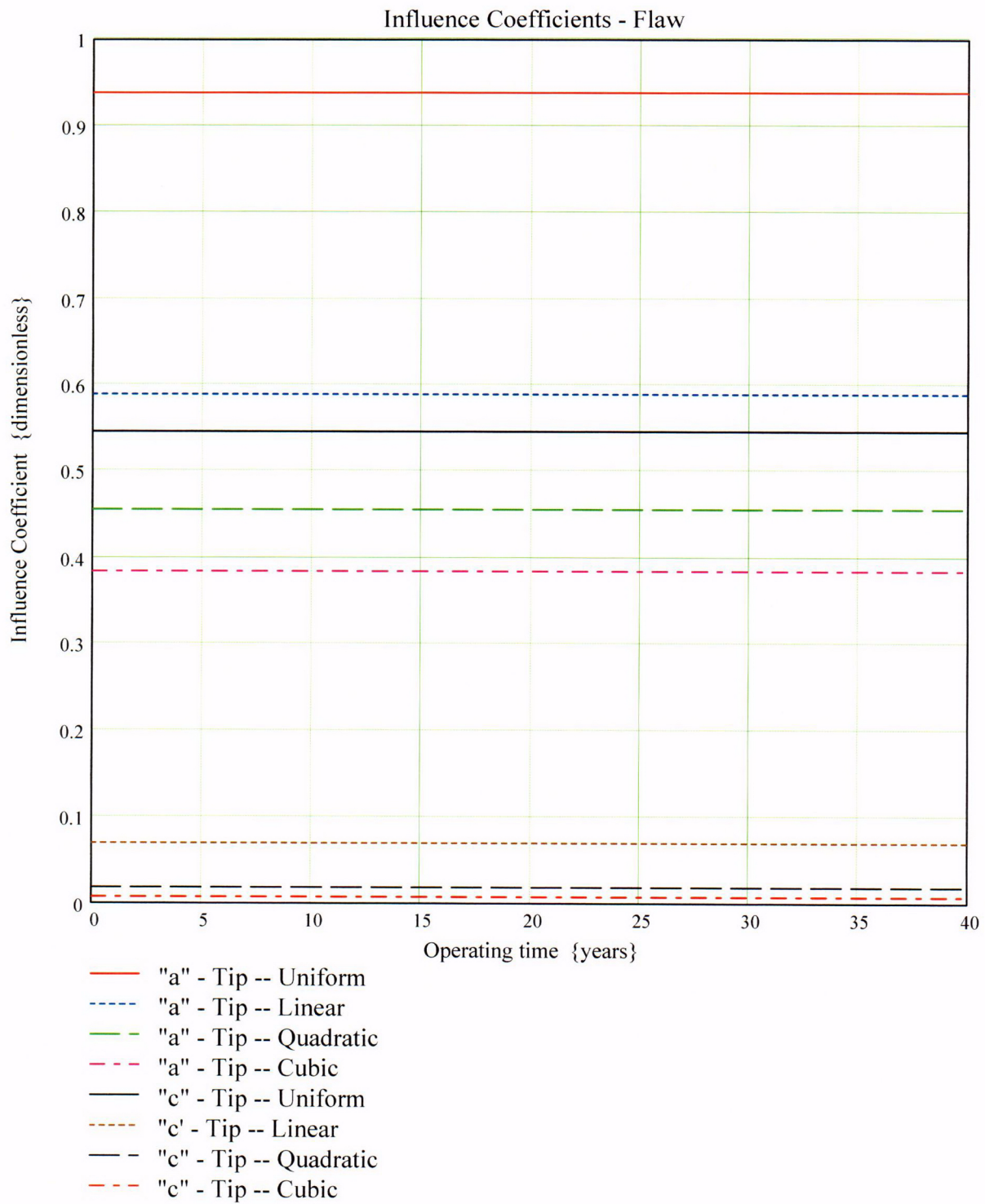
This implies that a flaw initially within the blindzone must grow 0.4 inch to become detectable via UT.

The curve below shows the flaw growth along the length of the ICI nozzle and the operating time (in years) it takes to reach the Prop_Length value defined above.



Thus, a flaw initially 0.4-inch in length, and 0.04-inch in depth (10% through-wall) will not grow in a 40 year operating period.





Arkansas Nuclear One Unit 2

Primary Water Stress Corrosion Crack Growth Analysis for an ICI ID Surface Flaw
Uphill (180°), in the Blind Zone above the Top of the J-Groove Weld
Developed by Central Engineering Programs, Entergy Operations Inc.

Flaw Case 3: 25% Through-Wall Flaw with a 4-to-1 Flaw Length-to-Depth Aspect Ratio, Located at the Center of the Blind Zone

Calculation Basis: MRP 75 th Percentile and Flaw Face Pressurized

Mean Radius -to- Thickness Ratio:- " R_m/t " – between 1.0 and 300.0

Note : *The Metric form of the equation from EPRI MRP was used 55-Rev. 1 . A correction factor is applied in the determination of the crack extension to convert the units of meters per second to the value in inches per hour .*

ID Surface Flaw

User Input:

The Dominion Engineering Inc. (DEI) finite element model nodal elevations and hoop stresses for the uphill side (180° azimuth) of the ICI nozzle are brought into the Mathcad worksheet from data supplied in Reference 6d. The data are composed of the nodal elevations (in inches), along with the ID, 25% through-wall (tw), 50% tw, 75% tw, and OD hoop stresses, beginning at the top of the weld (nodal line 81301) and extending to the top of the nozzle in the FEA model, which is at the point where the nozzle intersects the reactor vessel head.

The DEI FEA data has elevation referenced from the bottom of the ICI nozzle. The elevations of the node points in the DEI FEA model, beginning at the top of the weld (nodal line 81301), are as follows:

$i := 0..9$

$\text{Node_line}_i := \text{ID_elev_fea}_i := \text{QT_elev_fea}_i := \text{MD_elev_fea}_i := \text{TQ_elev_fea}_i := \text{OD_elev_fea}_i :=$

81301	4.2276	4.2276	4.2276	4.2276	4.2276
81401	4.4536	4.4536	4.4536	4.4536	4.4536
81501	4.8639	4.8639	4.8639	4.8639	4.8639
81601	5.1825	5.2486	5.3148	5.3810	5.4472
81701	6.2761	6.2761	6.2761	6.2761	6.2761
81801	7.4543	7.4543	7.4543	7.4543	7.4543
81901	9.1289	9.1289	9.1289	9.1289	9.1289
82001	11.5090	11.5090	11.5090	11.5090	11.5090
82101	14.8917	14.8917	14.8917	14.8917	14.8917
82201	17.8288	17.8288	17.8288	17.8288	17.8288

The corresponding stresses at these nodes are

ID_stress_fea_i := QT_stress_fea_i := MD_stress_fea_i := TQ_stress_fea_i := OD_stress_fea_i :=

26.390
23.147
19.425
15.065
16.707
17.399
17.412
17.115
15.304
10.308

25.687
21.559
18.188
14.581
16.175
17.177
17.487
15.794
13.024
10.119

24.607
19.292
15.780
13.132
15.560
15.044
12.883
11.377
10.766
10.032

22.680
16.085
11.381
6.189
8.890
8.136
7.180
7.821
9.067
9.951

44.523
9.729
8.207
-0.109
2.74
2.316
2.298
4.387
7.453
9.936

Blind Zone and Counterbore Reference dimensions:

From design drawings (Ref. 2a and 2b) and the design input of Attachment 1, the following dimensions are used to locate the counterbore bottom and blind zone locations (bottom, top, and middle) as referenced from the nodal coordinates of the DEI FEA model.

$$\text{Actual_cbore_bottom_elev} := \text{ID_elev_fea}_0 + 1.377$$

$$\text{Actual_cbore_bottom_elev} = 5.6046$$

$$\text{topweld_to_bottom_BZ} := 1.08$$

$$\text{BZ_length} := 0.88$$

$$\text{elev_to_mid_BZ} := \text{ID_elev_fea}_0 + \text{topweld_to_bottom_BZ} + \frac{\text{BZ_length}}{2}$$

$$\text{elev_to_mid_BZ} = 5.7476$$

$$\text{bottom_of_BZ} := \text{ID_elev_fea}_0 + \text{topweld_to_bottom_BZ}$$

$$\text{bottom_of_BZ} = 5.3076$$

$\text{top_of_BZ} := \text{ID_elev_fea}_0 + \text{topweld_to_bottom_BZ} + \text{BZ_length}$

$\text{top_of_BZ} = 6.1876$

For stress averaging and fracture mechanics purposes, the reference coordinate system--with a "0" elevation at the bottom of the nozzle, at the ID corner--must be converted into a new coordinate system with the top of the nozzle (nodal line 82201) as the new "0" elevation.. The positive direction along this new coordinate system will be towards nodal line 81301, which is the top of the weld. This modification facilitates a fracture mechanics model more ammenable to the surface flaw loop structure previously developed in Reference 7.

The following iterative loops convert the five (5) through-wall stress components--ID, 25% tw (QT), 50% tw (MD), 75% tw (TQ), and OD--and the associated elevations, initially given in the DEI FEA model, into the "new" coordinate system, referenced from the top of the nozzle where it meets the reactor vessel head.

```

ID_conv := | Top ← ID_elev_fea9
            | j ← 9
            | i ← 0
            | while j ≥ 0
            |   | ID_elev_convi ← Top - ID_elev_feaj
            |   | ID_stressi ← ID_stress_feaj
            |   | output(i, 0) ← ID_elev_convi
            |   | output(i, 1) ← ID_stressi
            |   | j ← j - 1
            |   | i ← i + 1
            | output
  
```

$\text{ID_elev} := \text{ID_conv}^{\langle 0 \rangle}$

$\text{ID_stress} := \text{ID_conv}^{\langle 1 \rangle}$

```

QT_conv := | Top ← QT_elev_fea9
            | j ← 9
            | i ← 0
            | while j ≥ 0
            |   | QT_elev_convi ← Top - QT_elev_feaj
            |   | QT_stressi ← QT_stress_feaj
            |   | output(i, 0) ← QT_elev_convi
            |   | output(i, 1) ← QT_stressi
            |   | j ← j - 1
            |   | i ← i + 1
            | output
  
```

QT_elev := QT_conv⁽⁰⁾

QT_stress := QT_conv⁽¹⁾

```

MD_conv := | Top ← MD_elev_fea9
            | j ← 9
            | i ← 0
            | while j ≥ 0
            |   | MD_elev_convi ← Top - MD_elev_feaj
            |   | MD_stressi ← MD_stress_feaj
            |   | output(i, 0) ← MD_elev_convi
            |   | output(i, 1) ← MD_stressi
            |   | j ← j - 1
            |   | i ← i + 1
            | output
  
```

MD_elev := MD_conv⁽⁰⁾

MD_stress := MD_conv⁽¹⁾


```

TQ_conv := | Top ← TQ_elev_fea9
           | j ← 9
           | i ← 0
           | while j ≥ 0
           |   | TQ_elev_convi ← Top – TQ_elev_feaj
           |   | TQ_stressi ← TQ_stress_feaj
           |   | output(i,0) ← TQ_elev_convi
           |   | output(i,1) ← TQ_stressi
           |   | j ← j – 1
           |   | i ← i + 1
           | output

```

TQ_elev := TQ_conv⁽⁰⁾

TQ_stress := TQ_conv⁽¹⁾

```

OD_conv := | Top ← OD_elev_fea9
           | j ← 9
           | i ← 0
           | while j ≥ 0
           |   | OD_elev_convi ← Top – OD_elev_feaj
           |   | OD_stressi ← OD_stress_feaj
           |   | output(i,0) ← OD_elev_convi
           |   | output(i,1) ← OD_stressi
           |   | j ← j – 1
           |   | i ← i + 1
           | output

```

OD_elev := OD_conv⁽⁰⁾

OD_stress := OD_conv⁽¹⁾

ID_elev_i =

0
2.9371
6.3198
8.6999
10.3745
11.5527
12.6463
12.9649
13.3752
13.6012

QT_elev_i =

0
2.9371
6.3198
8.6999
10.3745
11.5527
12.5802
12.9649
13.3752
13.6012

MD_elev_i =

0
2.9371
6.3198
8.6999
10.3745
11.5527
12.514
12.9649
13.3752
13.6012

TQ_elev_i =

0
2.9371
6.3198
8.6999
10.3745
11.5527
12.4478
12.9649
13.3752
13.6012

OD_elev_i =

0
2.9371
6.3198
8.6999
10.3745
11.5527
12.3816
12.9649
13.3752
13.6012

ID_stress_i =

10.308
15.304
17.115
17.412
17.399
16.707
15.065
19.425
23.147
26.39

QT_stress_i =

10.119
13.024
15.794
17.487
17.177
16.175
14.581
18.188
21.559
25.687

MD_stress_i =

10.032
10.766
11.377
12.883
15.044
15.56
13.132
15.78
19.292
24.607

TQ_stress_i =

9.951
9.067
7.821
7.18
8.136
8.89
6.189
11.381
16.085
22.68

OD_stress_i =

9.936
7.453
4.387
2.298
2.316
2.74
-0.109
8.207
9.729
44.523

The two sets of five arrays given above are the elevations measured from the top of the ICI nozzle from the FEA model down to the top of the J-weld and the corresponding hoop stresses in the modified coordinate system (MCS).

Additional Geometry in Modified Coordinate System

The top of the J-groove weld in the MCS is equal to the last entry in the ID_elev array:

$$\text{Top_Jweld} := \text{ID_elev}_9$$

$$\text{Top_Jweld} = 13.6012$$

The location of the top of the UT blind zone (BZ) in the MCS (as measured from the ID surface) is

$$\text{BZ_top} := \text{Top_Jweld} - (\text{topweld_to_bottom_BZ} + \text{BZ_length})$$

$$\text{BZ_top} = 11.6412$$

The midpoint of the BZ in the MCS is

$$\text{BZ_mid} := \text{BZ_top} + \frac{\text{BZ_length}}{2}$$

$$\text{BZ_mid} = 12.0812$$

The bottom of the BZ in the MCS is

$$\text{BZ_bottom} := \text{BZ_top} + \text{BZ_length}$$

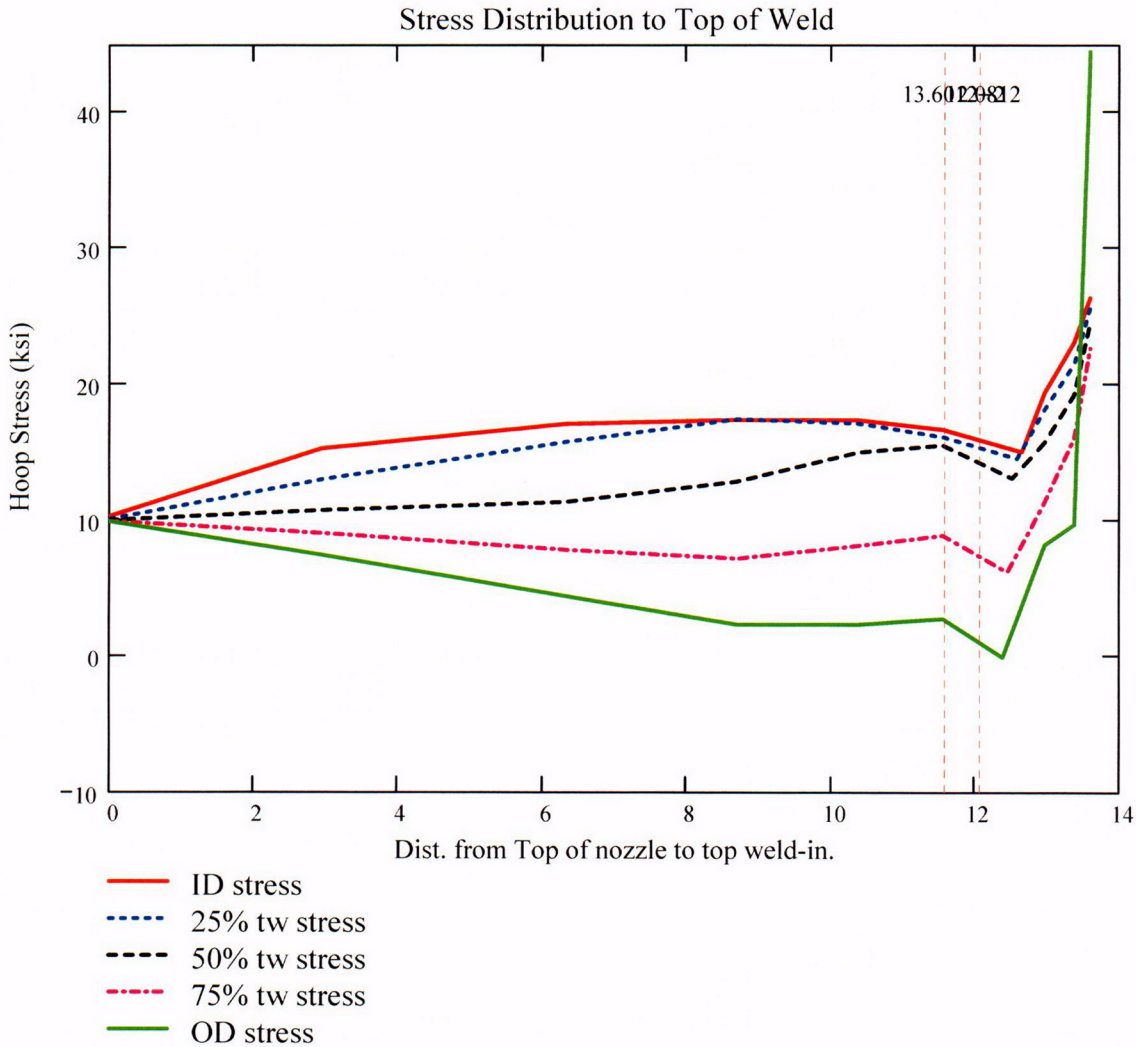
$$\text{BZ_bottom} = 12.5212$$

The location of the actual counterbore (from design drawings) in the MCS:

$$\text{cbore_elev} := \text{Top_Jweld} - 1.377$$

$$\text{cbore_elev} = 12.2242$$

From the MCS, the stress distribution from elevation 0 (the top of the ICI nozzle where it intersects the RV head) to the top of the weld is graphically shown below.



For the ID surface flaw model, the reference point is the location along the axis of the nozzle used to locate the flaw. For this analysis, the reference point is considered at the mid-height of the blind zone.

Ref_{Point} := BZ_{mid}

To place the flaw with respect to the reference point, the flaw tips and center can be located as follows:

- 1) The Upper "c- tip" located at the reference point (Enter 1)
- 2) The Center of the flaw at the reference point (Enter 2)
- 3) The lower "c- tip" located at the reference point (Enter 3).

Val := 2

The Input Below is the point below the blind zone region where stresses will be considered for curve-fitting. This point is taken as the top of the weld, since the stress distribution changes drastically within the weld region. Enter this dimension or variable below.

Elev_{Strs.Dist} := Top_Jweld The elevation to the point of maximum stress to consider
(Axial distance from elevation 0 in the MCS).

ICI Nozzle Geometry Input Data:

od := 5.563 – 0.001 Tube OD, in inches (The value from Ref. 2a, is 5.563" +0.00/-0.001)

id1 := 4.625 + 0.01 Maximum Tube ID above counterbore, in inches
(The value from Ref. 2b is 4.625" +/- 0.010")

id2 := 4.750 + 0.01 Maximum Tube ID below counterbore, in inches
(The value from Ref. 2b is 4.750" +/- 0.010")

$$t1 := \frac{(od - id1)}{2}$$

Minimum wall thickness above the counterbore, in inches

$$t1 = 0.4635$$

$$t2 := \frac{(od - id2)}{2}$$

Minimum wall thickness below the counterbore, in inches

$$t2 = 0.401$$

$$R_o := \frac{od}{2}$$

$$R_o = 2.781$$

$$R_{id1} := \frac{id1}{2}$$

$$R_{id1} = 2.3175$$

$$R_{id2} := \frac{id2}{2} \quad R_{id2} = 2.38$$

$$R_{m1} := R_{id1} + \frac{t1}{2} \quad R_{m1} = 2.54925$$

$$R_{m2} := R_{id2} + \frac{t2}{2} \quad R_{m2} = 2.5805$$

$$R_t := \frac{R_{m2}}{t2} \quad R_t = 6.43516$$

$$\frac{R_o}{t2} = 6.93516$$

Flaw Geometry Input Data:

A postulated flaw could exist in the 0.88" UT Blindzone that occurs 1.08" above the top of the J-weld at the uphill (180°) location. The flaw length (c) and depth (a) constitute the input parameters. This flaw represents an internal surface crack in a cylinder, as described in Reference 8.

$AR_0 := 4$ The flaw length-to-depth aspect ratio. This ratio (4-to-1) is potentially more conducive for through-wall growth than the 6-to-1 ratio used in ASME Section XI, and one sufficient to promote flaw growth through the thickness.

$$t2 \cdot 25 = 0.10025$$

$a_0 := 0.1$ Initial Flaw Depth of the ID surface flaw in the blind zone above the top of the weld on the uphill side. The minimum detectable depth of a surface flaw from UT demonstrations [Ref. 11] was 8% throughwall. Conservatively, a 25% throughwall flaw is assumed. This flaw is sufficiently deep to see the stress field developed through the thickness.

$L_m := a_0 \cdot AR_0$ Initial Flaw Length of an ID surface flaw in the counterbore region, in inches. The length was determined by assuming a 4-to-1 flaw length-to-depth aspect ratio. Half the flaw length (0.2 inch) was placed below the mid-height of the blind zone, while the other half was placed above the mid-height.

$$L = 0.4$$

$c_0 := \frac{L}{2}$ The half flaw length used in the fracture mechanics model

Additional Input Data:

$P_{Int} := 2.235$ Design Operating Pressure (internal) [Ref. 3]

Years := 40 Number of Operating Years

$I_{lim} := 8000$ Iteration limit for Crack Growth loop

$T_m := 604$ Conservative Operating Temperature for the head, in degrees F. Ref. 4 gives a value of 594.8 deg. F following power uprate.

$\alpha_{0c} := 2.67 \cdot 10^{-12}$ Constant in MRP-55 PWSCC Model for I-600 Wrought @ 617 deg. F [Ref. 9]

$Q_g := 31.0$ Thermal activation Energy for Crack Growth {MRP} [Ref. 9]

$T_{ref} := 617$ Reference Temperature for normalizing Data deg. F [Ref. 9]

$Tim_{opr} := 365.2422 \cdot 24 \cdot \text{Years}$ Numer of operating hours in a year

$CF_{inhr} := 1.417 \cdot 10^5$ Correction factor to convert meters per second to inches per hour

$C_{blk} := \frac{Tim_{opr}}{I_{lim}}$ Calculation block size for the crack growth iteration loop

$C_{blk} = 43.82906$

$Prnt_{blk} := \left\lceil \frac{I_{lim}}{50} \right\rceil$

$C_{01} := e^{\left[\frac{-Q_g}{1.103 \cdot 10^{-3}} \left(\frac{1}{T+459.67} - \frac{1}{T_{ref}+459.67} \right) \right]} \cdot \alpha_{0c}$ Temperature Correction for Coefficient Alpha from EPRI MRP-55, Revision 1 [Ref. 9]

$C_0 := 1.0C_{01}$ 75th percentile from MRP-55 Revision 1 [Ref. 9]

The flaw model used for a postulated flaw within the counterbore region on the uphill side of the ICI nozzle is an internal surface flaw in a cylinder, subject to an arbitrary stress distribution.

To allow for a "moving average" of through-thickness stress values as the flaw extends along the length of the ICI ID surface, the length from the bottom tip of the of the initial flaw in the blind zone to the stress distribution upper limit--ElevStrs.Dist--is broken into 20 equal segments. Note that due to the MCS used, with a 0 elevation occurring at the TOP of the nozzle, the term "U_{Tip}" (implying the upper tip of the flaw) is actually the physical bottom tip of the flaw, closer to the top of the weld. U_{Tip} is the term used in Reference 7 for the CEDM nozzles, and thus it will continue to be used in the ICI nozzle evaluation.

$$FL_{Cntr} := \begin{cases} Ref_{Point} - c_0 & \text{if Val} = 1 \\ Ref_{Point} & \text{if Val} = 2 \\ Ref_{Point} + c_0 & \text{otherwise} \end{cases} \quad \begin{array}{l} \text{Flaw center Location at the mid-point of} \\ \text{the blind zone region} \end{array}$$

$$U_{Tip} := FL_{Cntr} + c_0$$

$$U_{Tip} = 12.2812$$

$$Inc_{Strs.avg} := \frac{Elev_{Strs.Dist} - U_{Tip}}{20}$$

$$Inc_{Strs.avg} = 0.066$$

No User Input is required beyond this Point

Regression of Through-Thickness Stresses as a Function of Axial Elevation

Because of the minor variation in stresses occurring at the top of the nozzle where it intersects the reactor head and the need to accurately curve fit stresses in the region of interest in the BZ, the entire range of stresses is not appropriate to curve fit. To accommodate an area below and above the BZ region, the first two data points in each of the elevation and stress arrays were removed from consideration in the curve fitting equations. This is a reasonable assumption, given that in the completely through-wall tensile stress field that exists in the nozzle above the top of the J-weld, a flaw centered in the BZ region is likely to grow through the thickness entirely (in addition to growth along the surface of the nozzle) rather than grow very long into an area close to the top of the head or below the top of the J-weld (i.e., elevation ranges not included in the stress polynomial curve fit). Initially, a **fourth (4th)** order polynomial was chosen for axial stress regression. After regression, the stress at the mid-height of the blind zone (12.0812 inches in the MCS) is checked.

Regression for ID stresses:

$k := 0..6$

$$ID_elev_cf := \begin{pmatrix} 8.6999 \\ 10.3745 \\ 11.5527 \\ 12.6463 \\ 12.9649 \\ 13.3752 \\ 13.6012 \end{pmatrix}$$

$$ID_stress_cf := \begin{pmatrix} 17.412 \\ 17.399 \\ 16.707 \\ 15.065 \\ 19.425 \\ 23.147 \\ 26.39 \end{pmatrix}$$

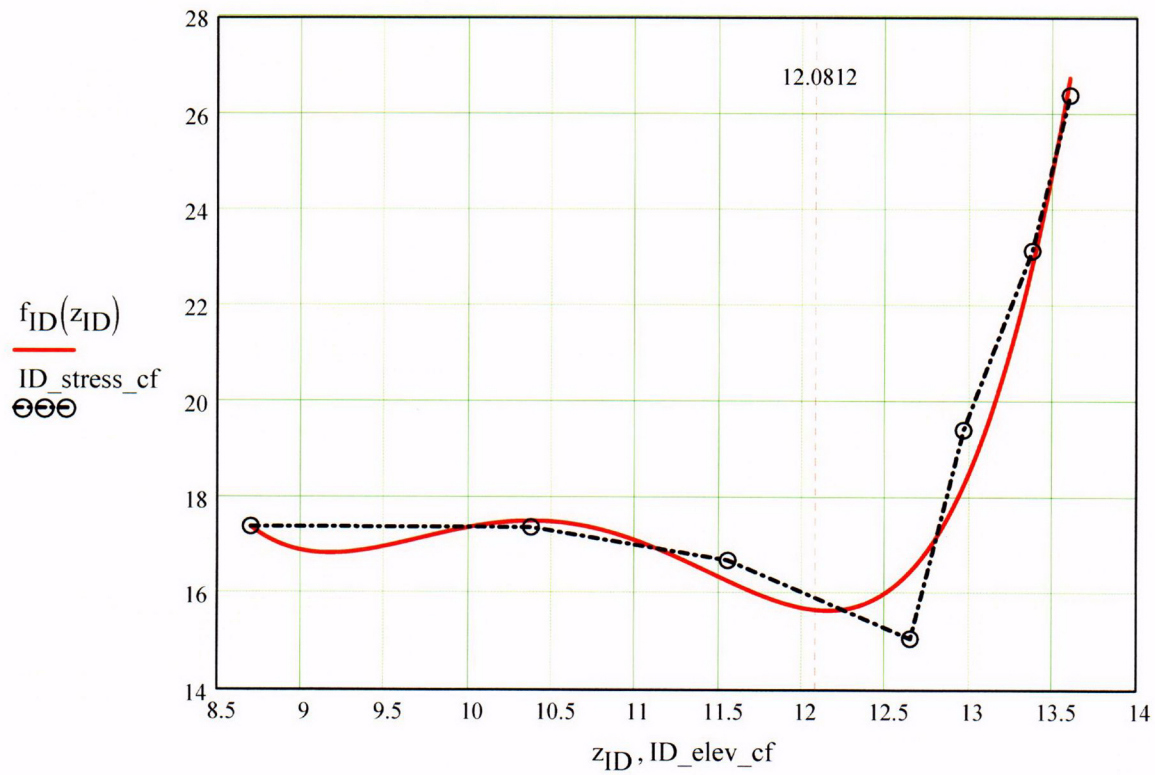
$$R_{ID} := \text{regress}(ID_elev_cf, ID_stress_cf, 4)$$

$$z_{ID} := 8.6999, 8.701.. \text{Top_Jweld}$$

$$R_{ID} = \begin{pmatrix} 3 \\ 3 \\ 4 \\ 2920.01158 \\ -1120.32621 \\ 161.1276 \\ -10.23275 \\ 0.24206 \end{pmatrix}$$

ID_elev _i =	ID_stress _i =
0	10.308
2.9371	15.304
6.3198	17.115
8.6999	17.412
10.3745	17.399
11.5527	16.707
12.6463	15.065
12.9649	19.425
13.3752	23.147
13.6012	26.39

$$f_{ID}(z_{ID}) := \text{interp}(R_{ID}, ID_elev_cf, ID_stress_cf, z_{ID})$$



$$f_{ID}(12.0812) = 15.66367$$

Regression for 25% throughwall stresses:

$$QT_elev_cf := \begin{pmatrix} 8.6999 \\ 10.3745 \\ 11.5527 \\ 12.5802 \\ 12.9649 \\ 13.3752 \\ 13.6012 \end{pmatrix} \quad QT_stress_cf := \begin{pmatrix} 17.487 \\ 17.177 \\ 16.175 \\ 14.581 \\ 18.188 \\ 21.559 \\ 25.687 \end{pmatrix}$$

$R_{QT} := \text{regress}(QT_elev_cf, QT_stress_cf, 4)$
 $z_{QT} := 8.6999, 8.701 \dots \text{Top_Jweld}$

$R_{QT} = \begin{pmatrix} 3 \\ 3 \\ 4 \\ 3362.70255 \\ -1281.45936 \\ 182.93207 \\ -11.53275 \\ 0.27085 \end{pmatrix}$

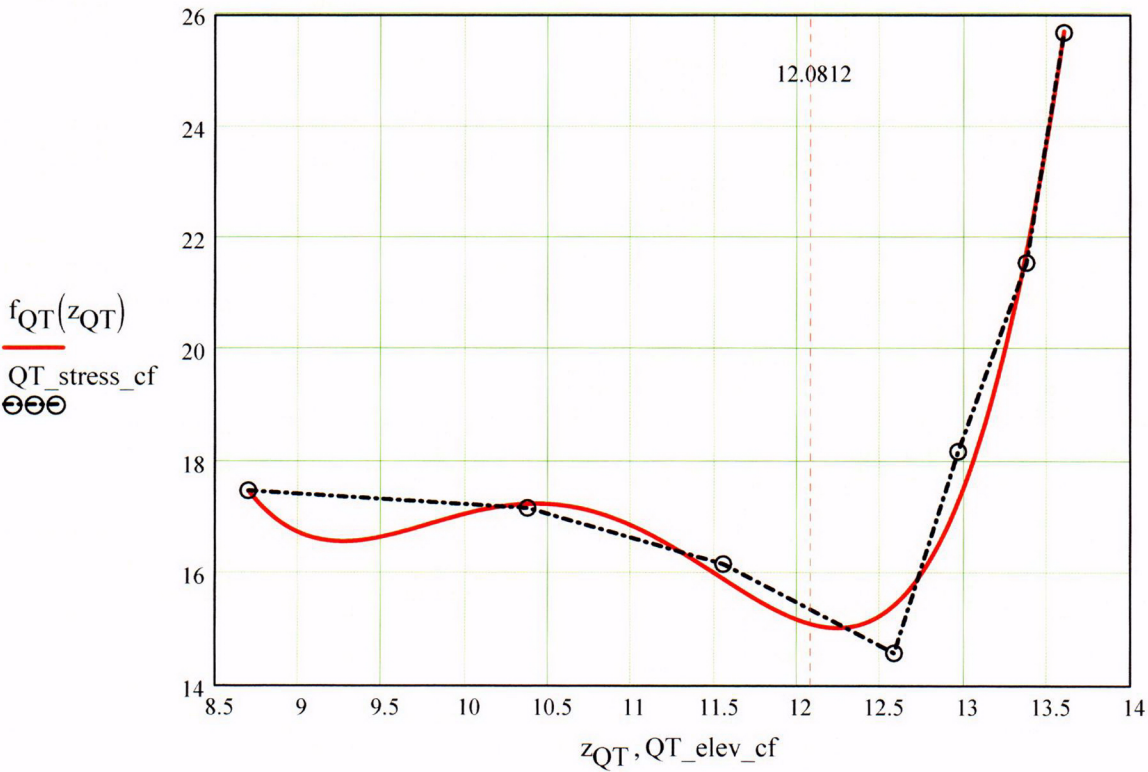
$QT_elev_i =$

0
2.9371
6.3198
8.6999
10.3745
11.5527
12.5802
12.9649
13.3752
13.6012

$QT_stress_i =$

10.119
13.024
15.794
17.487
17.177
16.175
14.581
18.188
21.559
25.687

$f_{QT}(z_{QT}) := \text{interp}(R_{QT}, QT_elev_cf, QT_stress_cf, z_{QT})$



$f_{QT}(12.0812) = 15.09487$

Regression for 50% throughwall stresses:

$$\text{MD_elev_cf} := \begin{pmatrix} 8.6999 \\ 10.3745 \\ 11.5527 \\ 12.514 \\ 12.9649 \\ 13.3752 \\ 13.6012 \end{pmatrix} \quad \text{MD_stress_cf} := \begin{pmatrix} 12.883 \\ 15.044 \\ 15.56 \\ 13.132 \\ 15.78 \\ 19.292 \\ 24.607 \end{pmatrix}$$

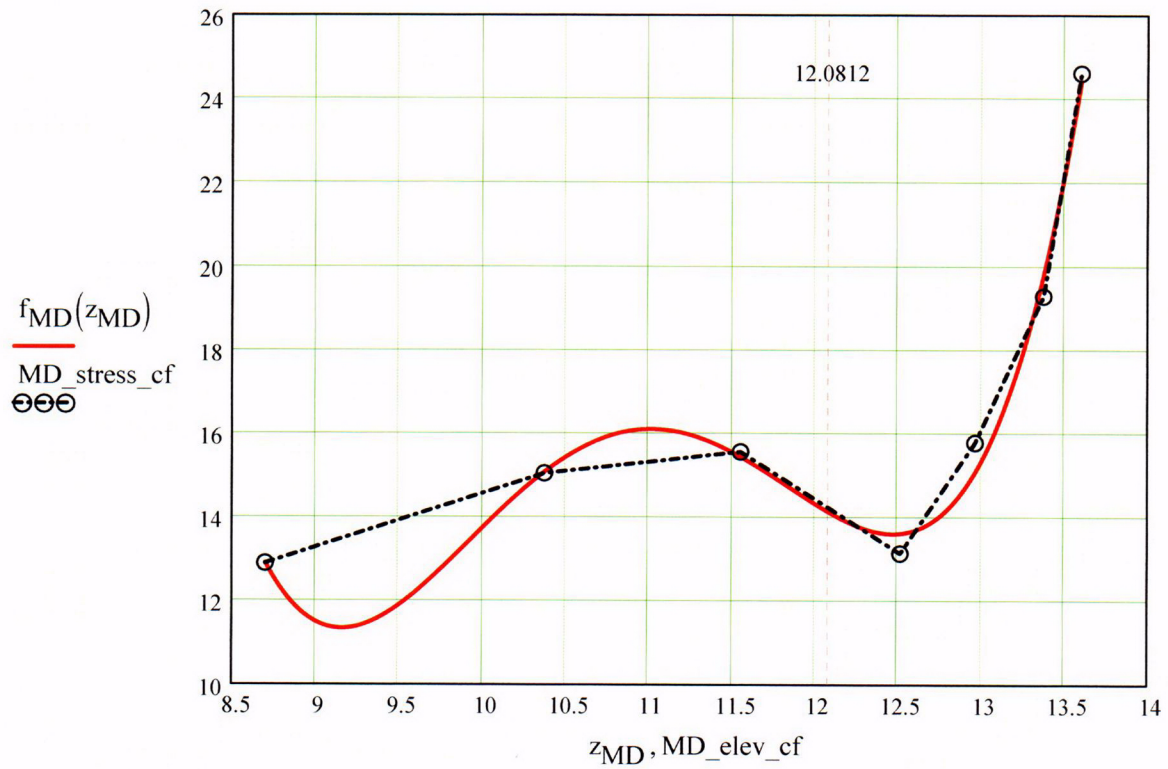
$$R_{\text{MD}} := \text{regress}(\text{MD_elev_cf}, \text{MD_stress_cf}, 4)$$

$$z_{\text{MD}} := 8.6999, 8.701 \dots \text{Top_Jweld}$$

$$R_{\text{MD}} = \begin{pmatrix} 3 \\ 3 \\ 4 \\ 6270.57353 \\ -2357.44561 \\ 330.23769 \\ -20.39106 \\ 0.46849 \end{pmatrix}$$

MD_elev _i	MD_stress _i
0	10.032
2.9371	10.766
6.3198	11.377
8.6999	12.883
10.3745	15.044
11.5527	15.56
12.514	13.132
12.9649	15.78
13.3752	19.292
13.6012	24.607

$$f_{\text{MD}}(z_{\text{MD}}) := \text{interp}(R_{\text{MD}}, \text{MD_elev_cf}, \text{MD_stress_cf}, z_{\text{MD}})$$



$$f_{MD}(12.0812) = 14.11569$$

Regression for 75% throughwall stresses:

$$TQ_elev_cf := \begin{pmatrix} 8.6999 \\ 10.3745 \\ 11.5527 \\ 12.4478 \\ 12.9649 \\ 13.3752 \\ 13.6012 \end{pmatrix}$$

$$TQ_stress_cf := \begin{pmatrix} 7.18 \\ 8.136 \\ 8.89 \\ 6.189 \\ 11.381 \\ 16.085 \\ 22.68 \end{pmatrix}$$

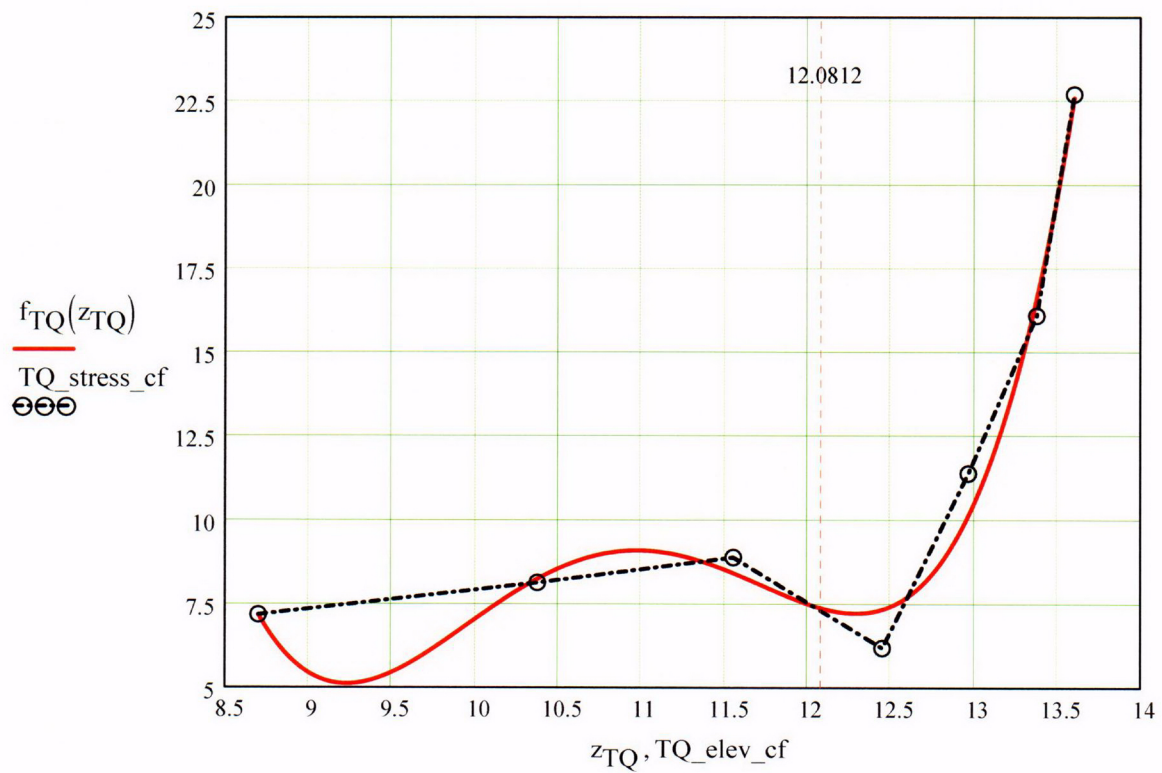
$$R_{TQ} := \text{regress}(TQ_elev_cf, TQ_stress_cf, 4)$$

$$z_{TQ} := 8.6999, 8.701 \dots \text{Top_Jweld}$$

$$R_{TQ} = \begin{pmatrix} 3 \\ 3 \\ 4 \\ 6772.44513 \\ -2552.34739 \\ 358.42617 \\ -22.21167 \\ 0.51271 \end{pmatrix}$$

$TQ_elev_i =$	$TQ_stress_i =$
0	9.951
2.9371	9.067
6.3198	7.821
8.6999	7.18
10.3745	8.136
11.5527	8.89
12.4478	6.189
12.9649	11.381
13.3752	16.085
13.6012	22.68

$$f_{TQ}(z_{TQ}) := \text{interp}(R_{TQ}, TQ_elev_cf, TQ_stress_cf, z_{TQ})$$



$$f_{TQ}(12.0812) = 7.37343$$

C24

Regression for OD stresses:

kk := 0..5

$$\text{OD_elev_cf} := \begin{pmatrix} 10.3745 \\ 11.5527 \\ 12.3816 \\ 12.9649 \\ 13.3752 \\ 13.6012 \end{pmatrix} \quad \text{OD_stress_cf} := \begin{pmatrix} 2.316 \\ 2.74 \\ -0.109 \\ 8.207 \\ 9.729 \\ 44.523 \end{pmatrix}$$

$R_{OD} := \text{regress}(\text{OD_elev_cf}, \text{OD_stress_cf}, 4$

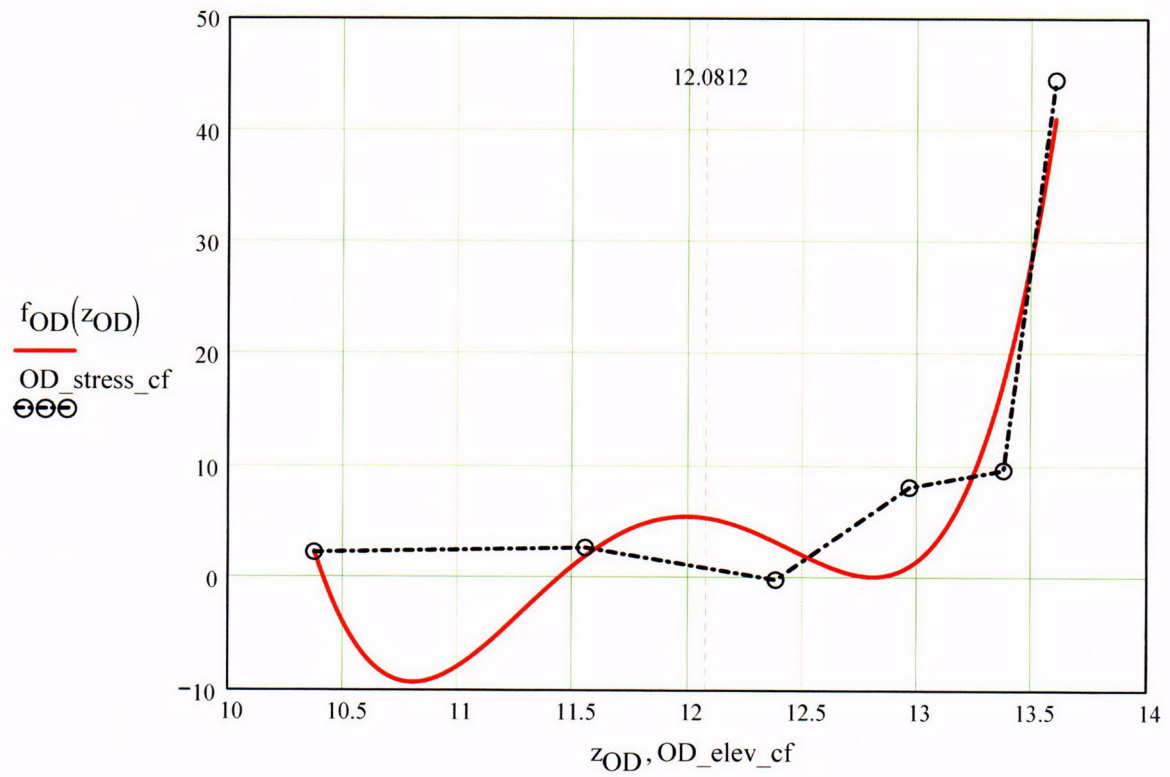
$z_{OD} := 10.3745, 10.376 \dots \text{Top_Jweld}$

$$R_{OD} = \begin{pmatrix} 3 \\ 3 \\ 4 \\ 1.83727 \times 10^5 \\ -62394.03658 \\ 7925.4618 \\ -446.31291 \\ 9.40247 \end{pmatrix}$$

OD_elev_i = OD_stress_i =

OD_elev _i	OD_stress _i
0	9.936
2.9371	7.453
6.3198	4.387
8.6999	2.298
10.3745	2.316
11.5527	2.74
12.3816	-0.109
12.9649	8.207
13.3752	9.729
13.6012	44.523

$f_{OD}(z_{OD}) := \text{interp}(R_{OD}, \text{OD_elev_cf}, \text{OD_stress_cf}, z_{OD})$



$$f_{OD}(12.0812) = 5.39079$$

Calculation to develop Stress Profiles for Analysis

This analysis for the axial stress regression and the through-wall stress regression is the same as that used for the CEDM Nozzles (in Ref. 7) with the exception that the axial stresses are fit with a fourth-order polynomial, rather than a third-order polynomial, to accommodate greater precision.

$$N_{\text{w}} := 20 \quad \text{Number of locations for stress profiles}$$

$$\text{Loc}_0 := \text{FL}_{\text{Cntr}} - L$$

$$\text{FL}_{\text{Cntr}} = 12.0812$$

$$L = 0.4$$

$$i := 1..N + 3$$

$$\text{Incr}_i := \begin{cases} c_0 & \text{if } i < 4 \\ \text{IncStrs.avg} & \text{otherwise} \end{cases}$$

$$\text{Loc}_i := \text{Loc}_{i-1} + \text{Incr}_i$$

$$\text{SID}_i := R_{\text{ID}_3} + R_{\text{ID}_4} \cdot \text{Loc}_i + R_{\text{ID}_5} \cdot (\text{Loc}_i)^2 + R_{\text{ID}_6} \cdot (\text{Loc}_i)^3 + R_{\text{ID}_7} \cdot (\text{Loc}_i)^4$$

$$\text{SQT}_i := R_{\text{QT}_3} + R_{\text{QT}_4} \cdot \text{Loc}_i + R_{\text{QT}_5} \cdot (\text{Loc}_i)^2 + R_{\text{QT}_6} \cdot (\text{Loc}_i)^3 + R_{\text{QT}_7} \cdot (\text{Loc}_i)^4$$

$$\text{SMD}_i := R_{\text{MD}_3} + R_{\text{MD}_4} \cdot \text{Loc}_i + R_{\text{MD}_5} \cdot (\text{Loc}_i)^2 + R_{\text{MD}_6} \cdot (\text{Loc}_i)^3 + R_{\text{MD}_7} \cdot (\text{Loc}_i)^4$$

$$\text{STQ}_i := R_{\text{TQ}_3} + R_{\text{TQ}_4} \cdot \text{Loc}_i + R_{\text{TQ}_5} \cdot (\text{Loc}_i)^2 + R_{\text{TQ}_6} \cdot (\text{Loc}_i)^3 + R_{\text{TQ}_7} \cdot (\text{Loc}_i)^4$$

$$\text{SOD}_i := R_{\text{OD}_3} + R_{\text{OD}_4} \cdot \text{Loc}_i + R_{\text{OD}_5} \cdot (\text{Loc}_i)^2 + R_{\text{OD}_6} \cdot (\text{Loc}_i)^3 + R_{\text{OD}_7} \cdot (\text{Loc}_i)^4$$

$$j := 1..N$$

$$S_{\text{id}_j} := \begin{cases} \frac{\text{SID}_j + \text{SID}_{j+1} + \text{SID}_{j+2}}{3} & \text{if } j = 1 \\ \frac{S_{\text{id}_{j-1}} \cdot (j+1) + \text{SID}_{j+2}}{j+2} & \text{otherwise} \end{cases}$$

$$S_{\text{qt}_j} := \begin{cases} \frac{\text{SQT}_j + \text{SQT}_{j+1} + \text{SQT}_{j+2}}{3} & \text{if } j = 1 \\ \frac{S_{\text{qt}_{j-1}} \cdot (j+1) + \text{SQT}_{j+2}}{j+2} & \text{otherwise} \end{cases}$$

$$S_{md_j} := \begin{cases} \frac{SMD_j + SMD_{j+1} + SMD_{j+2}}{3} & \text{if } j = 1 \\ \frac{S_{md_{j-1}} \cdot (j+1) + SMD_{j+2}}{j+2} & \text{otherwise} \end{cases}$$

$$S_{tq_j} := \begin{cases} \frac{STQ_j + STQ_{j+1} + STQ_{j+2}}{3} & \text{if } j = 1 \\ \frac{S_{tq_{j-1}} \cdot (j+1) + STQ_{j+2}}{j+2} & \text{otherwise} \end{cases}$$

$$S_{od_j} := \begin{cases} \frac{SOD_j + SOD_{j+1} + SOD_{j+2}}{3} & \text{if } j = 1 \\ \frac{S_{od_{j-1}} \cdot (j+1) + SOD_{j+2}}{j+2} & \text{otherwise} \end{cases}$$

Through-Wall Stress Distribution for ID Flaws (i.e. ID to OD Stress distribution)

$$u_0 := 0.000$$

$$u_1 := 0.25$$

$$u_2 := 0.50$$

$$u_3 := 0.75$$

$$u_4 := 1.00$$

$$Y := \text{stack}(u_0, u_1, u_2, u_3, u_4)$$

$$\text{SIG}_1 := \text{stack}(S_{id_1}, S_{qt_1}, S_{md_1}, S_{tq_1}, S_{od_1})$$

$$\text{SIG}_2 := \text{stack}(S_{id_2}, S_{qt_2}, S_{md_2}, S_{tq_2}, S_{od_2})$$

$$\text{SIG}_3 := \text{stack}(S_{id_3}, S_{qt_3}, S_{md_3}, S_{tq_3}, S_{od_3})$$

$$\text{SIG}_4 := \text{stack}(S_{id_4}, S_{qt_4}, S_{md_4}, S_{tq_4}, S_{od_4})$$

$$\text{SIG}_5 := \text{stack}(S_{id_5}, S_{qt_5}, S_{md_5}, S_{tq_5}, S_{od_5})$$

$$\text{SIG}_6 := \text{stack}(S_{id_6}, S_{qt_6}, S_{md_6}, S_{tq_6}, S_{od_6})$$

$$\text{SIG}_7 := \text{stack}(S_{id_7}, S_{qt_7}, S_{md_7}, S_{tq_7}, S_{od_7})$$

$$\text{SIG}_8 := \text{stack}(S_{id_8}, S_{qt_8}, S_{md_8}, S_{tq_8}, S_{od_8})$$

$$\text{SIG}_9 := \text{stack}(S_{id_9}, S_{qt_9}, S_{md_9}, S_{tq_9}, S_{od_9})$$

$$\text{SIG}_{10} := \text{stack}(S_{id_{10}}, S_{qt_{10}}, S_{md_{10}}, S_{tq_{10}}, S_{od_{10}})$$

$$\text{SIG}_{11} := \text{stack}(S_{id_{11}}, S_{qt_{11}}, S_{md_{11}}, S_{tq_{11}}, S_{od_{11}})$$

$$\text{SIG}_{12} := \text{stack}(S_{id_{12}}, S_{qt_{12}}, S_{md_{12}}, S_{tq_{12}}, S_{od_{12}})$$

$$\text{SIG}_{13} := \text{stack}(S_{id_{13}}, S_{qt_{13}}, S_{md_{13}}, S_{tq_{13}}, S_{od_{13}})$$

$$\text{SIG}_{14} := \text{stack}(S_{id_{14}}, S_{qt_{14}}, S_{md_{14}}, S_{tq_{14}}, S_{od_{14}})$$

$$\text{SIG}_{15} := \text{stack}(S_{id_{15}}, S_{qt_{15}}, S_{md_{15}}, S_{tq_{15}}, S_{od_{15}})$$

$$\text{SIG}_{16} := \text{stack}(S_{id_{16}}, S_{qt_{16}}, S_{md_{16}}, S_{tq_{16}}, S_{od_{16}})$$

$$\text{SIG}_{17} := \text{stack}(S_{id_{17}}, S_{qt_{17}}, S_{md_{17}}, S_{tq_{17}}, S_{od_{17}})$$

$$\text{SIG}_{18} := \text{stack}(S_{id_{18}}, S_{qt_{18}}, S_{md_{18}}, S_{tq_{18}}, S_{od_{18}})$$

$$\text{SIG}_{19} := \text{stack}(S_{id_{19}}, S_{qt_{19}}, S_{md_{19}}, S_{tq_{19}}, S_{od_{19}})$$

$$\text{SIG}_{20} := \text{stack}(S_{id_{20}}, S_{qt_{20}}, S_{md_{20}}, S_{tq_{20}}, S_{od_{20}})$$

Regression of Through-Wall Stress distribution to Obtain Stress Coefficients Using a Third Order Polynomial

$$\text{IDRG}_1 := \text{regress}(Y, \text{SIG}_1, 3)$$

$$\text{IDRG}_2 := \text{regress}(Y, \text{SIG}_2, 3)$$

$$\text{IDRG}_3 := \text{regress}(Y, \text{SIG}_3, 3)$$

$$\text{IDRG}_4 := \text{regress}(Y, \text{SIG}_4, 3)$$

$$\text{IDRG}_5 := \text{regress}(Y, \text{SIG}_5, 3)$$

$$\text{IDRG}_6 := \text{regress}(Y, \text{SIG}_6, 3)$$

$$\text{IDRG}_7 := \text{regress}(Y, \text{SIG}_7, 3)$$

$$\text{IDRG}_8 := \text{regress}(Y, \text{SIG}_8, 3)$$

$$\text{IDRG}_9 := \text{regress}(Y, \text{SIG}_9, 3)$$

$$\text{IDRG}_{10} := \text{regress}(Y, \text{SIG}_{10}, 3)$$

$$\text{IDRG}_{11} := \text{regress}(Y, \text{SIG}_{11}, 3)$$

$$\text{IDRG}_{12} := \text{regress}(Y, \text{SIG}_{12}, 3)$$

$$\text{IDRG}_{13} := \text{regress}(Y, \text{SIG}_{13}, 3)$$

$$\text{IDRG}_{14} := \text{regress}(Y, \text{SIG}_{14}, 3)$$

$$\text{IDRG}_{15} := \text{regress}(Y, \text{SIG}_{15}, 3)$$

$$\text{IDRG}_{16} := \text{regress}(Y, \text{SIG}_{16}, 3)$$

$$\text{IDRG}_{17} := \text{regress}(Y, \text{SIG}_{17}, 3)$$

$$\text{IDRG}_{18} := \text{regress}(Y, \text{SIG}_{18}, 3)$$

$$\text{IDRG}_{19} := \text{regress}(Y, \text{SIG}_{19}, 3)$$

$$\text{IDRG}_{20} := \text{regress}(Y, \text{SIG}_{20}, 3)$$

***Stress Distribution in the tube. Stress influence coefficients obtained from
third-order polynomial curve fit to the throughwall stress distribution***

Data Files for Flaw Shape Factors from NASA SC04 Model [Ref. 8]

{NO INPUT Required}

**Mettu Raju Newman Sivakumar Forman Solution of ID Part throughwall
Flaw in Cyinder**

Jsb :=

	0	1	2
0	1.000	0.200	0.000
1	1.000	0.200	0.200
2	1.000	0.200	0.500
3	1.000	0.200	0.800
4	1.000	0.200	1.000
5	1.000	0.400	0.000
6	1.000	0.400	0.200
7	1.000	0.400	0.500
8	1.000	0.400	0.800
9	1.000	0.400	1.000
10	1.000	1.000	0.000
11	1.000	1.000	0.200
12	1.000	1.000	0.500
13	1.000	1.000	0.800
14	1.000	1.000	1.000
15	2.000	0.200	0.000
16	2.000	0.200	0.200
17	2.000	0.200	0.500
18	2.000	0.200	0.800
19	2.000	0.200	1.000
20	2.000	0.400	0.000
21	2.000	0.400	0.200
22	2.000	0.400	0.500
23	2.000	0.400	0.800
24	2.000	0.400	1.000
25	2.000	1.000	0.000
26	2.000	1.000	0.200
27	2.000	1.000	0.500
28	2.000	1.000	0.800
29	2.000	1.000	1.000
30	4.000	0.200	0.000
31	4.000	0.200	0.200
32	4.000	0.200	0.500
33	4.000	0.200	0.800

34	4.000	0.200	1.000
35	4.000	0.400	0.000
36	4.000	0.400	0.200
37	4.000	0.400	0.500
38	4.000	0.400	0.800
39	4.000	0.400	1.000
40	4.000	1.000	0.000
41	4.000	1.000	0.200
42	4.000	1.000	0.500
43	4.000	1.000	0.800
44	4.000	1.000	1.000
45	10.000	0.200	0.000
46	10.000	0.200	0.200
47	10.000	0.200	0.500
48	10.000	0.200	0.800
49	10.000	0.200	1.000
50	10.000	0.400	0.000
51	10.000	0.400	0.200
52	10.000	0.400	0.500
53	10.000	0.400	0.800
54	10.000	0.400	1.000
55	10.000	1.000	0.000
56	10.000	1.000	0.200
57	10.000	1.000	0.500
58	10.000	1.000	0.800
59	10.000	1.000	1.000
60	300.000	0.200	0.000
61	300.000	0.200	0.200
62	300.000	0.200	0.500
63	300.000	0.200	0.800
64	300.000	0.200	1.000
65	300.000	0.400	0.000
66	300.000	0.400	0.200
67	300.000	0.400	0.500
68	300.000	0.400	0.800
69	300.000	0.400	1.000
70	300.000	1.000	0.000
71	300.000	1.000	0.200
72	300.000	1.000	0.500
73	300.000	1.000	0.800
74	300.000	1.000	1.000

Sambi :=

	0	1	2	3	4	5	6	7
0	1.076	0.693	0.531	0.434	0.608	0.083	0.023	0.009
1	1.056	0.647	0.495	0.408	0.615	0.085	0.027	0.013
2	1.395	0.767	0.557	0.446	0.871	0.171	0.069	0.038
3	2.53	1.174	0.772	0.58	1.554	0.363	0.155	0.085
4	3.846	1.615	0.995	0.716	2.277	0.544	0.233	0.127
5	1.051	0.689	0.536	0.444	0.74	0.112	0.035	0.015
6	1.011	0.646	0.504	0.421	0.745	0.119	0.041	0.02
7	1.149	0.694	0.529	0.435	0.916	0.181	0.073	0.04
8	1.6	0.889	0.642	0.51	1.334	0.307	0.132	0.073
9	2.087	1.093	0.761	0.589	1.752	0.421	0.183	0.101
10	0.992	0.704	0.534	0.506	1.044	0.169	0.064	0.032
11	0.987	0.701	0.554	0.491	1.08	0.182	0.067	0.034
12	1.01	0.709	0.577	0.493	1.116	0.2	0.078	0.041
13	1.07	0.73	0.623	0.523	1.132	0.218	0.095	0.051
14	1.128	0.75	0.675	0.556	1.131	0.229	0.11	0.06
15	1.049	0.673	0.519	0.427	0.6	0.078	0.021	0.008
16	1.091	0.661	0.502	0.413	0.614	0.083	0.025	0.012
17	1.384	0.764	0.556	0.446	0.817	0.15	0.058	0.031
18	2.059	1.033	0.708	0.545	1.3	0.291	0.123	0.067
19	2.739	1.301	0.858	0.643	1.783	0.421	0.18	0.099
20	1.075	0.674	0.527	0.436	0.73	0.072	0.044	0.021
21	1.045	0.659	0.511	0.425	0.76	0.122	0.043	0.021
22	1.16	0.71	0.536	0.441	0.919	0.197	0.064	0.034
23	1.51	0.854	0.623	0.498	1.231	0.271	0.114	0.062
24	1.876	0.995	0.71	0.555	1.519	0.317	0.161	0.089
25	1.037	0.732	0.594	0.505	1.132	0.192	0.07	0.035
26	1.003	0.707	0.577	0.493	1.113	0.19	0.071	0.036
27	1.023	0.714	0.58	0.495	1.155	0.207	0.08	0.042
28	1.129	0.774	0.619	0.521	1.286	0.247	0.098	0.052
29	1.242	0.84	0.661	0.549	1.416	0.285	0.115	0.061
30	1.003	0.649	0.511	0.43	0.577	0.07	0.015	0.005
31	1.097	0.666	0.511	0.426	0.606	0.079	0.023	0.01
32	1.405	0.776	0.567	0.46	0.797	0.141	0.054	0.028
33	1.959	0.996	0.692	0.542	1.201	0.262	0.108	0.059
34	2.461	1.197	0.808	0.619	1.586	0.37	0.154	0.085
35	1.024	0.668	0.528	0.451	0.737	0.11	0.033	0.015
36	1.057	0.666	0.52	0.439	0.77	0.123	0.042	0.021
37	1.193	0.715	0.545	0.454	0.924	0.174	0.068	0.036
38	1.443	0.828	0.614	0.509	1.219	0.263	0.109	0.059
39	1.665	0.934	0.681	0.565	1.487	0.339	0.143	0.078
40	1.005	0.72	0.597	0.518	1.119	0.188	0.068	0.034

	1.000	0.712	0.588	0.511	1.118	0.194	0.072	0.037
41	1.009	0.713	0.588	0.511	1.128	0.194	0.072	0.037
42	1.041	0.726	0.594	0.515	1.191	0.214	0.082	0.043
43	1.105	0.768	0.623	0.536	1.316	0.248	0.097	0.05
44	1.162	0.81	0.653	0.558	1.428	0.277	0.109	0.055
45	0.973	0.635	0.499	0.446	0.579	0.07	0.016	0.005
46	1.115	0.673	0.514	0.438	0.607	0.079	0.023	0.01
47	1.427	0.783	0.571	0.462	0.791	0.138	0.052	0.027
48	1.872	0.96	0.671	0.529	1.179	0.253	0.104	0.056
49	2.23	1.108	0.757	0.594	1.548	0.356	0.149	0.081
50	0.992	0.656	0.52	0.443	0.733	0.109	0.032	0.014
51	1.072	0.672	0.523	0.441	0.777	0.125	0.043	0.021
52	1.217	0.723	0.549	0.456	0.936	0.176	0.069	0.036
53	1.393	0.806	0.601	0.493	1.219	0.259	0.106	0.056
54	1.521	0.875	0.647	0.528	1.469	0.328	0.135	0.071
55	0.994	0.715	0.59	0.518	1.114	0.187	0.068	0.035
56	1.015	0.715	0.588	0.512	1.14	0.197	0.074	0.038
57	1.05	0.729	0.596	0.515	1.219	0.221	0.085	0.044
58	1.09	0.76	0.618	0.532	1.348	0.255	0.099	0.051
59	1.118	0.788	0.639	0.55	1.456	0.282	0.109	0.056
60	0.936	0.62	0.486	0.405	0.582	0.068	0.015	0.005
61	1.145	0.681	0.514	0.42	0.613	0.081	0.024	0.011
62	1.459	0.79	0.569	0.454	0.79	0.138	0.051	0.026
63	1.774	0.917	0.641	0.501	1.148	0.239	0.096	0.051
64	1.974	1.008	0.696	0.537	1.482	0.328	0.134	0.07
65	0.982	0.651	0.512	0.427	0.721	0.103	0.031	0.013
66	1.095	0.677	0.52	0.431	0.782	0.127	0.045	0.022
67	1.244	0.727	0.546	0.446	0.946	0.18	0.071	0.037
68	1.37	0.791	0.585	0.473	1.201	0.253	0.102	0.054
69	1.438	0.838	0.618	0.496	1.413	0.31	0.126	0.066

$$W_{mm} := Js_b^{(0)}$$

$$X := Js_b^{(1)}$$

$$Y := Js_b^{(2)}$$

$$a_U := Sambi^{(0)}$$

$$a_L := Sambi^{(1)}$$

$$a_Q := Sambi^{(2)}$$

$$a_C := Sambi^{(3)}$$

$$c_U := Sambi^{(4)}$$

$$c_L := Sambi^{(5)}$$

$$c_Q := Sambi^{(6)}$$

$$c_C := Sambi^{(7)}$$

$$n := \begin{cases} 3 & \text{if } R_t \leq 4.0 \\ 2 & \text{otherwise} \end{cases}$$

"a-Tip" Uniform Term

$$M_{aU} := \text{augment}(W, X, Y) \quad V_{aU} := a_U \quad R_{aU} := \text{regress}(M_{aU}, V_{aU}, n)$$

$$f_{aU}(W, X, Y) := \text{interp} \left[R_{aU}, M_{aU}, V_{aU}, \begin{pmatrix} W \\ X \\ Y \end{pmatrix} \right]$$

$$f_{aU}(4, .4, .8) = 1.7089$$

Check Calculation

Linear Term

$$M_{aL} := \text{augment}(W, X, Y) \quad V_{aL} := a_L \quad R_{aL} := \text{regress}(M_{aL}, V_{aL}, n)$$

$$f_{aL}(W, X, Y) := \text{interp} \left[R_{aL}, M_{aL}, V_{aL}, \begin{pmatrix} W \\ X \\ Y \end{pmatrix} \right]$$

$$f_{aL}(4, .4, .8) = 0.93393$$

Check Calculation

Quadratic Term

$$M_{aQ} := \text{augment}(W, X, Y) \quad V_{aQ} := a_Q \quad R_{aQ} := \text{regress}(M_{aQ}, V_{aQ}, n)$$

$$f_{aQ}(W, X, Y) := \text{interp} \left[R_{aQ}, M_{aQ}, V_{aQ}, \begin{pmatrix} W \\ X \\ Y \end{pmatrix} \right]$$

$$f_{aQ}(4, .4, .8) = 0.67668 \quad \text{Check Calculation}$$

Cubic Term

$$M_{aC} := \text{augment}(W, X, Y) \quad V_{aC} := a_C \quad R_{aC} := \text{regress}(M_{aC}, V_{aC}, n)$$

$$f_{aC}(W, X, Y) := \text{interp} \left[R_{aC}, M_{aC}, V_{aC}, \begin{pmatrix} W \\ X \\ Y \end{pmatrix} \right]$$

$$f_{aC}(4, .4, .8) = 0.54151 \quad \text{Check Calculation}$$

"C" Tip Coefficients

Uniform Term

$$M_{cU} := \text{augment}(W, X, Y) \quad V_{cU} := c_U \quad R_{cU} := \text{regress}(M_{cU}, V_{cU}, n)$$

$$f_{cU}(W, X, Y) := \text{interp} \left[R_{cU}, M_{cU}, V_{cU}, \begin{pmatrix} W \\ X \\ Y \end{pmatrix} \right]$$

$$f_{cU}(4, .4, .8) = 1.31015 \quad \text{Check Calculation}$$

Linear Term

$$M_{cL} := \text{augment}(W, X, Y) \quad V_{cL} := c_L \quad R_{cL} := \text{regress}(M_{cL}, V_{cL}, n)$$

$$f_{cL}(W, X, Y) := \text{interp} \left[R_{cL}, M_{cL}, V_{cL}, \begin{pmatrix} W \\ X \\ Y \end{pmatrix} \right]$$

$$f_{cL}(2, .4, .8) = 0.28509 \quad \text{Check Calculation}$$

Quadratic Term

$$M_{cQ} := \text{augment}(W, X, Y) \quad V_{cQ} := c_Q \quad R_{cQ} := \text{regress}(M_{cQ}, V_{cQ}, n)$$

$$f_{cQ}(W, X, Y) := \text{interp} \left[R_{cQ}, M_{cQ}, V_{cQ}, \begin{pmatrix} W \\ X \\ Y \end{pmatrix} \right]$$

$$f_{cQ}(4, .4, .8) = 0.11797 \quad \text{Check Calculation}$$

Cubic Term

$$M_{cC} := \text{augment}(W, X, Y) \quad V_{cC} := c_C \quad R_{cC} := \text{regress}(M_{cC}, V_{cC}, n)$$

$$f_{cC}(W, X, Y) := \text{interp} \left[R_{cC}, M_{cC}, V_{cC}, \begin{pmatrix} W \\ X \\ Y \end{pmatrix} \right]$$

$$f_{cC}(4, .4, .8) = 0.06384 \quad \text{Check Calculation}$$

Calculations : Recursive calculations to estimate flaw growth

Recursive Loop for Calculation of PWSCC Crack Growth

```

CGRsambi := | j ← 0
              | a0 ← a0
              | c0 ← c0
              | t ← t2
              | NCB0 ← Cblk
              | while j ≤ Ilim
                |   | σ0 ← | IDRG13 if cj ≤ c0
                |   |   | IDRG23 if c0 < cj ≤ c0 + IncStrs.avg
                |   |   | IDRG33 if c0 + IncStrs.avg < cj ≤ c0 + 2·IncStrs.avg
                |   |   | IDRG43 if c0 + 2·IncStrs.avg < cj ≤ c0 + 3·IncStrs.avg
                |   |   | IDRG53 if c0 + 3·IncStrs.avg < cj ≤ c0 + 4·IncStrs.avg
                |   |   | IDRG63 if c0 + 4·IncStrs.avg < cj ≤ c0 + 5·IncStrs.avg
                |   |   | IDRG73 if c0 + 5·IncStrs.avg < cj ≤ c0 + 6·IncStrs.avg
                |   |   | IDRG83 if c0 + 6·IncStrs.avg < cj ≤ c0 + 7·IncStrs.avg
                |   |   | IDRG93 if c0 + 7·IncStrs.avg < cj ≤ c0 + 8·IncStrs.avg
                |   |   | IDRG103 if c0 + 8·IncStrs.avg < cj ≤ c0 + 9·IncStrs.avg
                |   |   | IDRG113 if c0 + 9·IncStrs.avg < cj ≤ c0 + 10·IncStrs.avg
                |   |   | IDRG123 if c0 + 10·IncStrs.avg < cj ≤ c0 + 11·IncStrs.avg
                |   |   | IDRG133 if c0 + 11·IncStrs.avg < cj ≤ c0 + 12·IncStrs.avg
                |   |   | IDRG143 if c0 + 12·IncStrs.avg < cj ≤ c0 + 13·IncStrs.avg
                |   |   | IDRG153 if c0 + 13·IncStrs.avg < cj ≤ c0 + 14·IncStrs.avg

```

	IDRG _{16₃} if $c_0 + 14 \cdot \text{IncStrs.avg} < c_j \leq c_0 + 15 \cdot \text{IncStrs.avg}$
	IDRG _{17₃} if $c_0 + 15 \cdot \text{IncStrs.avg} < c_j \leq c_0 + 16 \cdot \text{IncStrs.avg}$
	IDRG _{18₃} if $c_0 + 16 \cdot \text{IncStrs.avg} < c_j \leq c_0 + 17 \cdot \text{IncStrs.avg}$
	IDRG _{19₃} if $c_0 + 17 \cdot \text{IncStrs.avg} < c_j \leq c_0 + 18 \cdot \text{IncStrs.avg}$
	IDRG _{20₃} otherwise
$\sigma_1 \leftarrow$	IDRG _{1₄} if $c_j \leq c_0$
	IDRG _{2₄} if $c_0 < c_j \leq c_0 + \text{IncStrs.avg}$
	IDRG _{3₄} if $c_0 + \text{IncStrs.avg} < c_j \leq c_0 + 2 \cdot \text{IncStrs.avg}$
	IDRG _{4₄} if $c_0 + 2 \cdot \text{IncStrs.avg} < c_j \leq c_0 + 3 \cdot \text{IncStrs.avg}$
	IDRG _{5₄} if $c_0 + 3 \cdot \text{IncStrs.avg} < c_j \leq c_0 + 4 \cdot \text{IncStrs.avg}$
	IDRG _{6₄} if $c_0 + 4 \cdot \text{IncStrs.avg} < c_j \leq c_0 + 5 \cdot \text{IncStrs.avg}$
	IDRG _{7₄} if $c_0 + 5 \cdot \text{IncStrs.avg} < c_j \leq c_0 + 6 \cdot \text{IncStrs.avg}$
	IDRG _{8₄} if $c_0 + 6 \cdot \text{IncStrs.avg} < c_j \leq c_0 + 7 \cdot \text{IncStrs.avg}$
	IDRG _{9₄} if $c_0 + 7 \cdot \text{IncStrs.avg} < c_j \leq c_0 + 8 \cdot \text{IncStrs.avg}$
	IDRG _{10₄} if $c_0 + 8 \cdot \text{IncStrs.avg} < c_j \leq c_0 + 9 \cdot \text{IncStrs.avg}$
	IDRG _{11₄} if $c_0 + 9 \cdot \text{IncStrs.avg} < c_j \leq c_0 + 10 \cdot \text{IncStrs.avg}$
	IDRG _{12₄} if $c_0 + 10 \cdot \text{IncStrs.avg} < c_j \leq c_0 + 11 \cdot \text{IncStrs.avg}$
	IDRG _{13₄} if $c_0 + 11 \cdot \text{IncStrs.avg} < c_j \leq c_0 + 12 \cdot \text{IncStrs.avg}$
	IDRG _{14₄} if $c_0 + 12 \cdot \text{IncStrs.avg} < c_j \leq c_0 + 13 \cdot \text{IncStrs.avg}$
	IDRG _{15₄} if $c_0 + 13 \cdot \text{IncStrs.avg} < c_j \leq c_0 + 14 \cdot \text{IncStrs.avg}$
	IDRG _{16₄} if $c_0 + 14 \cdot \text{IncStrs.avg} < c_j \leq c_0 + 15 \cdot \text{IncStrs.avg}$

	IDRG _{17,4}	if $c_0 + 15 \cdot \text{IncStrs.avg} < c_j \leq c_0 + 16 \cdot \text{IncStrs.avg}$
	IDRG _{18,4}	if $c_0 + 16 \cdot \text{IncStrs.avg} < c_j \leq c_0 + 17 \cdot \text{IncStrs.avg}$
	IDRG _{19,4}	if $c_0 + 17 \cdot \text{IncStrs.avg} < c_j \leq c_0 + 18 \cdot \text{IncStrs.avg}$
	IDRG _{20,4}	otherwise
$\sigma_2 \leftarrow$	IDRG _{1,5}	if $c_j \leq c_0$
	IDRG _{2,5}	if $c_0 < c_j \leq c_0 + \text{IncStrs.avg}$
	IDRG _{3,5}	if $c_0 + \text{IncStrs.avg} < c_j \leq c_0 + 2 \cdot \text{IncStrs.avg}$
	IDRG _{4,5}	if $c_0 + 2 \cdot \text{IncStrs.avg} < c_j \leq c_0 + 3 \cdot \text{IncStrs.avg}$
	IDRG _{5,5}	if $c_0 + 3 \cdot \text{IncStrs.avg} < c_j \leq c_0 + 4 \cdot \text{IncStrs.avg}$
	IDRG _{6,5}	if $c_0 + 4 \cdot \text{IncStrs.avg} < c_j \leq c_0 + 5 \cdot \text{IncStrs.avg}$
	IDRG _{7,5}	if $c_0 + 5 \cdot \text{IncStrs.avg} < c_j \leq c_0 + 6 \cdot \text{IncStrs.avg}$
	IDRG _{8,5}	if $c_0 + 6 \cdot \text{IncStrs.avg} < c_j \leq c_0 + 7 \cdot \text{IncStrs.avg}$
	IDRG _{9,5}	if $c_0 + 7 \cdot \text{IncStrs.avg} < c_j \leq c_0 + 8 \cdot \text{IncStrs.avg}$
	IDRG _{10,5}	if $c_0 + 8 \cdot \text{IncStrs.avg} < c_j \leq c_0 + 9 \cdot \text{IncStrs.avg}$
	IDRG _{11,5}	if $c_0 + 9 \cdot \text{IncStrs.avg} < c_j \leq c_0 + 10 \cdot \text{IncStrs.avg}$
	IDRG _{12,5}	if $c_0 + 10 \cdot \text{IncStrs.avg} < c_j \leq c_0 + 11 \cdot \text{IncStrs.avg}$
	IDRG _{13,5}	if $c_0 + 11 \cdot \text{IncStrs.avg} < c_j \leq c_0 + 12 \cdot \text{IncStrs.avg}$
	IDRG _{14,5}	if $c_0 + 12 \cdot \text{IncStrs.avg} < c_j \leq c_0 + 13 \cdot \text{IncStrs.avg}$
	IDRG _{15,5}	if $c_0 + 13 \cdot \text{IncStrs.avg} < c_j \leq c_0 + 14 \cdot \text{IncStrs.avg}$
	IDRG _{16,5}	if $c_0 + 14 \cdot \text{IncStrs.avg} < c_j \leq c_0 + 15 \cdot \text{IncStrs.avg}$
	IDRG _{17,5}	if $c_0 + 15 \cdot \text{IncStrs.avg} < c_j \leq c_0 + 16 \cdot \text{IncStrs.avg}$
	IDRG ₁₈	if $c_0 + 16 \cdot \text{IncStrs.avg} < c_j \leq c_0 + 17 \cdot \text{IncStrs.avg}$

		IDRG_{19_5} if $c_0 + 17 \cdot \text{IncStrs.avg} < c_j \leq c_0 + 18 \cdot \text{IncStrs.avg}$ IDRG_{20_5} otherwise
$\sigma_3 \leftarrow$		IDRG_{1_6} if $c_j \leq c_0$ IDRG_{2_6} if $c_0 < c_j \leq c_0 + \text{IncStrs.avg}$ IDRG_{3_6} if $c_0 + \text{IncStrs.avg} < c_j \leq c_0 + 2 \cdot \text{IncStrs.avg}$ IDRG_{4_6} if $c_0 + 2 \cdot \text{IncStrs.avg} < c_j \leq c_0 + 3 \cdot \text{IncStrs.avg}$ IDRG_{5_6} if $c_0 + 3 \cdot \text{IncStrs.avg} < c_j \leq c_0 + 4 \cdot \text{IncStrs.avg}$ IDRG_{6_6} if $c_0 + 4 \cdot \text{IncStrs.avg} < c_j \leq c_0 + 5 \cdot \text{IncStrs.avg}$ IDRG_{7_6} if $c_0 + 5 \cdot \text{IncStrs.avg} < c_j \leq c_0 + 6 \cdot \text{IncStrs.avg}$ IDRG_{8_6} if $c_0 + 6 \cdot \text{IncStrs.avg} < c_j \leq c_0 + 7 \cdot \text{IncStrs.avg}$ IDRG_{9_6} if $c_0 + 7 \cdot \text{IncStrs.avg} < c_j \leq c_0 + 8 \cdot \text{IncStrs.avg}$ IDRG_{10_6} if $c_0 + 8 \cdot \text{IncStrs.avg} < c_j \leq c_0 + 9 \cdot \text{IncStrs.avg}$ IDRG_{11_6} if $c_0 + 9 \cdot \text{IncStrs.avg} < c_j \leq c_0 + 10 \cdot \text{IncStrs.avg}$ IDRG_{12_6} if $c_0 + 10 \cdot \text{IncStrs.avg} < c_j \leq c_0 + 11 \cdot \text{IncStrs.avg}$ IDRG_{13_6} if $c_0 + 11 \cdot \text{IncStrs.avg} < c_j \leq c_0 + 12 \cdot \text{IncStrs.avg}$ IDRG_{14_6} if $c_0 + 12 \cdot \text{IncStrs.avg} < c_j \leq c_0 + 13 \cdot \text{IncStrs.avg}$ IDRG_{15_6} if $c_0 + 13 \cdot \text{IncStrs.avg} < c_j \leq c_0 + 14 \cdot \text{IncStrs.avg}$ IDRG_{16_6} if $c_0 + 14 \cdot \text{IncStrs.avg} < c_j \leq c_0 + 15 \cdot \text{IncStrs.avg}$ IDRG_{17_6} if $c_0 + 15 \cdot \text{IncStrs.avg} < c_j \leq c_0 + 16 \cdot \text{IncStrs.avg}$ IDRG_{18_6} if $c_0 + 16 \cdot \text{IncStrs.avg} < c_j \leq c_0 + 17 \cdot \text{IncStrs.avg}$ IDRG_{19_6} if $c_0 + 17 \cdot \text{IncStrs.avg} < c_j \leq c_0 + 18 \cdot \text{IncStrs.avg}$

```

IDRG206 otherwise
ξ0 ← σ0
ξ1 ← σ0 + σ1 ·  $\left(\frac{0.25 \cdot a_j}{t}\right) + \sigma_2 \cdot \left(\frac{0.25 \cdot a_j}{t}\right)^2 + \sigma_3 \cdot \left(\frac{0.25 \cdot a_j}{t}\right)^3$ 
ξ2 ← σ0 + σ1 ·  $\left(\frac{0.5 \cdot a_j}{t}\right) + \sigma_2 \cdot \left(\frac{0.5 \cdot a_j}{t}\right)^2 + \sigma_3 \cdot \left(\frac{0.5 \cdot a_j}{t}\right)^3$ 
ξ3 ← σ0 + σ1 ·  $\left(\frac{0.75 \cdot a_j}{t}\right) + \sigma_2 \cdot \left(\frac{0.75 \cdot a_j}{t}\right)^2 + \sigma_3 \cdot \left(\frac{0.75 \cdot a_j}{t}\right)^3$ 
ξ4 ← σ0 + σ1 ·  $\left(\frac{1.0 \cdot a_j}{t}\right) + \sigma_2 \cdot \left(\frac{1.0 \cdot a_j}{t}\right)^2 + \sigma_3 \cdot \left(\frac{1.0 \cdot a_j}{t}\right)^3$ 
x0 ← 0.0
x1 ← 0.25
x2 ← 0.5
x3 ← 0.75
x4 ← 1.0
X ← stack(x0, x1, x2, x3, x4)
ST ← stack(ξ0, ξ1, ξ2, ξ3, ξ4)
RG ← regress(X, ST, 3)
σ00 ← RG3 + PInt
σ10 ← RG4
σ20 ← RG5
σ30 ← RG6
ARj ←  $\frac{a_j}{c_j}$ 
ATj ←  $\frac{a_j}{t}$ 
G... ← f...(R..., AR..., AT...)

```


$$G_{au_j} \leftarrow f_{aU}(R_t, AR_j, AT_j)$$

$$G_{al_j} \leftarrow f_{aL}(R_t, AR_j, AT_j)$$

$$G_{aq_j} \leftarrow f_{aQ}(R_t, AR_j, AT_j)$$

$$G_{ac_j} \leftarrow f_{aC}(R_t, AR_j, AT_j)$$

$$G_{cu_j} \leftarrow f_{cU}(R_t, AR_j, AT_j)$$

$$G_{cl_j} \leftarrow f_{cL}(R_t, AR_j, AT_j)$$

$$G_{cq_j} \leftarrow f_{cQ}(R_t, AR_j, AT_j)$$

$$G_{cc_j} \leftarrow f_{cC}(R_t, AR_j, AT_j)$$

$$Q_j \leftarrow \begin{cases} 1 + 1.464 \cdot \left(\frac{a_j}{c_j}\right)^{1.65} & \text{if } c_j \geq a_j \\ 1 + 1.464 \cdot \left(\frac{c_j}{a_j}\right)^{1.65} & \text{otherwise} \end{cases}$$

$$K_{a_j} \leftarrow \left(\frac{\pi \cdot a_j}{Q_j}\right)^{0.5} \cdot (\sigma_{00} \cdot G_{au_j} + \sigma_{10} \cdot G_{al_j} + \sigma_{20} \cdot G_{aq_j} + \sigma_{30} \cdot G_{ac_j})$$

$$K_{c_j} \leftarrow \left(\frac{\pi \cdot c_j}{Q_j}\right)^{0.5} \cdot (\sigma_{00} \cdot G_{cu_j} + \sigma_{10} \cdot G_{cl_j} + \sigma_{20} \cdot G_{cq_j} + \sigma_{30} \cdot G_{cc_j})$$

$$K_{\alpha_j} \leftarrow K_{a_j} \cdot 1.099$$

$$K_{\gamma_j} \leftarrow K_{c_j} \cdot 1.099$$

$$K_{\alpha_j} \leftarrow \begin{cases} 9.0 & \text{if } K_{\alpha_j} \leq 9.0 \\ K_{\alpha_j} & \text{otherwise} \end{cases}$$

$$K_{\gamma_j} \leftarrow \begin{cases} 9.0 & \text{if } K_{\gamma_j} \leq 9.0 \\ K_{\gamma_j} & \text{otherwise} \end{cases}$$

$$D_{a_j} \leftarrow C_0 \cdot (K_{\alpha_j} - 9.0)^{1.16}$$

$$D_{c_j} \leftarrow \begin{cases} D_{a_j} \cdot C_F & \text{if } K_{\gamma_j} \leq 9.0 \end{cases}$$

$$D_{ag_j} \leftarrow \begin{cases} a_j \cdot CF_{inhr} \cdot C_{blk} & \text{if } K_{\gamma_j} > 80.0 \\ 4 \cdot 10^{-10} \cdot CF_{inhr} \cdot C_{blk} & \text{otherwise} \end{cases}$$

$$D_{c_j} \leftarrow C_0 \cdot (K_{\gamma_j} - 9.0)^{1.16}$$

$$D_{cg_j} \leftarrow \begin{cases} D_{c_j} \cdot CF_{inhr} \cdot C_{blk} & \text{if } K_{\gamma_j} < 80.0 \\ 4 \cdot 10^{-10} \cdot CF_{inhr} \cdot C_{blk} & \text{otherwise} \end{cases}$$

$$\text{output}(j, 0) \leftarrow j$$

$$\text{output}(j, 1) \leftarrow a_j$$

$$\text{output}(j, 2) \leftarrow c_j - c_0$$

$$\text{output}(j, 3) \leftarrow D_{ag_j}$$

$$\text{output}(j, 4) \leftarrow D_{cg_j}$$

$$\text{output}(j, 5) \leftarrow K_{a_j}$$

$$\text{output}(j, 6) \leftarrow K_{c_j}$$

$$\text{output}(j, 7) \leftarrow \frac{NCB_j}{365 \cdot 24}$$

$$\text{output}(j, 8) \leftarrow G_{au_j}$$

$$\text{output}(j, 9) \leftarrow G_{al_j}$$

$$\text{output}(j, 10) \leftarrow G_{aq_j}$$

$$\text{output}(j, 11) \leftarrow G_{ac_j}$$

$$\text{output}(j, 12) \leftarrow G_{cu_j}$$

$$\text{output}(j, 13) \leftarrow G_{cl_j}$$

$$\text{output}(j, 14) \leftarrow G_{cq_j}$$

$$\text{output}(j, 15) \leftarrow G_{cc_j}$$

$$j \leftarrow j + 1$$

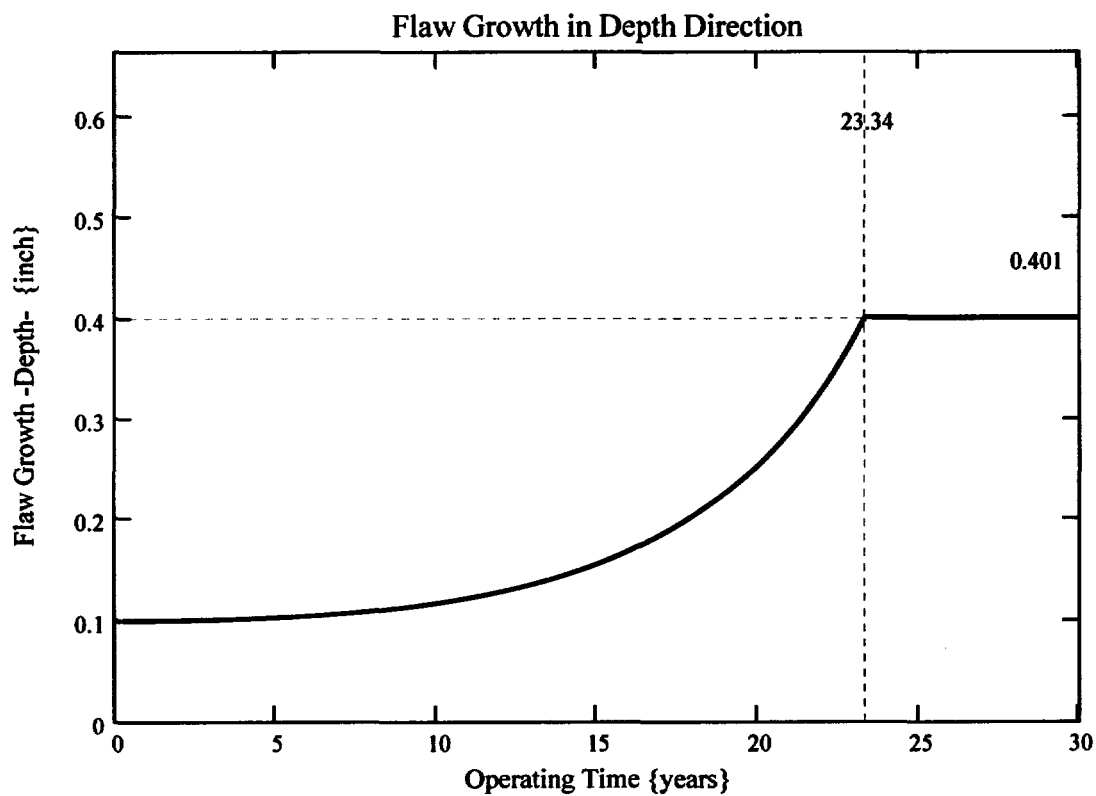
$$a_i \leftarrow a_{i-1} + D_{a_i}$$

```

       $\epsilon_{j-1}$ 
       $c_j \leftarrow c_{j-1} + D_{cg_{j-1}}$ 
       $a_j \leftarrow \begin{cases} t & \text{if } a_j \geq t \\ a_j & \text{otherwise} \end{cases}$ 
       $NCB_j \leftarrow NCB_{j-1} + C_{blk}$ 
    output
  
```

$k_w := 0..I_{lim}$

The curve below shows the flaw growth through-wall and the operating time (in years) it takes to go through-wall.



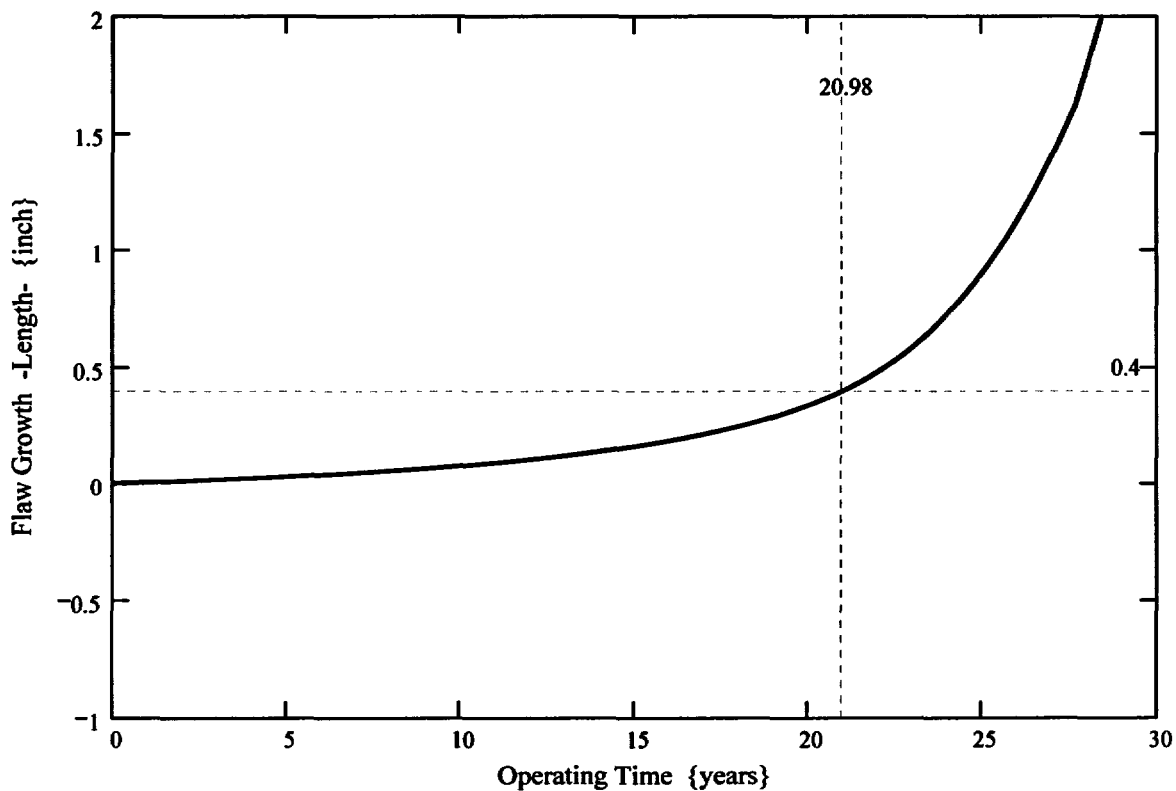
The propagation length for the ICI nozzles is defined as the length for which the initial flaw in the blind zone would extend out of the blind zone and grow to a detectable flaw. Reference 11 gives the minimum detectable flaw size of 4 mm (0.16) in length; thus, 0.16 inch was considered as this minimum detectable flaw length. This dimension is added to the end of the blind zone.

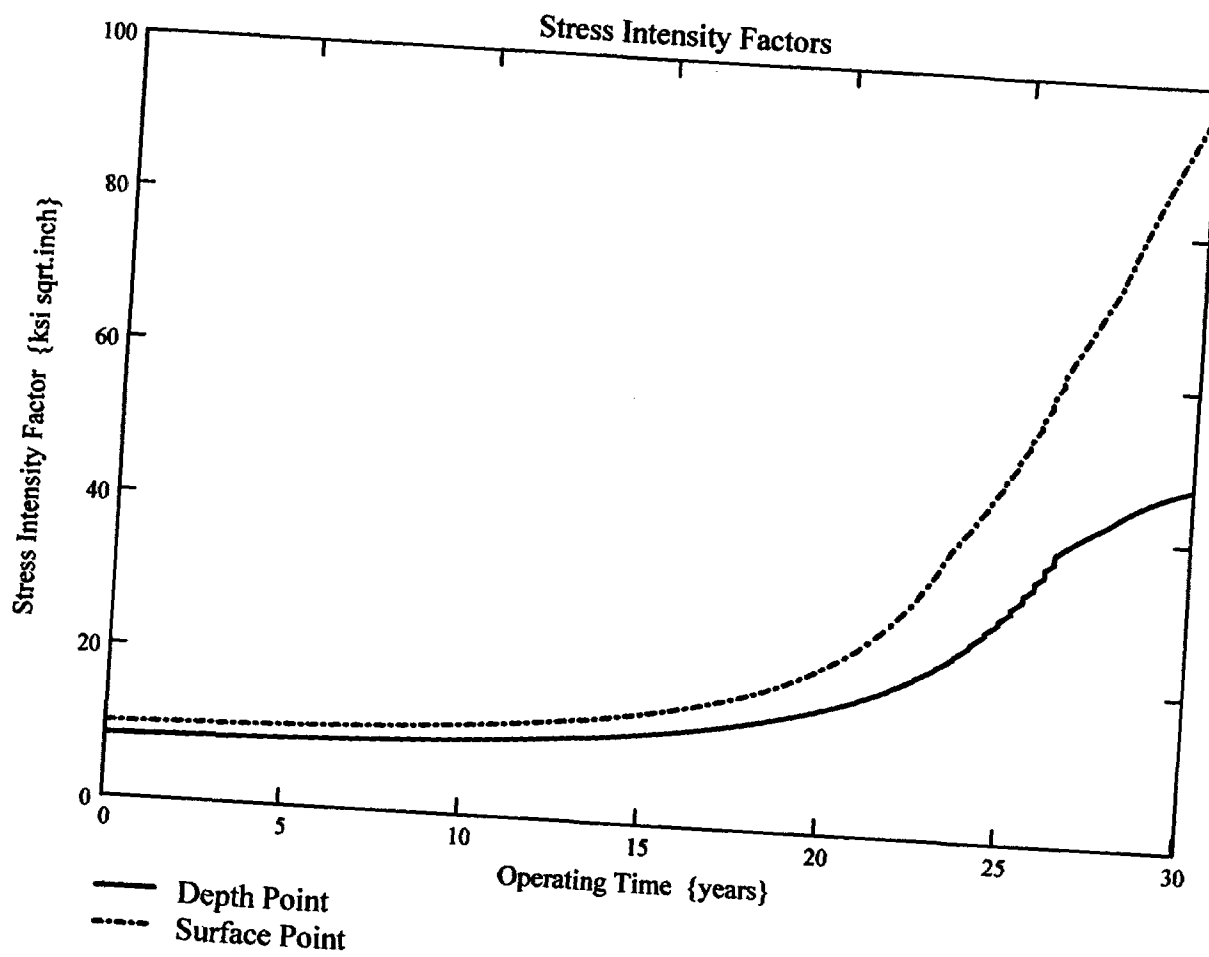
$$\text{Prop_Length} := \frac{\text{BZ_length}}{2} - c_0 + 0.16$$

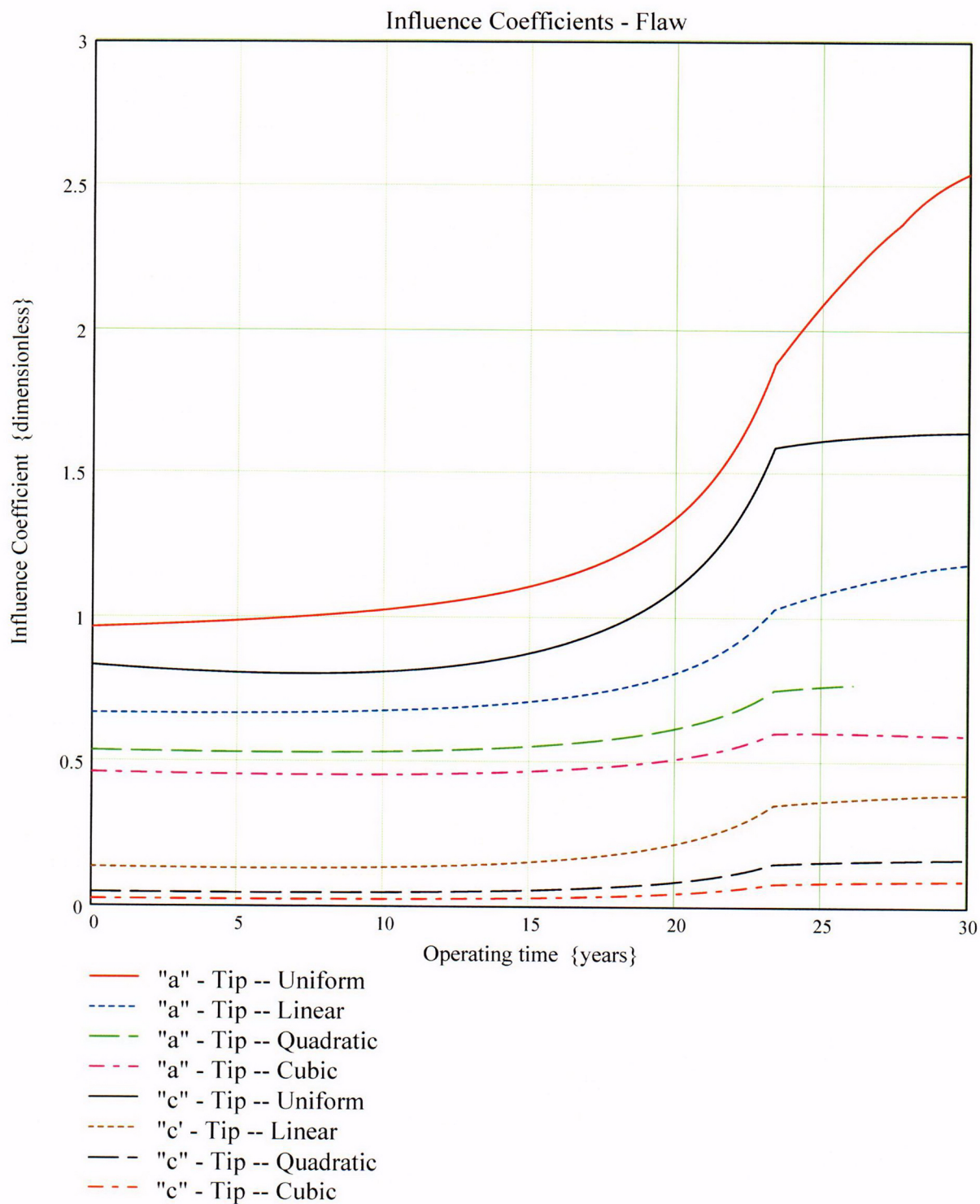
$$\text{Prop_Length} = 0.4$$

This implies that a flaw initially within the blindzone must grow 0.4 inch to become detectable via UT.

The curve below shows the flaw growth along the length of the ICI nozzle and the operating time (in years) it takes to reach the Prop_Length value defined above.







c26

Arkansas Nuclear One Unit 2

Primary Water Stress Corrosion Crack Growth Analysis for an ICI ID Surface Flaw
Uphill (180°), in the Blind Zone above the Top of the J-Groove Weld
Developed by Central Engineering Programs, Entergy Operations Inc.

Flaw Case 4: Flaw Spanning the Full Length of the Blind Zone (0.88 Inch) with a 6-to-1 Aspect Ratio

Calculation Basis: MRP 75 th Percentile and Flaw Face Pressurized

Mean Radius -to- Thickness Ratio:- " R_m/t " – between 1.0 and 300.0

Note : *The Metric form of the equation from EPRI MRP was used 55-Rev. 1 . A correction factor is applied in the determination of the crack extension to convert the units of meters per second to the value in inches per hour .*

ID Surface Flaw

User Input:

The Dominion Engineering Inc. (DEI) finite element model nodal elevations and hoop stresses for the uphill side (180° azimuth) of the ICI nozzle are brought into the Mathcad worksheet from data supplied in Reference 6d. The data are composed of the nodal elevations (in inches), along with the ID, 25% through-wall (tw), 50% tw, 75% tw, and OD hoop stresses, beginning at the top of the weld (nodal line 81301) and extending to the top of the nozzle in the FEA model, which is at the point where the nozzle intersects the reactor vessel head.

The DEI FEA data has elevation referenced from the bottom of the ICI nozzle. The elevations of the node points in the DEI FEA model, beginning at the top of the weld (nodal line 81301), are as follows:

$i := 0..9$

Node_line_i := ID_elev_fea_i := QT_elev_fea_i := MD_elev_fea_i := TQ_elev_fea_i := OD_elev_fea_i :=

81301	4.2276	4.2276	4.2276	4.2276	4.2276
81401	4.4536	4.4536	4.4536	4.4536	4.4536
81501	4.8639	4.8639	4.8639	4.8639	4.8639
81601	5.1825	5.2486	5.3148	5.3810	5.4472
81701	6.2761	6.2761	6.2761	6.2761	6.2761
81801	7.4543	7.4543	7.4543	7.4543	7.4543
81901	9.1289	9.1289	9.1289	9.1289	9.1289
82001	11.5090	11.5090	11.5090	11.5090	11.5090
82101	14.8917	14.8917	14.8917	14.8917	14.8917
82201	17.8288	17.8288	17.8288	17.8288	17.8288

The corresponding stresses at these nodes are

ID_stress_fea_i := QT_stress_fea_i := MD_stress_fea_i := TQ_stress_fea_i := OD_stress_fea_i :=

26.390	25.687	24.607	22.680	44.523
23.147	21.559	19.292	16.085	9.729
19.425	18.188	15.780	11.381	8.207
15.065	14.581	13.132	6.189	-0.109
16.707	16.175	15.560	8.890	2.74
17.399	17.177	15.044	8.136	2.316
17.412	17.487	12.883	7.180	2.298
17.115	15.794	11.377	7.821	4.387
15.304	13.024	10.766	9.067	7.453
10.308	10.119	10.032	9.951	9.936

Blind Zone and Counterbore Reference dimensions:

From design drawings (Ref. 2a and 2b) and the design input of Attachment 1, the following dimensions are used to locate the counterbore bottom and blind zone locations (bottom, top, and middle) as referenced from the nodal coordinates of the DEI FEA model.

$$\text{Actual_cbore_bottom_elev} := \text{ID_elev_fea}_0 + 1.377$$

$$\text{Actual_cbore_bottom_elev} = 5.6046$$

$$\text{topweld_to_bottom_BZ} := 1.08$$

$$\text{BZ_length} := 0.88$$

$$\text{elev_to_mid_BZ} := \text{ID_elev_fea}_0 + \text{topweld_to_bottom_BZ} + \frac{\text{BZ_length}}{2}$$

$$\text{elev_to_mid_BZ} = 5.7476$$

$$\text{bottom_of_BZ} := \text{ID_elev_fea}_0 + \text{topweld_to_bottom_BZ}$$

$$\text{bottom_of_BZ} = 5.3076$$

$$\text{top_of_BZ} := \text{ID_elev_fea}_0 + \text{topweld_to_bottom_BZ} + \text{BZ_length}$$

$$\text{top_of_BZ} = 6.1876$$

For stress averaging and fracture mechanics purposes, the reference coordinate system--with a "0" elevation at the bottom of the nozzle, at the ID corner--must be converted into a new coordinate system with the top of the nozzle (nodal line 82201) as the new "0" elevation.. The positive direction along this new coordinate system will be towards nodal line 81301, which is the top of the weld. This modification facilitates a fracture mechanics model more ammenable to the surface flaw loop structure previously developed in Reference 7.

The following iterative loops convert the five (5) through-wall stress components--ID, 25% tw (QT), 50% tw (MD), 75% tw (TQ), and OD--and the associated elevations, initially given in the DEI FEA model, into the "new" coordinate system, referenced from the top of the nozzle where it meets the reactor vessel head.

```

ID_conv := | Top ← ID_elev_fea9
            | j ← 9
            | i ← 0
            | while j ≥ 0
            |   | ID_elev_convi ← Top - ID_elev_feaj
            |   | ID_stressi ← ID_stress_feaj
            |   | output(i,0) ← ID_elev_convi
            |   | output(i,1) ← ID_stressi
            |   | j ← j - 1
            |   | i ← i + 1
            | output
  
```

$$\text{ID_elev} := \text{ID_conv}^{\langle 0 \rangle}$$

$$\text{ID_stress} := \text{ID_conv}^{\langle 1 \rangle}$$

```

QT_conv := | Top ← QT_elev_fea9
            | j ← 9
            | i ← 0
            | while j ≥ 0
            |   | QT_elev_convi ← Top - QT_elev_feaj
            |   | QT_stressi ← QT_stress_feaj
            |   | output(i, 0) ← QT_elev_convi
            |   | output(i, 1) ← QT_stressi
            |   | j ← j - 1
            |   | i ← i + 1
            | output

```

QT_elev := QT_conv⁽⁰⁾

QT_stress := QT_conv⁽¹⁾

```

MD_conv := | Top ← MD_elev_fea9
            | j ← 9
            | i ← 0
            | while j ≥ 0
            |   | MD_elev_convi ← Top - MD_elev_feaj
            |   | MD_stressi ← MD_stress_feaj
            |   | output(i, 0) ← MD_elev_convi
            |   | output(i, 1) ← MD_stressi
            |   | j ← j - 1
            |   | i ← i + 1
            | output

```

MD_elev := MD_conv⁽⁰⁾

MD_stress := MD_conv⁽¹⁾

```

TQ_conv := | Top ← TQ_elev_fea9
            | j ← 9
            | i ← 0
            | while j ≥ 0
            |   | TQ_elev_convi ← Top – TQ_elev_feaj
            |   | TQ_stressi ← TQ_stress_feaj
            |   | output(i, 0) ← TQ_elev_convi
            |   | output(i, 1) ← TQ_stressi
            |   | j ← j – 1
            |   | i ← i + 1
            | output

```

TQ_elev := TQ_conv^{⟨0⟩}

TQ_stress := TQ_conv^{⟨1⟩}

```

OD_conv := | Top ← OD_elev_fea9
            | j ← 9
            | i ← 0
            | while j ≥ 0
            |   | OD_elev_convi ← Top – OD_elev_feaj
            |   | OD_stressi ← OD_stress_feaj
            |   | output(i, 0) ← OD_elev_convi
            |   | output(i, 1) ← OD_stressi
            |   | j ← j – 1
            |   | i ← i + 1
            | output

```

OD_elev := OD_conv^{⟨0⟩}

OD_stress := OD_conv^{⟨1⟩}

ID_elev_i =

0
2.9371
6.3198
8.6999
10.3745
11.5527
12.6463
12.9649
13.3752
13.6012

QT_elev_i =

0
2.9371
6.3198
8.6999
10.3745
11.5527
12.5802
12.9649
13.3752
13.6012

MD_elev_i =

0
2.9371
6.3198
8.6999
10.3745
11.5527
12.514
12.9649
13.3752
13.6012

TQ_elev_i =

0
2.9371
6.3198
8.6999
10.3745
11.5527
12.4478
12.9649
13.3752
13.6012

OD_elev_i =

0
2.9371
6.3198
8.6999
10.3745
11.5527
12.3816
12.9649
13.3752
13.6012

ID_stress_i =

10.308
15.304
17.115
17.412
17.399
16.707
15.065
19.425
23.147
26.39

QT_stress_i =

10.119
13.024
15.794
17.487
17.177
16.175
14.581
18.188
21.559
25.687

MD_stress_i =

10.032
10.766
11.377
12.883
15.044
15.56
13.132
15.78
19.292
24.607

TQ_stress_i =

9.951
9.067
7.821
7.18
8.136
8.89
6.189
11.381
16.085
22.68

OD_stress_i =

9.936
7.453
4.387
2.298
2.316
2.74
-0.109
8.207
9.729
44.523

The two sets of five arrays given above are the elevations measured from the top of the ICI nozzle from the FEA model down to the top of the J-weld and the corresponding hoop stresses in the modified coordinate system (MCS).

Additional Geometry in Modified Coordinate System

The top of the J-groove weld in the MCS is equal to the last entry in the ID_elev array:

$$\text{Top_Jweld} := \text{ID_elev}_9$$

$$\text{Top_Jweld} = 13.6012$$

The location of the top of the UT blind zone (BZ) in the MCS (as measured from the ID surface) is

$$\text{BZ_top} := \text{Top_Jweld} - (\text{topweld_to_bottom_BZ} + \text{BZ_length})$$

$$\text{BZ_top} = 11.6412$$

The midpoint of the BZ in the MCS is

$$\text{BZ_mid} := \text{BZ_top} + \frac{\text{BZ_length}}{2}$$

$$\text{BZ_mid} = 12.0812$$

The bottom of the BZ in the MCS is

$$\text{BZ_bottom} := \text{BZ_top} + \text{BZ_length}$$

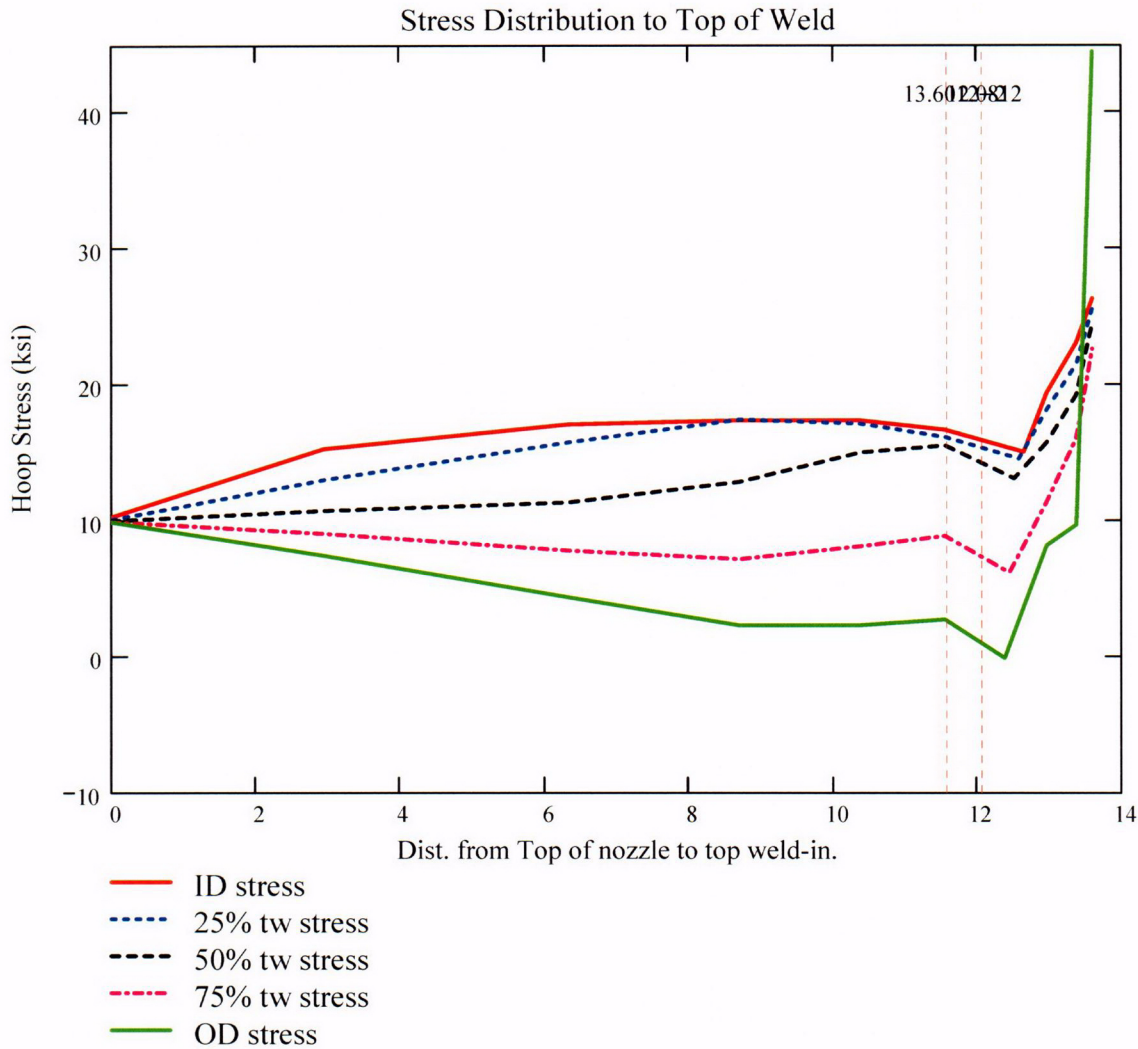
$$\text{BZ_bottom} = 12.5212$$

The location of the actual counterbore (from design drawings) in the MCS:

$$\text{cbore_elev} := \text{Top_Jweld} - 1.377$$

$$\text{cbore_elev} = 12.2242$$

From the MCS, the stress distribution from elevation 0 (the top of the ICI nozzle where it intersects the RV head) to the top of the weld is graphically shown below.



For the ID surface flaw model, the reference point is the location along the axis of the nozzle used to locate the flaw. For this analysis, the reference point is considered at the mid-height of the blind zone.

Ref_{point} := BZ_{mid}

To place the flaw with respect to the reference point, the flaw tips and center can be located as follows:

- 1) The Upper "c- tip" located at the reference point (Enter 1)
- 2) The Center of the flaw at the reference point (Enter 2)
- 3) The lower "c- tip" located at the reference point (Enter 3).

Val := 2

The Input Below is the point below the blind zone region where stresses will be considered for curve-fitting. This point is taken as the top of the weld, since the stress distribution changes drastically within the weld region Enter this dimension or variable below.

Elev_{Strs.Dist} := Top_Jweld The elevation to the point of maximum stress to consider
(Axial distance from elevation 0 in the MCS).

ICI Nozzle Geometry Input Data:

od := 5.563 - 0.001 Tube OD, in inches (The value from Ref. 2a, is 5.563" +0.00/-0.001)

id1 := 4.625 + 0.01 Maximum Tube ID above counterbore, in inches
(The value from Ref. 2b is 4.625" +/- 0.010")

id2 := 4.750 + 0.01 Maximum Tube ID below counterbore, in inches
(The value from Ref. 2b is 4.750" +/- 0.010")

$$t1 := \frac{(od - id1)}{2}$$

Minmum wall thickness above the counterbore, in inches

$$t1 = 0.4635$$

$$t2 := \frac{(od - id2)}{2}$$

Minimum wall thickness below the counterbore, in inches

$$t2 = 0.401$$

$$R_o := \frac{od}{2}$$

$$R_o = 2.781$$

$$R_{id1} := \frac{id1}{2}$$

$$R_{id1} = 2.3175$$

$$R_{id2} := \frac{id2}{2} \quad R_{id2} = 2.38$$

$$R_{m1} := R_{id1} + \frac{t1}{2} \quad R_{m1} = 2.54925$$

$$R_{m2} := R_{id2} + \frac{t2}{2} \quad R_{m2} = 2.5805$$

$$R_t := \frac{R_{m2}}{t2} \quad R_t = 6.43516$$

$$\frac{R_o}{t2} = 6.93516$$

Flaw Geometry Input Data:

A postulated flaw could exist in the 0.88" UT Blindzone that occurs 1.08" above the top of the J-weld at the uphill (180°) location. The flaw length (c) and depth (a) constitute the input parameters. This flaw represents an internal surface crack in a cylinder, as described in Reference 8.

$AR_0 := 6$ The flaw length-to-depth aspect ratio. This is a ratio common to ASME Section XI, and one sufficient to promote flaw growth through the thickness.

$L_{in} := BZ_length$ Initial Flaw Length of an ID surface flaw in the counterbore region, in inches. The length was set equal to the full length of the UT blind zone (0.88 inch). Flaw depth was based on a common length-to-depth aspect ratio of 6-to-1. Half the flaw length (0.44 inch) was placed below the mid-height of the blind zone, while the other half was placed above the mid-height.

$$L = 0.88$$

$a_0 := \frac{L}{AR_0}$ Initial Flaw Depth of the ID surface flaw in the blind zone above the top of the weld on the uphill side. The minimum detectable depth of a surface flaw from UT demonstrations [Ref. 11] was 8% throughwall. This flaw equates to 36.58% through-wall. This flaw is sufficiently deep to see the stress field developed through the thickness.

$$a_0 = 0.14667$$

$$t2 \cdot 36575 = 0.14667$$

$c_0 := \frac{L}{2}$ The half flaw length used in the fracture mechanics model

Additional Input Data:

$P_{Int} := 2.235$ Design Operating Pressure (internal) [Ref. 3]

Years := 40 Number of Operating Years

$I_{lim} := 8000$ Iteration limit for Crack Growth loop

$T_m := 604$ Conservative Operating Temperature for the head, in degrees F. Ref. 4 gives a value of 594.8 deg. F following power uprate.

$\alpha_{0c} := 2.67 \cdot 10^{-12}$ Constant in MRP-55 PWSCC Model for I-600 Wrought @ 617 deg. F [Ref. 9]

$Q_g := 31.0$ Thermal activation Energy for Crack Growth {MRP} [Ref. 9]

$T_{ref} := 617$ Reference Temperature for normalizing Data deg. F [Ref. 9]

$Tim_{opr} := 365.2422 \cdot 24 \cdot \text{Years}$ Numer of operating hours in a year

$CF_{inhr} := 1.417 \cdot 10^5$ Correction factor to convert meters per second to inches per hour

$C_{blk} := \frac{Tim_{opr}}{I_{lim}}$ Calculation block size for the crack growth iteration loop

$C_{blk} = 43.82906$

$Prnt_{blk} := \left\lceil \frac{I_{lim}}{50} \right\rceil$

$C_{01} := e^{\left[\frac{-Q_g}{1.103 \cdot 10^{-3}} \cdot \left(\frac{1}{T+459.67} - \frac{1}{T_{ref}+459.67} \right) \right]} \cdot \alpha_{0c}$

Temperature Correction for Coefficient Alpha
from EPRI MRP-55, Revision 1 [Ref. 9]

$$C_0 := 1.0C_{01} \quad 75^{\text{th}} \text{ percentile from MRP-55 Revision 1 [Ref. 9]}$$

The flaw model used for a postulated flaw within the counterbore region on the uphill side of the ICI nozzle is an internal surface flaw in a cylinder, subject to an arbitrary stress distribution.

To allow for a "moving average" of through-thickness stress values as the flaw extends along the length of the ICI ID surface, the length from the bottom tip of the of the initial flaw in the blind zone to the stress distribution upper limit--ElevStrs.Dist--is broken into 20 equal segments. Note that due to the MCS used, with a 0 elevation occurring at the TOP of the nozzle, the term "U_{Tip}" (implying the upper tip of the flaw) is actually the physical bottom tip of the flaw, closer to the top of the weld. U_{Tip} is the term used in Reference 7 for the CEDM nozzles, and thus it will continue to be used in the ICI nozzle evaluation.

$$FL_{Cntr} := \begin{cases} Ref_{Point} - c_0 & \text{if Val} = 1 \\ Ref_{Point} & \text{if Val} = 2 \\ Ref_{Point} + c_0 & \text{otherwise} \end{cases} \quad \begin{array}{l} \text{Flaw center Location at the mid-point of} \\ \text{the blind zone region} \end{array}$$

$$U_{Tip} := FL_{Cntr} + c_0$$

$$U_{Tip} = 12.5212$$

$$Inc_{Strs.avg} := \frac{Elev_{Strs.Dist} - U_{Tip}}{20}$$

$$Inc_{Strs.avg} = 0.054$$

No User Input is required beyond this Point

Regression of Through-Thickness Stresses as a Function of Axial Elevation

Because of the minor variation in stresses occurring at the top of the nozzle where it intersects the reactor head and the need to accurately curve fit stresses in the region of interest in the BZ, the entire range of stresses is not appropriate to curve fit. To accommodate an area below and above the BZ region, the first two data points in each of the elevation and stress arrays were removed from consideration in the curve fitting equations. This is a reasonable assumption, given that in the completely through-wall tensile stress field that exists in the nozzle above the top of the J-weld, a flaw centered in the BZ region is likely to grow through the thickness entirely (in addition to growth along the surface of the nozzle) rather than grow very long into an area close to the top of the head or below the top of the J-weld (i.e., elevation ranges not included in the stress polynomial curve fit). Initially, a **fourth (4th)** order polynomial was chosen for axial stress regression. After regression, the stress at the mid-height of the blind zone (12.0812 inches in the MCS) is checked.

Regression for ID stresses:

$k := 0..6$

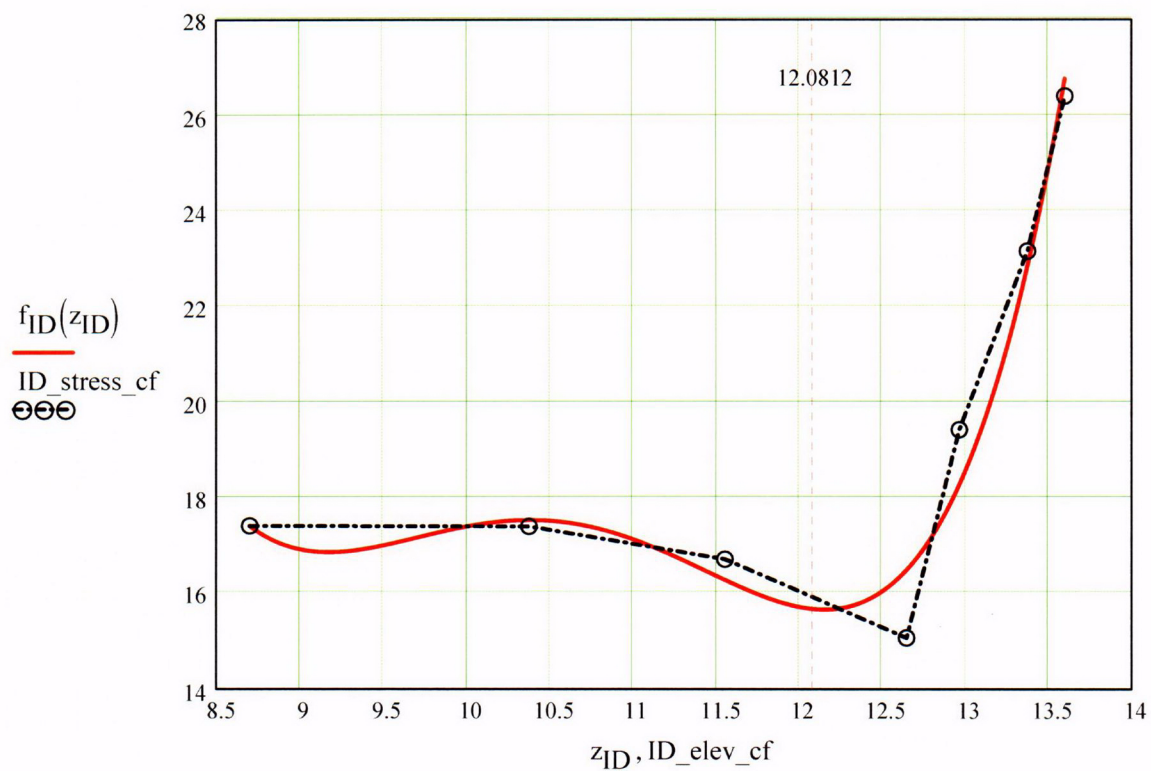
$$ID_elev_cf := \begin{pmatrix} 8.6999 \\ 10.3745 \\ 11.5527 \\ 12.6463 \\ 12.9649 \\ 13.3752 \\ 13.6012 \end{pmatrix} \quad ID_stress_cf := \begin{pmatrix} 17.412 \\ 17.399 \\ 16.707 \\ 15.065 \\ 19.425 \\ 23.147 \\ 26.39 \end{pmatrix}$$

$$R_{ID} := \text{regress}(ID_elev_cf, ID_stress_cf, 4)$$

$$R_{ID} = \begin{pmatrix} 3 \\ 3 \\ 4 \\ 2920.01158 \\ -1120.32621 \\ 161.1276 \\ -10.23275 \\ 0.24206 \end{pmatrix}$$

ID_elev _i =	ID_stress _i =
0	10.308
2.9371	15.304
6.3198	17.115
8.6999	17.412
10.3745	17.399
11.5527	16.707
12.6463	15.065
12.9649	19.425
13.3752	23.147
13.6012	26.39

$$f_{ID}(z_{ID}) := \text{interp}(R_{ID}, ID_elev_cf, ID_stress_cf, z_{ID})$$



$$f_{ID}(12.0812) = 15.66367$$

Regression for 25% throughwall stresses:

$$QT_elev_cf := \begin{pmatrix} 8.6999 \\ 10.3745 \\ 11.5527 \\ 12.5802 \\ 12.9649 \\ 13.3752 \\ 13.6012 \end{pmatrix} \quad QT_stress_cf := \begin{pmatrix} 17.487 \\ 17.177 \\ 16.175 \\ 14.581 \\ 18.188 \\ 21.559 \\ 25.687 \end{pmatrix}$$

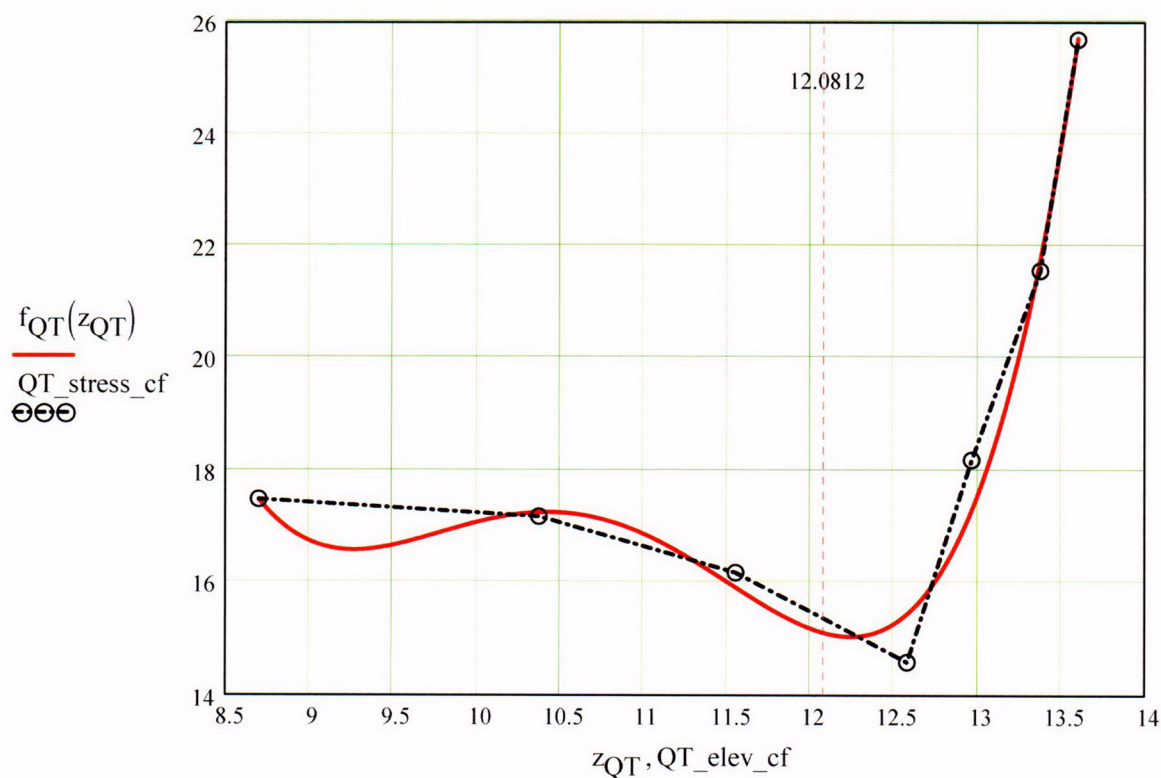
$$R_{QT} := \text{regress}(QT_elev_cf, QT_stress_cf, 4)$$

$$z_{QT} := 8.6999, 8.701 \dots \text{Top_Jweld}$$

$$R_{QT} = \begin{pmatrix} 3 \\ 3 \\ 4 \\ 3362.70255 \\ -1281.45936 \\ 182.93207 \\ -11.53275 \\ 0.27085 \end{pmatrix}$$

$QT_elev_i =$	$QT_stress_i =$
0	10.119
2.9371	13.024
6.3198	15.794
8.6999	17.487
10.3745	17.177
11.5527	16.175
12.5802	14.581
12.9649	18.188
13.3752	21.559
13.6012	25.687

$$f_{QT}(z_{QT}) := \text{interp}(R_{QT}, QT_elev_cf, QT_stress_cf, z_{QT})$$



$$f_{QT}(12.0812) = 15.09487$$

Regression for 50% throughwall stresses:

$$\text{MD_elev_cf} := \begin{pmatrix} 8.6999 \\ 10.3745 \\ 11.5527 \\ 12.514 \\ 12.9649 \\ 13.3752 \\ 13.6012 \end{pmatrix} \quad \text{MD_stress_cf} := \begin{pmatrix} 12.883 \\ 15.044 \\ 15.56 \\ 13.132 \\ 15.78 \\ 19.292 \\ 24.607 \end{pmatrix}$$

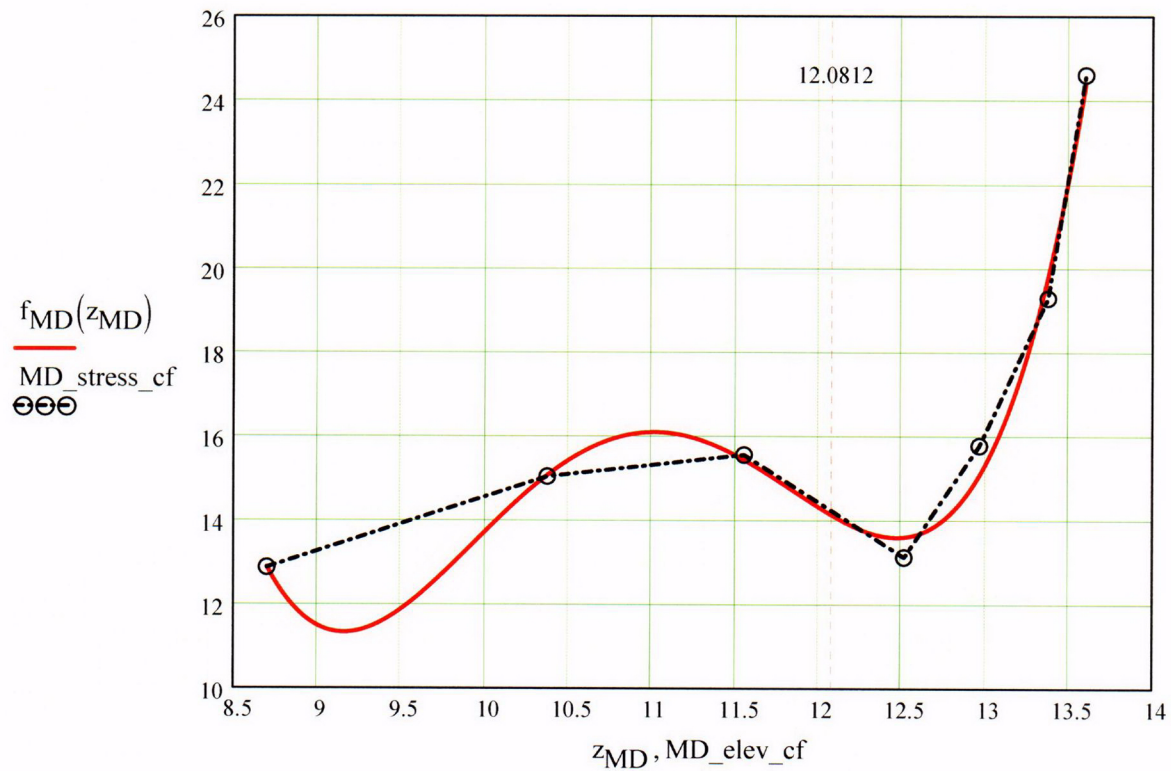
$$\text{R}_{\text{MD}} := \text{regress}(\text{MD_elev_cf}, \text{MD_stress_cf}, 4)$$

$$\text{z}_{\text{MD}} := 8.6999, 8.701 \dots \text{Top_Jweld}$$

$$\text{R}_{\text{MD}} = \begin{pmatrix} 3 \\ 3 \\ 4 \\ 6270.57353 \\ -2357.44561 \\ 330.23769 \\ -20.39106 \\ 0.46849 \end{pmatrix}$$

MD_elev _i	MD_stress _i
0	10.032
2.9371	10.766
6.3198	11.377
8.6999	12.883
10.3745	15.044
11.5527	15.56
12.514	13.132
12.9649	15.78
13.3752	19.292
13.6012	24.607

$$f_{\text{MD}}(z_{\text{MD}}) := \text{interp}(\text{R}_{\text{MD}}, \text{MD_elev_cf}, \text{MD_stress_cf}, z_{\text{MD}})$$



$$f_{MD}(12.0812) = 14.11569$$

Regression for 75% throughwall stresses:

$$TQ_elev_cf := \begin{pmatrix} 8.6999 \\ 10.3745 \\ 11.5527 \\ 12.4478 \\ 12.9649 \\ 13.3752 \\ 13.6012 \end{pmatrix} \quad TQ_stress_cf := \begin{pmatrix} 7.18 \\ 8.136 \\ 8.89 \\ 6.189 \\ 11.381 \\ 16.085 \\ 22.68 \end{pmatrix}$$

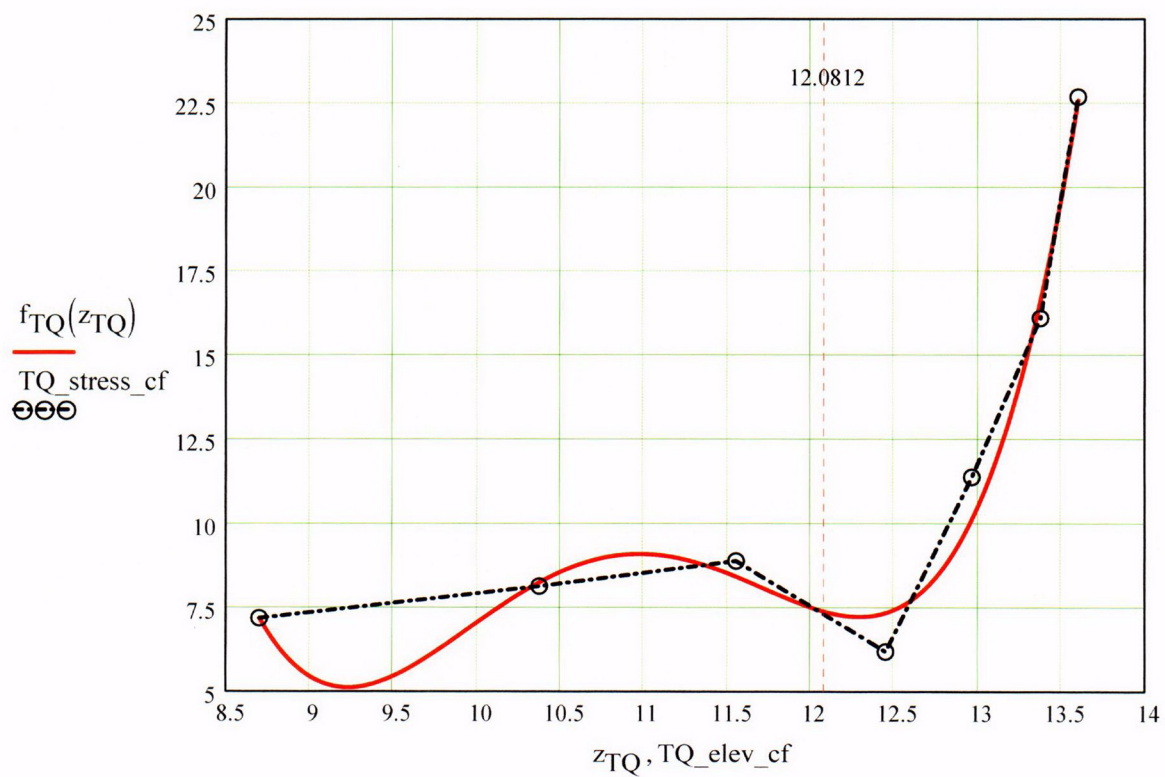
$$R_{TQ} := \text{regress}(TQ_elev_cf, TQ_stress_cf, 4)$$

$$z_{TQ} := 8.6999, 8.701 \dots \text{Top_Jweld}$$

$$R_{TQ} = \begin{pmatrix} 3 \\ 3 \\ 4 \\ 6772.44513 \\ -2552.34739 \\ 358.42617 \\ -22.21167 \\ 0.51271 \end{pmatrix}$$

$TQ_elev_i =$	$TQ_stress_i =$
0	9.951
2.9371	9.067
6.3198	7.821
8.6999	7.18
10.3745	8.136
11.5527	8.89
12.4478	6.189
12.9649	11.381
13.3752	16.085
13.6012	22.68

$$f_{TQ}(z_{TQ}) := \text{interp}(R_{TQ}, TQ_elev_cf, TQ_stress_cf, z_{TQ})$$



$$f_{TQ}(12.0812) = 7.37343$$

Regression for OD stresses:

kk := 0..5

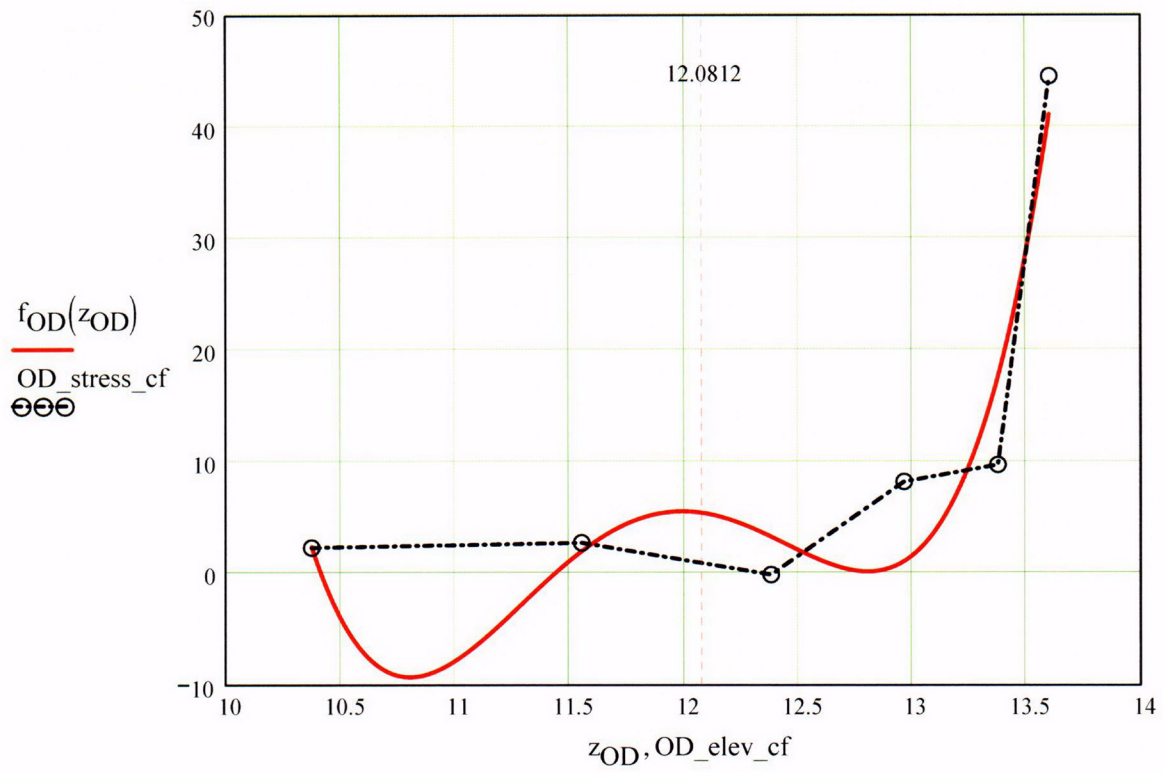
$$\text{OD_elev_cf} := \begin{pmatrix} 10.3745 \\ 11.5527 \\ 12.3816 \\ 12.9649 \\ 13.3752 \\ 13.6012 \end{pmatrix} \quad \text{OD_stress_cf} := \begin{pmatrix} 2.316 \\ 2.74 \\ -0.109 \\ 8.207 \\ 9.729 \\ 44.523 \end{pmatrix}$$

$$\begin{aligned} R_{\text{OD}} &:= \text{regress}(\text{OD_elev_cf}, \text{OD_stress_cf}, 4) \\ z_{\text{OD}} &:= 10.3745, 10.376 \dots \text{Top_Jweld} \end{aligned}$$

$$R_{\text{OD}} = \begin{pmatrix} 3 \\ 3 \\ 4 \\ 1.83727 \times 10^5 \\ -62394.03658 \\ 7925.4618 \\ -446.31291 \\ 9.40247 \end{pmatrix}$$

OD_elev _i	OD_stress _i
0	9.936
2.9371	7.453
6.3198	4.387
8.6999	2.298
10.3745	2.316
11.5527	2.74
12.3816	-0.109
12.9649	8.207
13.3752	9.729
13.6012	44.523

$$f_{\text{OD}}(z_{\text{OD}}) := \text{interp}(R_{\text{OD}}, \text{OD_elev_cf}, \text{OD_stress_cf}, z_{\text{OD}})$$



$$f_{OD}(12.0812) = 5.39079$$

C32

Calculation to develop Stress Profiles for Analysis

This analysis for the axial stress regression and the through-wall stress regression is the same as that used for the CEDM Nozzles (in Ref. 7) with the exception that the axial stresses are fit with a fourth-order polynomial, rather than a third-order polynomial, to accomodate greater precision.

$$N_w := 20$$

Number of locations for stress profiles

$$Loc_0 := FL_{Cntr} - L$$

$$FL_{Cntr} = 12.0812$$

$$L = 0.88$$

$$i := 1..N + 3$$

$$Incr_i := \begin{cases} c_0 & \text{if } i < 4 \\ Inc_{Strs.avg} & \text{otherwise} \end{cases}$$

$$Loc_i := Loc_{i-1} + Incr_i$$

$$SID_i := R_{ID_3} + R_{ID_4} \cdot Loc_i + R_{ID_5} \cdot (Loc_i)^2 + R_{ID_6} \cdot (Loc_i)^3 + R_{ID_7} \cdot (Loc_i)^4$$

$$SQT_i := R_{QT_3} + R_{QT_4} \cdot Loc_i + R_{QT_5} \cdot (Loc_i)^2 + R_{QT_6} \cdot (Loc_i)^3 + R_{QT_7} \cdot (Loc_i)^4$$

$$SMD_i := R_{MD_3} + R_{MD_4} \cdot Loc_i + R_{MD_5} \cdot (Loc_i)^2 + R_{MD_6} \cdot (Loc_i)^3 + R_{MD_7} \cdot (Loc_i)^4$$

$$STQ_i := R_{TQ_3} + R_{TQ_4} \cdot Loc_i + R_{TQ_5} \cdot (Loc_i)^2 + R_{TQ_6} \cdot (Loc_i)^3 + R_{TQ_7} \cdot (Loc_i)^4$$

$$SOD_i := R_{OD_3} + R_{OD_4} \cdot Loc_i + R_{OD_5} \cdot (Loc_i)^2 + R_{OD_6} \cdot (Loc_i)^3 + R_{OD_7} \cdot (Loc_i)^4$$

$$j := 1..N$$

$$S_{id_j} := \begin{cases} \frac{SID_j + SID_{j+1} + SID_{j+2}}{3} & \text{if } j = 1 \\ \frac{S_{id_{j-1}} \cdot (j+1) + SID_{j+2}}{j+2} & \text{otherwise} \end{cases}$$

$$S_{qt_j} := \begin{cases} \frac{SQT_j + SQT_{j+1} + SQT_{j+2}}{3} & \text{if } j = 1 \\ \frac{S_{qt_{(j-1)}} \cdot (j+1) + SQT_{j+2}}{j+2} & \text{otherwise} \end{cases}$$

$$S_{md_j} := \begin{cases} \frac{SMD_j + SMD_{j+1} + SMD_{j+2}}{3} & \text{if } j = 1 \\ \frac{S_{md_{j-1}} \cdot (j+1) + SMD_{j+2}}{j+2} & \text{otherwise} \end{cases}$$

$$S_{tq_j} := \begin{cases} \frac{STQ_j + STQ_{j+1} + STQ_{j+2}}{3} & \text{if } j = 1 \\ \frac{S_{tq_{j-1}} \cdot (j+1) + STQ_{j+2}}{j+2} & \text{otherwise} \end{cases}$$

$$S_{od_j} := \begin{cases} \frac{SOD_j + SOD_{j+1} + SOD_{j+2}}{3} & \text{if } j = 1 \\ \frac{S_{od_{j-1}} \cdot (j+1) + SOD_{j+2}}{j+2} & \text{otherwise} \end{cases}$$

Through-Wall Stress Distribution for ID Flaws (i.e. ID to OD Stress distribution)

$$u_0 := 0.000$$

$$u_1 := 0.25$$

$$u_2 := 0.50$$

$$u_3 := 0.75$$

$$u_4 := 1.00$$

$$Y := \text{stack}(u_0, u_1, u_2, u_3, u_4)$$

$$\text{SIG}_1 := \text{stack}(S_{id_1}, S_{qt_1}, S_{md_1}, S_{tq_1}, S_{od_1})$$

$$\text{SIG}_2 := \text{stack}(S_{id_2}, S_{qt_2}, S_{md_2}, S_{tq_2}, S_{od_2})$$

$$\text{SIG}_3 := \text{stack}(S_{id_3}, S_{qt_3}, S_{md_3}, S_{tq_3}, S_{od_3})$$

$$\text{SIG}_4 := \text{stack}(S_{id_4}, S_{qt_4}, S_{md_4}, S_{tq_4}, S_{od_4})$$

$$\text{SIG}_5 := \text{stack}(S_{id_5}, S_{qt_5}, S_{md_5}, S_{tq_5}, S_{od_5})$$

$$\text{SIG}_6 := \text{stack}(S_{id_6}, S_{qt_6}, S_{md_6}, S_{tq_6}, S_{od_6})$$

$$\text{SIG}_7 := \text{stack}(S_{id_7}, S_{qt_7}, S_{md_7}, S_{tq_7}, S_{od_7})$$

$$\text{SIG}_8 := \text{stack}(S_{id_8}, S_{qt_8}, S_{md_8}, S_{tq_8}, S_{od_8})$$

$$\text{SIG}_9 := \text{stack}(S_{id_9}, S_{qt_9}, S_{md_9}, S_{tq_9}, S_{od_9})$$

$$\text{SIG}_{10} := \text{stack}(S_{id_{10}}, S_{qt_{10}}, S_{md_{10}}, S_{tq_{10}}, S_{od_{10}})$$

$$\text{SIG}_{11} := \text{stack}(S_{id_{11}}, S_{qt_{11}}, S_{md_{11}}, S_{tq_{11}}, S_{od_{11}})$$

$$\text{SIG}_{12} := \text{stack}(S_{id_{12}}, S_{qt_{12}}, S_{md_{12}}, S_{tq_{12}}, S_{od_{12}})$$

$$\text{SIG}_{13} := \text{stack}(S_{id_{13}}, S_{qt_{13}}, S_{md_{13}}, S_{tq_{13}}, S_{od_{13}})$$

$$\text{SIG}_{14} := \text{stack}(S_{id_{14}}, S_{qt_{14}}, S_{md_{14}}, S_{tq_{14}}, S_{od_{14}})$$

$$\text{SIG}_{15} := \text{stack}(S_{id_{15}}, S_{qt_{15}}, S_{md_{15}}, S_{tq_{15}}, S_{od_{15}})$$

$$\text{SIG}_{16} := \text{stack}(S_{id_{16}}, S_{qt_{16}}, S_{md_{16}}, S_{tq_{16}}, S_{od_{16}})$$

$$\text{SIG}_{17} := \text{stack}(S_{id_{17}}, S_{qt_{17}}, S_{md_{17}}, S_{tq_{17}}, S_{od_{17}})$$

$$\text{SIG}_{18} := \text{stack}(S_{id_{18}}, S_{qt_{18}}, S_{md_{18}}, S_{tq_{18}}, S_{od_{18}})$$

$$\text{SIG}_{19} := \text{stack}(S_{id_{19}}, S_{qt_{19}}, S_{md_{19}}, S_{tq_{19}}, S_{od_{19}})$$

$$\text{SIG}_{20} := \text{stack}(S_{id_{20}}, S_{qt_{20}}, S_{md_{20}}, S_{tq_{20}}, S_{od_{20}})$$

Regression of Through-Wall Stress distribution to Obtain Stress Coefficients Using a Third Order Polynomial

$$\text{IDRG}_1 := \text{regress}(Y, \text{SIG}_1, 3)$$

$$\text{IDRG}_2 := \text{regress}(Y, \text{SIG}_2, 3)$$

$$\text{IDRG}_3 := \text{regress}(Y, \text{SIG}_3, 3)$$

$$\text{IDRG}_4 := \text{regress}(Y, \text{SIG}_4, 3)$$

$$\text{IDRG}_5 := \text{regress}(Y, \text{SIG}_5, 3)$$

$$\text{IDRG}_6 := \text{regress}(Y, \text{SIG}_6, 3)$$

$$\text{IDRG}_7 := \text{regress}(Y, \text{SIG}_7, 3)$$

$$\text{IDRG}_8 := \text{regress}(Y, \text{SIG}_8, 3)$$

$$\text{IDRG}_9 := \text{regress}(Y, \text{SIG}_9, 3)$$

$$\text{IDRG}_{10} := \text{regress}(Y, \text{SIG}_{10}, 3)$$

$$\text{IDRG}_{11} := \text{regress}(Y, \text{SIG}_{11}, 3)$$

$$\text{IDRG}_{12} := \text{regress}(Y, \text{SIG}_{12}, 3)$$

$$\text{IDRG}_{13} := \text{regress}(Y, \text{SIG}_{13}, 3)$$

$$\text{IDRG}_{14} := \text{regress}(Y, \text{SIG}_{14}, 3)$$

$$\text{IDRG}_{15} := \text{regress}(Y, \text{SIG}_{15}, 3)$$

$$\text{IDRG}_{16} := \text{regress}(Y, \text{SIG}_{16}, 3)$$

$$\text{IDRG}_{17} := \text{regress}(Y, \text{SIG}_{17}, 3)$$

$$\text{IDRG}_{18} := \text{regress}(Y, \text{SIG}_{18}, 3)$$

$$\text{IDRG}_{19} := \text{regress}(Y, \text{SIG}_{19}, 3)$$

$$\text{IDRG}_{20} := \text{regress}(Y, \text{SIG}_{20}, 3)$$

***Stress Distribution in the tube. Stress influence coefficients obtained from
third-order polynomial curve fit to the throughwall stress distribution***

Data Files for Flaw Shape Factors from NASA SC04 Model [Ref. 8]

{NO INPUT Required}

Mettu Raju Newman Sivakumar Forman Solution of ID Part throughwall Flaw in Cyinder

Jsb :=

	0	1	2
0	1.000	0.200	0.000
1	1.000	0.200	0.200
2	1.000	0.200	0.500
3	1.000	0.200	0.800
4	1.000	0.200	1.000
5	1.000	0.400	0.000
6	1.000	0.400	0.200
7	1.000	0.400	0.500
8	1.000	0.400	0.800
9	1.000	0.400	1.000
10	1.000	1.000	0.000
11	1.000	1.000	0.200
12	1.000	1.000	0.500
13	1.000	1.000	0.800
14	1.000	1.000	1.000
15	2.000	0.200	0.000
16	2.000	0.200	0.200
17	2.000	0.200	0.500
18	2.000	0.200	0.800
19	2.000	0.200	1.000
20	2.000	0.400	0.000
21	2.000	0.400	0.200
22	2.000	0.400	0.500
23	2.000	0.400	0.800
24	2.000	0.400	1.000
25	2.000	1.000	0.000
26	2.000	1.000	0.200
27	2.000	1.000	0.500
28	2.000	1.000	0.800
29	2.000	1.000	1.000
30	4.000	0.200	0.000
31	4.000	0.200	0.200
32	4.000	0.200	0.500
33	4.000	0.200	0.800

34	4.000	0.200	1.000
35	4.000	0.400	0.000
36	4.000	0.400	0.200
37	4.000	0.400	0.500
38	4.000	0.400	0.800
39	4.000	0.400	1.000
40	4.000	1.000	0.000
41	4.000	1.000	0.200
42	4.000	1.000	0.500
43	4.000	1.000	0.800
44	4.000	1.000	1.000
45	10.000	0.200	0.000
46	10.000	0.200	0.200
47	10.000	0.200	0.500
48	10.000	0.200	0.800
49	10.000	0.200	1.000
50	10.000	0.400	0.000
51	10.000	0.400	0.200
52	10.000	0.400	0.500
53	10.000	0.400	0.800
54	10.000	0.400	1.000
55	10.000	1.000	0.000
56	10.000	1.000	0.200
57	10.000	1.000	0.500
58	10.000	1.000	0.800
59	10.000	1.000	1.000
60	300.000	0.200	0.000
61	300.000	0.200	0.200
62	300.000	0.200	0.500
63	300.000	0.200	0.800
64	300.000	0.200	1.000
65	300.000	0.400	0.000
66	300.000	0.400	0.200
67	300.000	0.400	0.500
68	300.000	0.400	0.800
69	300.000	0.400	1.000
70	300.000	1.000	0.000
71	300.000	1.000	0.200
72	300.000	1.000	0.500
73	300.000	1.000	0.800
74	300.000	1.000	1.000

Sambi :=

	0	1	2	3	4	5	6	7
0	1.076	0.693	0.531	0.434	0.608	0.083	0.023	0.009
1	1.056	0.647	0.495	0.408	0.615	0.085	0.027	0.013
2	1.395	0.767	0.557	0.446	0.871	0.171	0.069	0.038
3	2.53	1.174	0.772	0.58	1.554	0.363	0.155	0.085
4	3.846	1.615	0.995	0.716	2.277	0.544	0.233	0.127
5	1.051	0.689	0.536	0.444	0.74	0.112	0.035	0.015
6	1.011	0.646	0.504	0.421	0.745	0.119	0.041	0.02
7	1.149	0.694	0.529	0.435	0.916	0.181	0.073	0.04
8	1.6	0.889	0.642	0.51	1.334	0.307	0.132	0.073
9	2.087	1.093	0.761	0.589	1.752	0.421	0.183	0.101
10	0.992	0.704	0.534	0.506	1.044	0.169	0.064	0.032
11	0.987	0.701	0.554	0.491	1.08	0.182	0.067	0.034
12	1.01	0.709	0.577	0.493	1.116	0.2	0.078	0.041
13	1.07	0.73	0.623	0.523	1.132	0.218	0.095	0.051
14	1.128	0.75	0.675	0.556	1.131	0.229	0.11	0.06
15	1.049	0.673	0.519	0.427	0.6	0.078	0.021	0.008
16	1.091	0.661	0.502	0.413	0.614	0.083	0.025	0.012
17	1.384	0.764	0.556	0.446	0.817	0.15	0.058	0.031
18	2.059	1.033	0.708	0.545	1.3	0.291	0.123	0.067
19	2.739	1.301	0.858	0.643	1.783	0.421	0.18	0.099
20	1.075	0.674	0.527	0.436	0.73	0.072	0.044	0.021
21	1.045	0.659	0.511	0.425	0.76	0.122	0.043	0.021
22	1.16	0.71	0.536	0.441	0.919	0.197	0.064	0.034
23	1.51	0.854	0.623	0.498	1.231	0.271	0.114	0.062
24	1.876	0.995	0.71	0.555	1.519	0.317	0.161	0.089
25	1.037	0.732	0.594	0.505	1.132	0.192	0.07	0.035
26	1.003	0.707	0.577	0.493	1.113	0.19	0.071	0.036
27	1.023	0.714	0.58	0.495	1.155	0.207	0.08	0.042
28	1.129	0.774	0.619	0.521	1.286	0.247	0.098	0.052
29	1.242	0.84	0.661	0.549	1.416	0.285	0.115	0.061
30	1.003	0.649	0.511	0.43	0.577	0.07	0.015	0.005
31	1.097	0.666	0.511	0.426	0.606	0.079	0.023	0.01
32	1.405	0.776	0.567	0.46	0.797	0.141	0.054	0.028
33	1.959	0.996	0.692	0.542	1.201	0.262	0.108	0.059
34	2.461	1.197	0.808	0.619	1.586	0.37	0.154	0.085
35	1.024	0.668	0.528	0.451	0.737	0.11	0.033	0.015
36	1.057	0.666	0.52	0.439	0.77	0.123	0.042	0.021
37	1.193	0.715	0.545	0.454	0.924	0.174	0.068	0.036
38	1.443	0.828	0.614	0.509	1.219	0.263	0.109	0.059
39	1.665	0.934	0.681	0.565	1.487	0.339	0.143	0.078
40	1.005	0.72	0.507	0.418	1.110	0.188	0.068	0.034

	1.000	0.712	0.588	0.511	1.128	0.194	0.072	0.037
41	1.009	0.713	0.588	0.511	1.128	0.194	0.072	0.037
42	1.041	0.726	0.594	0.515	1.191	0.214	0.082	0.043
43	1.105	0.768	0.623	0.536	1.316	0.248	0.097	0.05
44	1.162	0.81	0.653	0.558	1.428	0.277	0.109	0.055
45	0.973	0.635	0.499	0.446	0.579	0.07	0.016	0.005
46	1.115	0.673	0.514	0.438	0.607	0.079	0.023	0.01
47	1.427	0.783	0.571	0.462	0.791	0.138	0.052	0.027
48	1.872	0.96	0.671	0.529	1.179	0.253	0.104	0.056
49	2.23	1.108	0.757	0.594	1.548	0.356	0.149	0.081
50	0.992	0.656	0.52	0.443	0.733	0.109	0.032	0.014
51	1.072	0.672	0.523	0.441	0.777	0.125	0.043	0.021
52	1.217	0.723	0.549	0.456	0.936	0.176	0.069	0.036
53	1.393	0.806	0.601	0.493	1.219	0.259	0.106	0.056
54	1.521	0.875	0.647	0.528	1.469	0.328	0.135	0.071
55	0.994	0.715	0.59	0.518	1.114	0.187	0.068	0.035
56	1.015	0.715	0.588	0.512	1.14	0.197	0.074	0.038
57	1.05	0.729	0.596	0.515	1.219	0.221	0.085	0.044
58	1.09	0.76	0.618	0.532	1.348	0.255	0.099	0.051
59	1.118	0.788	0.639	0.55	1.456	0.282	0.109	0.056
60	0.936	0.62	0.486	0.405	0.582	0.068	0.015	0.005
61	1.145	0.681	0.514	0.42	0.613	0.081	0.024	0.011
62	1.459	0.79	0.569	0.454	0.79	0.138	0.051	0.026
63	1.774	0.917	0.641	0.501	1.148	0.239	0.096	0.051
64	1.974	1.008	0.696	0.537	1.482	0.328	0.134	0.07
65	0.982	0.651	0.512	0.427	0.721	0.103	0.031	0.013
66	1.095	0.677	0.52	0.431	0.782	0.127	0.045	0.022
67	1.244	0.727	0.546	0.446	0.946	0.18	0.071	0.037
68	1.37	0.791	0.585	0.473	1.201	0.253	0.102	0.054
69	1.438	0.838	0.618	0.496	1.413	0.31	0.126	0.066

$$W_{\text{mm}} := \text{Jsb}^{(0)}$$

$$X := \text{Jsb}^{(1)}$$

$$Y := \text{Jsb}^{(2)}$$

$$a_U := \text{Sambi}^{(0)}$$

$$a_L := \text{Sambi}^{(1)}$$

$$a_Q := \text{Sambi}^{(2)}$$

$$a_C := \text{Sambi}^{(3)}$$

$$c_U := \text{Sambi}^{(4)}$$

$$c_L := \text{Sambi}^{(5)}$$

$$c_Q := \text{Sambi}^{(6)}$$

$$c_C := \text{Sambi}^{(7)}$$

$$n := \begin{cases} 3 & \text{if } R_t \leq 4.0 \\ 2 & \text{otherwise} \end{cases}$$

"a-Tip" Uniform Term

$$M_{aU} := \text{augment}(W, X, Y) \quad V_{aU} := a_U \quad R_{aU} := \text{regress}(M_{aU}, V_{aU}, n)$$

$$f_{aU}(W, X, Y) := \text{interp} \left[R_{aU}, M_{aU}, V_{aU}, \begin{pmatrix} W \\ X \\ Y \end{pmatrix} \right]$$

$$f_{aU}(4, .4, .8) = 1.7089$$

Check Calculation

Linear Term

$$M_{aL} := \text{augment}(W, X, Y) \quad V_{aL} := a_L \quad R_{aL} := \text{regress}(M_{aL}, V_{aL}, n)$$

$$f_{aL}(W, X, Y) := \text{interp} \left[R_{aL}, M_{aL}, V_{aL}, \begin{pmatrix} W \\ X \\ Y \end{pmatrix} \right]$$

$$f_{aL}(4, .4, .8) = 0.93393$$

Check Calculation

Quadratic Term

$$M_{aQ} := \text{augment}(W, X, Y) \quad V_{aQ} := a_Q \quad R_{aQ} := \text{regress}(M_{aQ}, V_{aQ}, n)$$

$$f_{aQ}(W, X, Y) := \text{interp} \left[R_{aQ}, M_{aQ}, V_{aQ}, \begin{pmatrix} W \\ X \\ Y \end{pmatrix} \right]$$

$$f_{aQ}(4, .4, .8) = 0.67668 \quad \text{Check Calculation}$$

Cubic Term

$$M_{aC} := \text{augment}(W, X, Y) \quad V_{aC} := a_C$$

$$R_{aC} := \text{regress}(M_{aC}, V_{aC}, n)$$

$$f_{aC}(W, X, Y) := \text{interp} \left[R_{aC}, M_{aC}, V_{aC}, \begin{pmatrix} W \\ X \\ Y \end{pmatrix} \right]$$

$$f_{aC}(4, .4, .8) = 0.54151 \quad \text{Check Calculation}$$

"C" Tip Coefficients

Uniform Term

$$M_{cU} := \text{augment}(W, X, Y) \quad V_{cU} := c_U$$

$$R_{cU} := \text{regress}(M_{cU}, V_{cU}, n)$$

$$f_{cU}(W, X, Y) := \text{interp} \left[R_{cU}, M_{cU}, V_{cU}, \begin{pmatrix} W \\ X \\ Y \end{pmatrix} \right]$$

$$f_{cU}(4, .4, .8) = 1.31015 \quad \text{Check Calculation}$$

Linear Term

$$M_{cL} := \text{augment}(W, X, Y) \quad V_{cL} := c_L$$

$$R_{cL} := \text{regress}(M_{cL}, V_{cL}, n)$$

$$f_{cL}(W, X, Y) := \text{interp} \left[R_{cL}, M_{cL}, V_{cL}, \begin{pmatrix} W \\ X \\ Y \end{pmatrix} \right]$$

$$f_{cL}(2, .4, .8) = 0.28509 \quad \text{Check Calculation}$$

Quadratic Term

$$M_{cQ} := \text{augment}(W, X, Y) \quad V_{cQ} := c_Q \quad R_{cQ} := \text{regress}(M_{cQ}, V_{cQ}, n)$$

$$f_{cQ}(W, X, Y) := \text{interp} \left[R_{cQ}, M_{cQ}, V_{cQ}, \begin{pmatrix} W \\ X \\ Y \end{pmatrix} \right]$$

$$f_{cQ}(4, .4, .8) = 0.11797 \quad \text{Check Calculation}$$

Cubic Term

$$M_{cC} := \text{augment}(W, X, Y) \quad V_{cC} := c_C \quad R_{cC} := \text{regress}(M_{cC}, V_{cC}, n)$$

$$f_{cC}(W, X, Y) := \text{interp} \left[R_{cC}, M_{cC}, V_{cC}, \begin{pmatrix} W \\ X \\ Y \end{pmatrix} \right]$$

$$f_{cC}(4, .4, .8) = 0.06384 \quad \text{Check Calculation}$$

Calculations : Recursive calculations to estimate flaw growth

Recursive Loop for Calculation of PWSCC Crack Growth

```

CGRsambi := | j ← 0
              | a0 ← a0
              | c0 ← c0
              | t ← t2
              | NCB0 ← Cblk
              | while j ≤ Ilim
                |   σ0 ← | IDRG1,3 if cj ≤ c0
                |         | IDRG2,3 if c0 < cj ≤ c0 + IncStrs.avg
                |         | IDRG3,3 if c0 + IncStrs.avg < cj ≤ c0 + 2·IncStrs.avg
                |         | IDRG4,3 if c0 + 2·IncStrs.avg < cj ≤ c0 + 3·IncStrs.avg
                |         | IDRG5,3 if c0 + 3·IncStrs.avg < cj ≤ c0 + 4·IncStrs.avg
                |         | IDRG6,3 if c0 + 4·IncStrs.avg < cj ≤ c0 + 5·IncStrs.avg
                |         | IDRG7,3 if c0 + 5·IncStrs.avg < cj ≤ c0 + 6·IncStrs.avg
                |         | IDRG8,3 if c0 + 6·IncStrs.avg < cj ≤ c0 + 7·IncStrs.avg
                |         | IDRG9,3 if c0 + 7·IncStrs.avg < cj ≤ c0 + 8·IncStrs.avg
                |         | IDRG10,3 if c0 + 8·IncStrs.avg < cj ≤ c0 + 9·IncStrs.avg
                |         | IDRG11,3 if c0 + 9·IncStrs.avg < cj ≤ c0 + 10·IncStrs.avg
                |         | IDRG12,3 if c0 + 10·IncStrs.avg < cj ≤ c0 + 11·IncStrs.avg
                |         | IDRG13,3 if c0 + 11·IncStrs.avg < cj ≤ c0 + 12·IncStrs.avg
                |         | IDRG14,3 if c0 + 12·IncStrs.avg < cj ≤ c0 + 13·IncStrs.avg
                |         | IDRG15,3 if c0 + 13·IncStrs.avg < cj ≤ c0 + 14·IncStrs.avg

```

	IDRG _{16₃} if $c_0 + 14 \cdot \text{IncStrs.avg} < c_j \leq c_0 + 15 \cdot \text{IncStrs.avg}$
	IDRG _{17₃} if $c_0 + 15 \cdot \text{IncStrs.avg} < c_j \leq c_0 + 16 \cdot \text{IncStrs.avg}$
	IDRG _{18₃} if $c_0 + 16 \cdot \text{IncStrs.avg} < c_j \leq c_0 + 17 \cdot \text{IncStrs.avg}$
	IDRG _{19₃} if $c_0 + 17 \cdot \text{IncStrs.avg} < c_j \leq c_0 + 18 \cdot \text{IncStrs.avg}$
	IDRG _{20₃} otherwise
$\sigma_1 \leftarrow$	IDRG _{1₄} if $c_j \leq c_0$
	IDRG _{2₄} if $c_0 < c_j \leq c_0 + \text{IncStrs.avg}$
	IDRG _{3₄} if $c_0 + \text{IncStrs.avg} < c_j \leq c_0 + 2 \cdot \text{IncStrs.avg}$
	IDRG _{4₄} if $c_0 + 2 \cdot \text{IncStrs.avg} < c_j \leq c_0 + 3 \cdot \text{IncStrs.avg}$
	IDRG _{5₄} if $c_0 + 3 \cdot \text{IncStrs.avg} < c_j \leq c_0 + 4 \cdot \text{IncStrs.avg}$
	IDRG _{6₄} if $c_0 + 4 \cdot \text{IncStrs.avg} < c_j \leq c_0 + 5 \cdot \text{IncStrs.avg}$
	IDRG _{7₄} if $c_0 + 5 \cdot \text{IncStrs.avg} < c_j \leq c_0 + 6 \cdot \text{IncStrs.avg}$
	IDRG _{8₄} if $c_0 + 6 \cdot \text{IncStrs.avg} < c_j \leq c_0 + 7 \cdot \text{IncStrs.avg}$
	IDRG _{9₄} if $c_0 + 7 \cdot \text{IncStrs.avg} < c_j \leq c_0 + 8 \cdot \text{IncStrs.avg}$
	IDRG _{10₄} if $c_0 + 8 \cdot \text{IncStrs.avg} < c_j \leq c_0 + 9 \cdot \text{IncStrs.avg}$
	IDRG _{11₄} if $c_0 + 9 \cdot \text{IncStrs.avg} < c_j \leq c_0 + 10 \cdot \text{IncStrs.avg}$
	IDRG _{12₄} if $c_0 + 10 \cdot \text{IncStrs.avg} < c_j \leq c_0 + 11 \cdot \text{IncStrs.avg}$
	IDRG _{13₄} if $c_0 + 11 \cdot \text{IncStrs.avg} < c_j \leq c_0 + 12 \cdot \text{IncStrs.avg}$
	IDRG _{14₄} if $c_0 + 12 \cdot \text{IncStrs.avg} < c_j \leq c_0 + 13 \cdot \text{IncStrs.avg}$
	IDRG _{15₄} if $c_0 + 13 \cdot \text{IncStrs.avg} < c_j \leq c_0 + 14 \cdot \text{IncStrs.avg}$
	IDRG _{16₄} if $c_0 + 14 \cdot \text{IncStrs.avg} < c_j \leq c_0 + 15 \cdot \text{IncStrs.avg}$

	IDRG ₁₇ ₄	if $c_0 + 15 \cdot \text{IncStrs.avg} < c_j \leq c_0 + 16 \cdot \text{IncStrs.avg}$
	IDRG ₁₈ ₄	if $c_0 + 16 \cdot \text{IncStrs.avg} < c_j \leq c_0 + 17 \cdot \text{IncStrs.avg}$
	IDRG ₁₉ ₄	if $c_0 + 17 \cdot \text{IncStrs.avg} < c_j \leq c_0 + 18 \cdot \text{IncStrs.avg}$
	IDRG ₂₀ ₄	otherwise
$\sigma_2 \leftarrow$	IDRG ₁ ₅	if $c_j \leq c_0$
	IDRG ₂ ₅	if $c_0 < c_j \leq c_0 + \text{IncStrs.avg}$
	IDRG ₃ ₅	if $c_0 + \text{IncStrs.avg} < c_j \leq c_0 + 2 \cdot \text{IncStrs.avg}$
	IDRG ₄ ₅	if $c_0 + 2 \cdot \text{IncStrs.avg} < c_j \leq c_0 + 3 \cdot \text{IncStrs.avg}$
	IDRG ₅ ₅	if $c_0 + 3 \cdot \text{IncStrs.avg} < c_j \leq c_0 + 4 \cdot \text{IncStrs.avg}$
	IDRG ₆ ₅	if $c_0 + 4 \cdot \text{IncStrs.avg} < c_j \leq c_0 + 5 \cdot \text{IncStrs.avg}$
	IDRG ₇ ₅	if $c_0 + 5 \cdot \text{IncStrs.avg} < c_j \leq c_0 + 6 \cdot \text{IncStrs.avg}$
	IDRG ₈ ₅	if $c_0 + 6 \cdot \text{IncStrs.avg} < c_j \leq c_0 + 7 \cdot \text{IncStrs.avg}$
	IDRG ₉ ₅	if $c_0 + 7 \cdot \text{IncStrs.avg} < c_j \leq c_0 + 8 \cdot \text{IncStrs.avg}$
	IDRG ₁₀ ₅	if $c_0 + 8 \cdot \text{IncStrs.avg} < c_j \leq c_0 + 9 \cdot \text{IncStrs.avg}$
	IDRG ₁₁ ₅	if $c_0 + 9 \cdot \text{IncStrs.avg} < c_j \leq c_0 + 10 \cdot \text{IncStrs.avg}$
	IDRG ₁₂ ₅	if $c_0 + 10 \cdot \text{IncStrs.avg} < c_j \leq c_0 + 11 \cdot \text{IncStrs.avg}$
	IDRG ₁₃ ₅	if $c_0 + 11 \cdot \text{IncStrs.avg} < c_j \leq c_0 + 12 \cdot \text{IncStrs.avg}$
	IDRG ₁₄ ₅	if $c_0 + 12 \cdot \text{IncStrs.avg} < c_j \leq c_0 + 13 \cdot \text{IncStrs.avg}$
	IDRG ₁₅ ₅	if $c_0 + 13 \cdot \text{IncStrs.avg} < c_j \leq c_0 + 14 \cdot \text{IncStrs.avg}$
	IDRG ₁₆ ₅	if $c_0 + 14 \cdot \text{IncStrs.avg} < c_j \leq c_0 + 15 \cdot \text{IncStrs.avg}$
	IDRG ₁₇ ₅	if $c_0 + 15 \cdot \text{IncStrs.avg} < c_j \leq c_0 + 16 \cdot \text{IncStrs.avg}$
	IDRG ₁₈	if $c_0 + 16 \cdot \text{IncStrs.avg} < c_j \leq c_0 + 17 \cdot \text{IncStrs.avg}$

		$\text{IDRG}_{19_5} \text{ if } c_0 + 17 \cdot \text{IncStrs.avg} < c_j \leq c_0 + 18 \cdot \text{IncStrs.avg}$ $\text{IDRG}_{20_5} \text{ otherwise}$
$\sigma_3 \leftarrow$		$\text{IDRG}_{1_6} \text{ if } c_j \leq c_0$ $\text{IDRG}_{2_6} \text{ if } c_0 < c_j \leq c_0 + \text{IncStrs.avg}$ $\text{IDRG}_{3_6} \text{ if } c_0 + \text{IncStrs.avg} < c_j \leq c_0 + 2 \cdot \text{IncStrs.avg}$ $\text{IDRG}_{4_6} \text{ if } c_0 + 2 \cdot \text{IncStrs.avg} < c_j \leq c_0 + 3 \cdot \text{IncStrs.avg}$ $\text{IDRG}_{5_6} \text{ if } c_0 + 3 \cdot \text{IncStrs.avg} < c_j \leq c_0 + 4 \cdot \text{IncStrs.avg}$ $\text{IDRG}_{6_6} \text{ if } c_0 + 4 \cdot \text{IncStrs.avg} < c_j \leq c_0 + 5 \cdot \text{IncStrs.avg}$ $\text{IDRG}_{7_6} \text{ if } c_0 + 5 \cdot \text{IncStrs.avg} < c_j \leq c_0 + 6 \cdot \text{IncStrs.avg}$ $\text{IDRG}_{8_6} \text{ if } c_0 + 6 \cdot \text{IncStrs.avg} < c_j \leq c_0 + 7 \cdot \text{IncStrs.avg}$ $\text{IDRG}_{9_6} \text{ if } c_0 + 7 \cdot \text{IncStrs.avg} < c_j \leq c_0 + 8 \cdot \text{IncStrs.avg}$ $\text{IDRG}_{10_6} \text{ if } c_0 + 8 \cdot \text{IncStrs.avg} < c_j \leq c_0 + 9 \cdot \text{IncStrs.avg}$ $\text{IDRG}_{11_6} \text{ if } c_0 + 9 \cdot \text{IncStrs.avg} < c_j \leq c_0 + 10 \cdot \text{IncStrs.avg}$ $\text{IDRG}_{12_6} \text{ if } c_0 + 10 \cdot \text{IncStrs.avg} < c_j \leq c_0 + 11 \cdot \text{IncStrs.avg}$ $\text{IDRG}_{13_6} \text{ if } c_0 + 11 \cdot \text{IncStrs.avg} < c_j \leq c_0 + 12 \cdot \text{IncStrs.avg}$ $\text{IDRG}_{14_6} \text{ if } c_0 + 12 \cdot \text{IncStrs.avg} < c_j \leq c_0 + 13 \cdot \text{IncStrs.avg}$ $\text{IDRG}_{15_6} \text{ if } c_0 + 13 \cdot \text{IncStrs.avg} < c_j \leq c_0 + 14 \cdot \text{IncStrs.avg}$ $\text{IDRG}_{16_6} \text{ if } c_0 + 14 \cdot \text{IncStrs.avg} < c_j \leq c_0 + 15 \cdot \text{IncStrs.avg}$ $\text{IDRG}_{17_6} \text{ if } c_0 + 15 \cdot \text{IncStrs.avg} < c_j \leq c_0 + 16 \cdot \text{IncStrs.avg}$ $\text{IDRG}_{18_6} \text{ if } c_0 + 16 \cdot \text{IncStrs.avg} < c_j \leq c_0 + 17 \cdot \text{IncStrs.avg}$ $\text{IDRG}_{19_6} \text{ if } c_0 + 17 \cdot \text{IncStrs.avg} < c_j \leq c_0 + 18 \cdot \text{IncStrs.avg}$

```

IDRG206 otherwise
ξ0 ← σ0
ξ1 ← σ0 + σ1 ·  $\left(\frac{0.25 \cdot a_j}{t}\right) + \sigma_2 \cdot \left(\frac{0.25 \cdot a_j}{t}\right)^2 + \sigma_3 \cdot \left(\frac{0.25 \cdot a_j}{t}\right)^3$ 
ξ2 ← σ0 + σ1 ·  $\left(\frac{0.5 \cdot a_j}{t}\right) + \sigma_2 \cdot \left(\frac{0.5 \cdot a_j}{t}\right)^2 + \sigma_3 \cdot \left(\frac{0.5 \cdot a_j}{t}\right)^3$ 
ξ3 ← σ0 + σ1 ·  $\left(\frac{0.75 \cdot a_j}{t}\right) + \sigma_2 \cdot \left(\frac{0.75 \cdot a_j}{t}\right)^2 + \sigma_3 \cdot \left(\frac{0.75 \cdot a_j}{t}\right)^3$ 
ξ4 ← σ0 + σ1 ·  $\left(\frac{1.0 \cdot a_j}{t}\right) + \sigma_2 \cdot \left(\frac{1.0 \cdot a_j}{t}\right)^2 + \sigma_3 \cdot \left(\frac{1.0 \cdot a_j}{t}\right)^3$ 
x0 ← 0.0
x1 ← 0.25
x2 ← 0.5
x3 ← 0.75
x4 ← 1.0
X ← stack(x0, x1, x2, x3, x4)
ST ← stack(ξ0, ξ1, ξ2, ξ3, ξ4)
RG ← regress(X, ST, 3)
σ00 ← RG3 + PInt
σ10 ← RG4
σ20 ← RG5
σ30 ← RG6
ARj ←  $\frac{a_j}{c_j}$ 
ATj ←  $\frac{a_j}{t}$ 
G... ← f...(R..., AR..., AT...)

```

$$G_{au_j} \leftarrow f_{au}(R_t, AR_j, AT_j)$$

$$G_{al_j} \leftarrow f_{aL}(R_t, AR_j, AT_j)$$

$$G_{aq_j} \leftarrow f_{aQ}(R_t, AR_j, AT_j)$$

$$G_{ac_j} \leftarrow f_{aC}(R_t, AR_j, AT_j)$$

$$G_{cu_j} \leftarrow f_{cU}(R_t, AR_j, AT_j)$$

$$G_{cl_j} \leftarrow f_{cL}(R_t, AR_j, AT_j)$$

$$G_{cq_j} \leftarrow f_{cQ}(R_t, AR_j, AT_j)$$

$$G_{cc_j} \leftarrow f_{cC}(R_t, AR_j, AT_j)$$

$$Q_j \leftarrow \begin{cases} 1 + 1.464 \cdot \left(\frac{a_j}{c_j}\right)^{1.65} & \text{if } c_j \geq a_j \\ 1 + 1.464 \cdot \left(\frac{c_j}{a_j}\right)^{1.65} & \text{otherwise} \end{cases}$$

$$K_{a_j} \leftarrow \left(\frac{\pi \cdot a_j}{Q_j}\right)^{0.5} \cdot (\sigma_{00} \cdot G_{au_j} + \sigma_{10} \cdot G_{al_j} + \sigma_{20} \cdot G_{aq_j} + \sigma_{30} \cdot G_{ac_j})$$

$$K_{c_j} \leftarrow \left(\frac{\pi \cdot c_j}{Q_j}\right)^{0.5} \cdot (\sigma_{00} \cdot G_{cu_j} + \sigma_{10} \cdot G_{cl_j} + \sigma_{20} \cdot G_{cq_j} + \sigma_{30} \cdot G_{cc_j})$$

$$K_{\alpha_j} \leftarrow K_{a_j} \cdot 1.099$$

$$K_{\gamma_j} \leftarrow K_{c_j} \cdot 1.099$$

$$K_{\alpha_j} \leftarrow \begin{cases} 9.0 & \text{if } K_{\alpha_j} \leq 9.0 \\ K_{\alpha_j} & \text{otherwise} \end{cases}$$

$$K_{\gamma_j} \leftarrow \begin{cases} 9.0 & \text{if } K_{\gamma_j} \leq 9.0 \\ K_{\gamma_j} & \text{otherwise} \end{cases}$$

$$D_{a_j} \leftarrow C_0 \cdot (K_{\alpha_j} - 9.0)^{1.16}$$

$$D_{c_j} \leftarrow C_0 \cdot (K_{\gamma_j} - 9.0)^{1.16} \quad \text{if } K_{\gamma_j} > 9.0$$

$$D_{ag_j} \leftarrow \begin{cases} a_j \cdot CF_{inhr} \cdot C_{blk} & \text{if } K_{\gamma_j} > 80.0 \\ 4 \cdot 10^{-10} \cdot CF_{inhr} \cdot C_{blk} & \text{otherwise} \end{cases}$$

$$D_{c_j} \leftarrow C_0 \cdot (K_{\gamma_j} - 9.0)^{1.16}$$

$$D_{cg_j} \leftarrow \begin{cases} D_{c_j} \cdot CF_{inhr} \cdot C_{blk} & \text{if } K_{\gamma_j} < 80.0 \\ 4 \cdot 10^{-10} \cdot CF_{inhr} \cdot C_{blk} & \text{otherwise} \end{cases}$$

$$\text{output}(j, 0) \leftarrow j$$

$$\text{output}(j, 1) \leftarrow a_j$$

$$\text{output}(j, 2) \leftarrow c_j - c_0$$

$$\text{output}(j, 3) \leftarrow D_{ag_j}$$

$$\text{output}(j, 4) \leftarrow D_{cg_j}$$

$$\text{output}(j, 5) \leftarrow K_{a_j}$$

$$\text{output}(j, 6) \leftarrow K_{c_j}$$

$$\text{output}(j, 7) \leftarrow \frac{NCB_j}{365 \cdot 24}$$

$$\text{output}(j, 8) \leftarrow G_{au_j}$$

$$\text{output}(j, 9) \leftarrow G_{al_j}$$

$$\text{output}(j, 10) \leftarrow G_{aq_j}$$

$$\text{output}(j, 11) \leftarrow G_{ac_j}$$

$$\text{output}(j, 12) \leftarrow G_{cu_j}$$

$$\text{output}(j, 13) \leftarrow G_{cl_j}$$

$$\text{output}(j, 14) \leftarrow G_{cq_j}$$

$$\text{output}(j, 15) \leftarrow G_{cc_j}$$

$$j \leftarrow j + 1$$

$$a_i \leftarrow a_{i-1} + D_{a_i}$$

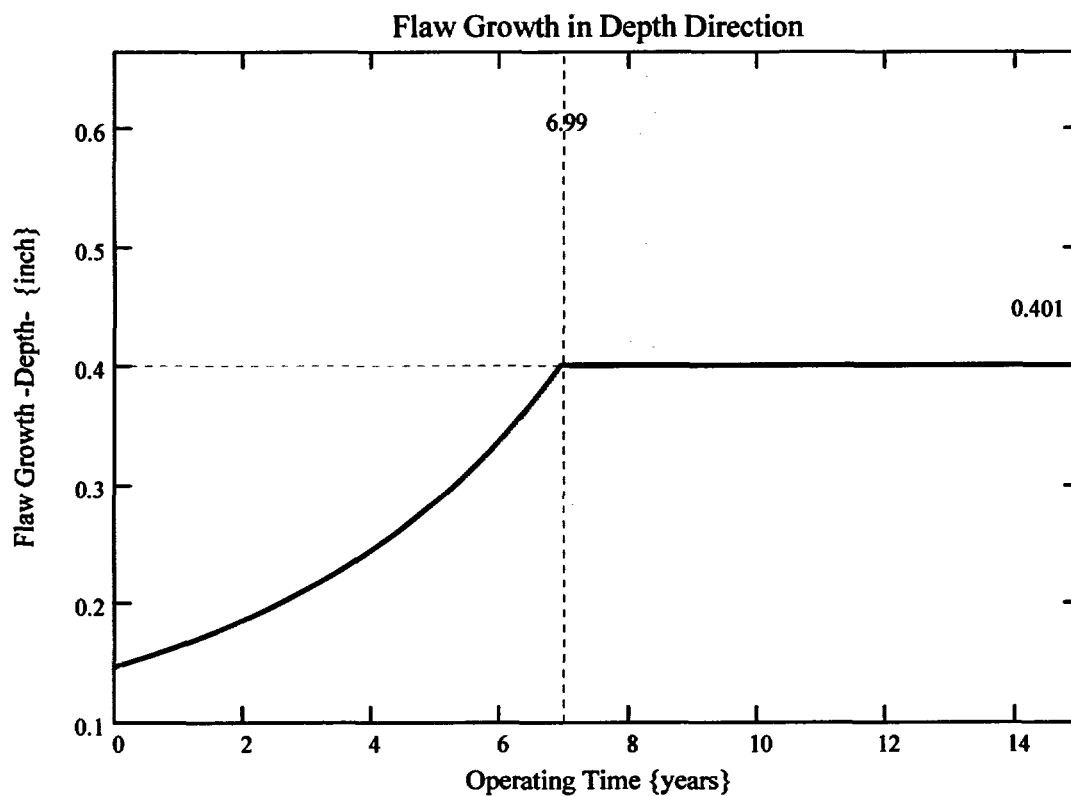
```

       $\epsilon_{j-1}$ 
       $c_j \leftarrow c_{j-1} + D_{cg_{j-1}}$ 
       $a_j \leftarrow \begin{cases} t & \text{if } a_j \geq t \\ a_j & \text{otherwise} \end{cases}$ 
       $NCB_j \leftarrow NCB_{j-1} + C_{blk}$ 
      output

```

$k_w := 0..I_{lim}$

The curve below shows the flaw growth through-wall and the operating time (in years) it takes to go through-wall.



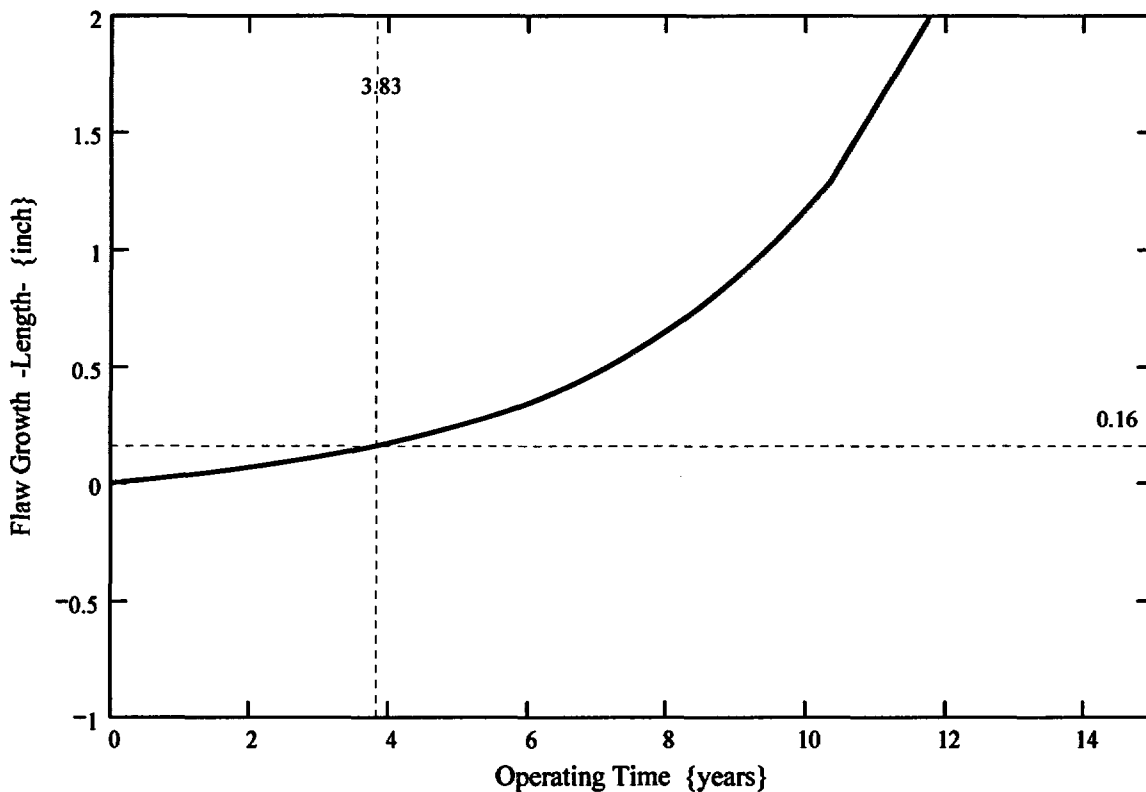
The propagation length for the ICI nozzles is defined as the length for which the initial flaw in the blind zone would extend out of the blind zone and grow to a detectable flaw. Reference 11 gives the minimum detectable flaw size of 4 mm (0.16) in length; thus, 0.16 inch was considered as this minimum detectable flaw length. This dimension is added to the end of the blind zone.

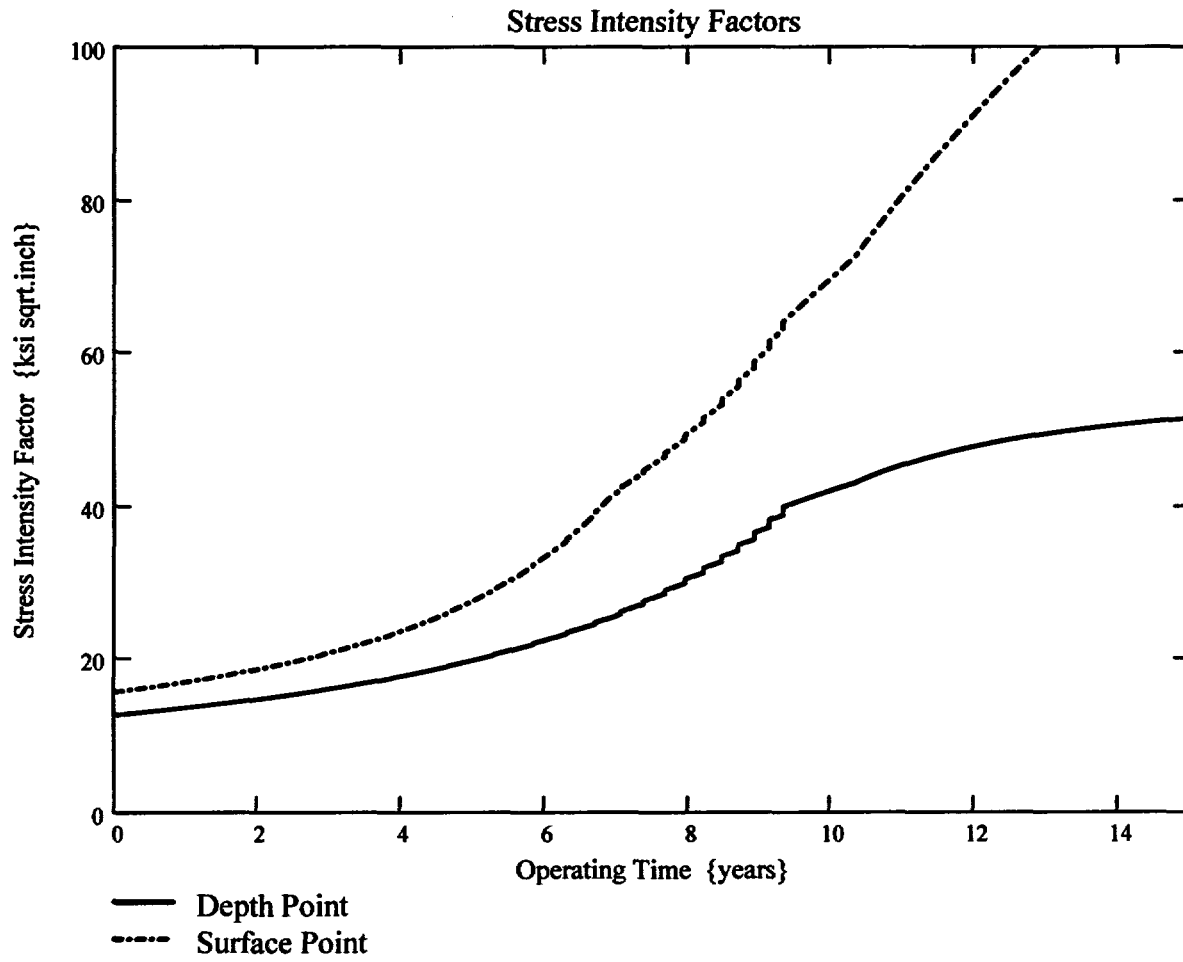
$$\text{Prop_Length} := \frac{\text{BZ_length}}{2} - c_0 + 0.16$$

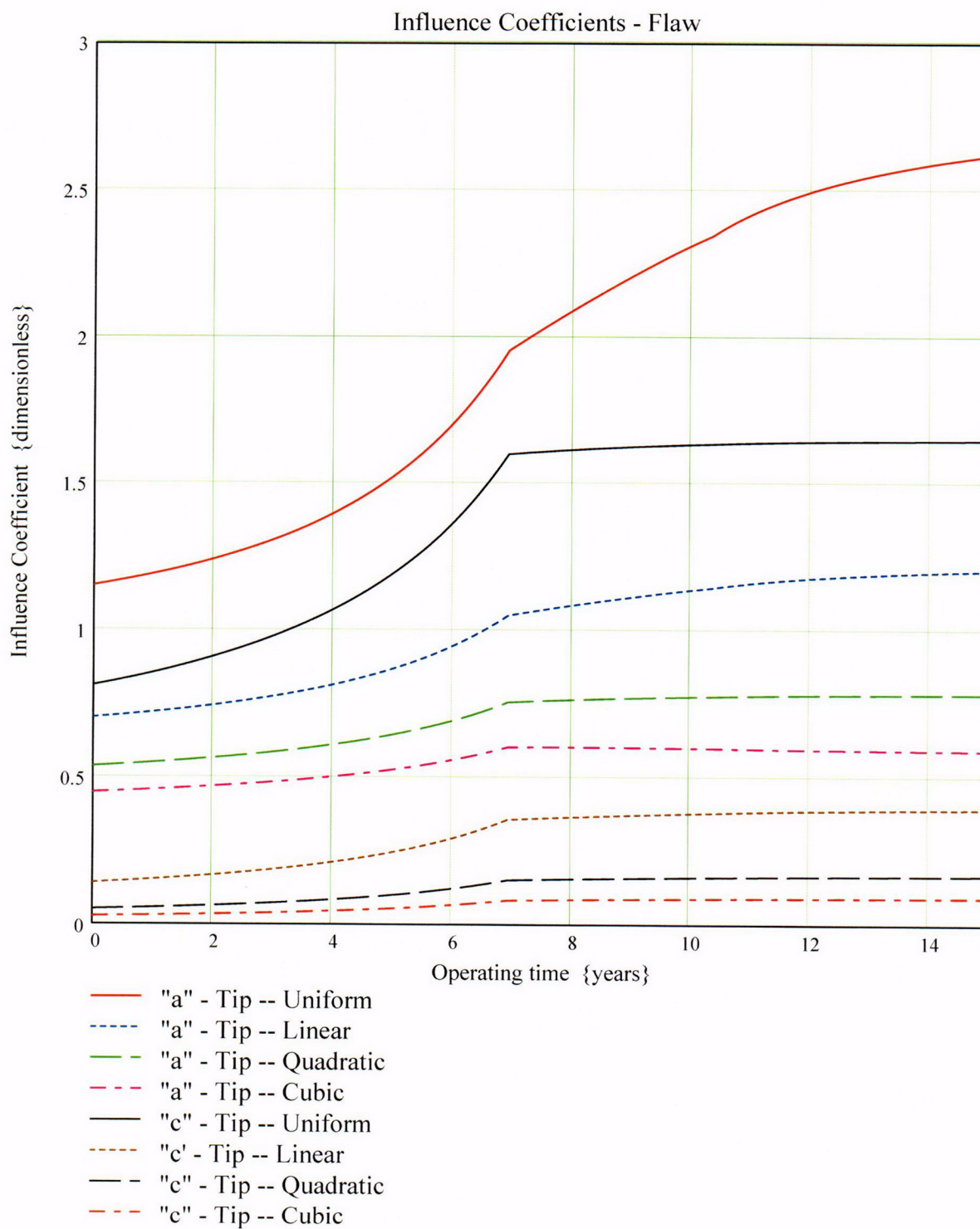
$$\text{Prop_Length} = 0.16$$

This implies that a flaw initially spanning the length of the blindzone must grow 0.16 inch to become detectable via UT.

The curve below shows the flaw growth along the length of the ICI nozzle and the operating time (in years) it takes to reach the Prop_Length value defined above.







ENCLOSURE 3

CNRO-2003-00035

LICENSEE-IDENTIFIED COMMITMENTS

LICENSEE-IDENTIFIED COMMITMENTS

COMMITMENT	TYPE (Check one)		SCHEDULED COMPLETION DATE
	ONE-TIME ACTION	CONTINUING COMPLIANCE	
1. Entergy will provide in the 60-day report for ANO-2, as required by the Order, specific inspection information; i.e., extent of inspections and results of those inspections.	✓		60 days after startup from the next refueling outage
2. If the NRC staff finds that the crack-growth formula in MRP-55 is unacceptable, Entergy shall revise its analysis that justifies relaxation of the Order within 30 days after the NRC informs Entergy of an NRC-approved crack-growth formula.	✓		Within 30 days after the NRC informs Entergy of an NRC-approved crack-growth formula.
3. If Entergy's revised analysis (#2, above) shows that the crack growth acceptance criteria are exceeded prior to the end of Operating Cycle 17 (following the upcoming refueling outage), Entergy will, within 72 hours, submit to the NRC written justification for continued operation.	✓		Within 72 hours from completing the revised analysis in #2, above.
4. If the revised analysis (#2, above) shows that the crack growth acceptance criteria are exceeded during the subsequent operating cycle, Entergy shall, within 30 days, submit the revised analysis for NRC review.	✓		Within 30 days from completing the revised analysis in #2, above.
5. If the revised analysis (#2, above) shows that the crack growth acceptance criteria are not exceeded during either Operating Cycle 17 or the subsequent operating cycle, Entergy shall, within 30 days, submit a letter to the NRC confirming that its analysis has been revised.	✓		Within 30 days from completing the revised analysis in #2, above.
6. Any future crack-growth analyses performed for Operating Cycle 17 and future cycles for RPV head penetrations will be based on an acceptable crack growth rate formula.		✓	N/A